INFORMATION TO USERS

This manuscript has been reproduced from the microfilm master. UMI films the text directly from the original or copy submitted. Thus, some thesis and dissertation copies are in typewriter face, while others may be from any type of computer printer.

The quality of this reproduction is dependent upon the quality of the copy submitted. Broken or indistinct print, colored or poor quality illustrations and photographs, print bleedthrough, substandard margins, and improper alignment can adversely affect reproduction.

In the unlikely event that the author did not send UMI a complete manuscript and there are missing pages, these will be noted. Also, if unauthorized copyright material had to be removed, a note will indicate the deletion.

Oversize materials (e.g., maps, drawings, charts) are reproduced by sectioning the original, beginning at the upper left-hand corner and continuing from left to right in equal sections with small overlaps.

Photographs included in the original manuscript have been reproduced xerographically in this copy. Higher quality 6" x 9" black and white photographic prints are available for any photographs or illustrations appearing in this copy for an additional charge. Contact UMI directly to order.

Bell & Howell Information and Learning
300 North Zeeb Road, Ann Arbor, MI 48106-1346 USA
800-521-0600

Université d'Ottawa · University of Ottawa

CONFORMATIONAL EFFECTS OF LIPIDS AND LOCAL ANESTHETICS ON THE NICOTINIC ACETYLCHOLINE RECEPTOR

Stephen E. Ryan

Thesis submitted to the Department of Biochemistry in partial fulfillment of the requirements for the degree of Doctor of Philosophy

University of Ottawa
Ottawa, Ontario, Canada
June, 2000

To my parents, Sally and Murray Ryan. All that I am and everything I achieve I owe to you both.

ABSTRACT

The mechanisms by which both lipids and local anesthetics modulate the structure and function of the nicotinic acetylcholine receptor (nAChR) from *Torpedo* have been investigated using the technique of Fourier transform infrared (FTIR) difference spectroscopy. With respect to lipids, the results reveal that reconstitution of the nAChR into a highly fluid egg phosphatidylcholine (EPC) membrane stabilizes the receptor in a channel-inactive desensitized state. The addition of a variety of neutral and/or anionic lipids to the EPC membrane all induce an essentially identical pattern of vibrational changes in the nAChR suggesting that the presence of diverse lipid structures within a reconstituted membrane acts to stabilize the receptor in a channel-competent resting state. In addition, increasing levels of either the neutral lipid, cholesterol (Chol) or the anionic lipid, dioleoylphosphatidic acid (DOPA) within an EPC membrane increasingly stabilizes a larger proportion of nAChR's in a conformation(s) that is(are) capable of undergoing agonist-induced desensitization, although only high levels of DOPA were found to stabilize the receptor in a fully functional resting state. The results have been interpreted in terms of a speculative model that describes the mechanisms by which lipids modulate nAChR function. This model suggests that the composition of the lipid membrane surrounding the nAChR influences the conformational equilibrium of the receptor between the resting, desensitized and a novel intermediate state through an indirect effect on some physical property of the lipid bilayer, possibly bulk fluidity. The model also proposes that anionic lipids, in addition to proper membrane fluidity, are required to stabilize the nAChR in a fully functional resting conformation.

With respect to local anesthetics, the results support the current model of local anesthetic action at the nAChR and suggest that the binding of local anesthetics stabilize the receptor in a desensitized conformation. Contrary to the model, however, the FTIR data suggest that receptor desensitization occurs not through interactions at a distinct non-competitive blocker site, but solely as a consequence of local anesthetic binding to the neurotransmitter binding sites. The data also suggest that the binding of local anesthetics to the non-competitive blocker site stabilizes the nAChR in an intermediate conformation similar to that stabilized upon reconstitution of the nAChR into EPC membranes containing low concentrations of either Chol or DOPA. Additional studies employing the local anesthetic, proadifen and the hallucinogen, phencyclidine hydrochloride (PCP) support these findings and show conclusively that both local anesthetics and PCP bind to the non-competitive blocker site and stabilize the nAChR in a conformation that is structurally distinct from both the resting and desensitized states.

ACKNOWLEDGEMENTS

At this point I would like to express my sincere gratitude to some of the many people who have had to patiently endure my presence for so many years:

- First and foremost I would like to thank my supervisor Dr. John Baenziger whose guidance, patience and friendship over the years has enabled me to achieve levels of success that I never imagined possible. I am forever in your debt (well, at least until I graduate).
- I would like to thank Dr. Steven Evans for both his friendship and support and for providing me with the opportunity to experience both the excitement of x-ray crystallography and the sting of defeat in 'Tanks'.
- To Julie Aubé and Joanne Daniels. How will I ever survive without you both?
- To past and present labmates who have made my many years here more enjoyable: Caroline Demers, Marcin Kaminski, Roula Webbi, Mary-Lou Morris, Tim Darsaut, Hoa Phuc Nguyen, Blair Ritchie, Jeremy Cheeseman, Corey Yanofski and MaryLou Barone. A special thanks to Dr. Nathalie Méthot for her friendship, encouragement and valiant attempts to teach me French.
- To Anna and Anita for allowing me to share in their lives and for the many memories.
- To Paola, Dave, Pete, Ninan, Mike, Simon, Paul, Ricardo, Tim, Alan, and the many others who made both Thursday Morning Hockey and Friday Night Beer Club welcome distractions from the everyday grind of graduate school.
- A special thanks to Roxanne for both her patience and understanding and for helping me overcome the many neuronal 'hiccups' (and there were many) that surfaced during the writing of this thesis. Thank you for also shattering any dream I had of becoming a professional pool player (remember, the Chirp Gods are always listening).
- And last but not least, I would like to thank my family, Sal, Mur, Paul, Dave and Amanda for their unwavering support and encouragement throughout my education.

PREFACE

The work presented in this thesis has either been previously published or will be submitted for publication as described below:

CHAPTER 3

Ryan, S.E., Demers, C.N., Chew, J.P. and Baenziger, J.E. (1996) Structural effects of neutral and anionic lipids on the nicotinic acetylcholine receptor. *J. Biol. Chem.* **271**, 24590-24597.

CHAPTER 4

Baenziger, J.E., Morris, M.-L., Darsaut, T. and Ryan, S.E. (2000) The effect of membrane lipid composition on the conformational equilibria of the nicotinic acetylcholine receptor. *J. Biol. Chem.* **275**, 777-784.

CHAPTER 5

Ryan, S.E., Nguyen, H.P. and Baenziger, J.E. (1998) Anesthetic-induced changes in the nicotinic acetylcholine receptor. *Toxicol. Lett.* **100-101**, 179-183.

Ryan, S.E and Baenziger, J.E. (1999) A structure-based approach to nicotinic receptor pharmacology. *Mol. Pharm.* **55**, 348-355.

CHAPTER 6

Ryan, S.E., Blanton, M.P. and Baenziger, J.E. (2000) The identification of a structural intermediate between the resting and desensitized states of the nicotinic acetylcholine receptor. Manuscript in preparation.

The following people have contributed to the experimental work presented in this thesis: Caroline Demers acquired the Carb-difference spectra recorded from the nAChR reconstituted into lipid membranes composed of EPC/DOPA (3:1) and EPC/Chol (3:1); Mary-Lou Morris and Tim Darsaut assisted in the acquisition of both [^{13}C]-ACh difference spectra and Carb-difference spectra recorded from the nAChR reconstituted into lipid membranes composed of EPC and varying levels of either DOPA or Chol.

TABLE OF CONTENTS

LIST OF FIGURES AND TABLES

CHAPTER 1

CHAPTER 2

CHAPTER 3

CHAPTER 4

CHAPTER 5

CHAPTER 6

LIST OF ABBREVIATIONS

Å	Angstrom
α-btx	α-Bungarotoxin
ACh	Acetylcholine
ATP	Adenosine triphosphate
ATPase	Adenosine triphosphatase
ATR	Attenuated total reflectance
a.u.	Absorbance units
A_ω	Absorbance at wavenumber ω
BAC	Bromoacetylcholine chloride
c	Velocity of light
Ca^{2+}	Calcium ion
$CaCl_2$	Calcium chloride
Carb	Carbamylcholine
Chol	Cholesterol
Cl^-	Chlorine ion
C=O	Carbonyl group
Cys	Cysteine
d	Mirror displacement
δ	Optical path difference
Da	Dalton
DDF	p-(N,N-Dimethyl)aminobenzenediazonium
DOPA	Dioleoylphosphatidic acid
DOPC	Dioleoylphosphatidylcholine
DOPS	Dioleoylphosphatidylserine
d_p	Penetration depth
DTT	Dithiothreitol
$\Delta E_{0\rightarrow 1}$	Energy difference between vibrational levels 0 and 1
EDTA	Ethylenediaminetetraacetic acid

EGTA	Ethylene glycol-bis(β-aminoethyl ether) N,N,N',N'-tetraaceticacid
EPC	Egg phosphatidylcholine
E_v	Vibrational level energy
E_w	Energy of a wave
ε_ω	Molar absorption coefficient
F	Force constant
f	Frequency
f_v	Vibrational frequency
f_w	Frequency of a wave
FTIR	Fourier transform infrared
GABA	γ-Aminobutyric acid
h	Planck's constant
^1H	Hydrogen
^2H	Deuterium
^3H	Tritium
He	Helium
^2H_2O	Deuterium oxide
I	Intensity
I_o	Initial intensity
^{125}I-*TID*	3-Trifluoromethyl-3-(*m*-[^{125}I]iodophenyl)diazirine
IRE	Internal reflection element
K^+	Potassium ion
KCl	Potassium chloride
K_D	Dissociation constant
kDa	KiloDalton
L	Length
l	Sample thickness
λ	Wavelength
M	Molarity

m	Mass
M_c	Molar concentration
$MgCl_2$	Magnesium chloride
M_{red}	Reduced mass
mV	Millivolt
N	Number of atoms in a molecule
n	Quantum number
n_1	Refractive index of a dense medium
n_2	Refractive index of a rarer medium
Na^+	Sodium ion
$nAChR$	Nicotinic acetylcholine receptor
$NaCl$	Sodium Chloride
$NaHCO_3$	Sodium bicarbonate
NaH_2PO_4	Sodium dihydrogen phosphate
Na_2HPO_4	Disodium phosphate
NaN_3	Sodium azide
NCB	Non-competitive blocker
Ne	Neon
NMR	Nuclear magnetic resonance
N_r	Number of internal reflections
P	Probability
φ	Angle of refraction
PCP	Phencyclidine hydrochloride
$PMSF$	Phenylmethylsulphonyl fluoride
Q	Magnitude of charge
q	Change in charge separation
r	Distance between two charges
rpm	Rotations per minute
θ	Angle of incidence
θ_c	Critical angle

Tris	Tris(hydroxymethyl)aminomethane
Trp	Tryptophan
Tyr	Tyrosine
μ	Dipole moment
ν	Velocity
ω	Wavenumber
z	Distance from interface
ZPD	Zero path difference

General Introduction

The human brain is the ultimate product of biological evolution. Its intricate network of neurons rapidly acquire, integrate and transmit information providing the biological basis on which we perceive, act, learn and remember. Understanding how the brain functions thus requires intimate knowledge of how information is conveyed both within and between neurons, and in turn, how changes in the efficiency of these processes influence human behaviour.

To this end, research into the brain has recently focused on identifying and characterizing the specific molecular components of the neuron that confer upon the cell its unique signaling capabilities. One such component is a superfamily of neurotransmitter-gated ion channels located at specialized junctions between neurons called synapses. These integral membrane receptors mediate rapid inter-neuronal communication by converting the chemical signals that are released from the surface of one neuron into electrical signals at another. Since the activity of these receptors can be modulated by various endogenous factors, including phosphorylation and membrane lipid composition, it is believed that these proteins perform an essential role in higher brain functions such as thought, memory and learning. An understanding of neurotransmitter-gated ion channel structure and function is thus likely to have important implications for our understanding of the brain.

The research described in this thesis is centred on one neurotransmitter-gated ion channel, the nicotinic acetylcholine receptor (nAChR) from *Torpedo*. The *Torpedo* nAChR was the first neurotransmitter receptor to be purified and sequenced, and is

currently used extensively as a model for studying neurotransmitter-gated ion channel structure and function.

Initially, the aim of this work was to employ the novel technique of Fourier transform infrared (FTIR) *difference* spectroscopy to examine the nature of the physical interactions that form between the nAChR and the neurotransmitter analog carbamylcholine (Carb). It was hoped that this information would lead to a greater understanding of how neurotransmitter binding elicits both channel activation and receptor desensitization. Preliminary studies, however, revealed unexpected details regarding the mechanisms by which both lipids and local anesthetics modulate receptor activity. As a result, the focus of this research was redirected towards unravelling the structural and functional consequences of both lipid and local anesthetic action at the nAChR.

To place this work in perspective, a brief review of both neurotransmission and the role of neurotransmitter receptors in this process will first be presented. This will be followed by a summary of our current understanding of the nAChR in terms of both its structural and functional architecture and its mechanism of action as well as an outline of the concepts and/or goals of the research presented in each subsequent chapter.

CHAPTER 1

INTRODUCTION

NEUROTRANSMISSION

The Neuron. Information in the form of both electrical and chemical signals is transmitted throughout the central and peripheral nervous systems via a complex network of specialized cells called neurons. Although wide variations in neuronal morphology exist, a typical neuron is composed of five functionally distinct regions: the *cell body*, *dendrites*, *axon hillock*, *axon* and *synaptic terminals* (Figure 1.1). The cell body contains the nucleus, mitochondria and other typical intracellular organelles and is primarily responsible for the metabolic activity of the neuron. The dendrites receive signals from either adjacent neurons or sensory stimuli and convey these signals through the cell body to the axon hillock. When specific conditions are met (see below), the axon hillock transforms these incoming signals into an action potential that is transmitted away from the cell body along the axon to the synaptic terminals. The synaptic terminals then communicate the action potential to adjacent neurons or effector cells through a process referred to as synaptic transmission.

Resting Membrane Potential. At rest, neurons maintain an imbalance of electrical charge across their plasma membrane referred to as the resting membrane potential (Figure 1.2). The resting membrane potential is established through the activity of three integral membrane proteins: the Na^+-K^+ ATPase and both Na^+ and K^+ leak channels. The Na^+-K^+ ATPase utilizes the energy of ATP hydrolysis to actively drive Na^+ ions out of, and K^+ ions into, the cell. This generates a large concentration gradient across the neuronal membrane for both cations. At the same time, K^+ ions diffuse down their concentration gradient through the K^+ leak channels. This efflux of K^+ leads to the

Figure 1.1 Schematic diagram of a typical neuron showing the location of the dendrites, cell body, axon hillock, axon and synaptic terminals. Also identified are the myelin sheaths and nodes of Ranvier, both of which facilitate the rapid conduction of action potentials along the axonal membrane. Modified from Kandel *et al.* (1).

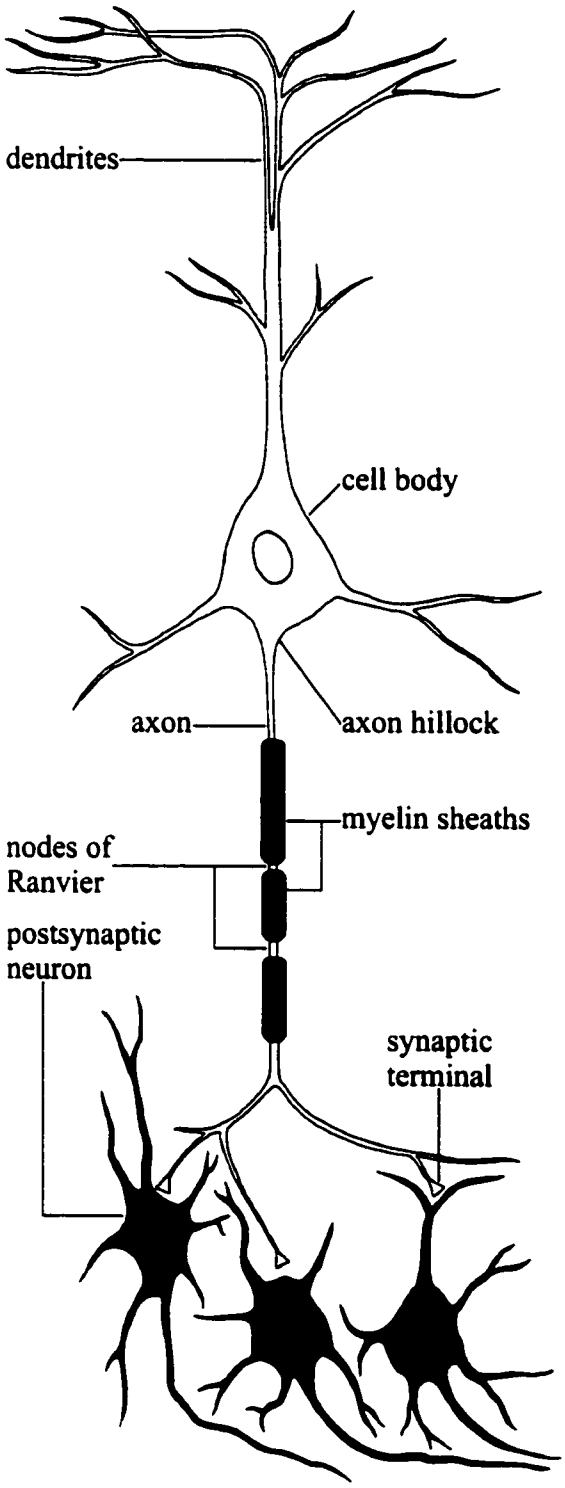
dendrites
cell body
axon
axon hillock
myelin sheaths
nodes of
Ranvier
postsynaptic
neuron
synaptic
terminal

Figure 1.2 Schematic diagram illustrating the cellular events involved in the formation of the neuronal resting membrane potential.

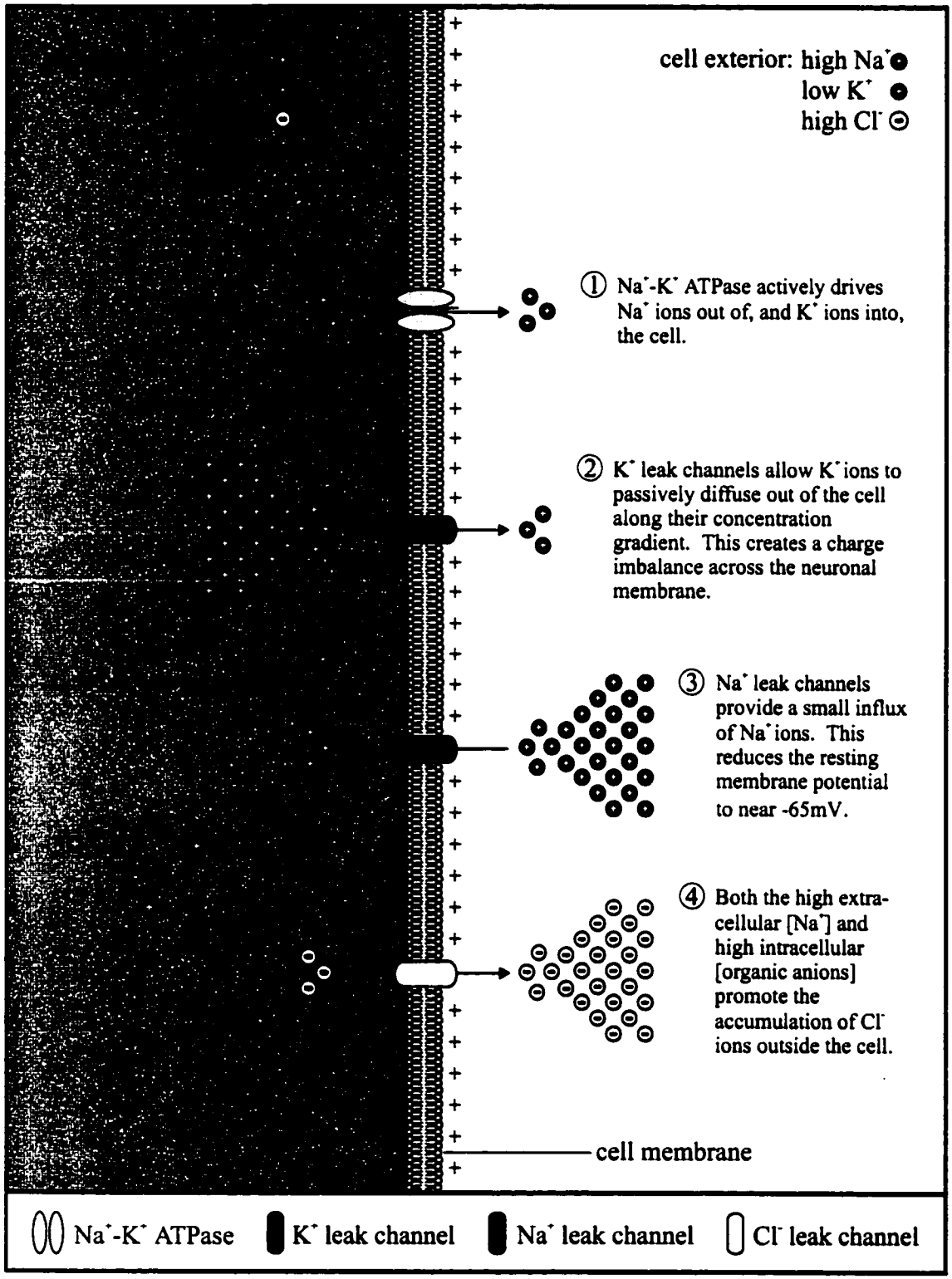
cell exterior: high Na+
low K+
high Cl-
① Na+-K+ ATPase actively drives Na+ ions out of, and K+ ions into, the cell.
② K+ leak channels allow K+ ions to passively diffuse out of the cell along their concentration gradient. This creates a charge imbalance across the neuronal membrane.
③ Na+ leak channels provide a small influx of Na+ ions. This reduces the resting membrane potential to near -65mV.
④ Both the high extracellular [Na+] and high intracellular [organic anions] promote the accumulation of Cl- ions outside the cell.
cell membrane
Na+-K+ ATPase
K+ leak channel
Na+ leak channel
Cl- leak channel

accumulation of unpaired negative and positive ions along the intracellular and extracellular sides of the cell membrane, respectively. The growing negative charge on the interior of the cell quickly counteracts the driving force of the K^+ concentration gradient, eventually ceasing the net flow of K^+ ions across the cell membrane. Although the Na^+ leak channels are few in number, they do provide the neuronal membrane with an appreciable permeability to Na^+ ions. This reduces the resting membrane potential of the neuron from near –75 mV, the equilibrium potential of K^+, to near –65 mV.

Note that Na^+ and K^+ are not the only ions with an uneven distribution across the resting neuronal membrane. Both the high extracellular concentration of Na^+ ions and the high intracellular concentration of organic anions act together to promote the accumulation of Cl^- ions outside of the cell. As will be seen in the following section, this Cl^- concentration gradient plays an important role in both the generation and integration of neuronal signals.

Signal Generation and Integration. All signals transmitted along a neuron are electrical in nature and result from transient changes in the electrical potential of the neuronal membrane. The initiation of an electrical signal occurs when a neuron is stimulated by either an adjacent nerve cell or an incoming sensory stimulus, such as light, temperature or pressure (Figure 1.3A). In either case, receptors located within the dendritic membrane respond by opening ion-specific transmembrane channels leading to an influx of either Na^+ or Cl^- ions down their respective concentration gradient. An influx of Na^+ ions reduces the neuronal membrane potential generating what is referred to as a depolarizing current. In contrast, an influx of Cl^- ions raises the neuronal membrane

Figure 1.3 Schematic diagram illustrating the cellular events involved in (**A**) the initiation and summation of electrical signals within the neuronal dendrites and (**B**) the propagation of an action potential along the neuronal axon.

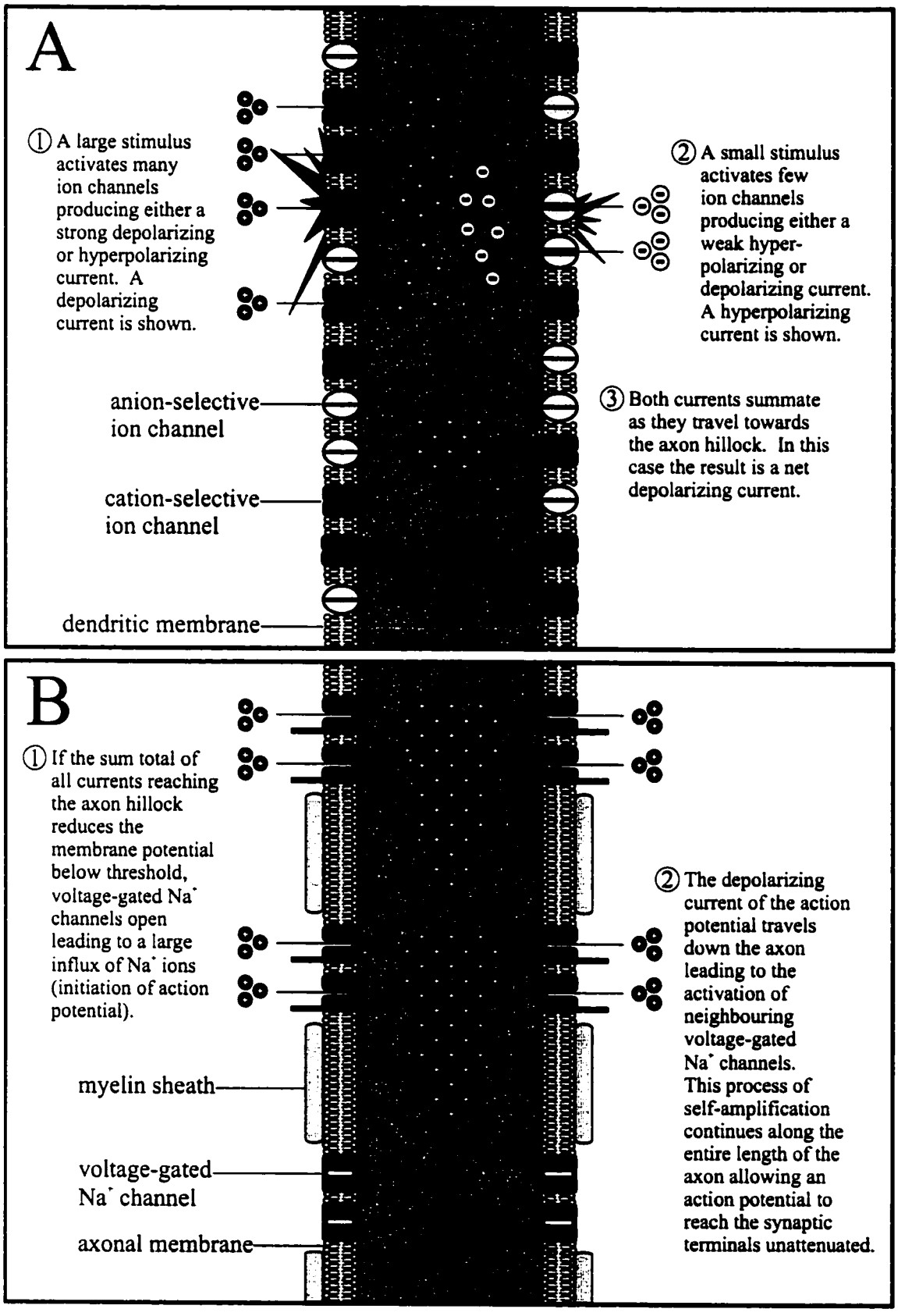
A
① A large stimulus activates many ion channels producing either a strong depolarizing or hyperpolarizing current. A depolarizing current is shown.
② A small stimulus activates few ion channels producing either a weak hyper-polarizing or depolarizing current. A hyperpolarizing current is shown.
③ Both currents summate as they travel towards the axon hillock. In this case the result is a net depolarizing current.
anion-selective ion channel
cation-selective ion channel
dendritic membrane
B
① If the sum total of all currents reaching the axon hillock reduces the membrane potential below threshold, voltage-gated Na⁺ channels open leading to a large influx of Na⁺ ions (initiation of action potential).
② The depolarizing current of the action potential travels down the axon leading to the activation of neighbouring voltage-gated Na⁺ channels. This process of self-amplification continues along the entire length of the axon allowing an action potential to reach the synaptic terminals unattenuated.
myelin sheath
voltage-gated Na⁺ channel
axonal membrane

potential generating what is referred to as a hyperpolarizing current. The magnitude of individual depolarizing or hyperpolarizing currents is directly proportional to the intensity and frequency of the stimulus from which they originate: weak and/or infrequent stimuli evoke small currents whereas strong and/or frequent stimuli evoke large currents. In addition, currents initiated at different sites along the dendrites summate, or integrate, as they travel along the plasma membrane towards the axon hillock. If the sum total of all depolarizing and hyperpolarizing currents reaching the axon hillock reduces the membrane potential below –55 mV, the threshold point, specialized voltage-gated ion channels open leading to the generation of an action potential. If, however, the sum total of all currents does not exceed threshold, the nerve remains silent.

Action Potential. An action potential consists of a wave of transient membrane depolarization that propagates along the neuronal axon (Figure 1.3B). When the membrane potential of the axon hillock is reduced below threshold, voltage-gated Na^+ channels open allowing Na^+ ions to flow into the cell along their concentration gradient. These Na^+ ions diffuse down the axon leading to the depolarization of the neuronal membrane at sites distal to the axon hillock and, consequently, the activation of neighboring voltage-gated Na^+ channels. This process of self-amplification occurs repetitively along the entire length of the axon allowing an action potential to reach the synaptic terminals unattenuated.

Shortly after an action potential is initiated, two factors combine to restore the axon's resting membrane potential. The first is the spontaneous closing of voltage-gated

Na^+ channels. The second is the concurrent activation of voltage-gated K^+ channels. The opening of K^+ channels allows K^+ ions to flow out of the cell along their concentration gradient thus driving the membrane potential back towards the K^+ equilibrium potential. Upon repolarization, the K^+ ion channels close allowing the membrane to regain its resting potential.

Synaptic Transmission. The communication of an action potential to either an adjacent neuron or effector cell occurs at cell-to-cell junctions called synapses and is thus referred to as synaptic transmission. Throughout the entire nervous system, two basic mechanisms of synaptic transmission are employed: electrical and chemical.

At electrical synapses, the distance between the presynaptic and postsynaptic membrane is small (~3.5 nm). In addition, special ion channels, called gap-junctions, link the presynaptic and postsynaptic cells providing a cytoplasmic continuity between the two cells. The high conductance of these gap-junctions permits the direct transfer of the action potential's depolarizing current from the presynaptic to the postsynaptic membrane. If the depolarizing current exceeds threshold, voltage-gated Na^+ channels open generating an action potential in the postsynaptic cell. Since the flow of depolarizing current can occur equally well from either the presynaptic to postsynaptic cell or vice versa, electrical synapses are often referred to as bi-directional.

The design of the electrical synapse provides certain functional advantages. First, signal transmission is extremely rapid, an important feature in responses that mediate escape from danger. Second, entire groups of neurons can be interconnected, thus allowing the electrical current flowing across the membrane of one cell to flow into and

out of all other electrically coupled cells. This enables a group of cells to fire synchronously, a property exploited, for example, in heart muscle contraction. Electrical synapses, however, do not readily allow inhibitory actions (hyperpolarizing currents) nor are they adaptable, thus limiting their functional capabilities.

At chemical synapses, there is no structural continuity between the presynaptic and postsynaptic cell (Figure 1.4). Instead, the cells are separated by a 20-40 nm space referred to as the *synaptic cleft*. As an action potential invades the presynaptic terminal, its depolarizing current activates voltage-gated Ca^{2+} channels allowing Ca^{2+} ions to flow across the presynaptic membrane and into the neuron. This increase in intracellular Ca^{2+} induces the fusion of neurotransmitter-containing vesicles with the presynaptic membrane and the consequent release of neurotransmitters into the synaptic cleft. Once released, the neurotransmitters diffuse across the synaptic cleft and bind to target neurotransmitter-gated ion channels located on the surface of the postsynaptic membrane. This interaction triggers the opening of the receptor's membrane-spanning ion channel resulting in an influx of ions and thus the generation of an electrical signal within the postsynaptic cell.

In contrast to electrical synapses, chemical synapses are more flexible and are amenable to complex regulation. As an example, chemical synapses often possess both cation- and anion-selective neurotransmitter receptors thereby allowing the generation of both inhibitory and excitatory (depolarizing) currents. In addition, both the number of neurotransmitter receptors and their efficiency of response can be modified permitting both short- and long-term changes in neuronal excitability. This property, referred to as

Figure 1.4 Schematic diagram illustrating the cellular events involved in chemical synaptic transmission. Modified from Schauf *et al.* (2)

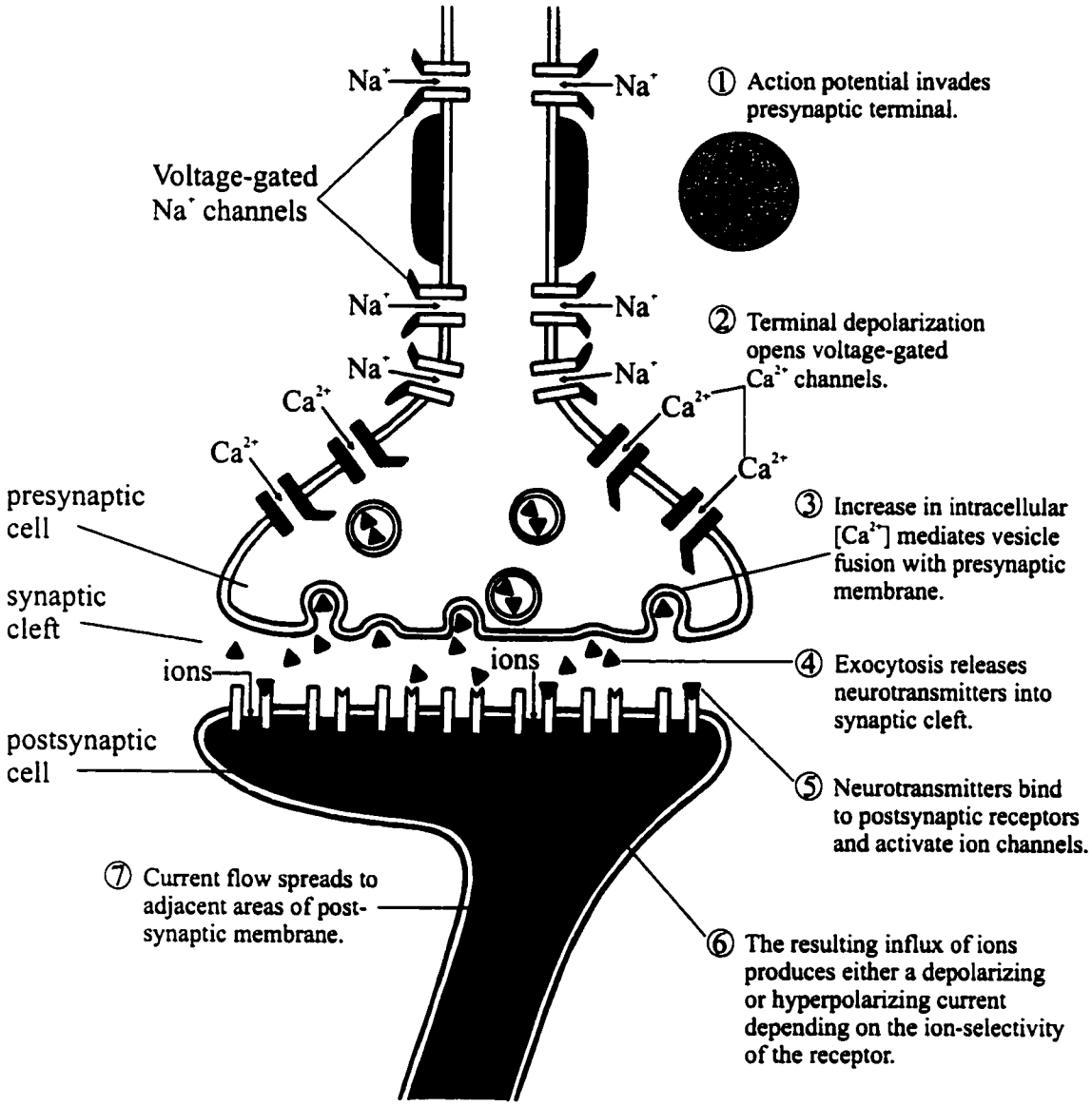
Na+
Na+
① Action potential invades presynaptic terminal.
Voltage-gated Na+ channels
Na+
Na+
Na+
Na+
② Terminal depolarization opens voltage-gated Ca2+ channels.
Ca2+
Ca2+
Ca2+
Ca2+
presynaptic cell
③ Increase in intracellular [Ca2+] mediates vesicle fusion with presynaptic membrane.
synaptic cleft
ions
ions
④ Exocytosis releases neurotransmitters into synaptic cleft.
postsynaptic cell
⑤ Neurotransmitters bind to postsynaptic receptors and activate ion channels.
⑦ Current flow spreads to adjacent areas of post-synaptic membrane.
⑥ The resulting influx of ions produces either a depolarizing or hyperpolarizing current depending on the ion-selectivity of the receptor.

synaptic plasticity, is believed to be central to higher brain functions such as memory and learning.

Clearly, neurotransmitter receptors perform an integral role in chemical synaptic transmission and ultimately in the mediation and modulation of electrical signals throughout the central and peripheral nervous systems. Insight into neurotransmitter receptor structure and mechanisms of activation and regulation is, therefore, essential in order to better understand the process of neurotransmission. Such knowledge should, in turn, lead to further advancement in our quest to unravel the functional complexity of the brain.

THE NICOTINIC ACETYLCHOLINE RECEPTOR

The nAChR is the most highly characterized member of a superfamily of genetically and structurally related neurotransmitter-gated ion channel receptors. Members of this family mediate the transfer of information throughout the central and peripheral nervous systems and include both the excitatory (cation-conducting) neuronal nAChRs, neuromuscular nAChRs and serotonin receptors and the inhibitory (anion-conducting) neuronal γ-aminobutyric acid (GABA) and glycine receptors. The excitatory neuronal glutamate receptor, although comprising both a neurotransmitter binding site and ion-conducting channel, differs in structure and thus may be distantly related.

The success of the nAChR as a model in the study of neurotransmitter-gated ion channel structure and function lies largely in its ability to be isolated in large quantities from the electroplaques of the electric ray *Torpedo* (*californica*, *marmorata* and

nobiliana) and the electric eel *Electrophorus*. The electrocytes that compose these electroplaques develop from muscle cells in the embryonic fish and their nAChRs are highly homologous in sequence and properties to those from mammalian neuromuscular junctions (3-5). Facilitating the identification, isolation, characterization and purification of electric organ nAChR has been the discovery of highly specific ligands, including small (7-8 kDa) protein α-neurotoxins from the venom of some Elapid snakes (*Bungarus multicinctus* and various *Naja* species). These α-neurotoxins, such as α-bungarotoxin (α-btx), compete with the nAChR's natural neurotransmitter, acetylcholine (ACh), and bind essentially irreversibly to the neurotransmitter binding site [dissociation constant (K_D) ~10^{-11} M].

Much of the driving force towards the elucidation of *Torpedo* nAChR structure and function has been two-fold. First, the significant sequence homology and architectural similarities observed between members of this superfamily suggest that the location of functionally important domains and mechanisms of activation, regulation and ion channel gating are likely to be similar within all members. This has led to the reasonable expectation that the information acquired from *Torpedo* nAChR will be relevant to the understanding of the structure and function of all members of the superfamily. Second, subtle variations in ligand binding properties, pharmacological sensitivity, ion channel function and regulatory characteristics, observed within subspecies of this superfamily, evokes the enticing possibility of identifying and/or designing novel pharmaceutical agents that could be targeted to specific receptors at

defined locations within the mammalian nervous system. This may, in turn, lead to the highly selective treatment of signaling disorders in the brain.

Structural Architecture

Subunit Composition, Sequence Homology and Quaternary Organization. The nAChR from *Torpedo* is a large, integral membrane protein (~290 000 Da) composed of five subunits arranged with quasi five-fold symmetry around a central ion pore that serves as the route of ion translocation across the postsynaptic membrane (Figure 1.5). Electron micrographs reveal that the receptor is ~125 Å long and ~80 Å in diameter at its widest point. Approximately 55% of the receptor's mass is found within the synaptic cleft, ~25% within the lipid bilayer and ~20% within the cytoplasm. The synaptic portion extends ~60 Å above the lipid headgroups of the postsynaptic membrane and the cytoplasmic portion extends ~20 Å below (7).

In *Torpedo*, the pentameric structure of the nAChR is created from four distinct gene products, designated α (52.4 kDa), β (56.2 kDa), γ (63.2 kDa), and δ (65.9 kDa), that assemble with a stoichiometry of $\alpha_2\beta\gamma\delta$ (8-10). A combination of anti-α subunit monoclonal antibody fragments and immunoelectron microscopy reveal that the two α subunits are not adjacent within the nAChR, but are in fact, separated by one subunit (11). The arrangement of the remaining subunits, however, is currently under debate. Immunoelectron microscopy and chemical cross-linking studies using nAChR from *Torpedo californica* and *marmorata* suggest the order αβαγδ as seen from the synaptic

Figure 1.5 Schematic diagram illustrating the quaternary organization of the nAChR. The nAChR is a large integral membrane protein composed of five subunits ($\alpha_2\beta\gamma\delta$) arranged with quasi five-fold symmetry around a central ion pore that serves as the route of ion translocation across the postsynaptic membrane. Each receptor pentamer contains two neurotransmitter binding sites, one on each of the two α subunits. Modified from Changeux (6).

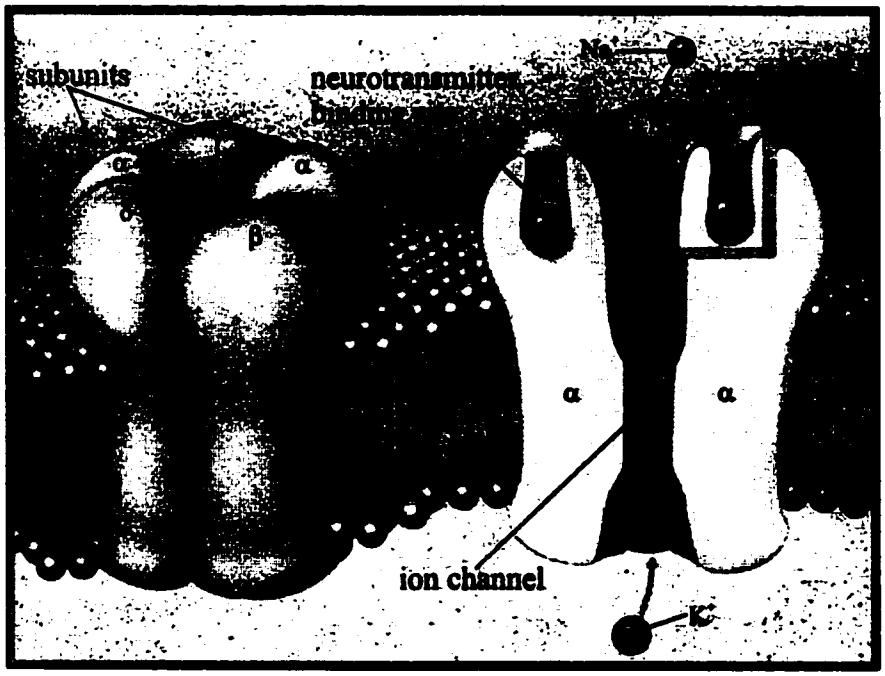
subunits
α
α
β
α
α
ion channel

cleft (12-14). In contrast, it has been proposed that the γ, rather than the β subunit, is located between the two α subunits (11).

Within mammalian muscle, the nAChR exists in two developmentally regulated isoforms. Embryonic muscle expresses nAChRs with a stoichiometry identical to that of *Torpedo* ($\alpha_2\beta\gamma\delta$), whereas in adults, the γ subunit is substituted by a homologous ε subunit to yield an $\alpha_2\beta\varepsilon\delta$ hetero-oligomer (15, 16). One additional isoform for each of the muscle α and β subunits has also been identified (17-19).

Unlike both *Torpedo* and muscular nAChRs, neuronal nAChRs are created from only two types of subunits, classified as either α or β according to their sequence homology with analogous subunits from muscle. To date, neuronal subunits designated α2-α9 and β2-β4 have been identified (20). In general, neuronal nAChRs have a stoichiometry of 2α3β, although the chicken α7 subunit and neuronal α subunits from *Drosophila* and locust can form functional homomeric nAChRs (21-25).

The nAChR subunits have been highly conserved throughout evolution as indicated by their high degree of sequence homology both between subunits and between species. Molecular cloning and protein sequencing of α, β, δ and γ subunits from *Torpedo* reveals ~19% sequence identity and ~54% homology between subunits (10, 26-31). The different muscle nAChR subunits share ~31 to 49% sequence homology whereas for neuronal nAChR subunits this value is between ~37 and 68%. Corresponding subunits from *Torpedo* and mammalian muscle nAChR share ~60-70% sequence homology.

Transmembrane Topology of the nAChR Subunits. Primary sequence analysis of individual nAChR subunits of *Torpedo*, muscle and neuronal origin reveals significant sequence homology as well as similar hydrophobicity profiles justifying a common subdivision of each subunit into three distinct structural domains (Figure 1.6). The first is a large hydrophilic amino-terminal domain comprising 210-224 amino acid residues found oriented towards the synaptic cleft. This orientation is supported by (a) the presence of a processed signal peptide of varying length in all subunits, indicating that the mature amino-terminus is extracellular, (b) the presence of asparagine-linked glycosylation sites, and (c) the location of residues within this region of the α subunit identified as being in or near the ACh binding site (26-28, 30-34).

The second is a hydrophobic domain consisting of ~90 residues that can be further subdivided into four segments designated M1 (27 residues), M2 (20 residues), M3 (20 residues) and M4 (19 residues). These hydrophobic segments display the highest sequence homology both between subunits and between species and are thought to represent four transmembrane α-helices (28, 30, 31). As α-helices, these segments would vary between 29.5 and 40.5 Å in length, a distance sufficient to span the ~32 Å thick hydrophobic portion of the lipid bilayer (35, 36). FTIR secondary structural analyses and covalent modification and chemical labeling studies all support each segment adopting a largely α-helical conformation (37-45). In contrast, high resolution electron micrographs of the nAChR from *Torpedo* suggest that only the ion channel-lining segment, M2, is α-helical and that segments M1, M3, and M4 form transmembrane β-strands (7).

Figure 1.6 Schematic diagram illustrating the transmembrane topology of the nAChR subunits. Each subunit contains (i) a large hydrophilic amino-terminal domain oriented towards the synaptic cleft, (ii) four hydrophobic segments designated M1-M4 that span the lipid bilayer as α-helices, and (iii) a small hydrophilic domain between segments M3 and M4 oriented towards the cytoplasm. The M2 segment from each of the five subunits is believed to form the lining of the ion channel. Modified from Changeux (6).

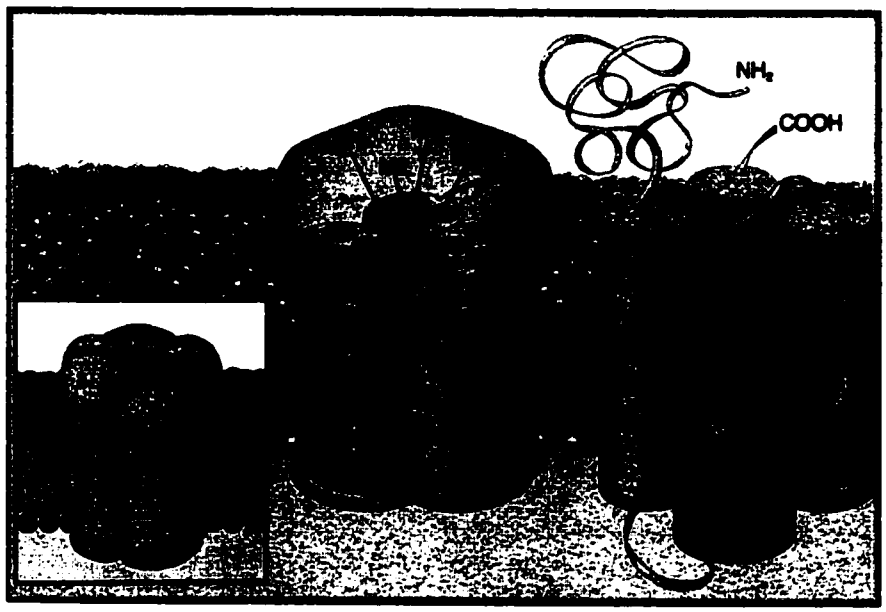
NH_2
COOH

The third is a small intracellular hydrophilic domain located between segments M3 and M4 (in *Torpedo*, comprising 109-142 amino acid residues). This region shows substantial diversity both between subunits and between species and is generally much larger in neuronal subunits. The location of this domain within the cytoplasm is supported by several studies using sequence-specific antibodies as well as by the identification of characteristic serine and tyrosine residues that are known sites of phosphorylation (46-51).

Functional Architecture

Neurotransmitter (ACh/Agonist/Competitive Antagonist) Binding Sites. Initial studies employing the use of radioactively labeled α-btx and various affinity labeling reagents established the presence of two ACh binding sites per receptor molecule, one on each of the two α subunits (Figure 1.5) (52-58). Both fluorescent energy transfer experiments and electron microscopy estimate these sites to be ~30 Å above the membrane surface and ~50 Å from the ion channel gate (59-61).

Sulfhydryl-directed labels suggest that two adjacent cysteine residues (αCys192 and αCys193) are located within the region that contributes to agonist binding (Figure 1.7B) (62). These cysteines form a disulphide bond in the native receptor and are found only within α subunits (63). Additional labeling compounds have identified several other residues including αTyr93, αTrp149, αTyr190 and αTyr198 (64-67). Significantly, these four residues, along with αCys192 and αCys193, are conserved at homologous positions in all α subunits from all species examined to date, consistent with their

Figure 1.7 Early (**A**) and current (**B**) models of the neurotransmitter binding sites of the nAChR. Each site consists primarily of amino acid residues residing in the large amino-terminal region of the α subunit. (A) Initial studies focusing on the physical properties of ACh proposed that the neurotransmitter binding sites consisted of both an anionic and esterophilic subsite that were responsible for interactions with ACh's quaternary ammonium and ester group, respectively. In the case of the anionic subsite, it was assumed to contain one or more aspartic and/or glutamic acid residues that could interact with the positive charge of the quaternary ammonium group through the formation of one or more salt bridges. More recent studies, however, have shown that the neurotransmitter binding sites consist primarily of aromatic residues that have been highly conserved throughout evolution (B). Those residues identified as being in or near the neurotransmitter binding site are shown (numbers refer to their position within the primary sequence of the α subunit from *Torpedo*). Amino acid residues from neighboring δ and γ subunits are also believed to contribute to agonist/competitive antagonist binding (identified as *x*). Modified from Changeux (6).

A

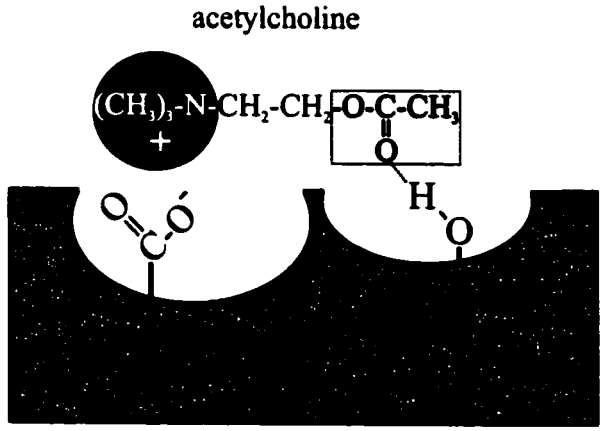

Neurotransmitter Binding Site

B

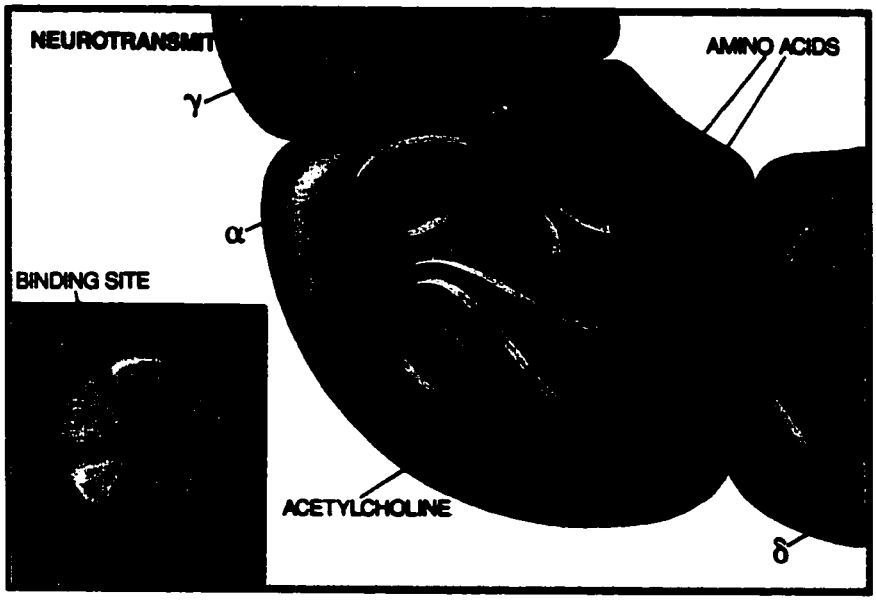

importance in agonist binding. The only exception is the neuronal α5 subunit, which does not contain amino acids homologous to αTyr93 and αTyr190 and does not form functional receptors when expressed in *Xenopus* oocytes (68). The contribution of each of these residues to agonist binding has also been confirmed by site directed mutagenesis (69-74)

A somewhat surprising observation from the above studies is the predominant role of aromatic residues in ACh binding. Early studies focusing on the physical properties of ACh proposed that the ACh binding site consisted of both an anionic and esterophilic subsite (Figure 1.7A). The anionic subsite was thought to interact with ACh's positively charged quaternary ammonium group while the esterophilic subsite was thought to interact with its highly polar ester group. In the case of the anionic subsite, it was assumed to contain one or more carboxylate anions, such as the side chains of aspartic and/or glutamic acids, that could stabilize ACh's quaternary ammonium group through the formation of one or more salt bridges. The recent work of Dougherty and Stauffer (75), however, has shown that a synthetic receptor composed primarily of aromatic residues is able to bind ACh with a dissociation constant similar to that of the nAChR and that this binding occurs through a stabilizing interaction between the aromatic π-electrons and ACh's positively charged quaternary ammonium group. The high resolution structures of acetylcholinesterase and of an anti-phosphocholine antibody also suggest the importance of aromatic residues in the binding of quaternary ammonium groups (76-78).

Although two ACh binding sites exist per nAChR, they are non-equivalent. Equilibrium binding curves indicate two distinct affinities for the competitive antagonist *d*-tubocurarine while the affinity reagents 4-(N-maleimido)-benzyltrimethyl-ammonium and bromoacetylcholine attach to both sites with different affinities (79-84). In addition, the expression of various subunit combinations indicates that the coexpression of either the γ or δ subunit with the α subunit is required for specific agonist binding (85). This has led to the proposal that the ACh binding sites are located at the α-γ and α-δ interfaces and that the different affinities of each site for agonists and antagonists is due to the different pairs of subunits that form the two sites (79, 81, 82, 86-90).

An alternative explanation for the disparate affinities of the two ACh binding sites arises from the electron micrographs of Unwin (60). At a resolution of 7.5 Å, each ACh binding site appears as a cavity encircled by three short α-helices oriented approximately normal to the membrane plane. Located near, but not at the α-δ and α-γ interfaces, these cavities differ in both size and shape. It is conceivable then that the different affinities displayed by the two ACh sites originates from the non-equivalent conformations of the cavity-lining α-helices. To accommodate the apparent role of the δ and γ subunits in agonist binding, it is possible that these neighboring subunits are involved in shaping these cavities as well as affecting access to them. With the entrance to the cavities being located presumably at the α-δ and α-γ interfaces, side chains from neighboring δ and γ subunits may extend close to, or into, these openings where they could interact with agonists and competitive antagonists as they travel towards the ACh binding sites. Such

a possibility would seem compatible both with the chemical labeling and site-directed mutagenesis data.

The Ion Channel. The ion channel of the nAChR is formed primarily from the M2 segment from each of its five subunits. Reagents that penetrate and block the ion channel label residues within this segment while the mutation of various M2 residues alters the ion-conductance properties of nAChRs expressed in *Xenopus* oocytes (91-96). Synthetic peptides corresponding to the M2 sequence are also capable of forming cation-conducting channels upon insertion into lipid bilayers (97).

The high resolution electron micrographs from Unwin (7) suggest that each M2 segment assumes a predominantly α-helical secondary structure and that together, these five helices arrange quasi-symmetrically around the central axis of the receptor to form the walls of the ion channel (Figure 1.6). These helices, however, do not traverse the lipid bilayer as uniform rods, but are in fact bent, or 'kinked', inwards near the middle of the bilayer. This kink results in a constriction in the circumference of the ion channel that is assumed to represent the location of the ion channel gate. In the closed conformation, this gate creates an impenetrable barrier to ions.

The similarity of the M2 sequences from different subunits and different species, coupled with the observation that the mutation of M2 residues at homologous positions in different subunits results in similar functional consequences, has lead to the proposal that aligned residues within the M2 segment of each subunit form a number of rings around the channel that play an important role in ion-conductance (Figure 1.8):

Figure 1.8 Schematic diagram illustrating the quaternary organization of the channel-lining M2 segments as well as the proposed alignment of M2 residues within the ion channel pore. The ion channel is formed from five α-helical M2 segments, one from each subunit, that arrange quasi-symmetrically around the central axis of the receptor (see inset; also Figure 1.6). Homologous residues located at equivalent M2 positions on each subunit are thought to form several rings around the channel that perform an important role in ion conductance (see text for details). Identified (from top to bottom): the outer charged ring, the leucine ring, the intermediate ring and the inner charged ring. Modified from Changeux (6).

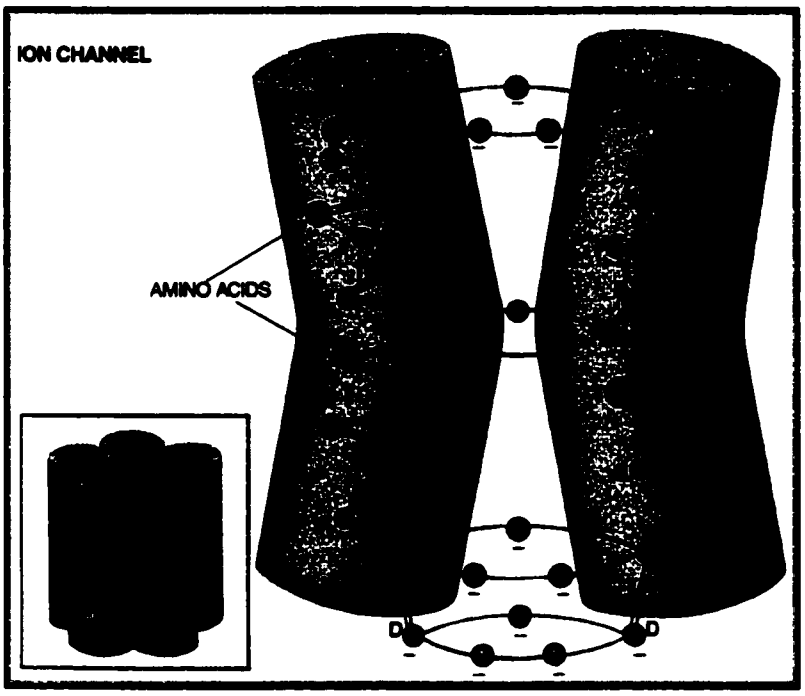
ION CHANNEL
AMINO ACIDS

The Inner and Outer Charged Rings. Located at the intracellular and extracellular entrances to the channel, respectively, these rings are comprised largely of negatively charged aspartic and/or glutamic acid residues. Initially, these rings were proposed to contribute to the ion-selectivity of the nAChR channel since their mutation moderately influenced cation-conductance (95). Their role in ion-selectivity, however, is currently in question since the inner ring of anion-conducting members of the neurotransmitter-gated ion channel superfamily is also negative. In addition, a negatively charged reagent has been shown to have access to the extracellular portion of the cation-conducting ion channel of the nAChR while a positively charged reagent is capable of accessing the extracellular portion of the anion-conducting channel of the $GABA_A$ receptor (44, 98, 99).

The Intermediate Ring. Located one helical turn up from the inner ring, this ring has a net negative charge in the cation-conducting nAChR, but is uncharged in the anion-conducting $GABA_A$ and glycine receptors. Although changes in the net charge of this ring produce the most significant effects on cation-conductance in the nAChR, recent work has shown that the intermediate ring is not the sole determinant of ion-selectivity (95, 100, 101).

The Serine and Threonine Rings. Located one and two helical turns up from the intermediate ring, respectively, these rings are highly conserved in almost all nAChR subunits sequenced to date. In the GABA and glycine receptors, only a threonine ring is present at a location analogous to that of the serine ring in nAChRs. These rings have

been proposed to perform a fundamental role in the process of ion-permeation by contributing to the exchange of water molecules surrounding transported ions (70).

The Leucine Ring. Located one helical turn up from the threonine ring, this ring is conserved in all known subunits of the nAChR, glycine and GABA receptors. It has been postulated that this ring represents the gate of the ion channel and that in the closed conformation, the aligned leucines from each subunit interdigitate to sterically block the transport of ions (7, 102). The mechanism of channel gating, however, appears to be more complicated than simple steric hindrance since the mutation of these leucines to serine in the homooligomer α7 nAChR does not prohibit channel gating (103).

The role of the M2 segment in the formation of both the ion channel and its gating mechanism, however, is not absolute. A number of residues towards the extracellular end of the M1 segment of the nAChR α subunit have also been shown to be exposed to the channel lumen (104, 105). In addition, the M1 segment contains a conserved proline-cysteine pair near the centre of M1 that has been suggested to perform a role in channel conductance. When located within an α-helix, proline's inability to form hydrogen bonds results in a localized disruption of secondary structure. This disruption may provide the M1 segment with the flexibility necessary to allow the M2 helices to adopt the different orientations required for the formation of the channel's distinct functional states (106).

Mechanisms of Function

Functional States of the Nicotinic Acetylcholine Receptor. Although the exact number of distinct conformational states of the nAChR is currently under investigation, there is sufficient evidence for the presence of at least three: *resting*, *open* and *desensitized* (Figure 1.9) (107-113). Fluorescence studies employing the conformationally sensitive probe dansyl-C_6-choline as well as [^{3}H]-ACh binding assays indicate that within its native membrane, the nAChR exists within a conformational equilibrium between a channel-competent resting (~80%) and channel-inactive desensitized state (~20%) (114). The binding of ACh to the resting state induces a conformational change in the receptor to the open state resulting in the translocation of ~10^4 Na^+ ions/msec across the postsynaptic membrane (115). This open state, however, is transient, lasting for only ~1 msec and thus has been difficult to study from both a structural and biochemical perspective. Prolonged or repeated exposure to ACh initiates a further conformational change in the nAChR to the desensitized state. This state is characterized by both its inability to conduct cations, even though ACh remains bound, and an approximate 1000-fold increase in ACh affinity (107, 114, 116). Since the desensitized state is stable for the duration of ACh exposure, it has become the primary focus of extensive structural and biochemical analyses.

Acetylcholine-Induced Structural Changes: Channel Activation. In order to induce channel activation, one molecule of ACh must bind to each of the nAChR's two ACh binding sites. The location of these sites within the extracellular domain of the α subunit, a distance of ~50 Å from the ion channel gate, imparts the requirement that the

Figure 1.9 Schematic diagram illustrating the known conformational states of the nAChR. In the absence of agonist, the nAChR exists within a conformational equilibrium between a channel-competent resting and channel-inactive desensitized state. The binding of agonist to the resting state induces a conformational change in the receptor to an open state. In this state, cations are free to diffuse across the postsynaptic membrane through the receptor's membrane-spanning ion channel. Upon prolonged or repeated exposure to agonist, the nAChR undergoes a further conformational change to the desensitized state. This state is characterized by both its inability to conduct cations, even though agonist remains bound, and an approximate 1000-fold increase in ACh affinity.

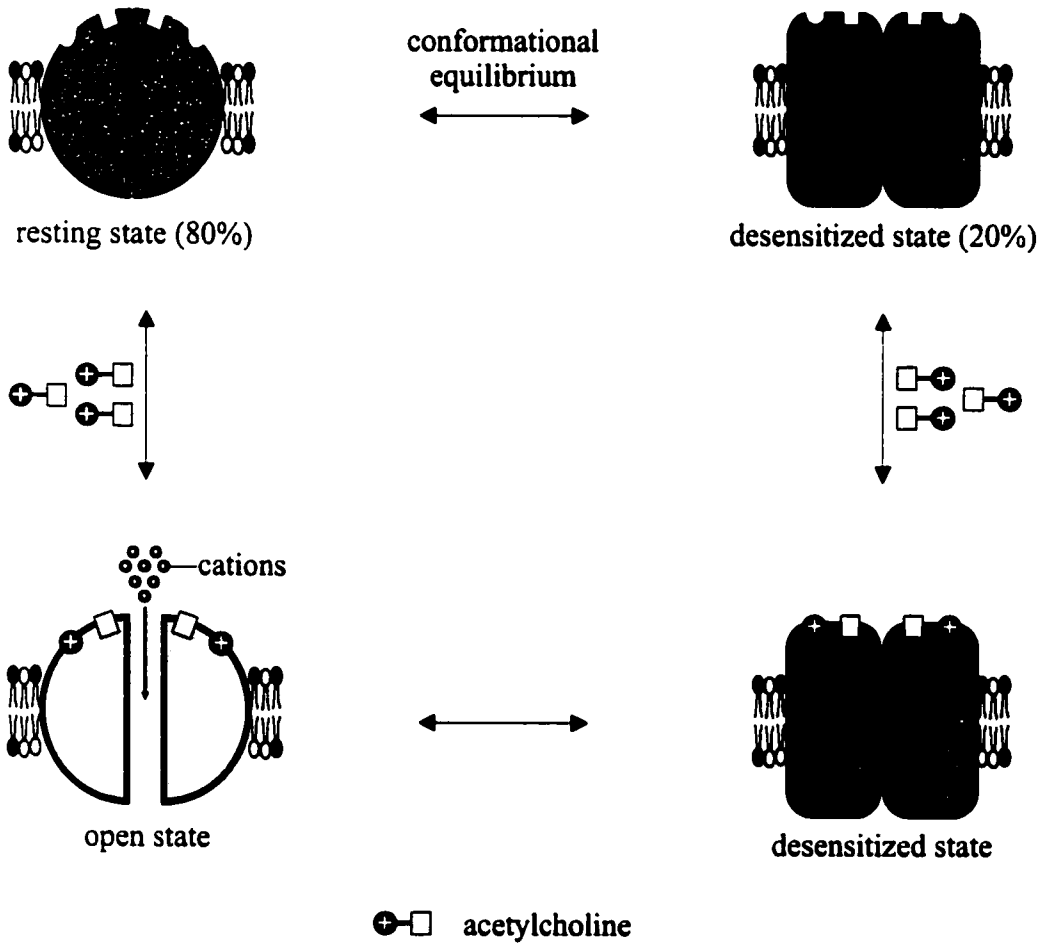
conformational
equilibrium
resting state (80%)
desensitized state (20%)
cations
open state
desensitized state
acetylcholine

opening of the ion channel occur through a propagated conformational change originating within the ACh binding site. Electron microscopic studies of the nAChR in both the resting and open states indicate that the binding of ACh triggers distinct localized disturbances in the three α-helical segments that comprise each ACh binding site (102). These disturbances appear to arise through a concerted twisting of the helices that are communicated to the transmembrane domain through small rotations of the subunits. These rotations, in turn, draw the gate-forming side chains of the leucine ring away from the center of the pore, thus removing the barrier to ion flow (60, 102, 117).

Acetylcholine-Induced Structural Changes: Desensitization. The structural changes that occur in the nAChR upon transition from the resting to the desensitized state have also been investigated by electron microscopy (118). A comparison of the three-dimensional structures of the nAChR in the absence (predominantly resting state) and presence (desensitized state) of ACh reveal small but significant changes in the quaternary arrangement of the receptor subunits. These changes, generated through both an ~10° tilt in the δ subunit tangential to the receptor axis and a slight displacement of the γ subunit radially outward, result in a less symmetrical arrangement of the subunits around the central ion channel.

Supporting the apparent structural role of the δ subunit in desensitization are a number of kinetic studies that show that the rate of nAChR desensitization is influenced by the degree of phosphorylation of the δ subunit (119, 120). In addition, the importance of the γ subunit in desensitization is corroborated by the labeling patterns of several non-competitive antagonists that bind to a distinct non-competitive blocker site located within

the ion channel pore. As an example, triphenylmethylphosphonium displays a reduced affinity for the γ subunit in the desensitized state while the rate of chlorpromazine incorporation into the γ subunit is significantly reduced. The displacement of the γ subunit away from the axis of the channel upon desensitization is consistent with these results.

The quaternary re-organization of the δ and γ subunits, however, is not the sole structural distinction that has been identified between the resting and desensitized states. Photo-labeling experiments employing the affinity probe p-(N,N-dimethyl)amino-benzenediazonium (DDF) indicate that the structure of the ACh binding sites is also altered during the resting to desensitized conformational transition (70). Stabilization of the nAChR in the desensitized state reveals an ~6-fold increase in the incorporation of DDF into the ACh binding site residues αTyr93 and αTrp149. These results suggest that the increased affinity displayed by the nAChR in the desensitized state is in part due to a localized structural change in the ACh binding sites that brings αTyr93 and αTrp149 closer to the bound agonist, thus strengthening their association.

CONCLUSIONS

Since 1906 when the British scientist T.R. Elliot first proposed that neurons communicate with one another and effector cells through chemical messengers, considerable progress has been made regarding our understanding of the molecular details surrounding chemical synaptic transmission and the role of neurotransmitter

receptors within this process. In the case of neurotransmitter receptors, much of our current understanding can be attributed to studies of the nAChR from electric fish organ, which has provided an accessible model for both structural and biochemical analyses.

Unfortunately, further insight into both neurotransmitter receptor structure/function and mechanisms of activation/desensitization have been hindered by the difficulties associated with the application of conventional high resolution structure elucidating techniques to the study of large integral membrane proteins, such as the nAChR. As a result, our laboratory has adapted the novel technique of FTIR difference spectroscopy and applied it to probe the structural and functional consequences of Carb binding to the nAChR. FTIR difference spectroscopy exists as one of the few techniques capable of abstracting detailed structural information from large integral membrane proteins by providing insight into the molecular vibrations of individual amino acid residues, which are extremely sensitive to changes in molecular structure and local environment.

As noted, the original objective of this research was to employ the FTIR difference technique to probe the nature of the physical interactions formed between Carb and neurotransmitter binding site residues in the hope that this information would lead to a greater understanding of how neurotransmitter binding elicits both channel activation and receptor desensitization. Based on preliminary results, however, the focus of this research was redirected towards unravelling the structural and functional consequences of both lipid and local anesthetic action at the nAChR. The results have lead to important new insight into the mechanisms by which both lipids and local anesthetics modulate

nAChR activity and reveal a conformational diversity of the nAChR that could play an important role in higher brain functions, such as memory and learning.

ORGANIZATION OF THESIS

Chapter 2 presents a brief review of the theory of vibrational spectroscopy, the acquisition of protein spectra using FTIR-ATR spectroscopy as well as the FTIR difference technique and its application to the study of the nAChR.

Chapter 3 focuses on the effects of both neutral and anionic lipids on the structure of the nAChR while Chapter 4 focuses on the specific structural requirement of the receptor for both cholesterol and dioleoylphosphatidic acid. The results have been interpreted in terms of a speculative model that suggests diverse lipid structures modulate nAChR structure and function through an indirect effect on some physical property of the lipid membrane, possibly bulk fluidity. The model also proposes that anionic lipids, in addition to proper membrane fluidity, are required to stabilize a fully functional nAChR.

Chapters 5 and 6 focus on the structural consequences of local anesthetic binding to the nAChR. The results reveal that the nAChR is capable of adopting a novel intermediate conformation that is structurally distinct from both the resting and desensitized states and suggest a revised model of local anesthetic action at the nAChR.

CHAPTER 2

FOURIER TRANSFORM INFRARED SPECTROSCOPY

INTRODUCTION

One of the greatest challenges facing structural biochemistry involves unravelling the intricate relationship that exists between protein structure and function. Included in this is an understanding of how various endogenous and exogenous factors exploit this relationship in order to exert their effects on protein activity. For the most part, accomplishing this task has necessitated the use of either x-ray crystallography or NMR spectroscopy, both of which are capable of providing protein structures at or near atomic resolution. Unfortunately, neither technique can be readily applied to the study of large integral membrane proteins, such as the nAChR.

With x-ray crystallography, the prerequisite high-quality protein crystals present a significant obstacle when dealing with integral membrane proteins. In addition, the conditions necessary to generate these crystals do not always mimic those of the protein's native environment, giving rise to concerns regarding the effect this may have on protein structure. Difficulties can also arise when attempting to translate the relatively 'static' structure of a protein crystal into the often dynamic and complex functional properties of a protein in solution.

NMR spectroscopy, on the other hand, provides a reasonable alternative to x-ray crystallography by allowing the structure of most proteins to be determined within their native environment. NMR spectroscopy, however, is currently restricted to proteins of less than ~40 kDa since larger molecular weight proteins generate complex spectra that make the interpretation and assignment of inter-proton distances infeasible. NMR

spectroscopy also can not be readily applied to the study of proteins within a membrane environment due to line-broadening effects associated with their motional restriction.

In light of these inherent limitations, considerable effort has been made towards the development and/or improvement of so-called 'low-resolution' spectroscopic methods that are capable of providing global insight into protein structure without being able to establish the precise three-dimensional location of individual structural elements. One such method that has emerged as an extremely useful tool is infrared spectroscopy. Infrared spectroscopy is a well established technique that provides information on protein structure through the frequency of its molecular vibrations, which are extremely sensitive to chemical structure, conformation and local environment. The most significant advantages of infrared spectroscopy are its flexibility and broad applicability. Infrared spectroscopy is not limited by the size of a protein or the nature of its environment. In fact, infrared spectroscopy exists as one of the few techniques capable of providing detailed structural information on large integral membrane proteins.

The correlation between the frequency of protein vibrational bands and protein structure was established early in the pioneering work of Elliot and Ambrose (121). Interest in infrared spectroscopy for studying protein structure, however, began to decrease due to the difficulties associated with both the acquisition of spectra and the extraction of the information contained within. These difficulties were largely a consequence of the low sensitivity of conventional dispersive infrared spectrometers that produced spectra with relatively low signal-to-noise ratios.

With the inception of FTIR spectrometers came a renewed interest in the application of infrared spectroscopy to protein conformational studies. FTIR spectrometers replaced the monochromator used in dispersive instruments with the Michelson interferometer. This, coupled with the development of microcomputers that allowed for the easy application of the fast Fourier transform algorithm, enabled protein spectra to be acquired much faster, with greater wavenumber precision and with far superior signal-to-noise ratios. The higher energy throughput of FTIR spectrometers also encouraged the use of infrared sampling techniques other than transmission, such as attenuated total reflectance (ATR). This enabled significant reductions in both the sample size and the difficulties associated with subtracting the overlapping absorption of water, the physiological medium in which proteins are dissolved.

Both the precision of FTIR spectrometers and the digitization of the data have also allowed for the reliable subtraction of spectra, a property exploited in FTIR difference spectroscopy. FTIR difference spectroscopy is an extremely effective technique for probing the molecular differences that exist between a protein's distinct conformational states and has already been successful in providing a detailed picture of the structural changes and proton movements during the photocycle of bacteriorhodopsin and other light activated proteins (122-126). In our laboratory, we have adapted this novel technique and applied it to the study of the nAChR to gain insight into the structural changes that occur in individual amino acid residues upon Carb binding and subsequent transition from the resting to the desensitized state (127-129). The objective of this chapter is to present a brief review of the theory of vibrational spectroscopy, the

acquisition of protein spectra using FTIR-ATR spectroscopy as well as the FTIR difference technique and its application to the study of the nAChR.

VIBRATIONAL SPECTROSCOPY

Molecular Vibrations. Infrared spectroscopy provides insight into molecular structure through the frequencies of a molecule's normal modes of vibration. A normal mode of vibration is one in which each atom executes a simple harmonic oscillation about its equilibrium position, such that a plot of each atom's nuclear displacement as a function of time yields a sinusoidal or cosinusoidal wave (Figure 2.1A). Although the relative amplitude and direction of each atom's displacement may be different, all atoms move in phase with the same frequency while the molecule's center of gravity remains constant.

For a linear polyatomic molecule, it can be shown that the number of independent normal modes of vibration is equal to 3N–5, where *N* represents the number of atoms in the molecule. If the molecule is non-linear, this number is reduced to 3N–6. In general, each normal mode of vibration can be classified as either *stretching* or *bending*, depending on the effect of the vibration on the molecule's chemical bonds. Stretching vibrations induce either symmetric or antisymmetric changes in bond length whereas bending vibrations induce either in-plane or out-of-plane changes in bond angle (Figure 2.1B).

Vibrational Energy. According to quantum mechanics, each of a molecule's normal modes of vibration can possess only one of a set of discrete amounts (or quanta)

Figure 2.1 Schematic diagram illustrating (**A**) a diatomic molecule executing a simple harmonic oscillation and (**B**) several independent modes of vibration of both a linear (i) and non-linear (ii) polyatomic molecule. (A) By definition, a simple harmonic oscillation is one in which each of a molecule's atoms move in phase with the same frequency while the molecule's center of gravity remains constant. A plot of each atom's nuclear displacement as a function of time yields a sinusoidal wave whose amplitude is proportional to the magnitude of each atom's displacement from equilibrium. (B) In general, each of a molecule's normal modes of vibration can be classified as either stretching (change in bond length) or bending (change in bond angle). Arrows indicate the movement of atoms along the plane of the page while positive (+) and negative (-) signs indicate the movement of atoms into or out of the page, respectively.

A

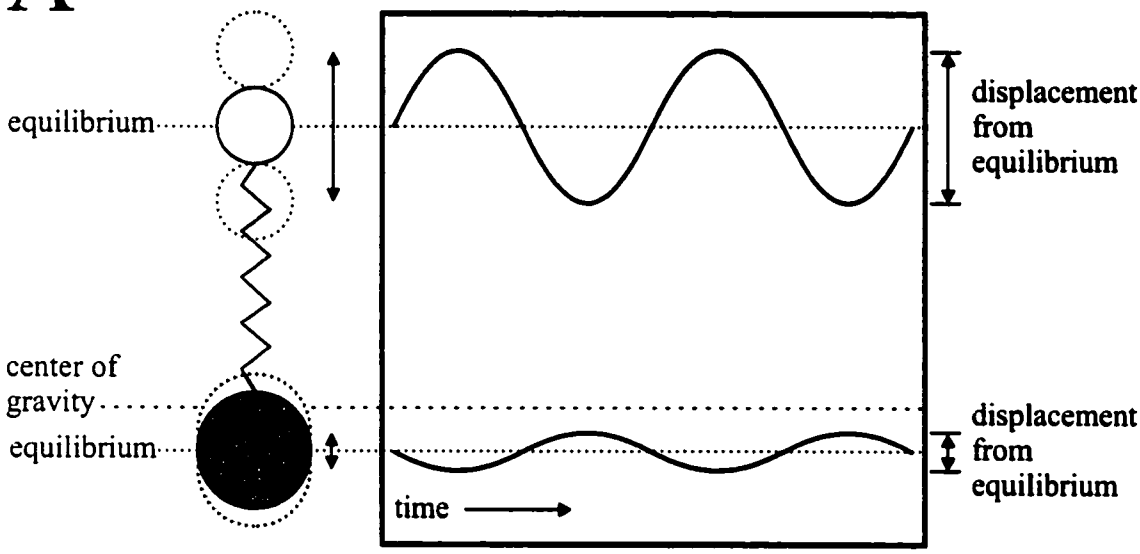
equilibrium
center of gravity
equilibrium
displacement from equilibrium
displacement from equilibrium
time

B

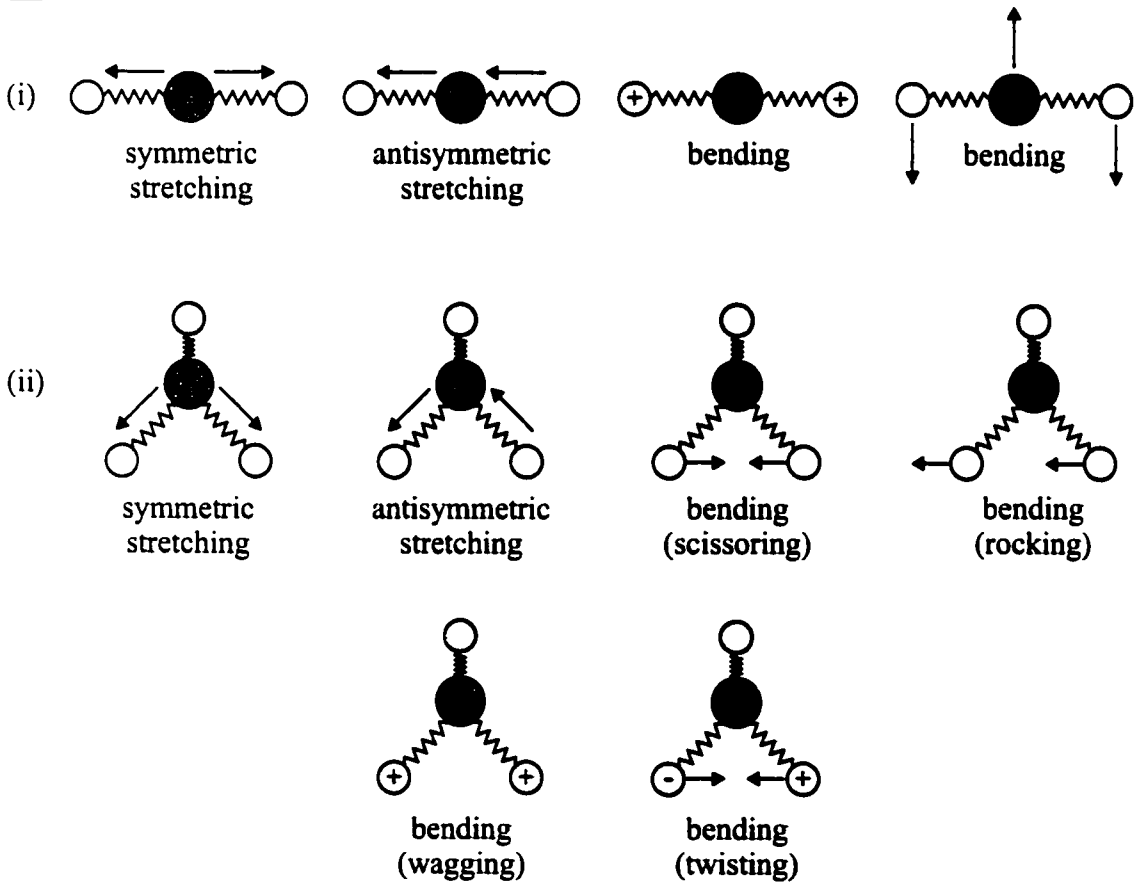
(i)
symmetric stretching
antisymmetric stretching
bending
bending
(ii)
symmetric stretching
antisymmetric stretching
bending (scissoring)
bending (rocking)
bending (wagging)
bending (twisting)

of energy, referred to as vibrational levels. The energy of each of these levels (E_v) is given by:

$$E_v = (n + \tfrac{1}{2})hf_v \qquad \text{(equation 2.1)}$$

where h is Planck's constant, f_v is the frequency of the normal mode of vibration and n is the vibrational quantum number, which can only have integer values (i.e. 0, 1, 2, 3...). From equation 2.1 it is evident that the energy difference between each vibrational level is equal to hf_v. In addition, even the lowest possible vibrational level, which occurs when $n=0$ (referred to as the ground state), retains vibrational energy equal to $\frac{1}{2}hf_v$. This is in accordance with Heisenberg's uncertainty principle, which states that both the position and momentum of a particle (i.e. an atom) can not be simultaneously known.

Vibrational Energy Transitions. Transitions between vibrational levels are induced when a molecule absorbs radiation in the infrared region of the electromagnetic spectrum. However, for a molecule to increase its vibrational energy, two conditions must be met. First, a transition can only occur if during a molecule's normal mode of vibration, its dipole moment is altered. In the case of a diatomic molecule possessing one atom with a net positive charge and one atom with an equivalent net negative charge, the dipole moment (μ) is defined as:

$$\mu = Qr \qquad \text{(equation 2.2)}$$

where Q is the magnitude of either charge and r is the distance between the two charges. For the transition from the ground state ($n=0$) to the first excited vibrational level ($n=1$), it can be shown that the probability (P) of this event is defined by:

$$P = \frac{\pi}{3hf_v M_{red}} \left(\frac{\partial \mu}{\partial q} \right)^2 \qquad \text{(equation 2.3)}$$

where q is a measure of the change in the charge separation that occurs during the transition and M_{red} is the reduced mass of the two atoms (m_1 and m_2) given by:

$$M_{red} = \frac{m_1 m_2}{m_1 + m_2} \qquad \text{(equation 2.4)}$$

From equation 2.3, it is clear that if the dipole moment does not change during a vibration, the value $\partial\mu/\partial q$ is zero and thus the probability of this transition is also zero. Such a vibration in which there is no change in dipole moment is often referred to as infrared inactive. Note, however, that a molecule with no permanent dipole moment may still be infrared active if during its vibration a change in dipole moment occurs.

Second, the incident electromagnetic radiation must have a frequency identical to that of the molecule's normal mode of vibration. To demonstrate this, consider the situation in which electromagnetic radiation strikes a diatomic molecule possessing a permanent dipole moment. As a wave, electromagnetic radiation can be characterized as consisting of mutually perpendicular electric and magnetic fields that oscillate sinusoidally as they propagate through space. The energy of this wave (E_w) is defined by:

$$E_w = hf_w \qquad \text{(equation 2.5)}$$

where f_w is the frequency of the wave. For this radiation to be absorbed by the molecule, its energy must be equivalent to the difference in energy between two vibrational levels.

In the case of the transition from the ground state ($n=0$) to the first excited vibrational level ($n=1$), this translates into:

$$E_{\cdot} = \Delta E_{0 \rightarrow 1} \qquad \text{(equation 2.6)}$$

where $\Delta E_{0 \rightarrow 1}$ is the energy difference between vibrational levels 0 and 1. Inserting equations 2.2 and 2.5 into equation 2.6 gives the following relationship:

$$f_{\cdot} = f_{\cdot} \qquad \text{(equation 2.7)}$$

In other words, the incident radiation that has the precise energy to induce the transition from the ground to the first excited state has a frequency that is identical to that of the normal mode of vibration of the molecule.

Schematically, the correlation between the frequency of the electromagnetic radiation absorbed by a molecule and the frequency of its normal mode of vibration is depicted in Figure 2.2. Since the wavelength of the incident radiation is far greater than the size of the molecule, the oscillating electric field vector of the wave can be considered uniform over the whole molecule. If its frequency matches the vibrational frequency of the molecule, the oscillating negative and positive fields will exert a force on the molecule's dipoles and, by definition, the force on opposite charges will be exerted in opposite directions. This will induce the molecule to absorb energy from the incident radiation thus increasing its own vibrational energy by vibrating with increased amplitude.

The value of infrared spectral analysis is derived from the fact that the frequency of each of a molecule's normal modes of vibration, and thus the frequency of the

Figure 2.2 Schematic diagram illustrating the interaction of electromagnetic radiation with a diatomic molecule. **(A)** When a polychromatic beam strikes a diatomic molecule possessing a permanent dipole moment, that component of the radiation oscillating at the same frequency as the molecule's normal mode of vibration will be absorbed. This is a consequence of the forces generated on the molecule's dipole by the oscillating electric field vector of the absorbed radiation **(B)**. The oscillating electric field alternately increases and decreases the length of the molecule's chemical bond resulting in an increase in the molecule's vibrational energy. This does not alter the frequency of the molecule's vibration, but rather the amplitude of each atom's displacement from equilibrium.

A

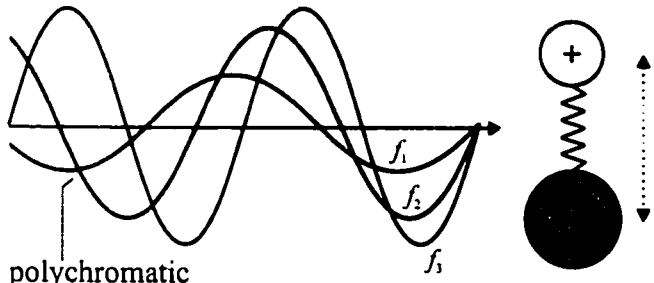

polychromatic radiation with component waves of frequency f_1, f_2 and f_3.

diatomic molecule possessing permanent dipole moment

① Vibrational energy before absorption.

② Vibrational energy after absorption of radiation with frequency f_3.

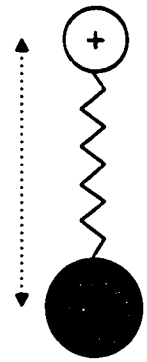

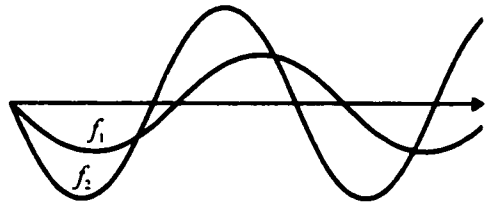

B

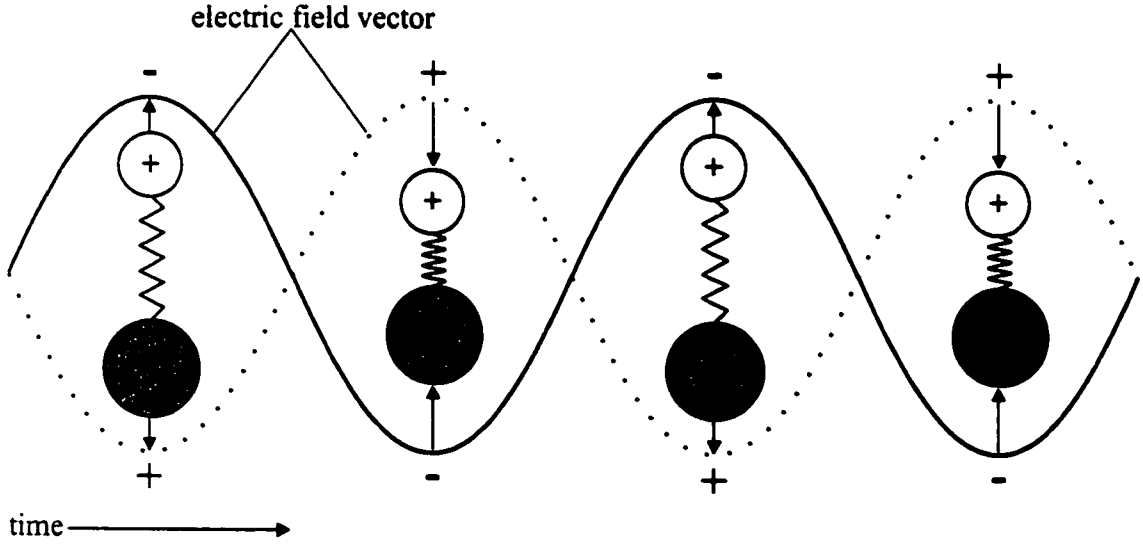

radiation that it absorbs, is extremely sensitive to molecular structure and local environment. To illustrate this, consider the linear diatomic molecule described above. For a diatomic molecule, the number of independent normal modes of vibration is equal to $3N-5 = 3(2) - 5 = 1$. According to classical mechanics, the frequency (f) of this vibration is given by:

$$f = \frac{1}{2\pi}\sqrt{\frac{F}{M_{red}}} \qquad \text{(equation 2.8)}$$

where F is the force constant binding the two atoms together (i.e. the chemical bond). From equation 2.8, it is evident that the frequency of this normal mode of vibration is directly proportional to the strength of the chemical bond. As a result, external factors that act to enhance the strength of this bond will increase the molecule's vibrational frequency while factors that act to reduce its strength will decrease the molecule's vibrational frequency. To relate this to the study of a macromolecule, such as a protein, consider the situation in which this diatomic molecule is substituted for a carbonyl group (C=O) located within a protein's polypeptide backbone. This carbonyl group will have a stretching vibration whose normal frequency of vibration can be approximated by equation 2.8. If the carbonyl oxygen is involved in a hydrogen bond, then the strength of the C=O bond will be reduced resulting in a decrease in the frequency of its stretching vibration and hence, a decrease in the frequency of its absorbed radiation. Similarly, dipole-ion or dipole-dipole interactions between the carbonyl group and neighboring amino acid side chains will also increase or decrease the strength of the C=O bond and thus increase or decrease the frequency of its stretching vibration.

Wavelength and Absorption Intensity. As mentioned, the region of the electromagnetic spectrum responsible for inducing vibrational transitions falls within the infrared. The frequencies of this radiation, however, are inconveniently large numbers (between 10^{11} to 10^{14} sec^{-1}). Thus, when referring to infrared radiation, the term wavenumber is more commonly used. The relationship between frequency and wavenumber (ω) is given by:

$$\omega = \frac{f}{c} \qquad \text{(equation 2.9)}$$

where c is the velocity of light in a vacuum.

In addition, although the frequency (or frequencies) of infrared radiation absorbed by a molecule is dependent upon the molecule's frequency (or frequencies) of vibration, the intensity of the absorption is dependent upon how efficiently the radiation energy is transferred to the molecule. This efficiency, which varies with the wavenumber of the incident radiation, is often described by the molecule's molar absorption coefficient (ε_ω). If radiation with wavenumber ω and initial intensity I_o is passed through a sample of thickness l and molar concentration M_c, such that the transmitted light has an intensity I, then the intensity of the absorbance of the sample (A_ω) will obey the Beer-Lambert law:

$$A_\omega = \log\left(\frac{I_o}{I}\right) = \varepsilon_\omega l M_c \qquad \text{(equation 2.10)}$$

A plot of the absorption intensity of a sample versus an entire range of wavenumbers (typically 400-4000 cm^{-1}) is referred to as an absorption spectrum. As will be discussed

in the following section, the absorption spectrum of a molecule can be acquired using either the dispersive or Fourier transform technique.

SPECTRAL ACQUISITION

Dispersive Infrared Spectrometers. Within dispersive infrared spectrometers, light from an infrared source is first passed through a sample and then into a monochromator (Figure 2.3). A monochromator is a device that employs either a prism or grating to disperse the polychromatic infrared beam into a spectrum of its component wavenumbers. This dispersed spectrum is focused by a mirror onto an exit slit that acts as a selective filter, allowing only a narrow range of the infrared spectrum to reach the detector at any given time. Subsequent wavelengths are then recorded by rotating the prism or grating. The use of a monochromator for spectral acquisition, however, has two important limitations. First, since only a narrow range of wavelengths is recorded at a time, spectral acquisition is very slow. Second, the selectivity of the exit slit means that only a fraction of the total light energy available strikes the detector at any given time, the result of which, is a relatively poor signal-to-noise ratio.

Note that the ultimate performance of any spectrometer is largely determined by its signal-to-noise ratio. The signal-to-noise ratio is a measure of the intensity of a sample absorbance band compared to that of the noise at some point nearby in the spectrum. Noise is observed as random fluctuations in the spectrum above and below the baseline. For any given sample and set of conditions, an instrument with a higher signal-to-noise ratio will be more sensitive, be applicable to a greater variety of samples and will

Figure 2.3 Schematic diagram illustrating the organization of a typical dispersive infrared spectrometer. The depicted monochromator employs a grating to disperse the polychromatic infrared beam into a spectrum of its component wavenumbers. The intensity of individual wavenumbers is recorded by rotating the grating thereby allowing different wavenumbers to pass through the exit slit and strike the detector.

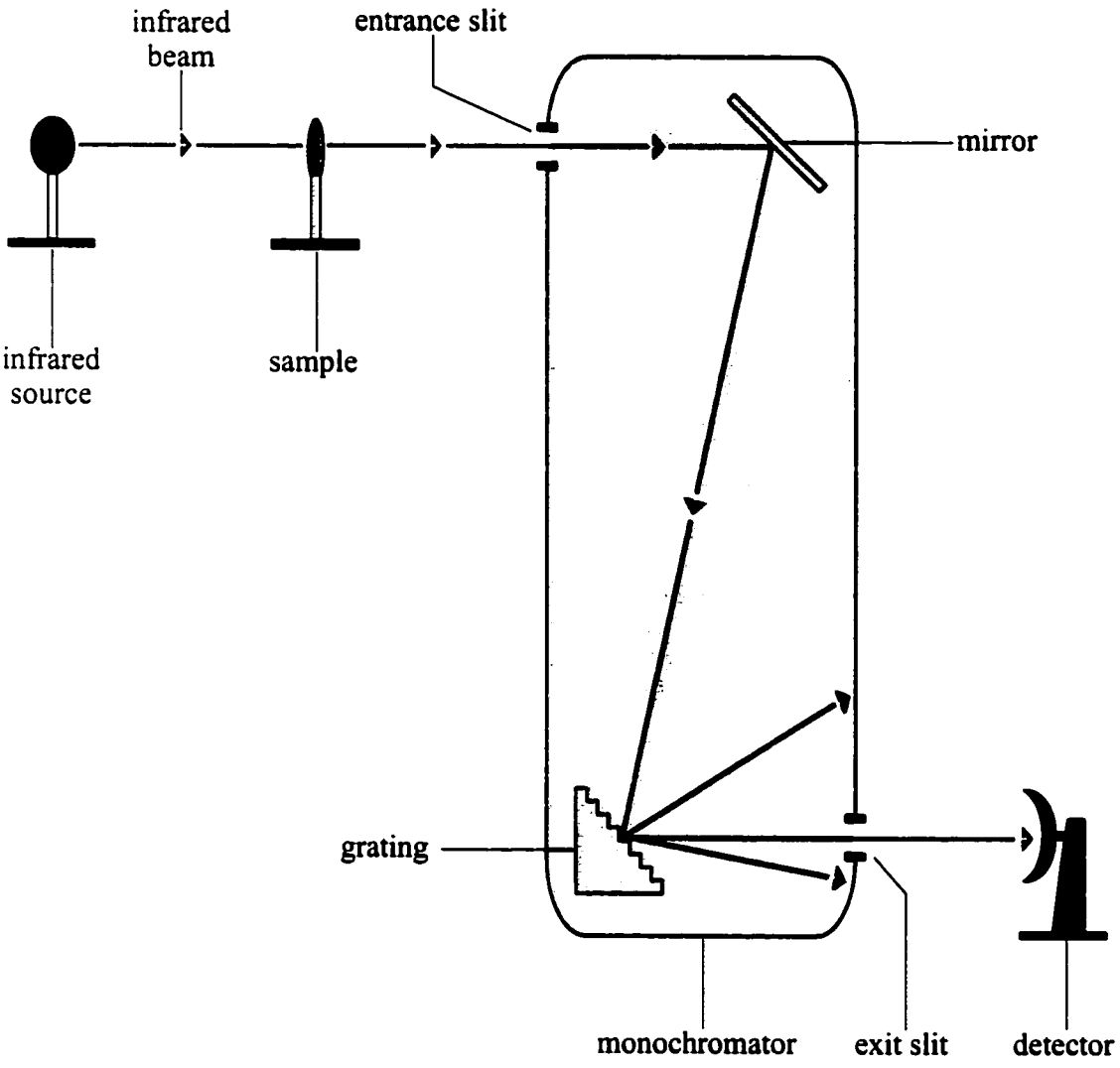
infrared
beam
entrance slit
mirror
infrared
source
sample
grating
monochromator
exit slit
detector

allow absorbances to be measured more accurately than an instrument with a low signal-to-noise ratio.

Fourier Transform Infrared Spectrometers. The inception of the Fourier transform technique for the acquisition of infrared spectra can be traced back to the turn of the nineteenth century when Albert Michelson first described the interferometer that now bears his name (130, 131). In general, an interferometer divides a beam of light into two, introduces a phase difference into one and then recombines the two beams so that constructive and destructive interference can occur. Within the Michelson interferometer, this is accomplished by mounting a beamsplitter at a 45° angle at the point of intersection of the planes of two perpendicular mirrors, one stationary and the other movable (Figure 2.4). Composed of a thin coating of germanium sandwiched between two pieces of potassium bromide, the beamsplitter is designed to transmit 50% of the incident radiation and reflect the other 50%. As a result, when a beam of infrared radiation enters the interferometer and strikes the beamsplitter, half of the radiation is transmitted towards the stationary mirror and half is reflected towards the movable mirror. After reflecting off their respective mirrors, the two beams are recombined at the beamsplitter where again, 50% is transmitted and 50% is reflected. The component of the recombined beam that is reflected leaves the interferometer where it first interacts with the sample before striking the detector.

When the moving mirror and the stationary mirror are an equivalent distance from the beamsplitter, the distance traveled by the transmitted and reflected beams prior to their recombination is identical. This position is referred to as the *zero path difference*

Figure 2.4 Schematic diagram illustrating the typical organization of a Michelson interferometer. Radiation from an infrared source entering the interferometer first strikes a beamsplitter where 50% of the incident radiation is transmitted to a stationary mirror and 50% is reflected to a movable mirror. By translating the movable mirror, an optical path, or phase difference, is introduced into the reflected beam that enables constructive and destructive interference to occur when the reflected beam is recombined with the transmitted beam at the beamsplitter. If the movable mirror is translated at a constant velocity, the intensity of the recombined beam will oscillate with a frequency that is unique to each wavelength component of the incident beam. A plot of intensity versus optical path difference after translating the movable mirror back and forth once is called an interferogram. An interferogram of a monochromatic source with wavelength λ is shown.

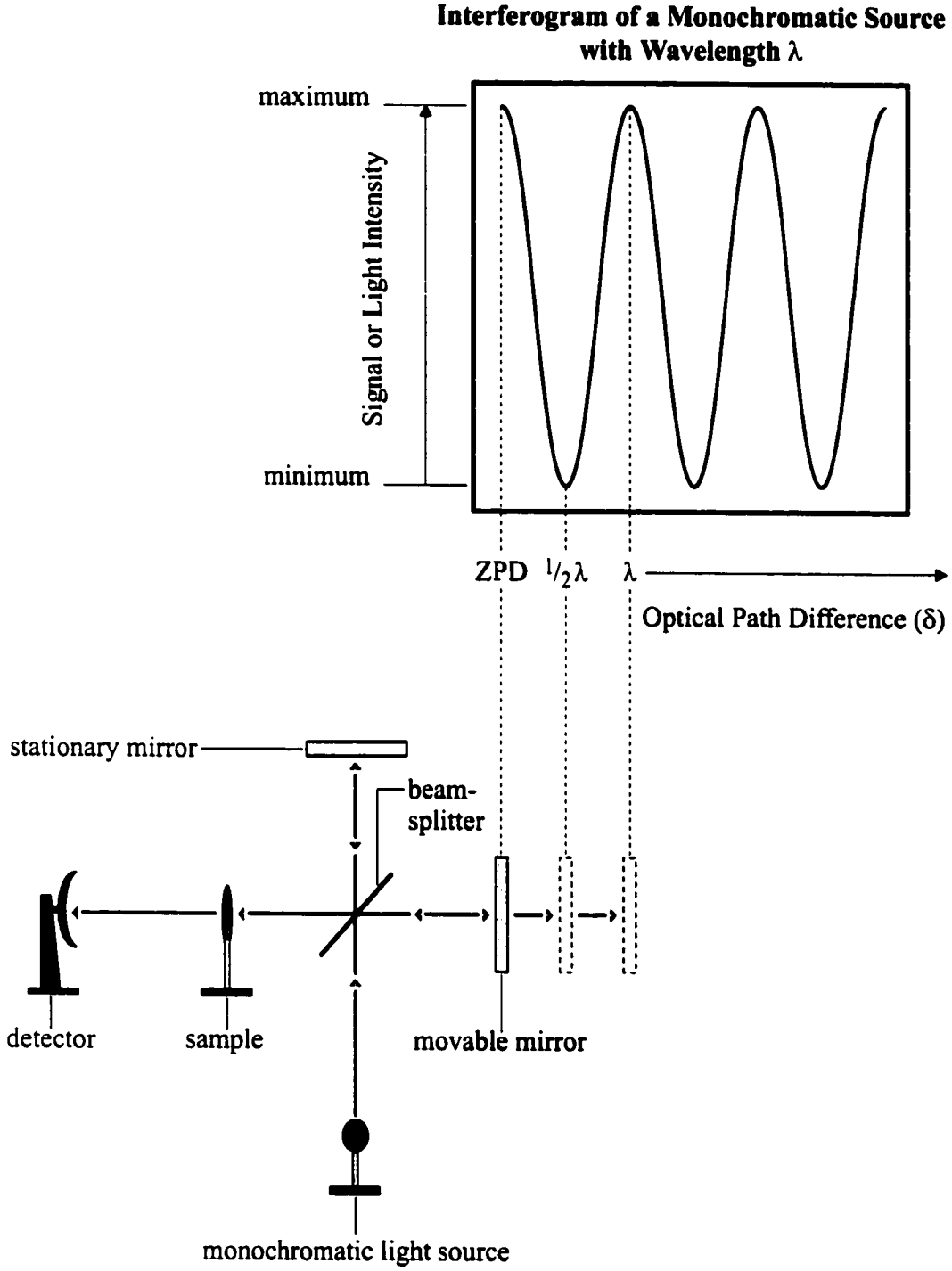

Michelson Interferometer

(ZPD). In the Michelson interferometer, a path difference, and thus a phase difference, is introduced into the reflected beam by translating the movable mirror away from the beamsplitter. The distance traveled by the movable mirror is called the *mirror displacement* and is denoted by d. Since the reflected beam must travel this distance both towards and away from the movable mirror, the relationship between the mirror displacement and the actual *optical path difference* (δ) is defined by:

$$\delta = 2d \qquad \text{(equation 2.11)}$$

If, for simplicity, it is assumed that the light source emits monochromatic radiation and that the movable mirror is at ZPD, then the transmitted and reflected beams will converge at the beamsplitter in phase. The result is complete constructive interference with the amplitude of the recombined beam being the sum of the amplitudes of the individual beams. Since the amplitude of the recombined beam is directly proportional to its intensity, the signal reaching the detector at this point will be at a maximum. As the movable mirror translates away from the beamsplitter, the transmitted and reflected beams converge at the beamsplitter out of phase and the amplitude of the recombined beam will decrease until $d = \frac{1}{4}\lambda$, where λ is the wavelength of the radiation. At this point the optical path difference is equal to $\frac{1}{2}\lambda$ and the reflected beam is exactly 180° out of phase with that of the transmitted beam. The result is complete destructive interference and the signal at the detector will be at a minimum. Further translation of the movable mirror will produce signal maxima at:

$$\delta = n\lambda \qquad \text{(equation 2.12)}$$

and signal minima at:

$$\delta = n + \tfrac{1}{2}\lambda \qquad \text{(equation 2.13)}$$

where n can have only integer values (i.e. 0, 1, 2, 3...). At optical path differences other than those described by equations 2.12 and 2.13, a combination of constructive and destructive interference occurs with the resulting amplitude of the recombined beam having a value somewhere between the maximum and the minimum. If the movable mirror is moved at a constant velocity, the amplitude of the monochromatic radiation, and thus the intensity of the signal reaching the detector, will increase and decrease uniformly. This variation in signal, or light intensity, with optical path difference is measured by the detector as a cosine wave whose frequency (f) is defined by:

$$f = \frac{v}{\lambda} = v\omega \qquad \text{(equation 2.14)}$$

where v is the constant velocity of the mirror and ω is the wavenumber of the monochromatic source. As indicated by equation 2.14, each wavenumber of light entering the interferometer gives rise to a cosine wave of unique frequency and it is this property that enables the signals arising from different wavenumbers to be distinguished by an FTIR spectrometer. A plot of signal intensity versus optical path difference after translating the moving mirror back and forth once is called an *interferogram.* A typical interferogram obtained from a Michelson interferometer using a monochromatic light source with a wavelength of λ is depicted in Figure 2.4.

If the monochromatic light source described above is replaced by a broadband infrared source similar to that found in a typical FTIR spectrometer, the radiation entering

the interferometer will contain a continuum of wavelengths, each one giving rise to a unique cosine wave whose frequency is defined by equation 2.14. The interferogram generated by the detector will, therefore, be the sum of each individual cosine wave. As depicted in Figure 2.5A, the interferogram generated from a polychromatic light source displays a sharp intensity spike at ZPD, termed the *centerburst*. This high intensity is the result of ZPD being the only point at which all component cosine waves interfere constructively. As the movable mirror translates away from ZPD, the phase differences introduced cause the individual cosine waves to interact in a destructive manner. Consequently, the intensity of the interferogram drops off rapidly with distance from ZPD.

To convert an interferogram into a spectrum, the fast Fourier algorithm developed by Cooley and Tukey (132) is applied. According to a theorem developed by Fourier, any mathematical function, such as an x, y plot, can be expressed as a sum of sinusoidal (or cosinusoidal) waves and vice versa. In essence, a Michelson interferometer Fourier transforms the intensity of each wavelength component of light that enters to produce an interferogram. This interferogram is then Fourier transformed back using the fast Fourier algorithm to generate a single beam spectrum of the sample, which divided by the spectrum of the incident beam without sample, gives rise to the familiar absorbance intensity versus wavenumber spectrum of the sample (Figure 2.5B).

There are several advantages to measuring infrared spectra interferometrically. The first is the multiplex (or Fellgett) advantage, which is derived from the fact that all wavelengths are detected simultaneously during each scan of the sample. This allows an

Figure 2.5 (**A**) A typical interferogram of a polychromatic infrared source produced by a Michelson interferometer. (**B**) From the interferogram, a single beam spectrum of a sample can be generated by applying the fast Fourier algorithm developed by Cooley and Tukey (132).

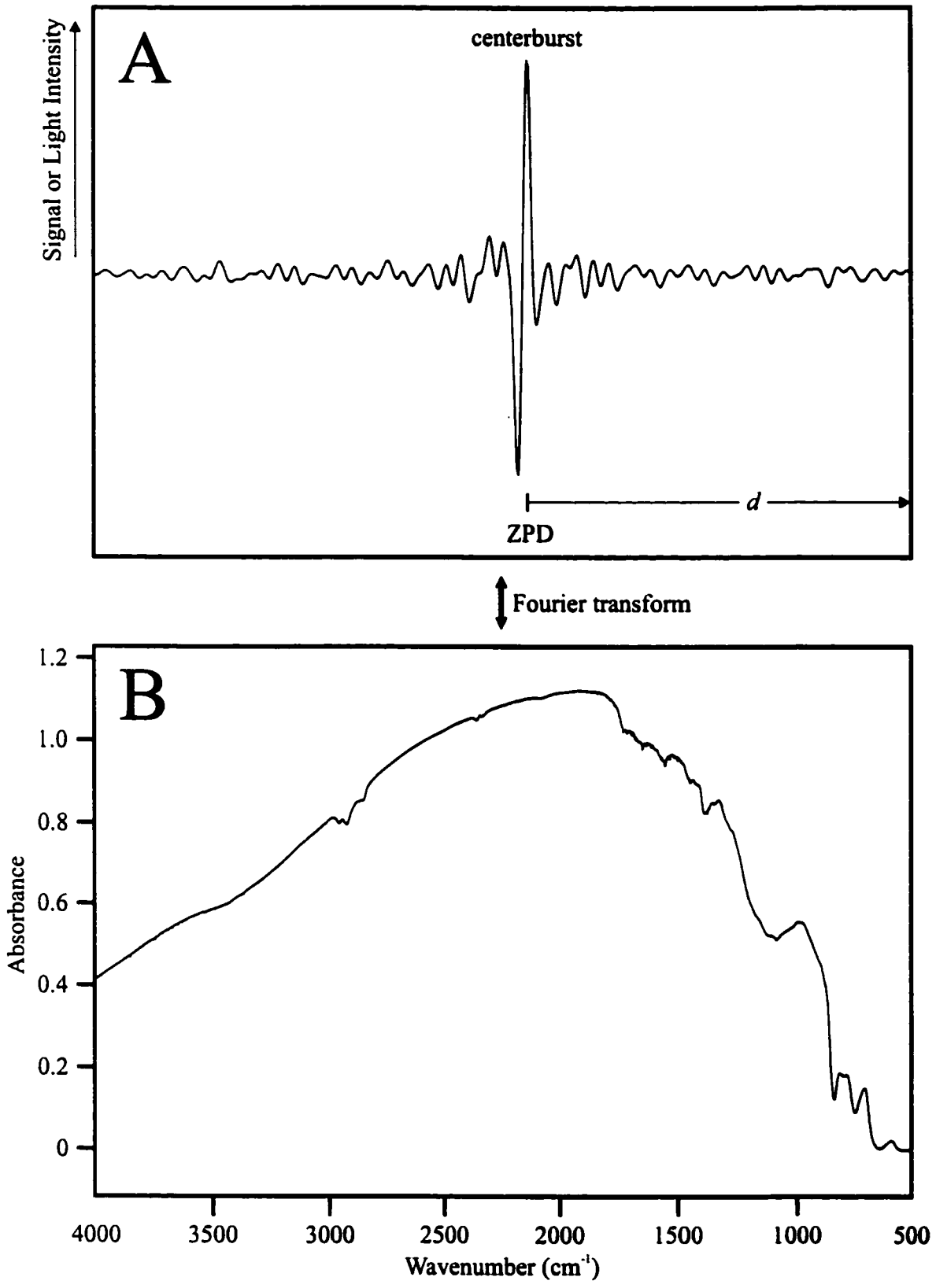
A
centerburst
Signal or Light Intensity
d
ZPD
Fourier transform
B
1.2
1.0
0.8
0.6
0.4
0.2
0
Absorbance
4000
3500
3000
2500
2000
1500
1000
500
Wavenumber (cm-1)

FTIR spectrometer to acquire a spectrum much faster than a dispersive instrument. Since the signal-to-noise ratio of any spectrum is proportional to the square root of the number of its averaged scans, over any given time range, an FTIR spectrometer will produce spectra with a significantly greater signal-to-noise ratio than a dispersive instrument. As an example, a scan from 4000 to 400 cm^{-1} at a resolution of 4 cm^{-1} will take approximately 10 minutes to record on a dispersive instrument. In that same time, an FTIR spectrometer can record and average approximately 600 scans, thus yielding an almost 25-fold improvement in the signal-to-noise ratio.

The second advantage is the throughput (or Jacquinot) advantage, which is derived from the fact that in an FTIR spectrometer, all infrared radiation passes through the sample and strikes the detector at once. Consequently, the detector sees the maximum amount of light at all points during a scan, again resulting in a far greater signal-to-noise ratio.

The third advantage is an extremely high wavenumber precision (Conne's advantage) due to the incorporation of a helium-neon (He-Ne) laser. A He-Ne laser produces light at precisely 17,798.637 cm^{-1} and thus is used as an internal wavelength standard. This allows the wavenumber reproducibility of most FTIR spectrometers to be 0.01 cm^{-1}, or better. In addition, the He-Ne laser is used to track the position of the movable mirror allowing the optical path difference to be measured with extreme accuracy.

The fourth advantage, which results in part from the improved signal-to-noise ratio and wavenumber precision of FTIR spectra, is the ease with which the spectral data

can be manipulated. Digitization of the spectra combined with the data processing power of the computer has enabled the development of a number of data treatment techniques that have yielded significant improvements in the qualitative interpretation of the vibrational bands observed within a sample spectrum. Examples include the reliable subtraction of one sample spectrum from that of another, (the foundation for the technique of FTIR difference spectroscopy, see below) and a number of resolution enhancement methods, such as Fourier self-deconvolution, that enable the visualisation and quantification of overlapping bands within a protein spectrum.

One specific limitation of FTIR spectroscopy, however, is that it is a single beam technique. This means that the background spectrum, which measures the contribution of the instrument and the environment to the spectrum, is measured at a different point in time than the sample spectrum. If special care is not taken, instrumental or environmental changes between the sample and the background spectrum can occur resulting in the appearance of spectral artifacts in the sample spectrum. A perfect example is the appearance of numerous sharp positive or negative vibrational bands within a sample spectrum due to variations in the level of atmospheric water vapour over time. To prevent this, most FTIR spectrometers are equipped with an air dryer to purge the sample compartment of water vapour.

Attenuated Total Reflection. The most common method for acquiring an absorbance spectrum of a sample is to employ what is referred to as a transmission cell (Figure 2.6A). In this case, the sample is placed between two transparent plates, called *windows*, that are separated by a spacer to fix the thickness of the sample. A sample

Figure 2.6 Schematic diagram illustrating the techniques of (**A**) transmission and (**B**) ATR. (A) In transmission, a sample is placed in a transmission cell that is comprised of two transparent plates (or windows) separated by a spacer to fix the thickness of the sample. A sample spectrum is then recorded by passing the infrared beam directly through the transmission cell. (B) In ATR, a thin layer of the sample is placed on the surface of an IRE. A sample spectrum is then recorded by passing the infrared beam through the IRE at an angle, such that the beam undergoes multiple internal reflections. Each time the beam strikes the interface between the sample and the IRE, a portion of the infrared radiation is absorbed by the sample. The effective penetration depth of the beam into the sample, however, is restricted to only a few microns, thus significantly reducing the contribution of water absorption to the sample spectrum.

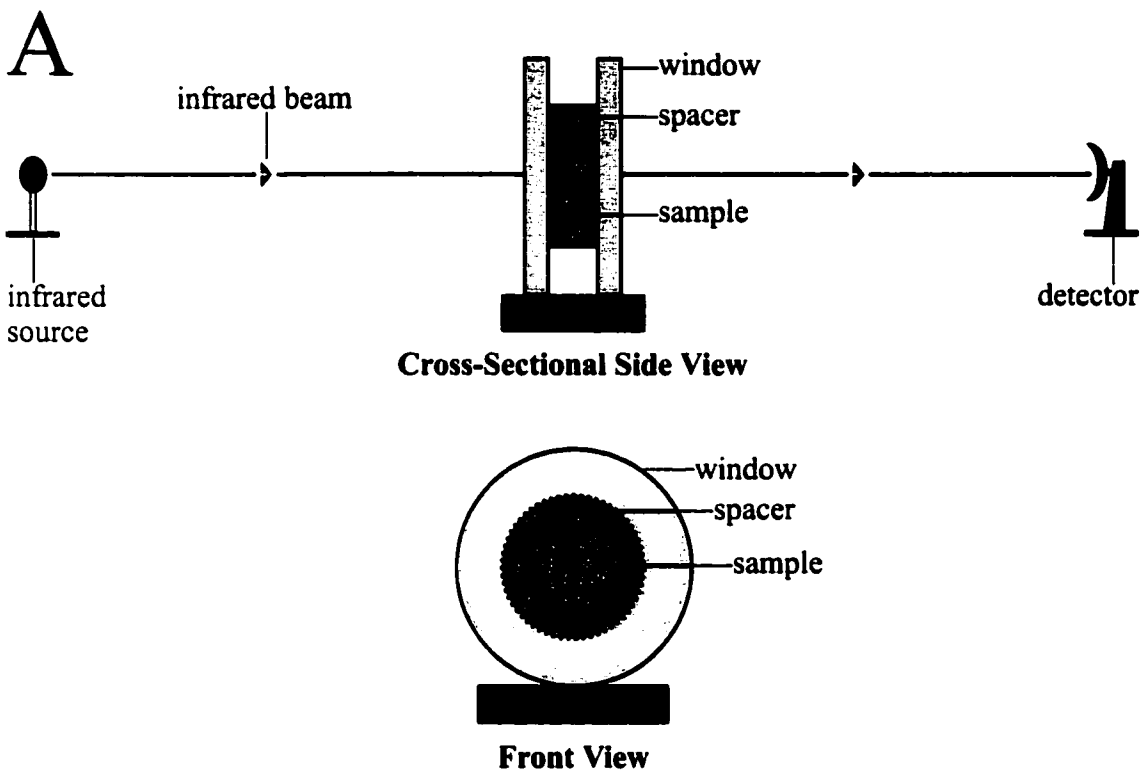
A
infrared beam
window
spacer
sample
infrared source
detector
Cross-Sectional Side View
window
spacer
sample
Front View

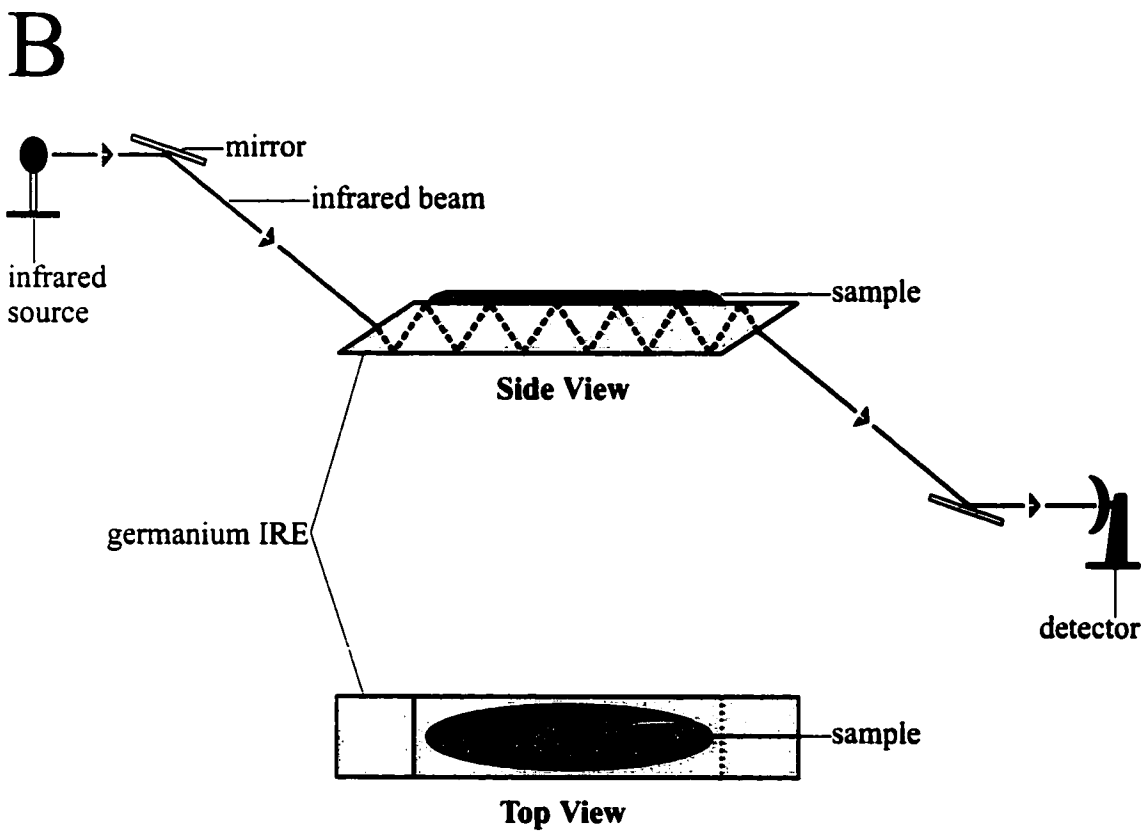
B
mirror
infrared beam
infrared source
sample
Side View
germanium IRE
detector
sample
Top View

spectrum is then recorded by passing an infrared beam directly through the transmission cell. For biological molecules, such as proteins, however, acquiring a sample spectrum by this method is often impeded by the intense and broad absorption of water, which overlaps a considerable part of the protein spectrum. For this reason, most transmission spectra of proteins must be acquired using very thin cells or under partially dehydrated conditions. Such methods, however, make it difficult to control the pH and ionic composition of the protein's aqueous environment, which can ultimately lead to undesirable effects on protein structure.

An attractive alternative to transmission is the technique of ATR (133-136). ATR essentially limits the effective thickness of a sample to a thin layer on the surface of an internal reflection element (IRE), thereby allowing for a significant reduction in the contribution of water to the absorbance spectrum (Figure 2.6B). In addition, the ATR technique allows the aqueous environment of the sample to be modified with little disturbance to the sample. One can thus study the conformational properties of proteins in different environments and under different physiological and non-physiological conditions. In the case of the nAChR, it also allows one to study the structural consequences of soluble ligand binding to the nAChR.

The technique of ATR, also referred to as multiple internal reflection spectroscopy, is based on the behaviour of light as it strikes the interface between two media of different refractive indices (n_1 and n_2). According to Snell's law, if a beam of light propagating through a dense medium (n_1), such as a prism, strikes the interface between the prism surface and a medium of lower refractive index (n_2), then the incident

beam will be partially reflected and partially transmitted (Figure 2.7A). For the reflected beam, the angle of reflection is equal to the angle of incidence (θ) whereas for the transmitted beam the angle of refraction (φ) is defined by:

$$\sin\varphi = \frac{n_1 \sin\theta}{n_2} \qquad \text{(equation 2.15)}$$

If, however, the incident beam strikes the interface such that $\sin\theta \geq \sin\theta_c$, where θ_c, referred to as the critical angle, is equal to $\sin^{-1}(n_2/n_1)$, then the angle of refraction is imaginary and the incident beam will be entirely reflected back into the denser medium (Figure 2.7B). In other words, the incident beam will undergo total internal reflection. Both experimental and theoretical studies have shown that in this special case, a standing wave retaining the same frequency (or frequencies) as the incident beam will be established at the interface between the two media producing an evanescent wave (or waves) that penetrates beyond the interface and into the rarer medium (Figure 2.7C). If the rarer medium is an absorbing sample, then the evanescent wave(s) is/are capable of interacting with the sample just beyond the interface leading to a reduction or *attenuation* of the totally reflected beam.

The intensity (I) of the evanescent wave(s) that penetrates into the sample decreases exponentially from its value I_0 at the interface such that:

$$I = I_0 e^{-z/d_p} \qquad \text{(equation 2.16)}$$

where z represents the distance from the interface and d_p represents the effective penetration depth, defined as the distance required for the intensity of the evanescent

Figure 2.7 (**A**) If a beam of radiation propagating through a prism with an index of refraction n_1 strikes the interface between the prism surface and a medium of lower refractive index, n_2, the incident beam will be partially transmitted and partially reflected as described by Snell's law. (**B**) If, however, the angle of incidence is greater than, or equal to, the critical angle (θ_c), the incident beam will be entirely reflected back into the prism, a situation referred to as total internal reflection. In this special case, a standing wave retaining the same frequency as the incident beam will be established at the prism interface producing an evanescent wave that penetrates beyond the interface and into the medium of lower refractive index (**C**).

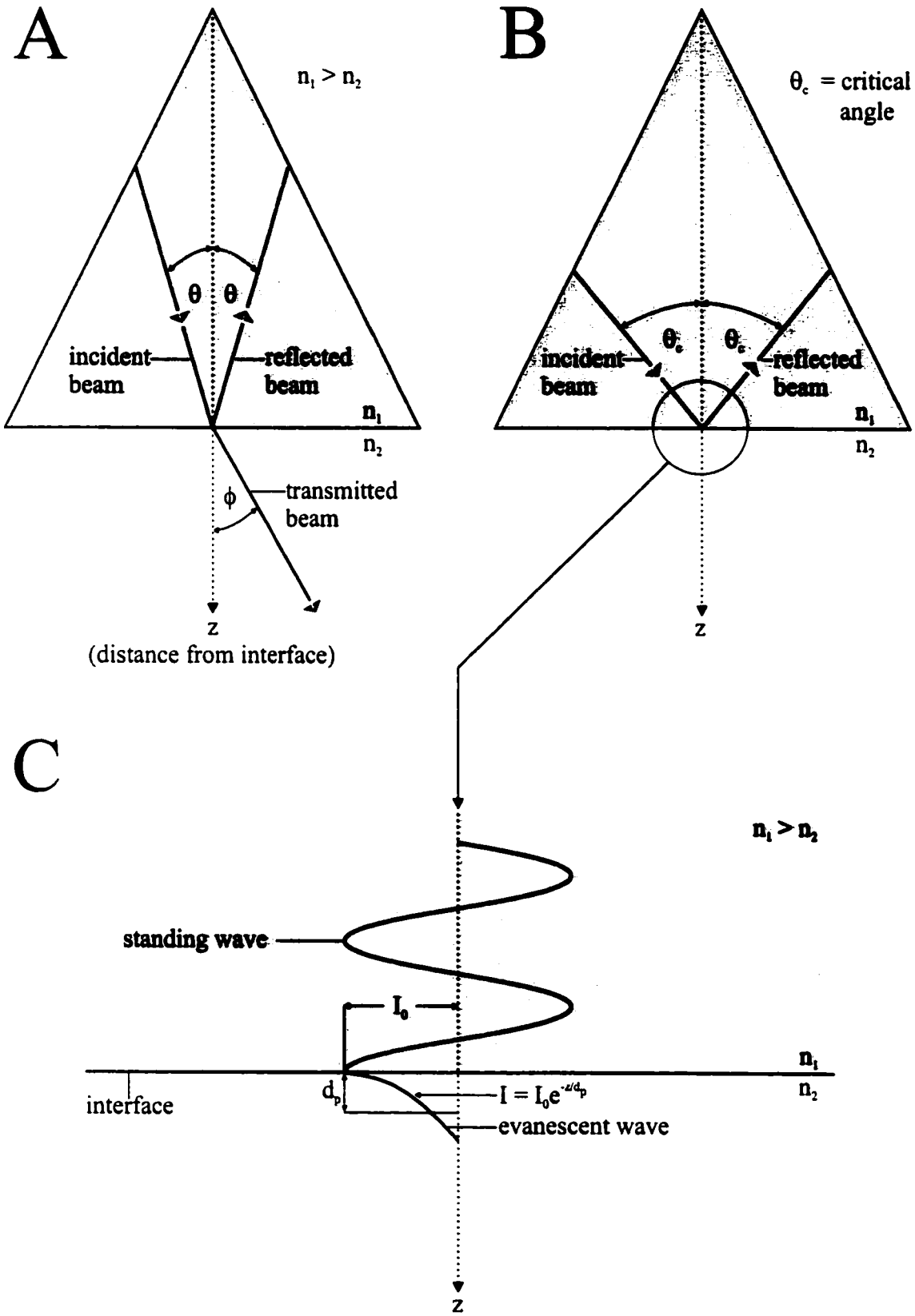
A
$n_1 > n_2$
θ θ
incident beam
reflected beam
n_1
n_2
ϕ
transmitted beam
z
(distance from interface)
B
θ_c = critical angle
θ_c θ_c
incident beam
reflected beam
n_1
n_2
z
C
$n_1 > n_2$
standing wave
I_0
n_1
n_2
interface
d_p
$I = I_0 e^{-z/d_p}$
evanescent wave
z

wave(s) to fall to e^{-1} of its value at the interface. As shown in equation 2.17 the effective penetration depth of the evanescent wave(s) into the rarer medium is a direct function of the wavelength(s) (λ) of the incident beam:

$$d_r = \frac{\lambda}{2\pi n_1 \sqrt{\sin^2\theta - \left(\frac{n_2}{n_1}\right)^2}} \qquad \text{(equation 2.17)}$$

Consequently, for an incident beam arising from a polychromatic light source, the effective penetration depth of its higher component wavelengths will be greater than that of its lower component wavelengths. Over the entire infrared spectrum, however, the effective penetration depth never exceeds more than a few microns.

To enhance the sensitivity of the ATR technique, a sample (rarer medium) is often placed in contact with a long thin IRE of high refractive index (denser medium) whose endfaces are cut at an angle, referred to as the angle of incidence (θ) (Figure 2.6B). Such an IRE enables multiple internal reflections to be produced leading to multiple interactions with the sample. As an example, all spectra presented in this thesis were acquired using a germanium IRE with the dimensions of 50 x 20 x 2 mm (length x width x depth) and an angle of incidence of 45°. The number of internal reflections (N_r) that occur as an infrared beam passes through this IRE is given by:

$$N_r = Ld\cot\theta \qquad \text{(equation 2.18)}$$

where L is the length of the IRE and d is its depth. For the germanium IRE employed in this research, this translates into ~25 internal reflections.

FTIR Difference Spectroscopy

In theory, FTIR spectroscopy, coupled to the technique of ATR, offers an attractive means of gaining insight into the structure and conformational dynamics of large integral membrane proteins, such as the nAChR. FTIR-ATR spectroscopy requires only small quantities (micrograms) of protein and is unaffected by the nature of the protein's environment. FTIR-ATR spectroscopy is also an extremely sensitive technique that has the potential to detect small alterations in protein structure. As an example, a change in hydrogen bonding distance of only 0.002 Å will shift the frequency of the N-H stretching vibration of an amide group within a peptide bond by approximately 1 cm^{-1}, which is well within the limits of detection of most FTIR instruments (137, 138). In addition, FTIR-ATR spectroscopy has a characteristically short acquisition time scale ($\sim 10^{-13}$ sec compared to 10^{-5} sec for NMR) making it possible to detect structural changes that occur on a time scale of fractions of a second.

In practice, however, it is often difficult to detect small localized structural changes in proteins with FTIR-ATR spectroscopy. Essentially all of a protein's functional groups have infrared-active vibrations and thus tend to give rise to a multitude of overlapping bands within the protein spectrum. As an example, the 1500-1700 cm^{-1} region of a protein spectrum has contributions from the many amide groups of a protein, which produce the intense and often broad amide I (predominantly the carbonyl stretching vibration of the amide group) and II (N-H bending and C-N stretching vibrations of the amide group) bands, as well as from the side chains of several amino

acid residues including aspartic acid, glutamic acid, tyrosine, tryptophan, lysine and arginine (123, 139, 140).

A simple solution to this problem is based on the principle of FTIR difference spectroscopy. FTIR difference spectroscopy is an extremely effective method for probing structural differences between a protein's various conformational states and exists as one of the few techniques capable of providing detailed structural information on large integral membrane proteins at the single amino acid level. FTIR difference spectroscopy is also technically simple. FTIR spectra of a protein in two different conformations (i.e. states A and B) are recorded and then digitally subtracted (B-A) to remove the infrared bands of those residues whose structure, and thus molecular vibrations, are unaffected by the conformational change. The result is a *difference* spectrum that contains vibrational bands reflecting only those residues whose structure and/or environment differ in the two states, thus providing key information about those residues that perform an important role in the conformational change. FTIR difference spectroscopy has already been successful in providing detailed information regarding the structural perturbations of the polypeptide backbone as well as changes in the orientation, protonation state, strength of hydrogen bonding and/or environments surrounding specific tyrosine, aspartic acid, glutamic acid, proline, tryptophan and histidine side chains upon the absorption of light by light activated proteins such as bacteriorhodopsin and the photosynthetic reaction center (122-126).

To apply the FTIR difference technique to the study of the nAChR, a small amount (~250 μg) of affinity purified nAChR from *Torpedo*, reconstituted into lipid

vesicles of defined composition, is deposited on the surface of a germanium IRE (for more details see Chapter 3, Experimental Procedures). After evaporating the bulk solvent with a gentle stream of N_2 gas, the germanium IRE is installed in an ATR liquid sample cell and the nAChR film rehydrated with excess Torpedo Ringer buffer. FTIR spectra are then acquired using the ATR technique. Initially, two consecutive spectra of the nAChR in the resting state are recorded while flowing buffer past the nAChR film (Figure 2.8A, buffer i and Figure 2.9A, top trace). The flowing solution is then switched to an identical one containing the ACh analogue Carb (Figure 2.8A, buffer ii) and a spectrum of the nAChR in the desensitized state is recorded (Figure 2.9A, middle trace). The difference between the two resting state spectra (referred to as a *control* spectrum) and the consecutive resting and desensitized state spectra (referred to as a *Carb-difference* spectrum) are calculated, stored and the flowing solution switched back to buffer without Carb. After a brief washing period to remove Carb from the film and to convert the nAChR back into the resting state, the process is repeated numerous times and the individual spectra averaged. Carb-difference spectra recorded under these stringent conditions exhibit a complex, yet highly reproducible pattern of positive and negative bands that provides a *'spectral map'* of the structural changes that occur in the nAChR upon Carb binding and subsequent desensitization (Figure 2.9A, bottom trace) (127-129). In general, negative bands reflect the vibrations of functional groups in the absence of Carb (resting state) while positive bands reflect the vibrations of the same functional groups in the presence of Carb (desensitized state), as well as those of nAChR-bound Carb itself. More specifically, these positive and negative vibrational bands within the Carb-difference spectra reflect three distinct consequences of Carb binding (Figure

Figure 2.8 Schematic diagram illustrating the acquisition of Carb-difference spectra using the ATR technique (see text for details).

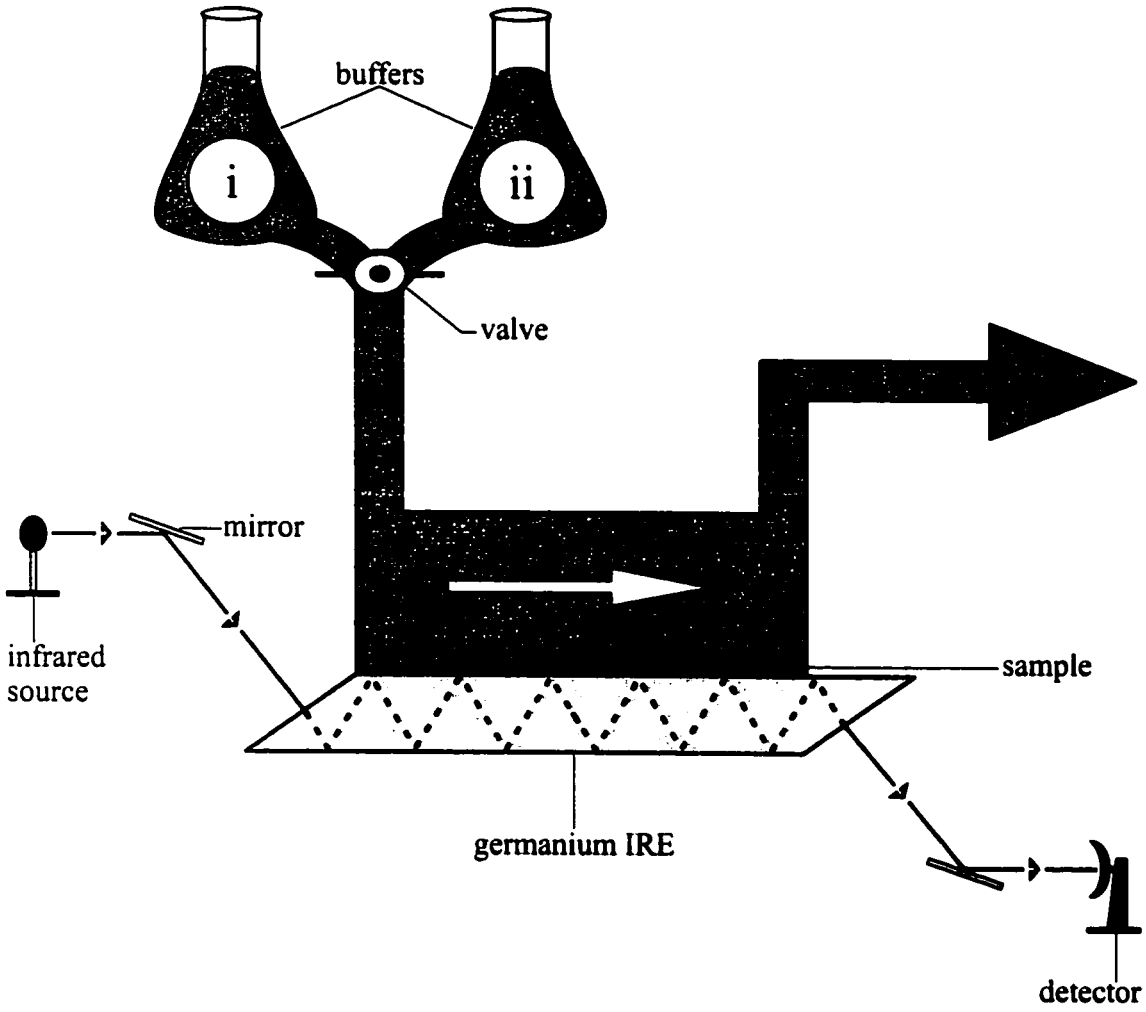
buffers
i
ii
valve
mirror
infrared
source
sample
germanium IRE
detector

Figure 2.9 (**A**) FTIR spectra recorded of the nAChR in the resting and desensitized states (the absorbance of the buffer has been subtracted) as well as the difference between the two (Carb-difference spectrum). The resting and desensitized state spectra are virtually superimposable indicating that the binding of Carb and subsequent transition to the desensitized state does not induce large alterations in nAChR structure. Carb-difference spectra do, however, reveal several positive and negative bands that provide a *'spectral map'* of those residues whose molecular vibrations, and thus structures, differ between the two states. The bar above each spectrum represents the relative absorbance intensity of the vibrational bands [in absorbance units (a.u.)]. (**B**) A schematic diagram illustrating the conformational changes in the nAChR that are reflected within a typical Carb-difference spectrum.

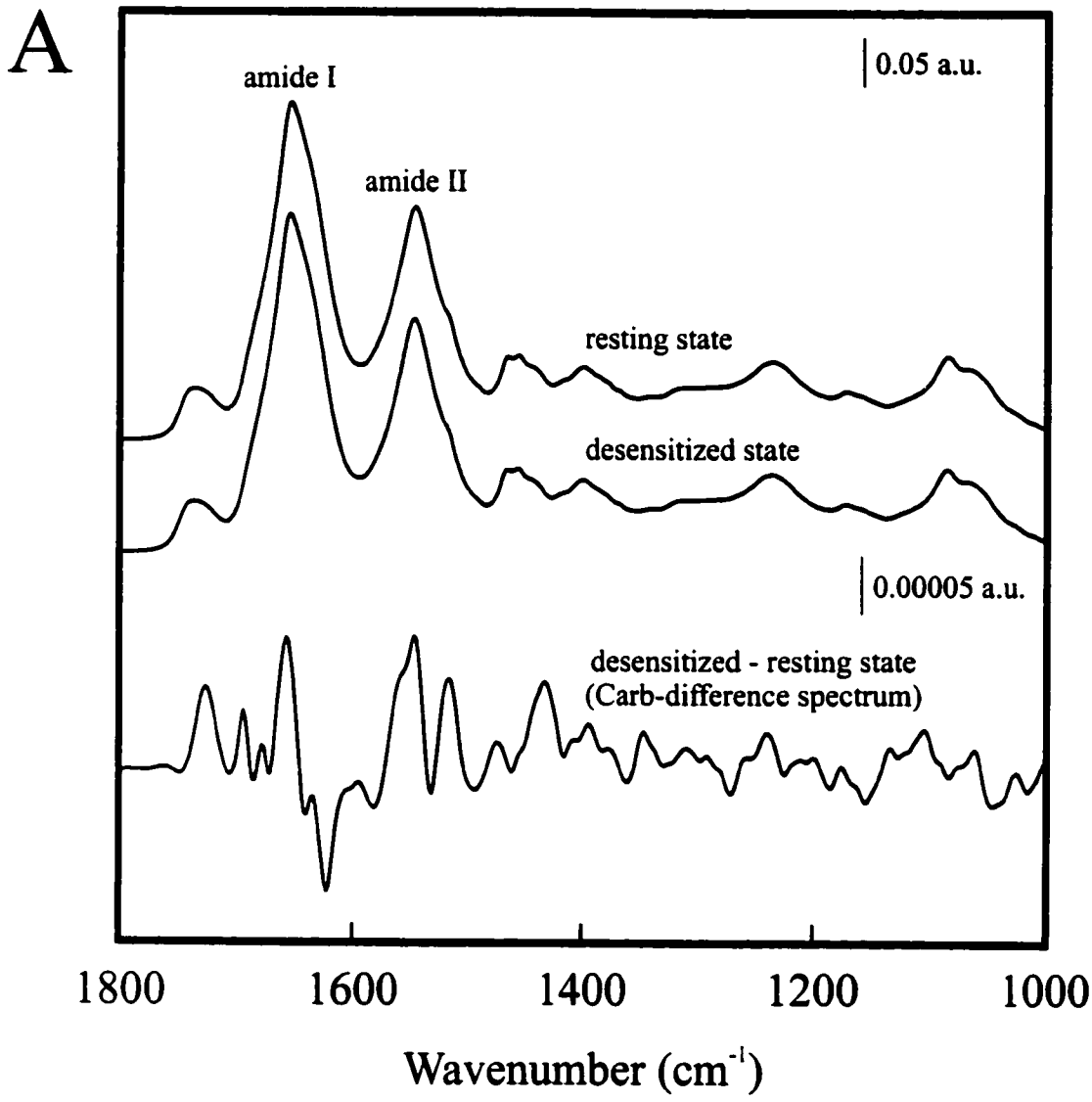
A
amide I
amide II
0.05 a.u.
resting state
desensitized state
0.00005 a.u.
desensitized - resting state
(Carb-difference spectrum)
1800
1600
1400
1200
1000
Wavenumber (cm-1)

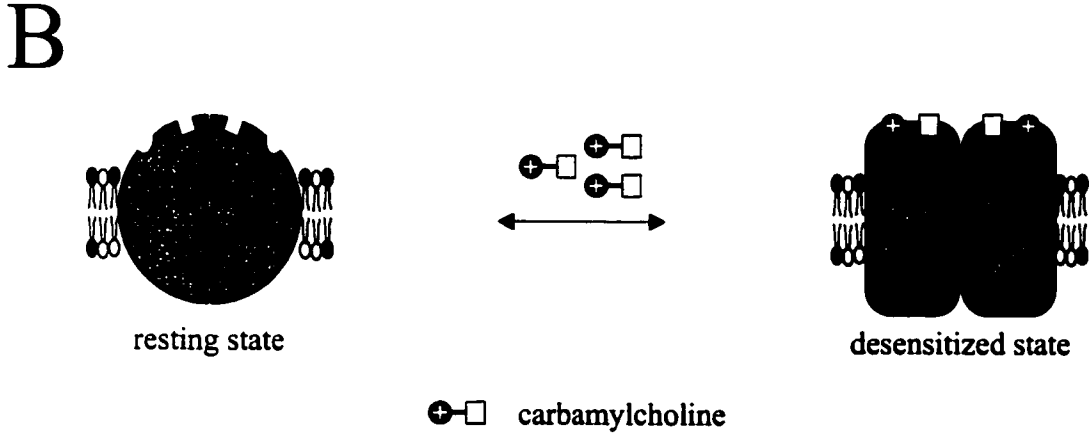
B
resting state
desensitized state
carbamylcholine

2.9B): i) variations in the molecular vibrations of individual amino acid residues within the neurotransmitter binding sites arising from specific interactions with Carb, ii) variations in the molecular vibrations of the polypeptide backbone and individual amino acid residues arising from the conformational transition from the resting to the desensitized state, and iii) the molecular vibrations of distinct functional groups within nAChR-bound Carb.

Initially, the objective of this research was to employ the FTIR difference technique to gain insight into the nature of the physical interactions (i.e. hydrogen bonds, salt-bridges, cation-π-electron interactions etc...) that form between Carb and individual neurotransmitter binding site residues. However, to accomplish this task, it was first necessary to identify those vibrational bands within the Carb-difference spectrum that reflect specific Carb-nAChR interactions. Bands reflecting the vibrations of nAChR-bound Carb were easily eliminated by comparing the frequency of the vibrational bands within the Carb-difference spectrum to those of a solution spectrum of Carb itself (Figure 2.10A) (129). Distinguishing between those vibrational bands reflecting specific Carb-nAChR interactions and those reflecting the resting-to-desensitized conformational transition presented a greater challenge. A possible solution arose from earlier studies focusing on the effects of local anesthetics and membrane composition on nAChR structure and function. These studies proposed that exposure to various local anesthetics or reconstitution of the nAChR into a highly fluid membrane stabilized the nAChR in a conformation that appeared to be analogous to the Carb-induced desensitized state. It was, therefore, hypothesized that by exploiting the effects of local anesthetics and membrane composition on nAChR structure, Carb-difference spectra could be acquired

Figure 2.10 (**A**) A comparison of a Carb-difference spectrum with that of a solution spectrum of Carb itself (the absorbance of the buffer has been subtracted). Those bands that have been labelled are assigned to the vibrations of nAChR-bound Carb. (**B**) A typical Carb-difference spectrum probes the structural changes induced in the nAChR upon Carb binding and subsequent transition from the resting to the desensitized state (scheme i). Previous studies, however, suggest that exposure of the nAChR to various local anesthetics or reconstitution of the nAChR into a highly fluid membrane (shown here) results in the nAChR being perpetually stabilized in the desensitized state (scheme ii). Carb-difference spectra recorded under these conditions, therefore, should reveal only those vibrational bands arising from either specific Carb-nAChR interactions or nAChR-bound Carb itself.

A

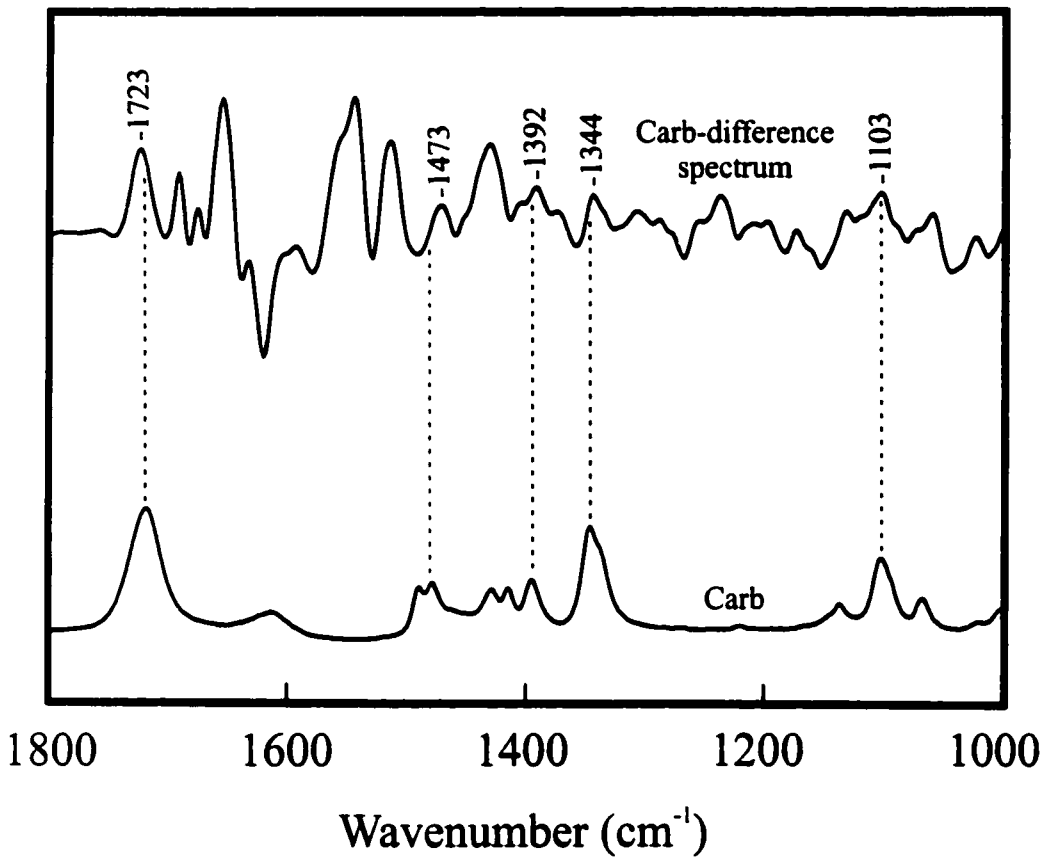
1723
1473
1392
1344
Carb-difference spectrum
1103
Carb
1800
1600
1400
1200
1000
Wavenumber (cm-1)

B

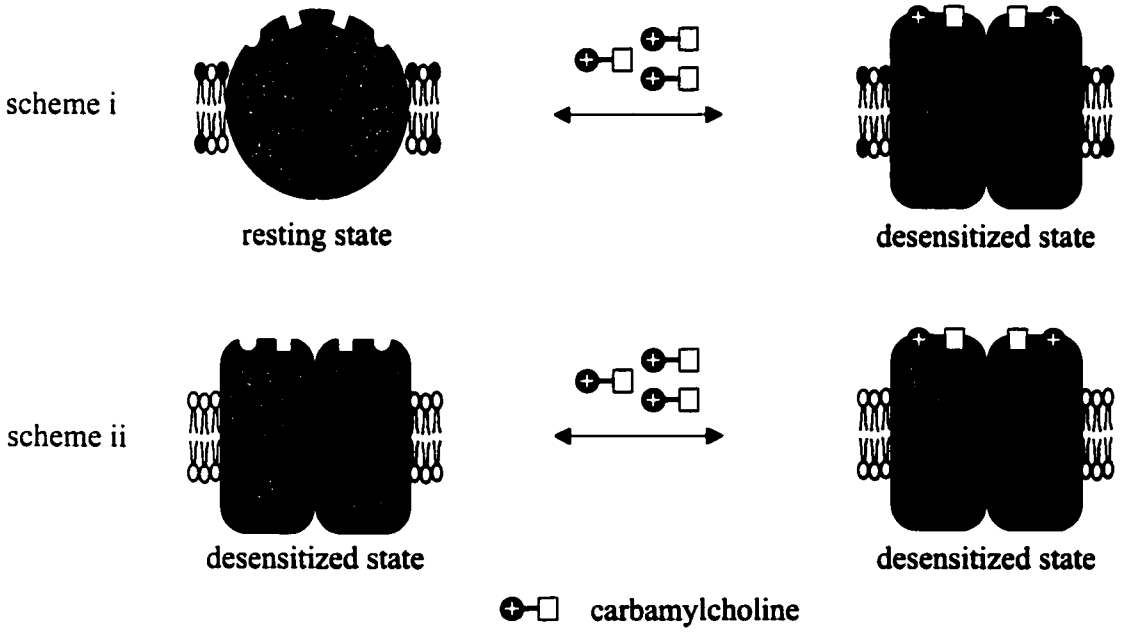
scheme i
resting state
desensitized state
scheme ii
desensitized state
desensitized state
carbamylcholine

of the nAChR perpetually stabilized in the desensitized state (Figure 2.10B, scheme ii). Carb-difference spectra acquired under these conditions would allow for the isolation and identification of vibrational bands arising from only specific Carb-nAChR interactions by eliminating those vibrational bands arising from the resting-to-desensitized conformational transition. However, as will be discussed in the following chapters, the unique band intensity variations revealed in these Carb-difference spectra compelled a more in-depth investigation, the results of which have lead to important new insight into the mechanisms by which both lipids and local anesthetics modulate nAChR activity.

CHAPTER 3

STRUCTURAL EFFECTS OF BOTH NEUTRAL AND ANIONIC LIPIDS ON THE NICOTINIC ACETYLCHOLINE RECEPTOR

INTRODUCTION

The ability of the nAChR to conduct cations across the membrane and undergo the resting-to-desensitized state transition is extremely sensitive to the composition of its surrounding lipid membrane. Previous studies suggest that the nAChR requires an optimal membrane fluidity as well as the presence of both a neutral lipid, such as cholesterol (Chol), and an anionic lipid, such as dioleoylphosphatidic acid (DOPA) to retain optimal flux and desensitization capabilities (141-145). In the absence of Chol and DOPA, the nAChR appears to adopt a channel-inactive conformation that is believed to be analogous to the agonist-induced desensitized state (143).

Although the effects of lipids on nAChR function have been well characterized, the lipid-induced changes in nAChR structure that generate these modulations in function are poorly understood. The functional requirement of the nAChR for neutral and anionic lipids has been attributed to the binding of each lipid to discrete sites at, or near, the protein-lipid interface with distinct effects on the receptor's gross secondary structure (146-149). Others have reported more dramatic alterations in the content of both α-helix and β-sheet with increasing levels of Chol in reconstituted neutral lipid-depleted soybean asolectin membranes (150). In contrast, an FTIR and hydrogen/deuterium ($^1H/^2H$) exchange study was unable to detect any definitive lipid-dependent alterations in nAChR secondary structure suggesting that both neutral and anionic lipids modulate nAChR function through subtle, but as yet unidentified, changes in nAChR structure (151).

The objective of this study was to exploit the structural sensitivity of FTIR difference spectroscopy to investigate the effects of both neutral and anionic lipids on the structure of the nAChR. The results suggest that the nAChR reconstituted into a membrane composed solely of egg phosphatidylcholine (EPC) is stabilized in a conformation similar to that stabilized by the local anesthetic, dibucaine, and one that is likely analogous to the agonist-induced desensitized state. The addition of a variety of neutral and/or anionic lipids to the EPC membrane all induce an essentially identical pattern of structural changes in the nAChR suggesting that both neutral and anionic lipids act to stabilize the receptor in an equivalent resting conformation. The proportion of receptors adopting either the resting or desensitized state, however, is dependent upon the final lipid composition of the reconstituted membrane. A lipid-dependent modulation of the equilibrium between the channel-competent resting and channel-inactive desensitized state is proposed to account for the effects of a variety of different lipids on the ion flux capabilities of the nAChR.

EXPERIMENTAL PROCEDURES

Preparation of Crude nAChR-Enriched Membrane Fraction. A crude nAChR-enriched membrane fraction was prepared from *Torpedo californica* electroplaques (Marinus; Long Beach, CA) as described by Ochoa *et al.* (141) with modifications (143). All steps were performed at 4 °C. Approximately 500 g of frozen electroplaques were

partially thawed, sliced into 2-4 cm^2 portions and added to 500 ml of homogenization buffer (10 mM Na_2HPO_4, 5 mM EDTA, 5 mM EGTA, 0.25 mM PMSF, 11 mM iodoacetamide and 0.2% NaN_3, pH 7.4). The electroplaques were then homogenized in a Waring blender using 3 x 30 second bursts. The resulting homogenate was centrifuged for 10 minutes at 5000 rpm in a Sorvall (model RC2-B) centrifuge and the supernatant collected after filtering through two layers of cheesecloth. The pellets were re-homogenized in 250 ml of homogenization buffer using a Brinkman Polytron and centrifuged as described above. The pooled supernatants were then centrifuged for 3.5 hours at 14000 rpm and the supernatant discarded. The crudely purified nAChR pellets were re-suspended in dialysis buffer (1 mM NaCl, 50 mM Na_2HPO_4, 1 mM EDTA and 0.2% NaN_3, pH 7.8) to a final volume of 50 ml, further dispersed using a 55 ml Wheaton hand homogenizer, and stored at –80 °C.

Synthesis of Bromoacetylcholine Chloride. For the affinity purification of the nAChR, bromoacetylcholine chloride (BAC) was used to derivatize Bio-Rad Affi-Gel 102 (Bio-Rad, Richmond, CA). BAC was synthesized according to Damle *et al.* (82). Over a period of 40 minutes, 0.15 moles of bromoacetyl chloride was added dropwise to 0.1 moles of choline bromide and the resulting mixture cooled in an ice bath for 1.5 hours. 75 ml of absolute ethanol was then added slowly over a period of 30 minutes and the resulting white precipitate (BAC) filtered using a Buchner funnel. BAC was re-crystallized twice using 200 ml of isopropanol, dried under vacuum overnight and stored at –20 °C.

Preparation of Bromoacetylcholine Affinity Column. The nAChR was affinity purified using a bromoacetylcholine column prepared as described by Ellena *et al.* (152). 20 ml (packed volume) of Affi-Gel 102 was added to 20 ml of thiolactone solution (1.44 M N-acetyl-DL-homocysteine thiolactone and 1 M $NaHCO_3$) and the pH adjusted to 9.7. This mixture was then left to stir overnight at 4 °C. The following morning, the gel was washed with 1 L of cold 0.1 M NaCl solution and re-suspended in 20 ml of DTT solution [0.2 M dithiothreitol and 0.2 mM tris(hydroxymethyl)aminomethane (Tris), pH 8.0]. The gel was stirred gently for 30 minutes, transferred to a 2.5 x 40 cm glass column (Amersham Pharmacia Biotech, Piscataway, NJ) and the DTT solution drained. 20 ml of fresh DTT solution was then added to the gel and the column agitated for 30 minutes. The DTT solution was again drained and the gel washed with 140 ml of buffer B (100 mM NaCl, 20 mM Na_2HPO_4, 0.02% NaN_3, pH 7.0). After re-suspending the gel in 15 ml of 50 mM Na_2HPO_4 buffer (pH 7.0), 0.4 g of BAC was added and the column agitated for 1 hour. The gel was then washed with 80 ml of buffer B, re-suspended in 15 ml of buffer B containing 0.14 g of iodoacetamide and the column again agitated for 20 minutes. The column was drained and the gel washed with 60 ml of unbuffered 0.2% NaN_3 solution. The column was then stored at 4°C until use.

Affinity Purification and Reconstitution of the nAChR. All steps were carried out at 4 °C. 20 ml of the crude nAChR-enriched membrane fraction was thawed and diluted with dialysis buffer to a final protein concentration of 4 mg/ml. To this was added an equal volume of dialysis buffer containing 2% cholate. The mixture was gently stirred

for 1 hour and then centrifuged at 35000 rpm for 1 hour using a Beckman (model L8-55M) ultracentrifuge. The supernatant, comprising cholate-solubilized nAChR, was applied to the bromoacetylcholine affinity column following a pre-wash of 60 ml of dialysis buffer. The column flow rate during this and all remaining steps was ~1.5 ml/minute.

To reconstitute the nAChR into different lipid mixtures, the affinity column was washed with the lipids of choice (Avanti Polar Lipids, Alabaster, AL). First, the column was washed with lipid solution B (80 ml dialysis buffer, 1.16 mM lipids and 1% cholate) to remove contaminating proteins. The column was then washed with lipid solution A (60 ml dialysis buffer, 2.85 mM lipids and 1% cholate) to exchange native lipids with defined lipids. Following this, the column was washed with lipid solution C (50 ml dialysis buffer, 0.116 mM lipids and 1% cholate) to lower the final lipid-to-protein ratio.

The nAChR was eluted from the affinity column using lipid solution D (10 mM Carb, 10 mM Na_2HPO_4, 50 mM NaCl, 0.1 mM EDTA, 0.02% NaN_3, 0.116 mM lipids and 0.5% cholate, pH 7.8). 3 ml fractions were collected and those with an absorbance greater than 0.05 a.u. at 280 nm were combined. The affinity purified nAChR solution was then placed in membrane tubing (molecular weight cut-off 12-14 kDa; Spectrum Laboratories, Gardena, CA) and dialyzed against 2 L of dialysis buffer. The dialysis buffer was changed four times, once every 12 hours, to ensure complete removal of both Carb and cholate and to reconstitute the nAChR into the defined lipids. Following dialysis, the purified nAChR was centrifuged for 2 hours at 41000 rpm, again using the

Beckman (model L8-55M) ultracentrifuge. The pellet was re-suspended in 1 ml phosphate buffer (1.2 mM NaH_2PO_4, 0.8 mM Na_2HPO_4, 0.02% NaN_3, pH 8.0) and further dispersed using a small glass hand homogenizer. Protein concentration was estimated by the method of Lowry *et al.* (153) as modified by Hartree (154) using bovine serum albumin as the standard and lipid solution D as the blank. The reconstituted nAChR was then separated into 250 μg aliquots and stored at –80 °C.

FTIR Difference Spectroscopy. FTIR samples were prepared by spreading 250 μg of the affinity purified nAChR on the surface of a 50 x 20 x 2 mm (length x width x depth) germanium IRE (Harrick, Ossining, NY). After evaporating the bulk solvent with a gentle stream of N_2 gas, the germanium IRE was installed in an ATR liquid sample cell (also from Harrick) and the nAChR film rehydrated with excess Torpedo Ringer buffer (250 mM NaCl, 5 mM KCl, 2 mM $MgCl_2$, 3 mM $CaCl_2$ and 20 mM Tris, pH 7.0). FTIR spectra of the nAChR film were then acquired using the ATR technique on either an FTS-40 or FTS-575 spectrometer (Bio-Rad, Cambridge, MA) equipped with a deuterated triglycine sulfate detector. Spectra were recorded at 8 cm^{-1} resolution using 512 scans each, which required roughly seven minutes per spectrum. For the difference measurements, two consecutive spectra of the nAChR in the resting state were recorded while flowing Torpedo Ringer buffer continuously through the sample compartment of the ATR cell at a rate of ~1.5 ml/min. The flowing buffer was then switched to an identical one containing 50 μM Carb. After one minute, a spectrum was recorded of the nAChR in the desensitized state. The difference between both the two resting state

spectra (referred to as a control spectrum) and the consecutive resting and desensitized state spectra (referred to as a Carb-difference spectrum) were calculated, stored and the flowing solution switched back to buffer without Carb. After a 20 minute washing period to remove Carb from the film and to convert the nAChR back into the resting conformation, the process was repeated several times and the individual Carb-difference spectra averaged to increase the signal-to-noise ratio. Each Carb-difference spectrum presented is an average of 30-90 spectra recorded from at least two separate affinity purifications and reconstitutions of the nAChR. All spectra were normalized by comparing the intensity of those bands that reflect the vibrations of nAChR-bound Carb.

Dibucaine Solution Spectrum. An absorbance spectrum of dibucaine (50 mM) in Torpedo Ringer buffer (pH 7.0) was recorded using the ATR technique. The spectrum is an average of 250 scans acquired at a resolution of 2 cm^{-1}. The overlapping absorbance bands of the buffer were subtracted.

RESULTS

Carb-difference spectra recorded from the nAChR reconstituted into a lipid membrane composed of EPC/DOPA/Chol (molar ratio 3:1:1) reveal a complex, yet highly reproducible pattern of positive and negative vibrational bands (Figure 3.1, top trace). Since an EPC/DOPA/Chol membrane has been shown previously to support a fully functional nAChR that is capable of undergoing both agonist-induced cation flux

Figure 3.1 A comparison of Carb-difference spectra recorded from affinity purified nAChR reconstituted into membranes composed of EPC/DOPA/Chol (3:1:1), EPC/DOPA (3:1), EPC/Chol (3:1) and EPC. The removal of either DOPA, Chol or both lipids from the reconstituted membrane results in a decrease in vibrational band intensity near 1740, 1663, 1655, 1547, 1430 and 1059 cm^{-1}. Note that it is a decrease in the intensity of a positive band near 1663 cm^{-1} that gives rise to the apparent increase in intensity of the overlapping negative band near 1668 cm^{-1}.

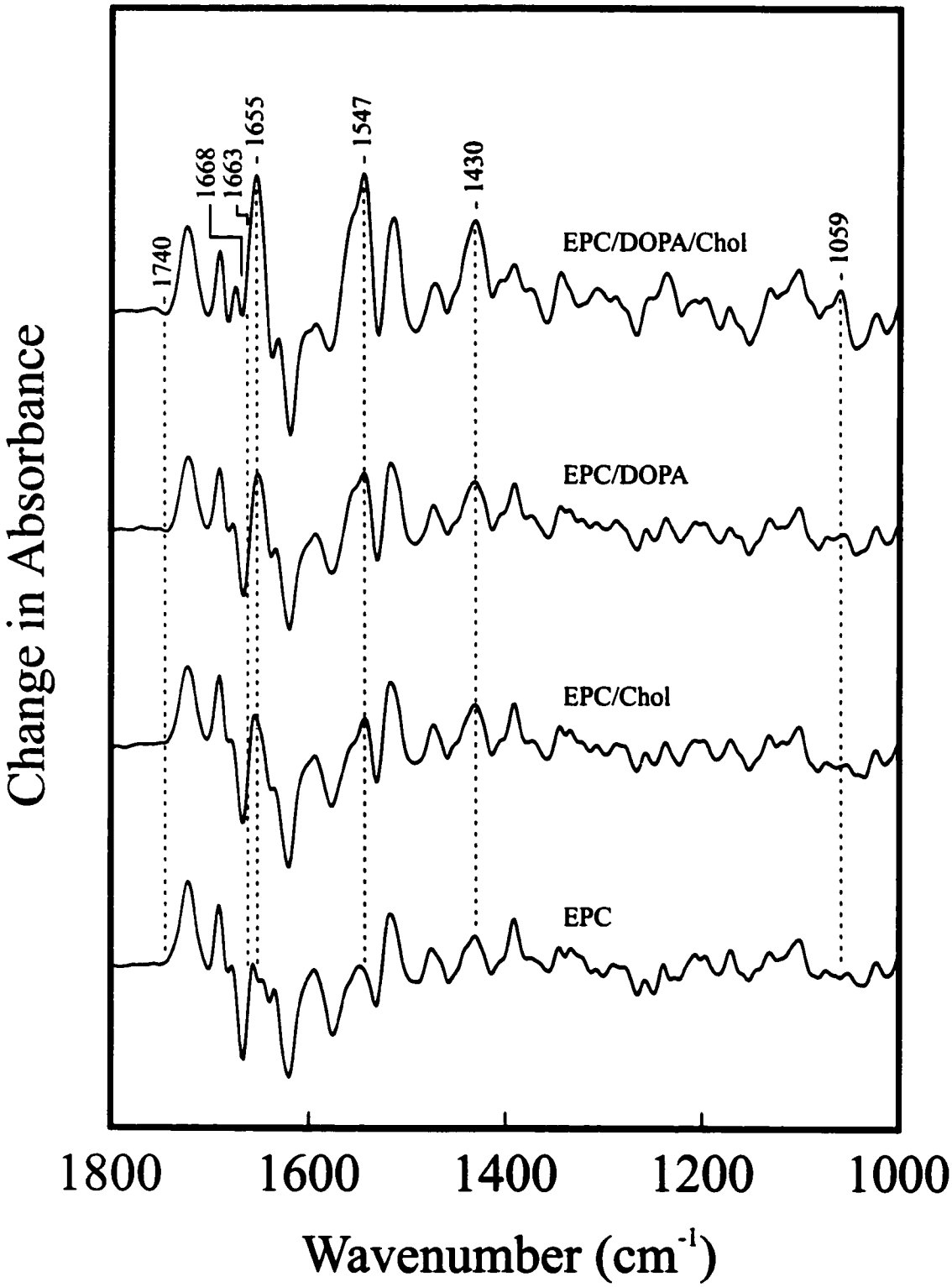
Change in Absorbance
1740
1668
1663
1655
1547
1430
1059
EPC/DOPA/Chol
EPC/DOPA
EPC/Chol
EPC
1800
1600
1400
1200
1000
Wavenumber (cm-1)

and the conformational transition from the resting to the desensitized state, these bands provide a *'spectral map'* of the structural changes that occur in the nAChR upon Carb binding and subsequent desensitization (129, 142, 143, 151). Note that the specificity of the vibrational bands to Carb-induced structural changes in the nAChR is also supported by both the absence of positive and negative bands in control Carb-difference spectra recorded from identical nAChR samples that have been pre-treated with the essentially irreversible competitive antagonist, α-btx, and the increasing intensity of the bands in Carb-difference spectra recorded from samples with increasing levels of nAChR purity (129, 155).

Addition of Chol and DOPA to EPC Membranes. To examine the effects of both Chol and DOPA on the structure of the nAChR, Carb-difference spectra were recorded from the nAChR reconstituted into either EPC/DOPA (3:1), EPC/Chol (3:1) or simply EPC membranes and compared to those recorded from the nAChR in EPC/DOPA/Chol (Figure 3.1). In general, both the frequencies and relative intensity of the majority of the bands in each spectrum are similar suggesting that neither Chol nor DOPA dramatically affect the structures and/or environments surrounding a large number of residues involved in both Carb binding and receptor desensitization. Closer inspection, however, reveals subtle variations in the intensity of six bands near 1740, 1663, 1655, 1547, 1430 and 1059 cm^{-1} that reflect lipid-induced changes in the structure of the nAChR that are likely responsible for modulations in nAChR function. Note that it is a decrease in the intensity

of a positive band near 1663 cm^{-1} that gives rise to the apparent increase in intensity of the overlapping negative band near 1668 cm^{-1} (see Chapter 5, Figure 5.5).

The lipid-sensitive bands near 1663, 1655 and 1547 cm^{-1} occur in either the amide I (1600-1700 cm^{-1}) or amide II (1520-1580 cm^{-1}) regions of the infrared spectrum. Bands within these regions arise largely from variations in the molecular vibrations of the amide group of the peptide bond and thus likely reflect a subtle lipid-induced change in the conformation of the receptor's polypeptide backbone. The assignment of these three bands to either amide I or amide II vibrations is consistent with the observed down shift in the frequency of these bands upon exposure of the nAChR to ^2H_2O (129). The other lipid-sensitive bands near 1740, 1430,and 1059 cm^{-1} could reflect either a lipid-induced change in the structure and/or environment surrounding amino acid side chains or possibly an alteration in the interactions between the nAChR and a 'bound' phospholipid (see Discussion).

Although a detailed interpretation of the individual band intensity variations is not yet possible, it is noteworthy that the absence of either Chol, DOPA, or both lipids each leads to a decrease in intensity near 1740, 1663, 1655, 1547, 1430 and 1059 cm^{-1}. The striking reproducibility of the *pattern* of band intensity variations suggests that the absence (and conversely the presence) of either or both lipids leads to a similar change in the structure of those residues within the nAChR that are involved in Carb binding and desensitization. The reproducibility of the spectral variations also suggests that both Chol and DOPA stabilize an equivalent conformational state of the nAChR.

In contrast, the relative magnitude of the intensity variations, and thus the degree of the conformational perturbation, appear to be dependent upon the final lipid composition of the reconstituted membrane. Relative to EPC/DOPA/Chol membranes, the variations in the intensity of all six bands are minimal for the nAChR in EPC/DOPA, slightly more substantial for the nAChR in EPC/Chol and relatively dramatic for the nAChR in EPC, where both the negative and positive bands near 1740, 1663, 1655 and 1059 cm^{-1} are completely absent and the two positive bands near 1547 cm^{-1} and 1430 cm^{-1} are both reduced in intensity by more than 50%. The differing magnitude of the variations in intensity of all six bands suggest that the structure of the nAChR is increasingly perturbed from a predominantly resting conformation in EPC/DOPA/Chol to an alternative, possibly desensitized conformation in EPC/DOPA, EPC/Chol, and EPC (see below). Chol and DOPA may, therefore, differ in their relative ability to stabilize the nAChR in a channel-competent resting conformation as opposed to their ability to stabilize the nAChR in distinct conformational states.

Asolectin, EPC/DOPS and EPC/Squalene Membranes. The possibility that diverse lipid structures stabilize an equivalent conformation of the nAChR was examined further by recording Carb-difference spectra from the nAChR reconstituted into soybean asolectin, EPC/dioleoylphosphatidylserine (DOPS) (3:1), and EPC/squalene (3:1) membranes (Figure 3.2). Asolectin is a complex mixture of neutral, anionic, and zwitterionic lipids whereas DOPS is an anionic lipid with a much larger head group than DOPA and squalene is a neutral isoprenoid polyene lipid with little structural

Figure 3.2 A comparison of Carb-difference spectra recorded from affinity purified nAChR reconstituted into membranes composed of EPC/DOPA/Chol (3:1:1), asolectin, EPC/squalene (3:1) and EPC/DOPS (3:1). Carb-difference spectra recorded from the nAChR reconstituted into asolectin membranes are essentially identical to those recorded from the nAChR reconstituted into EPC/DOPA/Chol suggesting a similar structure of the nAChR and resting-to-desensitized conformational transition. Reconstitution of the nAChR into EPC/squalene or EPC/DOPS membranes, however, reveal a similar pattern of band intensity variations, near 1740, 1663, 1655, 1547, 1430 and 1059 cm^{-1}, as that observed from the nAChR reconstituted into EPC/DOPA, EPC/Chol, or EPC membranes.

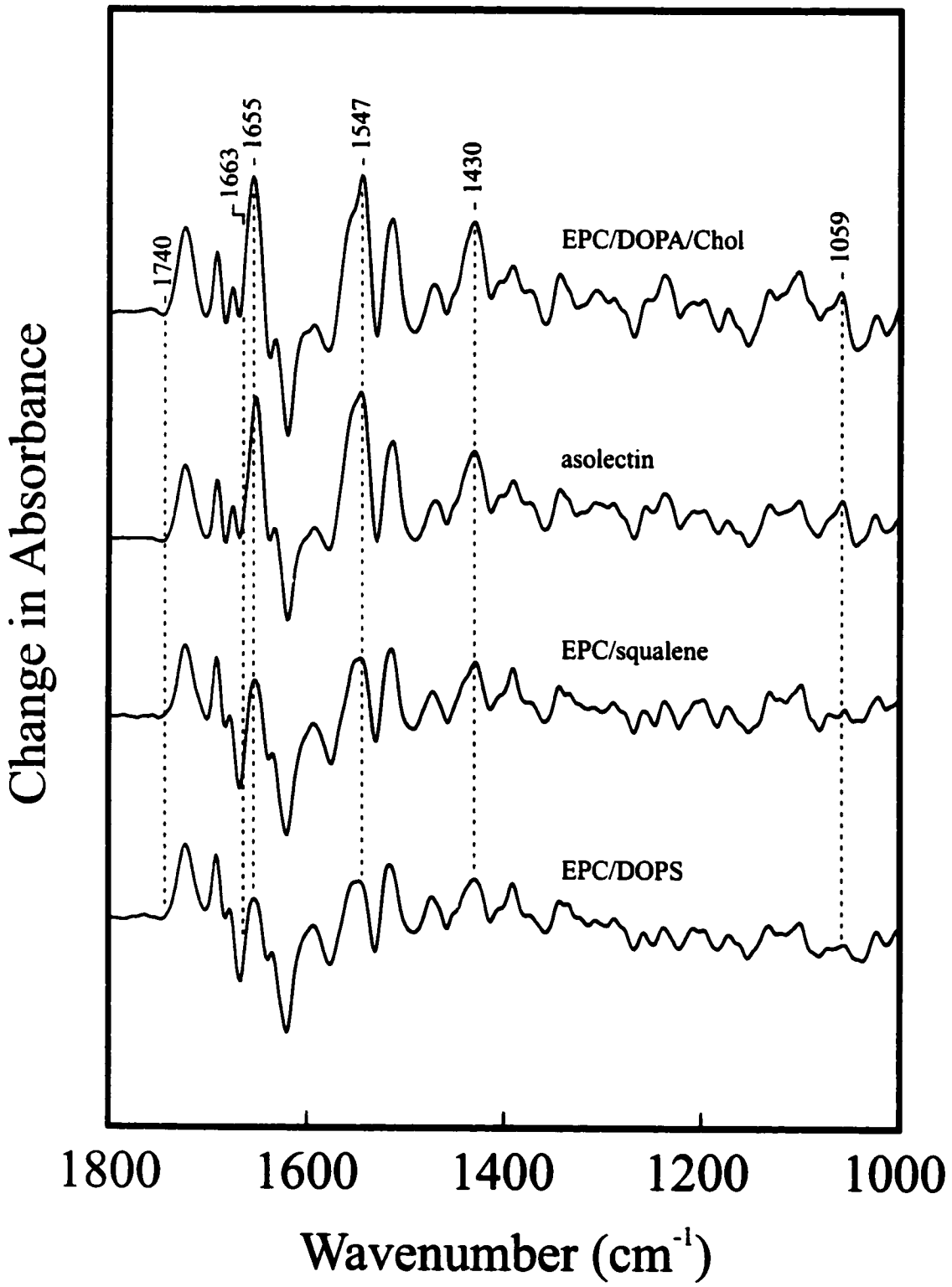
1740
1663
1655
1547
1430
1059
EPC/DOPA/Chol
asolectin
EPC/squalene
EPC/DOPS
Change in Absorbance
1800
1600
1400
1200
1000
Wavenumber (cm-1)

resemblance to either DOPA, DOPS or Chol. Carb-difference spectra recorded from the nAChR reconstituted into asolectin membranes are similar to those recorded from the nAChR in EPC/DOPA/Chol suggesting a similar structure of the nAChR and resting-to-desensitized conformational transition. Carb-difference spectra recorded from the nAChR in both EPC/DOPS and EPC/squalene, however, exhibit the same pattern of band intensity variations, near 1740, 1663, 1655, 1547, 1430 and 1059 cm^{-1}, as observed from the nAChR reconstituted into either EPC/DOPA, EPC/Chol or EPC. In addition, the magnitude of these variations is less in EPC/squalene than in EPC/DOPS suggesting that squalene is slightly more efficient than DOPS at stabilizing the nAChR in the resting conformation. The similarity of the pattern of band intensity variations observed in Carb-difference spectra recorded from the nAChR in EPC/Chol, EPC/DOPA, EPC/DOPS, and EPC/squalene relative to the Carb-difference spectra recorded from the nAChR in EPC strongly suggests that Chol, DOPA, DOPS, and squalene all stabilize the nAChR in an equivalent resting conformation.

Dibucaine-Induced Changes in nAChR Structure. There is some evidence suggesting that the nAChR is stabilized in a desensitized conformation in EPC membranes lacking both neutral and anionic lipids (143). This possibility implies that Carb-difference spectra recorded from the nAChR in EPC membranes will reflect only those changes in the structure and/or environment of individual residues within the nAChR that arise as a consequence of Carb binding to a predominantly desensitized population of receptors. To test this possibility, Carb-difference spectra were recorded

from the nAChR reconstituted into EPC/DOPA/Chol, but while continuously maintaining the receptor in contact with increasing concentrations of the desensitizing local anesthetic, dibucaine [i.e. dibucaine is included in both the plus Carb and minus Carb buffers (see Chapter 2, Figure 2.8, buffers i and ii)]. Dibucaine belongs to a class of structurally diverse compounds that bind to the nAChR at a distinct allosteric non-competitive blocker site located within the ion channel pore. Although exceptions exist, most of these compounds appear to modulate nAChR function by both sterically blocking the receptor's ion channel and stabilizing the receptor in the desensitized state (Figure 3.3, scheme i). Increasing concentrations of dibucaine lead to dose-dependent variations in the intensity of a number of bands including the same six bands noted above, near 1740, 1663, 1655, 1547, 1430 and 1059 cm^{-1}, that are sensitive to the absence of neutral and anionic lipids from the reconstituted membrane (Figure 3.4). The striking similarity of the subtle variations in the Carb-difference spectra (other variations are discussed below) suggest that both the presence of dibucaine and reconstitution of the nAChR into EPC membranes lacking neutral and/or anionic lipids lead to the stabilization of the same desensitized conformation (Figure 3.5).

Note that the dibucaine-induced variations in the Carb-difference spectra saturate at concentrations near 200 μM. This is consistent with earlier studies that report a dissociation constant for dibucaine near 30 μM (in the absence of Carb) when binding to the non-competitive blocker site of the nAChR reconstituted into EPC/DOPA/Chol membranes (this value is near 80 μM for the nAChR in native membranes) (156, 157).

Figure 3.3 Schematic diagram illustrating the structural changes observed in Carb-difference spectra recorded from the nAChR reconstituted into EPC/DOPA/Chol membranes, but while continuously maintaining the receptor in contact with increasing concentrations of the desensitizing local anesthetic, dibucaine. The dissociation constants for dibucaine binding to the non-competitive blocker site (in the absence of Carb) and the neurotransmitter binding sites are near 30 μM and 60 μM, respectively (156, 157). Low concentrations of dibucaine, where binding occurs predominantly to the non-competitive blocker site, are believed to induce a shift in the conformational equilibrium of the nAChR towards the desensitized state (scheme i). Higher concentrations of dibucaine, however, result in the additional binding to the neurotransmitter binding sites (scheme ii). In this situation, the addition of Carb causes the displacement of dibucaine from the neurotransmitter binding sites, and consequently, the appearance of negative dibucaine vibrational bands in the Carb-difference spectrum (scheme iii).

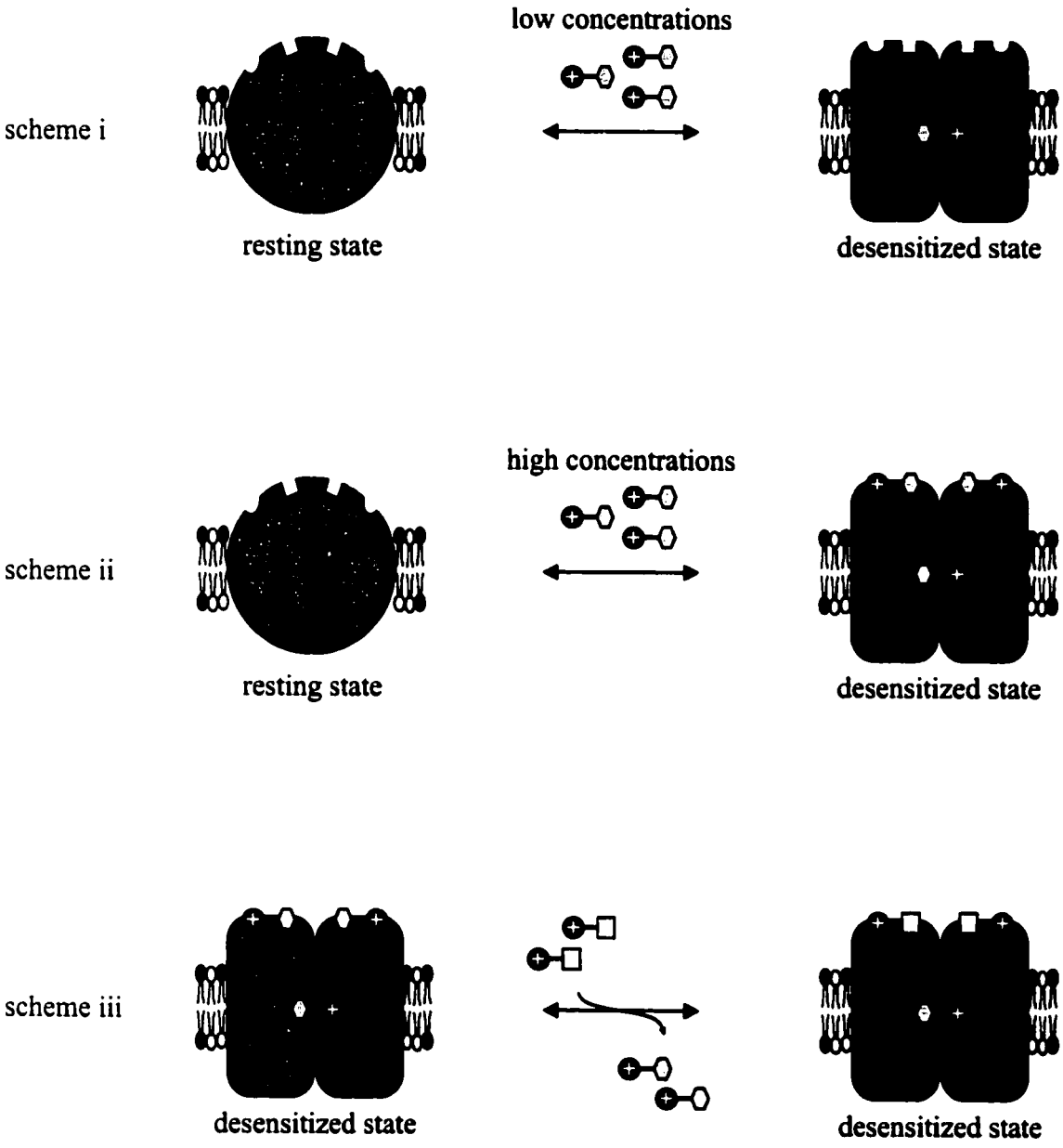
scheme i
low concentrations
resting state
desensitized state
scheme ii
high concentrations
resting state
desensitized state
scheme iii
desensitized state
desensitized state
dibucaine
carbamylcholine

Figure 3.4 A comparison of Carb-difference spectra recorded from affinity purified nAChR reconstituted into membranes composed of EPC/DOPA/Chol (3:1:1), but while continuously maintaining the receptor in contact with increasing concentrations of the desensitizing local anesthetic, dibucaine. Increasing concentrations of dibucaine lead to dose-dependent variations in the intensity of a number of bands including the same six bands, near 1740, 1663, 1655, 1547, 1430 and 1059 cm^{-1}, that are sensitive to the absence of neutral and anionic lipids from the reconstituted membrane.

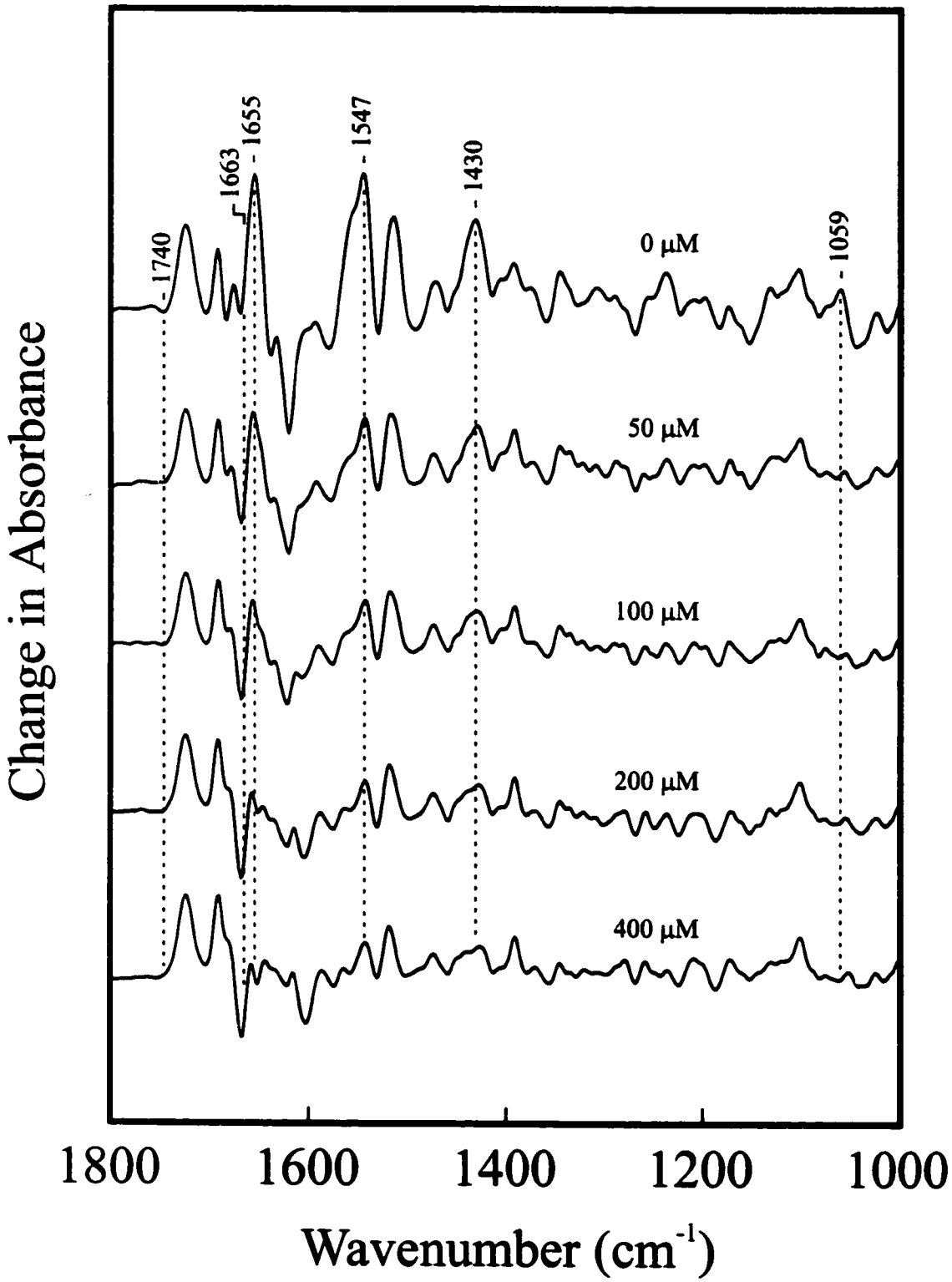
Change in Absorbance
1740
1663
1655
1547
1430
1059
0 μM
50 μM
100 μM
200 μM
400 μM
1800
1600
1400
1200
1000
Wavenumber (cm-1)

Figure 3.5 A comparison of Carb-difference spectra recorded from affinity purified nAChR reconstituted into membranes composed of EPC/DOPA/Chol (3:1:1), EPC and EPC/DOPA/Chol (3:1:1), but while continuously maintaining the receptor in contact with 200 μM dibucaine. The bottom trace is an absorbance spectrum recorded from a 50 mM aqueous solution of dibucaine (the overlapping absorbance bands of the buffer have been subtracted). The blue dashed lines identify negative vibrational bands that arise due to the displacement of dibucaine from the neurotransmitter binding sites upon the addition of Carb.

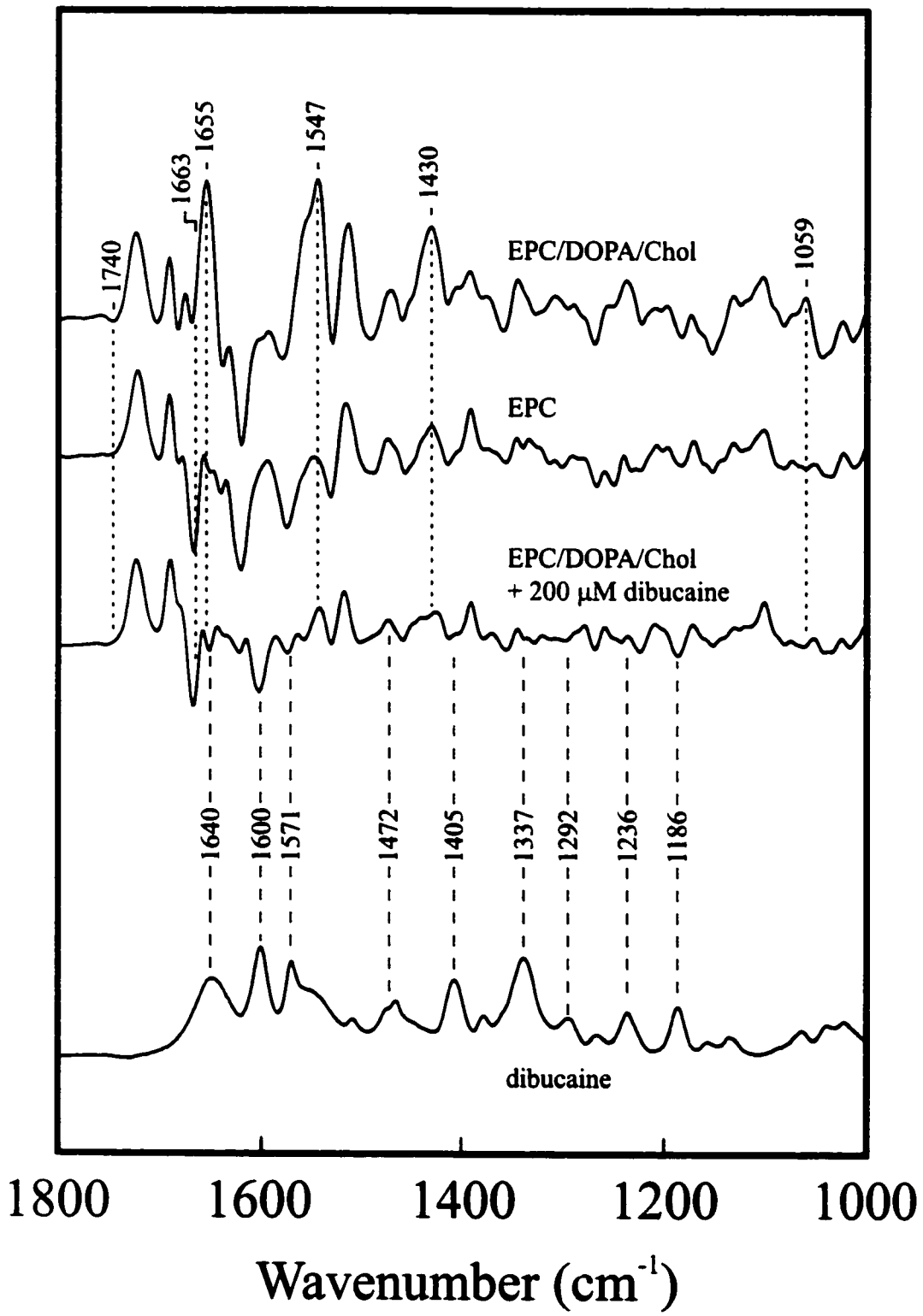
1740
1663
1655
1547
1430
1059
EPC/DOPA/Chol
EPC
EPC/DOPA/Chol
+ 200 μM dibucaine
1640
1600
1571
1472
1405
1337
1292
1236
1186
dibucaine
1800
1600
1400
1200
1000
Wavenumber (cm-1)

The Carb-difference spectra also exhibit a dose-dependent increase in negative band intensity at frequencies that correspond to the frequencies of vibrational bands observed in the solution spectrum of dibucaine itself (Figure 3.5). The latter is consistent with the additional binding of dibucaine to the nAChR's neurotransmitter binding sites (K_D near 60 μM for the nAChR in native membranes) and its subsequent displacement upon the addition of Carb (Figure 3.3, schemes ii and iii) (156).

DISCUSSION

In this study it is shown that the structural changes that occur within the nAChR upon Carb binding and subsequent desensitization are sensitive to both the composition of the lipid membrane that surrounds the nAChR and the presence of a local anesthetic, dibucaine. The lipid- and anesthetic-induced variations in the Carb-difference spectra suggest subtle changes in the conformation and/or orientation of the polypeptide backbone as well as perturbations in the structure of individual amino acid side chains and/or possible modulations of the interactions between the nAChR and a 'bound' phospholipid (see below). Significantly, the pattern of the lipid-induced variations in the Carb-difference spectra correlate with the pattern of the effects of the lipids on both the ion flux properties and the conformational state of the nAChR, as probed using various biochemical techniques (this correlation is discussed below). In addition, the effects of the local anesthetic, dibucaine, on the nAChR are dose-dependent and saturate at

concentrations consistent with the measured dissociation constants for the binding of dibucaine to both the non-competitive blocker and neurotransmitter binding sites. This close correlation between the spectroscopic and biochemical data suggests that the lipid-induced variations detected in the Carb-difference spectra are reflecting changes in the structure of the nAChR that are related to lipid-dependent modulations of nAChR activity. Together, the data presented in this study suggest three important features regarding the mechanism of lipid action at the nAChR.

(i) The most striking feature is that Carb-difference spectra recorded from the nAChR in diverse reconstituted membranes all exhibit an essentially identical pattern of band intensity variations, near 1740, 1663, 1655, 1547, 1430 and 1059 cm^{-1}, relative to Carb-difference spectra recorded from the nAChR reconstituted into EPC/DOPA/Chol. In particular, the reproducibility of the pattern of variations induced in the Carb-difference spectra by the inclusion of either a neutral lipid, such as Chol or squalene, or an anionic lipid, such as DOPA or DOPS, in an EPC membrane suggests that Chol, squalene, DOPA, and DOPS all have an essentially identical effect on the structures and/or environments surrounding those residues of the nAChR that are involved in Carb binding and desensitization. Given the sensitivity of the FTIR difference technique to subtle changes in protein structure, the reproducibility of these spectral variations implies that Chol, squalene, DOPA, and DOPS each stabilize the nAChR in an essentially identical resting conformation.

(ii) The second feature is the similarity of the pattern of band intensity variations observed in Carb-difference spectra recorded from the nAChR reconstituted into EPC membranes and from the nAChR reconstituted into EPC/DOPA/Chol, but while continuously maintaining the nAChR in contact with increasing concentrations of the local anesthetic, dibucaine. This similarity suggests that both the absence of neutral and anionic lipids and the presence of dibucaine lead to the stabilization of the same conformational state. Previous studies suggest that the binding of dibucaine to the non-competitive blocker site leads to the stabilization of a desensitized receptor (158, 159). Although the effects of dibucaine on nAChR function have been investigated primarily using receptors within their native membrane, the nAChR in EPC/DOPA/Chol retains the ability to conduct cations and undergoes an essentially identical resting-to-desensitized conformational change as judged by the similarity of the Carb-difference spectra recorded from the nAChR in native and EPC/DOPA/Chol membranes as well as other biochemical assays (127, 128, 141-144, 151, 155). In addition, as noted previously, the dibucaine-induced variations in the Carb-difference spectra saturate at concentrations consistent with the pharmacological properties of dibucaine at the nAChR (156). In all respects, the nAChR appears to be functional in EPC/DOPA/Chol and should respond to dibucaine by adopting a channel-inactive desensitized state. The absence of both neutral and anionic lipids from a reconstituted membrane thus appears to lead to the stabilization of a desensitized receptor.

(iii) The third feature is the magnitude of the band intensity variations observed in Carb-difference spectra recorded from the nAChR reconstituted into diverse lipid membranes. Although the pattern of band intensity variations is essentially the same in Carb-difference spectra recorded from the nAChR reconstituted into EPC membranes lacking neutral, anionic, or both types of lipids, the magnitude of these spectral variations differ according to the final lipid composition of the reconstituted membrane. This suggests a lipid-dependent modulation in the population of receptors found in the resting and desensitized states. Within Carb-difference spectra recorded from the nAChR reconstituted into EPC/DOPA/Chol or asolectin membranes, the variations in band intensity indicative of desensitization (i.e. a reduction in band intensity near 1740, 1663, 1655, 1547, 1430 and 1059 cm^{-1}) are minimal suggesting that membranes containing neutral, anionic, and zwitterionic lipids stabilize the majority of receptors in the resting conformation. The spectral variations, however, are slightly more intense in Carb-difference spectra recorded from the nAChR in EPC membranes with only a neutral or an anionic lipid, and are relatively dramatic in EPC membranes lacking both types of lipids. Within the four binary mixtures of lipids, there are also slight differences in the magnitude of the band intensity variations suggesting an increasing shift towards the desensitized state in the following order: EPC/DOPA → EPC/squalene → EPC/DOPS → EPC/Chol. While the nature of the conformational perturbation induced by the absence (or presence) of neutral and anionic lipids may be the same, the various lipid membranes

appear to differ in their relative ability to stabilize the nAChR in the resting conformation.

The results of this study suggest that when reconstituted into an EPC membrane void of both neutral and anionic lipids, the nAChR is stabilized predominantly in the desensitized state. Such a proposal is consistent with both the labeling pattern of the nAChR in EPC by the conformationally sensitive probe, 3-trifluoromethyl-3-(*m*-[^{125}I]iodophenyl)diazirine (^{125}I-TID) and the inability of the receptor within EPC membranes to either conduct cations across the membrane or undergo the resting-to-desensitized state transition (142, 143). A gradual increase in the proportion of receptors in the desensitized conformation in membranes with varying lipid compositions is also consistent with both ^{125}I-TID labeling and the relative ion flux responses of the nAChR in the different lipid membranes, although the latter types of experiments are usually interpreted in terms of the stabilization of either a channel-active or -inactive conformation. ^{125}I-TID labeling indicates that the nAChR in EPC/Chol adopts a conformation similar to that observed in EPC, whereas in EPC/DOPA the conformation resembles more closely that observed in both EPC/DOPA/Chol and native membranes (143). Although usually treated as non-functional, the nAChR in either EPC/Chol or EPC/DOPS has limited ability to conduct cations whereas the ability of the receptor to undergo the agonist-induced conformational transition from the resting to the desensitized state is enhanced in EPC/DOPA (141, 142, 144). These results correlate with the relative magnitude of the variations in band intensity found in the Carb-difference spectra and

thus the increasing proportion of receptors found in a channel-inactive desensitized state versus a channel-competent resting state in EPC/DOPA, EPC/DOPS, EPC/Chol, and EPC membranes. The close correlation between the relative magnitude of the spectral variations in the Carb-difference spectra and the relative ion flux activity of the nAChR in different lipid membranes suggests that a perturbation of the equilibrium between the resting and desensitized states may be the predominant effect of lipids on the structure of the nAChR.

In contrast, it has been suggested that the functional requirement of the nAChR for neutral and anionic lipids stems from the binding of each lipid to discrete sites on the nAChR with distinct effects on the receptor's gross secondary structure. McNamee and co-workers have proposed that the rigid sterol ring of Chol may intercalate into the grooves of α-helices, thus stabilizing transmembrane α-helical secondary structures (148, 149). Similarly, they propose that the negatively charged head group of anionic lipids may form electrostatic interactions with extramembranous regions of the nAChR, thus leading to the stabilization of β-sheet. Others have reported even more dramatic alterations in the content of both α-helix and β-sheet in the nAChR with increasing levels of Chol in reconstituted neutral lipid-depleted soybean asolectin membranes (150).

However, several lines of evidence argue against lipid-induced stabilization of nAChR secondary structures. First, the lipid-induced changes in the intensity of bands in both the amide I and amide II regions of the Carb-difference spectra correspond to less than 0.1% of the total amide I and amide II band intensities, respectively, indicating that

the lipid-induced conformational perturbations involve relatively few amino acid residues (compare the relative intensity of the amide I and II bands in the absorbance spectra recorded from the nAChR in the resting or desensitized state with those in the Carb-difference spectrum depicted in Chapter 2, Figure 2.9A) (160). Second, the frequencies and relative intensity of the majority of the bands in the Carb-difference spectra are unaffected when the nAChR is reconstituted into EPC membranes lacking neutral and/or anionic lipids. Large changes in the content of either α-helix or β-sheet should lead to changes in the structure and/or environment of a large number of residues, especially in the case of a compact, highly cooperative protein such as the nAChR. In turn, these changes should lead to variations in the frequencies and relative intensity of a large number of bands in the Carb-difference spectra, which is clearly not the case. Finally, an FTIR and $^{1}H/^{2}H$ exchange study was unable to detect any definitive lipid-dependent alterations in nAChR secondary structure and attributed the lipid-induced variations reported by others to either a previously unappreciated dependence of the shape of the secondary structure sensitive amide I band to the time of exposure of the nAChR to $^{2}H_{2}O$ or to errors resulting from uncompensated water vapor (151, 161). Lipid-dependent modulation of nAChR function must, therefore, occur through subtle changes in receptor structure as opposed to through the stabilization of α-helix and/or β-sheet secondary structures.

If neutral and anionic lipids are not required for the stabilization of α-helix and β-sheet secondary structures, and alter nAChR function through similar changes in

structure, then alternate mechanisms are required to explain the apparent functional requirement of the nAChR for both lipids. One possibility is that diverse lipid structures influence the conformation of the nAChR (i.e. the equilibrium between the resting and desensitized states) through non-specific alterations in the physical properties of the lipid membrane. Chol has a well characterized ordering effect on lipid bilayers in the liquid-crystalline state. In addition, the very small head group of DOPA should lead to a condensation, and thus a restriction, in the amplitudes of motion of the fatty acyl chains resulting in a more ordered and less fluid lipid bilayer (162, 163). The presence of both lipids could, therefore, lead to a relatively ordered lipid membrane that might be required for maintaining the nAChR in a predominantly resting conformation. Conversely, the absence of either or both lipids could lead to a more fluid membrane that might increasingly enhance the formation of the desensitized state. This possibility would account for both the reduced ion flux capabilities and the more substantial band intensity variations detected in the Carb-difference spectra recorded from the nAChR in EPC/DOPS relative to the nAChR in EPC/DOPA (142, 144). DOPS has a larger head group than DOPA and thus may be unable to reduce the fluidity of an EPC membrane as efficiently as DOPA. Note also that the nAChR is stabilized in a high-affinity conformation (likely desensitized) in the presence of several detergents that disrupt the integrity and thus modulate the fluidity of the lipid membrane (143).

A potential role for membrane fluidity in modulating nAChR function has been suggested previously, although modulations in fluidity, as monitored using either spin-

labeled fatty acid or fluorescent probes, can not completely explain lipid-dependent modulation of nAChR activity (142, 145). The lack of a clear correlation between membrane fluidity and nAChR function, however, could reflect an inability to accurately characterize the complex structure and dynamics of a lipid bilayer by monitoring the motions of either a rigid fluorescent or spin-labeled probe. Such spectroscopic methods are generally sensitive to motions occurring within a limited time frame and thus may not provide a comprehensive description of the complex variations in membrane structure and dynamics brought about by changes in membrane lipid composition (164, 165).

A second possibility to explain the apparent functional requirement of the nAChR for both neutral and anionic lipids is that each lipid binds to distinct sites on the receptor, but that the main effect of these interactions is a modulation of the equilibrium between the resting and desensitized states, as opposed to the stabilization of specific secondary structures. The lipid-sensitive band in the Carb-difference spectrum near 1740 cm^{-1} could reflect a change in a phospholipid ester carbonyl stretching vibration upon the binding of Carb to the nAChR and subsequent desensitization. Carb-difference spectra recorded in ^2H_2O buffer show that this band does not down shift in frequency, consistent with its assignment to a lipid ester carbonyl (166). A possible change in the structure of a lipid upon the binding of Carb to the nAChR would imply a tight association between the phospholipid and the receptor. Note, however, that the lipid-induced variations in the intensity of the weak band near 1740 cm^{-1} must be interpreted with caution given the sensitivity of this band to baseline fluctuations.

CONCLUSIONS

The objective of this study was to investigate the effects of both neutral and anionic lipids on the structure of the nAChR. Carb-difference spectra recorded from the nAChR reconstituted into EPC/DOPA/Chol membranes reveal a number of positive and negative bands that reflect variations in the molecular vibrations, and thus structures, of individual amino acid residues within the nAChR that arise as a consequence of Carb binding and subsequent desensitization. A comparison of Carb-difference spectra recorded from the nAChR reconstituted into EPC/DOPA/Chol with those recorded from the nAChR reconstituted into EPC/DOPA, EPC/Chol, EPC/DOPS, EPC/squalene and EPC, reveal an essentially identical pattern of vibrational band intensity variations, near 1740, 1663, 1655, 1547, 1430 and 1059 cm^{-1}. Significantly, this same pattern of band intensity variations is observed in Carb-difference spectra recorded from the nAChR reconstituted into EPC/DOPA/Chol membranes, but while continuously maintaining the nAChR in contact with increasing concentrations of the desensitizing local anesthetic, dibucaine. The results suggest that the predominant effect of neutral and/or anionic lipids within a reconstituted membrane is to stabilize the nAChR in the resting conformation. Removal of either, or both types of lipids appears to induce a shift in the conformational equilibrium of the nAChR towards a predominantly desensitized population of receptors, with the magnitude of this shift being dependent upon the final lipid composition of the reconstituted membrane (Figure 3.6). Although the precise mechanism of lipid action is unclear, it is possible that both neutral and anionic lipids exert their effects on nAChR

Figure 3.6 Schematic diagram illustrating the proposed effects of both neutral and anionic lipids on the structure of the nAChR. In the absence of Carb, the nAChR exists within a conformational equilibrium between a channel-competent resting (~80%) and channel-inactive desensitized state (~20%) (scheme i). The removal of either neutral or anionic lipids induces a shift in this equilibrium towards the desensitized state, with the magnitude being dependent upon the final lipid composition of the reconstituted membrane (scheme ii). For those binary lipid mixtures investigated in this study, the population of receptors adopting the desensitized state appears to increase in the following order: EPC/DOPA→EPC/squalene→ EPC/DOPS→ EPC/Chol. Reconstitution of the nAChR into an EPC membrane void of both neutral and anionic lipids induces a further shift in the equilibrium to a predominantly desensitized population of receptors (scheme iii). Although the precise mechanism of lipid action is unclear, it is possible that both neutral and anionic lipids exert their effects on nAChR structure and function through modulations in the fluidity of the lipid membrane surrounding the receptor.

scheme i

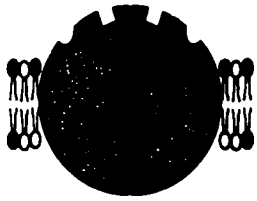

resting state (80%)

conformational equilibrium

desensitized state (20%)

scheme ii

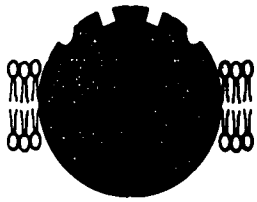

resting state

conformational equilibrium

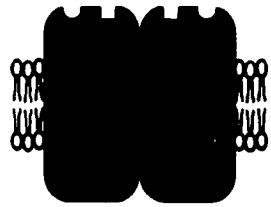

desensitized state

scheme iii

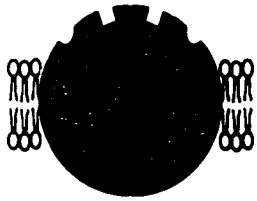

resting state

conformational equilibrium

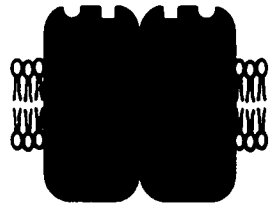

desensitized state

structure and function by modulating the fluidity of the lipid membrane surrounding the receptor.

Note that the results of this study also reveal that those vibrational bands within the Carb-difference spectrum near 1663, 1655, 1547, 1430 and 1059 cm^{-1} reflect structural changes in the nAChR that arise due to the conformational transition from the resting to the desensitized state (the 1740 cm^{-1} band is not included since it may represent a change in the structure of an nAChR-bound phospholipid). This, in turn, suggests that the remaining bands in the Carb-difference spectrum that have not been previously assigned to the vibrations of nAChR-bound Carb (see Chapter 2, Figure 2.10), must reflect structural changes in individual residues within the neurotransmitter binding sites that occur as a result of specific Carb-nAChR interactions.

CHAPTER 4

EFFECTS OF MEMBRANE LIPID COMPOSITION ON THE CONFORMATIONAL EQUILIBRIUM OF THE NICOTINIC ACETYLCHOLINE RECEPTOR

INTRODUCTION

Initial studies focussing on the effects of membrane lipid composition on the structure and function of the nAChR suggested that the receptor required the presence of both Chol and DOPA within its membrane environment in order to retain the ability to both conduct cations and undergo agonist-induced desensitization (142, 148). This functional requirement of the nAChR for both Chol and DOPA was attributed to both the formation of a lipid bilayer with optimal membrane fluidity and a specific structural requirement of the nAChR for each lipid. The latter was proposed to result from the binding of Chol and DOPA to distinct sites on the nAChR with the consequent formation of specific secondary structural features (147-150).

Subsequent work, however, has led to contradictory conclusions regarding the additional lipids that are required within the nAChR's membrane environment for the receptor to adopt a fully functional resting conformation. Based on chemical-labeling and α-btx rate-binding studies, McCarthy and Moore (143) proposed that anionic lipids, such as DOPA, are sufficient within an EPC membrane to stabilize the nAChR in a functional resting conformation. Their work also found that when reconstituted into membranes composed of either EPC/Chol or EPC alone, the nAChR adopts a predominantly desensitized conformation. In contrast, the binding kinetics of the structurally-sensitive fluorescent probe, ethidium bromide, led Rankin *et al.* (167) to suggest that mixtures of dioleoylphosphatidylcholine (DOPC)/Chol support a functional nAChR whereas in either DOPC/DOPA or DOPC alone, the nAChR is essentially 'locked' in the resting

conformation. Carb-difference spectra are consistent with the data of McCarthy and Moore (143) in that they suggest that the nAChR in EPC alone is desensitized. Contrary to both studies, however, Carb-difference spectra also show that the presence of small amounts of either neutral (Chol or squalene) or anionic (DOPA or DOPS) lipids in an EPC membrane is sufficient to stabilize a fraction of the nAChRs in a functional resting conformation that is capable of undergoing agonist-induced desensitization. This led to the proposal that lipids modulate the relative number of nAChRs in the resting and desensitized states in the absence of agonist. The apparent ability of a variety of structurally diverse neutral and anionic lipids to modulate the equilibrium between the resting and desensitized states suggested further that lipids influence the conformational equilibrium of the nAChR through an indirect effect on some physical property of the membrane.

The contradictory conclusions in the literature regarding the specific lipid requirements of the nAChR may reflect a variety of factors including the fact that the functional status of the receptor in most studies has been assessed in reconstituted DOPC or EPC membranes with the additional lipid of interest found at only a single molar percentage of the total membrane lipids (usually 25% or less). In many cases, the functional data have also been interpreted in terms of the stabilization of either a fully functional resting or a non-functional desensitized conformation. Both approaches, however, ignore the possibility that lipids modulate the equilibrium between different, and as yet unidentified, conformational states. The relative level of a given lipid in a

reconstituted phosphatidylcholine membrane may be an important factor in determining the relative percentage of nAChRs stabilized in a functional conformation and/or the kinetics of the nAChR conformational change.

To both gain a more conclusive picture of the specific lipid requirements of the nAChR and to test the above noted hypothesis regarding a lipid-dependent modulation of the conformational equilibrium of the receptor, the objective of this study was to examine the ability of the nAChR to undergo the agonist-induced resting-to-desensitized conformational transition in EPC membranes with varying levels of either DOPA or Chol. The results indicate that increasing levels of either lipid in an EPC membrane increasingly stabilizes a larger proportion of nAChRs in a conformation(s) that is(are) capable of undergoing agonist-induced desensitization. However, only high levels of DOPA were found to stabilize a structure of the nAChR that is fully equivalent to that found in native and EPC/DOPA/Chol membranes. This suggests that the presence of either DOPA or Chol in a reconstituted EPC membrane can influence the equilibrium between the resting and desensitized states, but that anionic lipids are required for the nAChR to adopt a fully functional resting conformation.

EXPERIMENTAL PROCEDURES

NAChR Affinity Purification, Reconstitution and FTIR Difference Spectroscopy. For a detailed description, see Chapter 3, Experimental Procedures.

[^{13}C]-Acetylcholine. [^{13}C]-ACh was synthesized from choline bromide and [^{13}C]-acetylchloride and purified according to Damle *et al.* (82). The infrared spectrum of the synthesized [^{13}C]-ACh was superimposable on a similar spectrum of commercially available [^{13}C]-ACh (168, 169).

RESULTS

Carb-difference spectra recorded from affinity purified nAChR reconstituted into membranes composed of EPC/DOPA/Chol (3:1:1), a membrane that gives rise to a strong Carb-induced cation flux, are similar to those recorded from the nAChR in native membranes and thus illustrate the pattern of difference bands expected for a functional receptor (Figures 4.1A, top trace and 4.1B, scheme i) (142, 155). Carb-difference spectra recorded from the nAChR reconstituted into EPC membranes lacking both neutral and anionic lipids are similar, but exhibit a number of band intensity variations (Figure 4.1A, middle trace). These variations reflect subtle lipid-induced alterations in the structure and/or environment of individual residues within the nAChR and include a marked decrease in the intensity of five positive bands centered near 1663, 1655, 1547, 1430 and 1059 cm^{-1} (the variation in band intensity near 1740 cm^{-1} is discussed below).

While the individual bands in the Carb-difference spectra remain to be assigned to specific residues, it is significant that the above noted changes in intensity are all observed in Carb-difference spectra recorded from the nAChR in EPC/DOPA/Chol, but

Figure 4.1 (**A**) A comparison of Carb-difference spectra recorded from the nAChR reconstituted into membranes composed of EPC/DOPA/Chol (3:1:1), EPC and EPC/DOPA/Chol (3:1:1), but while continuously maintaining the receptor in contact with 200 μM dibucaine. In the latter spectrum, the appearance of negative band intensity and/or a reduction in positive band intensity due to the displacement of dibucaine from the neurotransmitter binding sites upon the addition of Carb is denoted by a *d*. The red dashed lines identify those vibrational bands that are believed to reflect alterations in nAChR structure due to the transition from the resting to the desensitized state. (**B**) A typical Carb-difference spectrum exhibits vibrational bands that reflect the structural changes that occur in the nAChR as a result of Carb binding and subsequent transition from the resting to the desensitized state (scheme i). If the nAChR is maintained in the desensitized state prior to the addition of Carb by either a local anesthetic or reconstitution into a membrane composed solely of EPC (shown here), then the Carb-difference spectrum reflects mainly those vibrational changes associated with the formation of specific physical interactions between Carb and the nAChR (scheme ii). Note, however, that in both cases (schemes i and ii), positive bands due to the vibrations of nAChR-bound Carb are observed (denoted by a *c* in the top trace) (129).

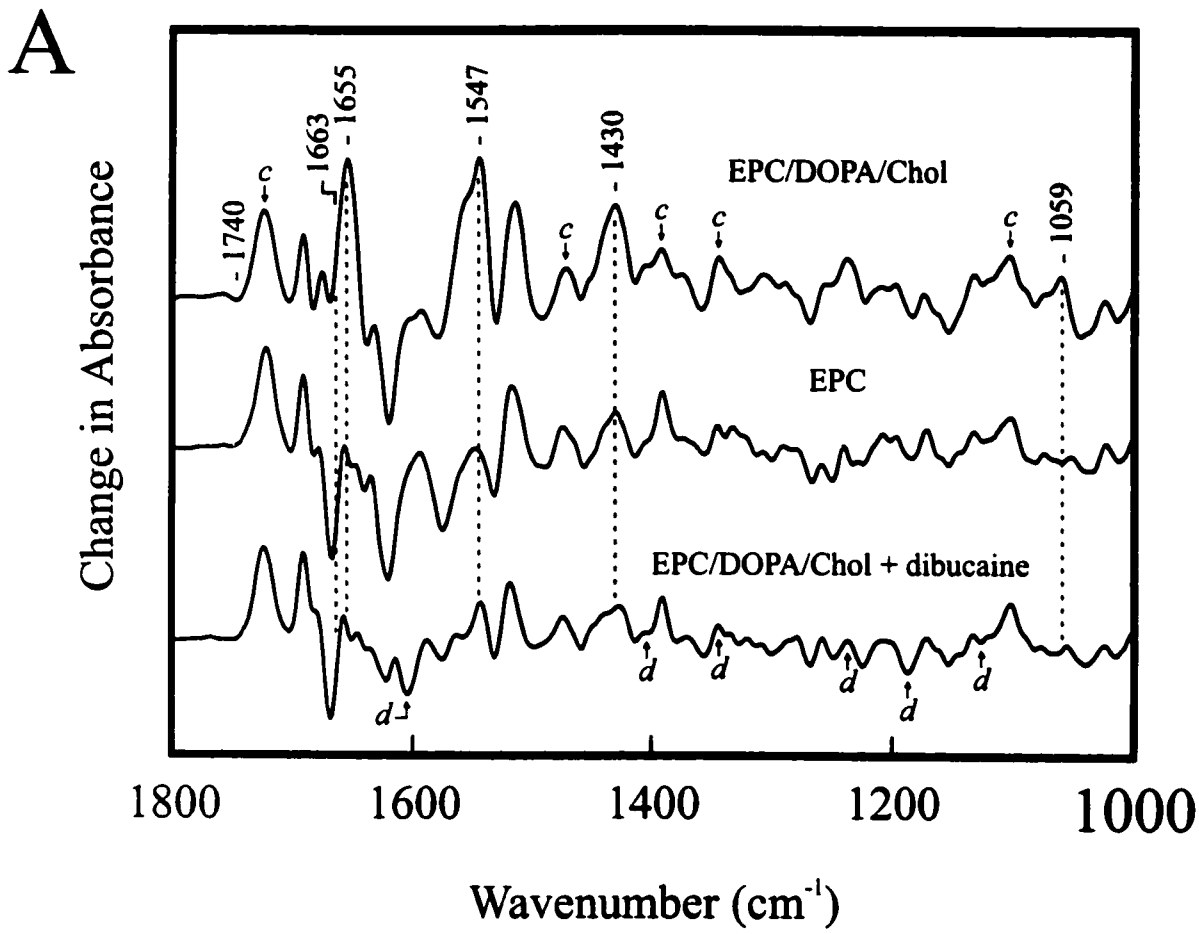
A
Change in Absorbance
1740
1663
1655
1547
1430
1059
EPC/DOPA/Chol
EPC
EPC/DOPA/Chol + dibucaine
c
d
1800
1600
1400
1200
1000
Wavenumber (cm-1)

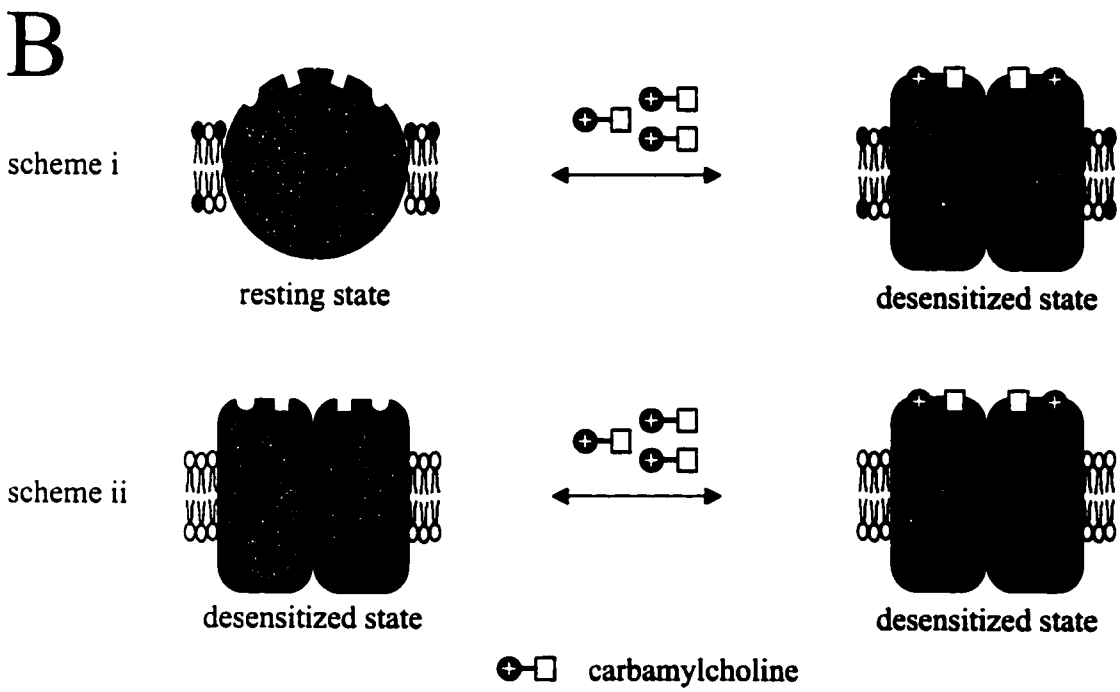
B
scheme i
resting state
desensitized state
scheme ii
desensitized state
desensitized state
carbamylcholine

while continuously maintaining the receptor in contact with the desensitizing local anesthetic, dibucaine (Figure 4.1A, bottom trace). This suggests that the five noted positive Carb-difference bands reflect changes in vibrational intensity that occur as a consequence of the resting-to-desensitized conformational transition itself (170). The absence of these five bands in Carb-difference spectra recorded from the nAChR reconstituted into EPC membranes indicates that within this membrane environment, the receptor does not undergo the resting-to-desensitized conformational transition upon the binding of Carb (Figure 4.1B, scheme ii). This result is consistent with photoaffinity labeling studies, which show that the nAChR in EPC is stabilized in the desensitized state (143).

In addition to the marked band intensity variations discussed above, more subtle lipid-sensitive spectral changes may occur in the regions between 1750 and 1700 cm^{-1}, 1580 and 1520 cm^{-1}, and 1400 and 1100 cm^{-1}. Variations in band intensity in the 1700 to 1750 cm^{-1} region are difficult to monitor due to the overlapping Carb vibration near 1720 cm^{-1} (Figure 4.2A). To circumvent this problem, difference spectra were recorded using isotopically-labeled ACh ([^{13}C]-label on the carbonyl carbon) instead of Carb to induce the resting-to-desensitized conformational transition. The resulting [^{13}C]-ACh-difference spectra exhibit a clear window in the 1750 to 1700 cm^{-1} region for viewing underlying protein and/or lipid vibrations (Figure 4.2B). [^{13}C]-ACh-difference spectra recorded from the nAChR in EPC/DOPA/Chol exhibit both a weak negative and positive band centered near 1740 and 1720 cm^{-1}, respectively, that could reflect changes in the vibrational

Figure 4.2 A comparison of difference spectra recorded from the nAChR using either Carb or [^{13}C]-ACh to induce the resting-to-desensitized conformational transition. In panel (**A**), a small region of a Carb-difference spectrum recorded from the nAChR reconstituted into EPC/DOPA/Chol (3:1:1) is compared to the solution absorbance spectrum of Carb. As can be seen, the possible presence of lipid and/or protein vibrational bands within this region is masked due to the overlapping carbonyl stretching vibration of Carb. In panel (**B**), the same region of a [^{13}C]-ACh-difference spectrum recorded from the nAChR reconstituted into EPC/DOPA/Chol (3:1:1) is compared to the solution absorbance spectrum of [^{13}C]-ACh. Isotopically labelling the carbonyl carbon (^{13}C=O) of ACh shifts the carbonyl stretching frequency down to near 1695 cm^{-1}, thereby allowing a clear window into the 1740-1720 cm^{-1} region of the difference spectrum. Panel (**C**) compares [^{13}C]-ACh-difference spectra recorded from the nAChR reconstituted into membranes composed of EPC/DOPA/Chol (3:1:1), EPC/DOPA (3:2), EPC/Chol (3:2), and EPC.

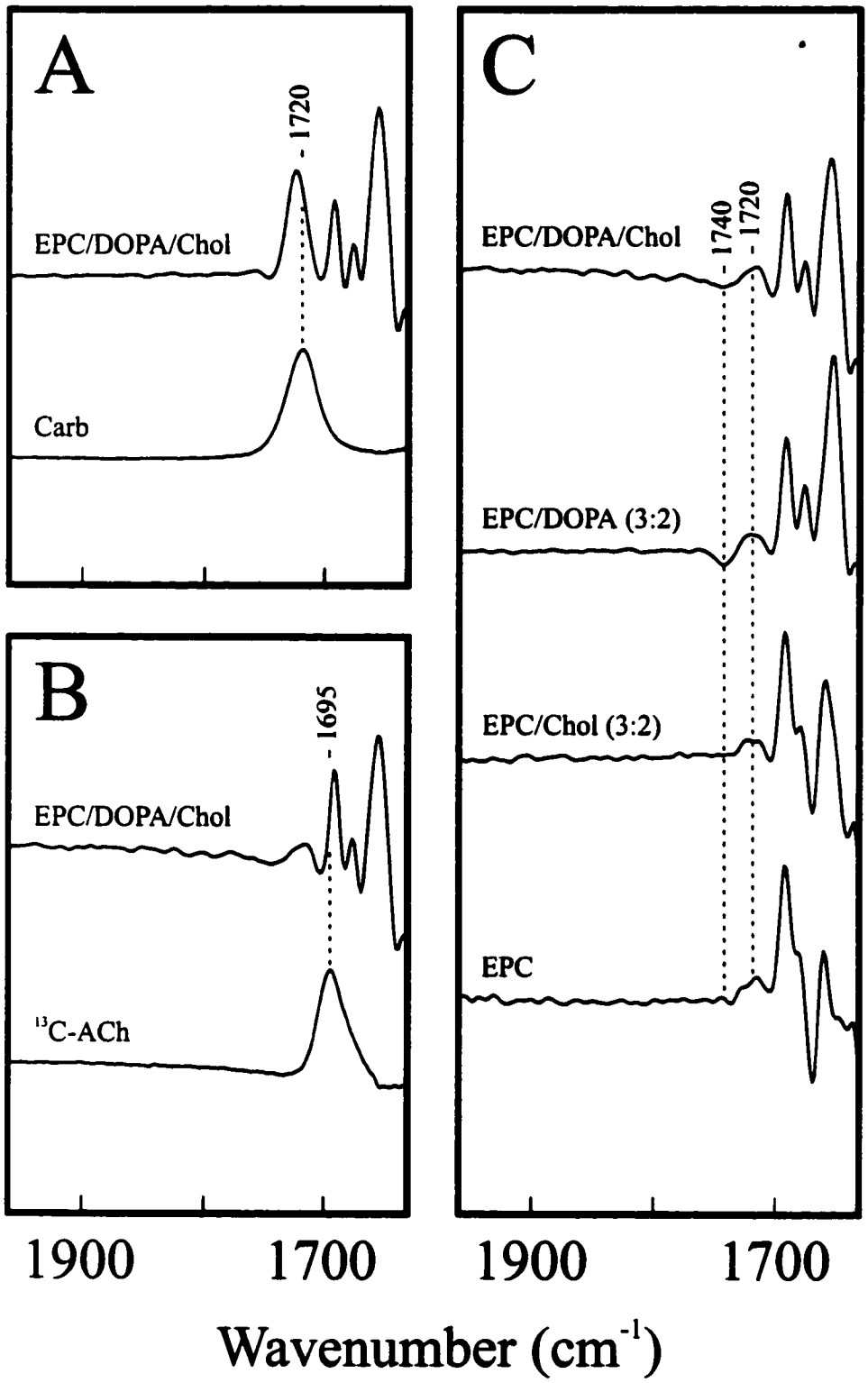
A
1720
EPC/DOPA/Chol
Carb
B
1695
EPC/DOPA/Chol
13C-ACh
C
1740
1720
EPC/DOPA/Chol
EPC/DOPA (3:2)
EPC/Chol (3:2)
EPC
1900
1700
1900
1700
Wavenumber (cm-1)

intensity and/or frequency of either a protonated carboxyl or a lipid ester carbonyl (Figure 4.2C, top trace). Note that the 1740 cm^{-1} vibration is absent in [^{13}C]-ACh-difference spectra recorded from the nAChR reconstituted into EPC membranes (Figure 4.2C, bottom trace).

Potential variations in intensity between 1520 and 1580 cm^{-1} and between 1400 and 1100 cm^{-1} are difficult to assess due to the possibility of temperature-sensitive baseline fluctuations that can occur in these regions and/or the relatively weak intensity of the Carb-difference bands. A comparison of potential spectral changes in these regions with those observed in Carb-difference spectra recorded in the presence of the desensitizing local anesthetic, dibucaine, are also complicated since negative vibrational bands due to the Carb-induced displacement of dibucaine from the neurotransmitter binding sites appear in the latter spectra (identified by a *d* in Figure 4.1A, bottom trace). It is thus difficult to assess both whether or not these spectral changes are present and, if present, whether the putative spectral changes are associated with the resting-to-desensitized conformational change. Further discussion will, therefore, focus mainly on the six lipid-sensitive bands near 1740, 1663, 1655, 1547, 1430 and 1059 cm^{-1}.

Increasing Levels of DOPA in EPC membranes. Carb-difference spectra recorded from the nAChR reconstituted into EPC membranes with increasing molar proportions of the anionic lipid DOPA exhibit a DOPA-dependent increase in positive intensity at the five noted conformationally sensitive band frequencies centered near 1663, 1655, 1547, 1430 and 1059 cm^{-1} (Figure 4.3). In general, the increase in intensity at these five

Figure 4.3 Selected regions of Carb-difference spectra recorded from the nAChR reconstituted into EPC membranes with increasing levels of DOPA. The molar ratio of EPC to DOPA is shown in parentheses. The top trace in each panel is a Carb-difference spectrum recorded from the nAChR reconstituted into EPC/DOPA/Chol (3:1:1) membranes.

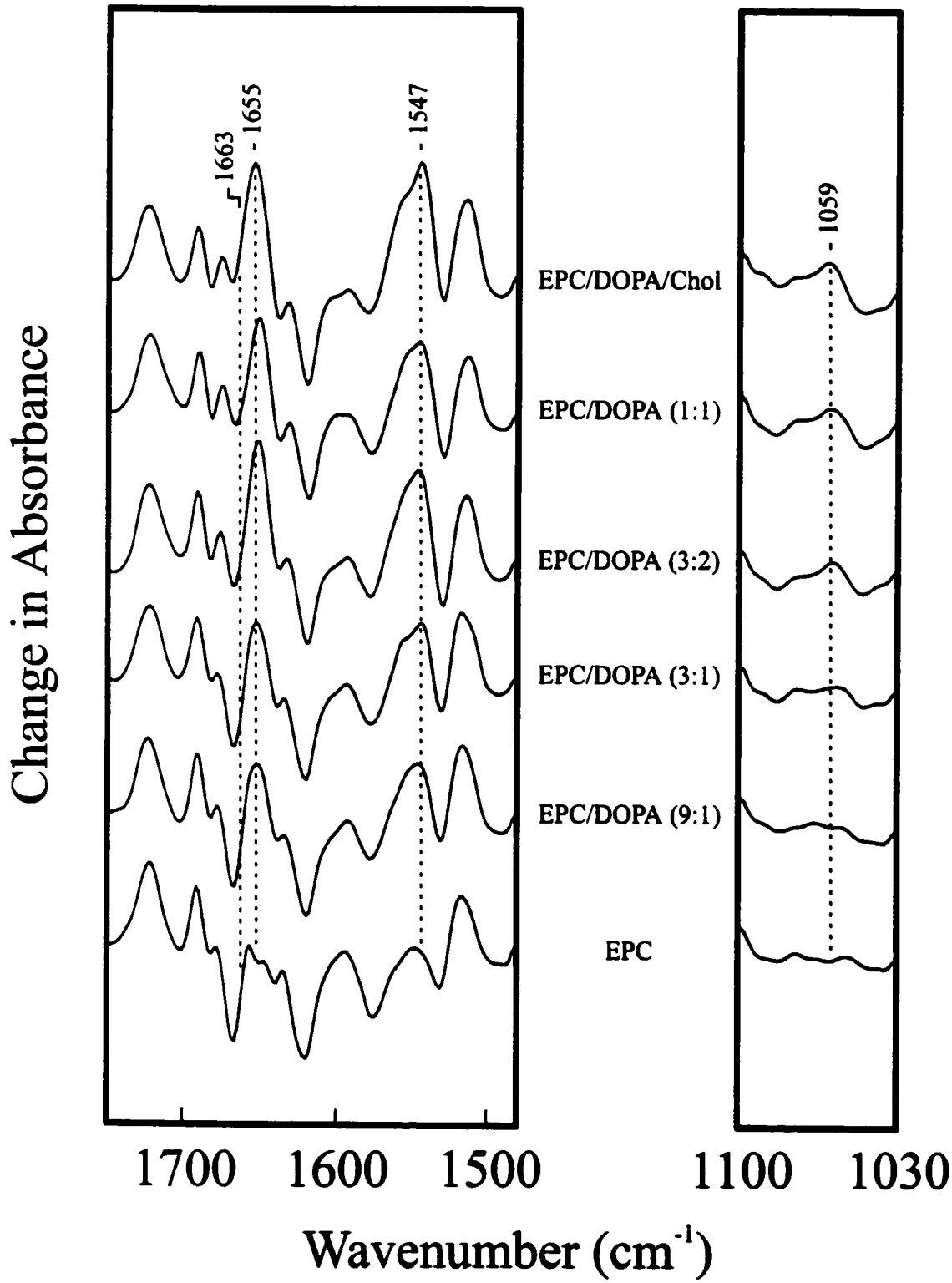
Change in Absorbance
1663
1655
1547
1059
EPC/DOPA/Chol
EPC/DOPA (1:1)
EPC/DOPA (3:2)
EPC/DOPA (3:1)
EPC/DOPA (9:1)
EPC
1700
1600
1500
1100
1030
Wavenumber (cm-1)

frequencies is modest at low levels of DOPA [up to the EPC/DOPA molar ratio of (3:1)] whereas in EPC/DOPA at both the (3:2) and (1:1) molar ratios, the intensity of these bands approach those observed in Carb-difference spectra recorded from the nAChR in EPC/DOPA/Chol. In addition, [^{13}C]-ACh-difference spectra recorded from the nAChR in EPC/DOPA (3:2) exhibit a relatively strong negative and positive band near 1740 and 1720 cm^{-1}, respectively (Figure 4.2C). The difference spectra thus indicate that the nAChR in EPC/DOPA at both the (3:2) and (1:1) molar ratios recovers its ability to undergo the resting-to-desensitized conformational transition and thus must be stabilized predominantly in a functional resting conformation. In terms of the FTIR difference technique, high levels of DOPA in an EPC membrane appear to be sufficient to stabilize the nAChR in a functional resting conformation that is equivalent to that found in EPC/DOPA/Chol, even in the absence of Chol.

Assuming that the nAChR in EPC membranes is stabilized in the desensitized state (see Discussion), the above data is consistent with a gradual shift in the conformational equilibrium of the receptor towards the resting state with increasing levels of DOPA. Closer examination of the data, however, reveals that the effects of DOPA may be more complex than the modulation of a simple two state conformational equilibrium. Carb-difference spectra recorded from the nAChR in both EPC/DOPA (3:1) and (9:1) membranes exhibit large positive intensity near 1655 and 1547 cm^{-1} relative to the intensity of the bands in Carb-difference spectra recorded from the nAChR in EPC (Figures 4.3 and 4.4A). In contrast, the intensity of the two vibrations near 1663 and

Figure 4.4 A comparison of Carb-difference spectra recorded from the nAChR reconstituted into (**A**) EPC/DOPA/Chol (3:1:1), EPC/DOPA (3:1), and EPC and (**B**) EPC/DOPA/Chol (3:1:1), EPC/Chol (3:1), and EPC. A multiple-point baseline correction was performed on all spectra to reduce subtle baseline fluctuations and thus allow superimposition of the spectra. The baseline corrections, however, do not have a substantial effect on the relative intensity of the bands as can be seen by comparing the spectra presented here with those that were not multiple-point baseline corrected in Figures 4.3 and 4.5.

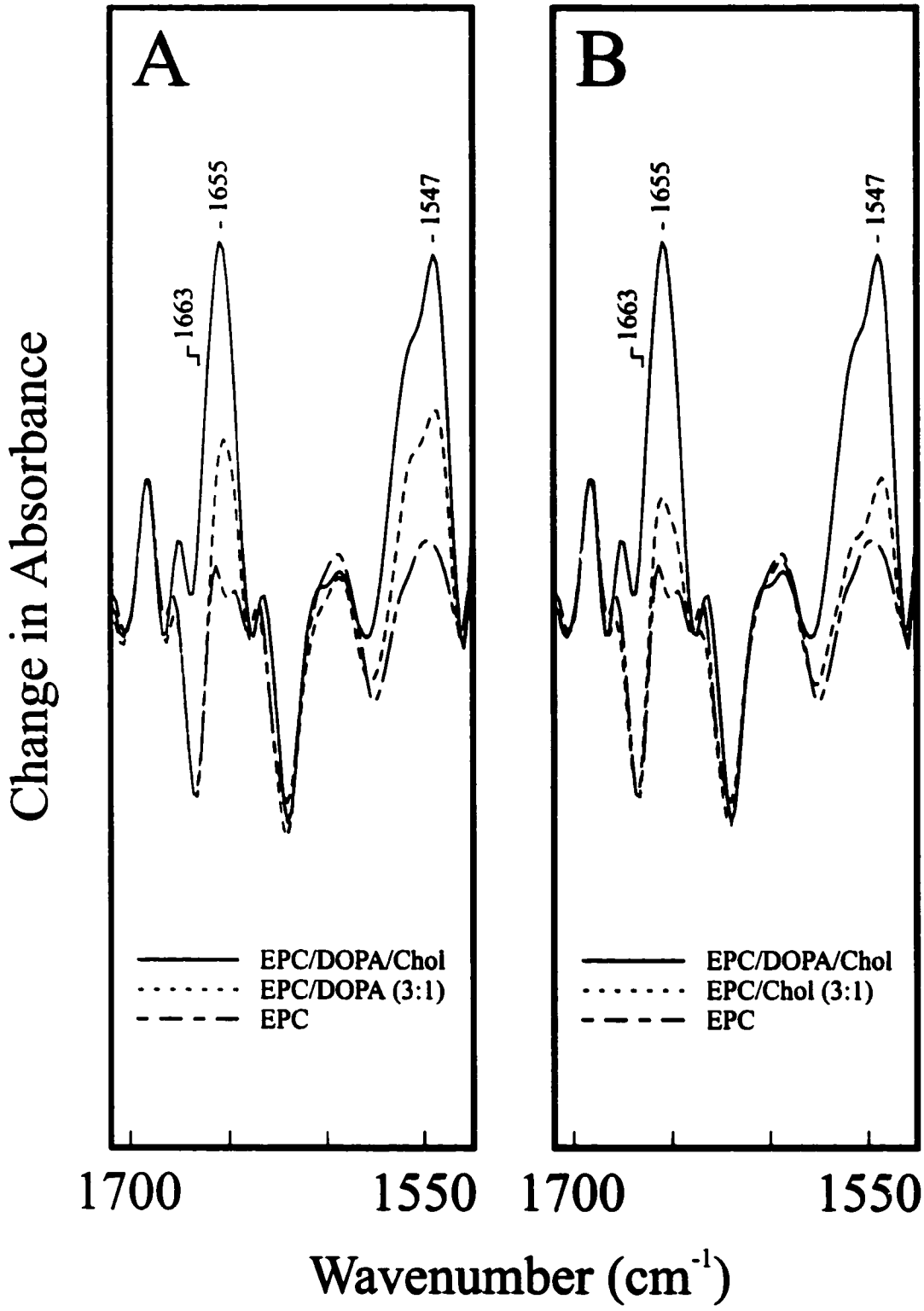
A
B
1663
1655
1547
EPC/DOPA/Chol
EPC/DOPA (3:1)
EPC
EPC/Chol (3:1)
Change in Absorbance
1700
1550
Wavenumber (cm-1)

1059 cm^{-1} remain weak and are similar to the intensity of the two bands in Carb-difference spectra recorded from the nAChR in EPC membranes completely lacking DOPA. This pattern of band intensity variations suggests that a large percentage of the conformationally-sensitive residues in the nAChR that contribute intensity to the Carb-difference bands near 1655 and 1547 cm^{-1} adopt a resting-like conformation in EPC/DOPA (3:1) while the majority of the residues that contribute intensity to the Carb-difference bands near 1663 and 1059 cm^{-1} adopt a desensitized-like conformation. The EPC/DOPA (9:1) and (3:1) membranes thus appear to stabilize a conformation that is a structural intermediate between the resting and desensitized states.

Increasing Levels of Chol in EPC membranes. Carb-difference spectra recorded from the nAChR reconstituted into EPC membranes with increasing proportions of the neutral lipid Chol are similar to those recorded from the nAChR in EPC membranes with increasing levels of DOPA. There is a Chol-dependent increase in the intensity of four of the five noted conformationally-sensitive bands near 1663, 1655, 1547 and 1430 cm^{-1} (Figure 4.5). The intensity of these four bands in the Carb-difference spectra recorded from the nAChR in EPC/Chol (3:2) approach the intensity of those recorded from the nAChR in EPC/DOPA/Chol suggesting that the nAChR has, for the most part, adopted a resting-like conformation. An EPC/Chol (3:1) membrane also appears to stabilize a conformational intermediate between the resting and desensitized states as indicated by the relatively large positive intensity near 1655 and 1547 cm^{-1} versus the relatively weak intensity near 1663 and 1059 cm^{-1} (Figures 4.5 and 4.4B). There are, however, subtle

Figure 4.5 Selected regions of Carb-difference spectra recorded from the nAChR reconstituted into EPC membranes with increasing levels of Chol. The molar ratio of EPC to Chol is shown in parentheses. The top trace in each panel is a Carb-difference spectrum recorded from the nAChR reconstituted into EPC/DOPA/Chol (3:1:1) membranes.

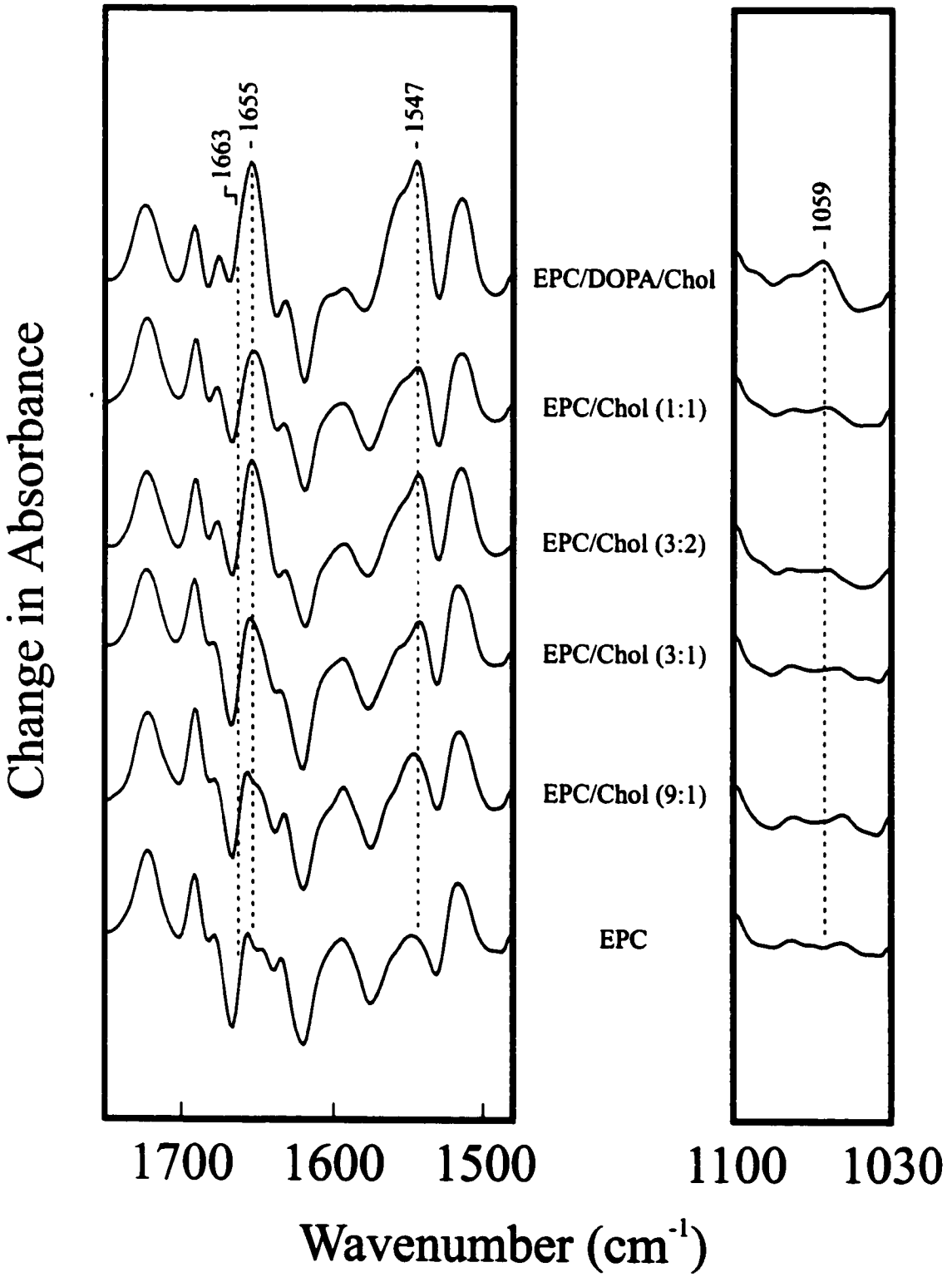
Change in Absorbance
1663
1655
1547
1059
EPC/DOPA/Chol
EPC/Chol (1:1)
EPC/Chol (3:2)
EPC/Chol (3:1)
EPC/Chol (9:1)
EPC
1700
1600
1500
1100
1030
Wavenumber (cm-1)

variations between the Carb-difference spectra recorded in the presence of increasing proportions of DOPA and Chol that suggest differences in the ability of these two lipids to modulate the conformational equilibrium of the nAChR.

First, at equivalent levels of either DOPA or Chol in the EPC membranes, the presence of DOPA leads to a greater recovery in the intensity of the conformationally-sensitive bands near 1663, 1655, 1547, 1430 and 1059 cm^{-1} implying that DOPA is slightly more effective at shifting the equilibrium towards the resting conformation (as an example, compare panels A and B in Figure 4.4)). This result is in agreement with the labeling studies of McCarthy and Moore (143), which suggest that the nAChR in EPC/Chol (3:1) is predominantly in the desensitized state whereas in EPC/DOPA (3:1) it is predominantly in the resting conformation.

Second, increasing proportions of Chol have weak, if any, effect on the intensity of the Carb-difference band centered near 1059 cm^{-1} (Figure 4.5, right panel). At all levels of Chol, the intensity near 1059 cm^{-1} remains essentially the same as the intensity of the band in Carb-difference spectra recorded from the nAChR in EPC alone. In contrast, the intensity of this band doubles in difference spectra recorded from the nAChR in either EPC/DOPA/Chol, EPC/DOPA (3:2), or EPC/DOPA (1:1) (Figure 4.3, right panel). The presence of Chol also does not lead to [^{13}C]-ACh-difference spectra with comparable negative intensity near 1740 cm^{-1} to that observed in spectra recorded from the nAChR in both EPC/DOPA/Chol and EPC/DOPA (3:2) (Figure 4.2C). The lack of an effect of Chol on the intensity of these two vibrations may indicate that there are subtle

structural differences between the nAChR in EPC membranes either with or without anionic lipids (see Discussion).

Finally, Carb-difference spectra recorded from the nAChR reconstituted into EPC/Chol (1:1) are similar to those recorded from the nAChR in EPC/Chol (3:1) (Figure 4.5). In other words, the pattern of increasing intensity at each of the conformationally-sensitive Carb-difference bands near 1663, 1655, 1547, and 1430 cm^{-1} with increasing Chol is reversed at very high levels of Chol. This reversal in the pattern of the band intensity variations suggests that the ability of Chol to stabilize the nAChR in a resting-like conformation is weakened at very high levels of Chol. A similar reversal in trend is observed with the peptide $^{1}H/^{2}H$ exchange kinetics of the nAChR upon reconstitution into EPC membranes with increasing levels of Chol (171).

DISCUSSION

The main goal of this work was to further investigate the structural requirement of the nAChR for both neutral and anionic lipids. Previously, it was shown that Carb-difference spectra recorded from the nAChR reveal several positive and negative vibrational bands, near 1663, 1655, 1547, 1430 and 1059 cm^{-1}, that serve as markers of the ability of the nAChR to undergo the resting-to-desensitized conformational transition. Significantly, these bands are absent in Carb-difference spectra recorded from the nAChR reconstituted into EPC membranes suggesting that the absence of both neutral and

anionic lipids leads to a receptor that is incapable of undergoing agonist-induced desensitization. In contrast, these bands are present with increasing intensity in Carb-difference spectra recorded from the nAChR reconstituted into EPC membranes with increasing levels of either DOPA or Chol. Both DOPA and Chol can thus individually influence the ability of the nAChR to undergo the resting-to-desensitized conformational transition in response to the binding of Carb. The level of either Chol or DOPA in the reconstituted membrane, however, is a critical factor in determining the efficacy of that lipid in stabilizing a 'functional' (i.e. resting state) receptor.

The variations in the intensity of vibrational bands observed in Carb-difference spectra recorded from the nAChR reconstituted into EPC membranes with increasing levels of either DOPA or Chol suggest several features regarding the mechanisms of lipid action at the nAChR. These features have been incorporated into a speculative model presented in Figure 4.6. The basic tenet of this model is that in the absence of agonist, lipid composition influences the conformational equilibrium of the nAChR between the resting and desensitized states through an indirect effect on some physical property of the lipid membrane, possibly bulk membrane fluidity. The model also proposes that anionic lipids, in addition to proper membrane fluidity, are required in order to stabilize a fully functional nAChR. The model is based on the following observations and arguments.

1) The postulate that lipid composition influences the conformational equilibrium of the nAChR is based on the observation that the receptor in EPC alone is incapable of undergoing the Carb-induced conformational change whereas in the presence of

Figure 4.6 A speculative model illustrating the effects of lipid composition on the conformational equilibrium of the nAChR. The model proposes that within a relatively fluid membrane, such as that formed by either EPC or DOPC, the nAChR is stabilized predominantly in the desensitized state. A decrease in fluidity, such as that found with increasing levels of either DOPA or Chol, leads initially to a shift in the nAChR into a conformation that is a structural intermediate between the resting and desensitized states, and then finally into the resting state. Anionic lipids such as DOPA, however, are required for the nAChR to adopt a fully functional resting conformation. In the absence of anionic lipids, the results suggest that the nAChR adopts a conformation similar to either the resting, intermediate, or desensitized states, as dictated by the membrane fluidity, but one that has an unidentified subtle structural difference. These putative conformational states are referred to as pseudo-resting, pseudo-intermediate, and pseudo-desensitized.

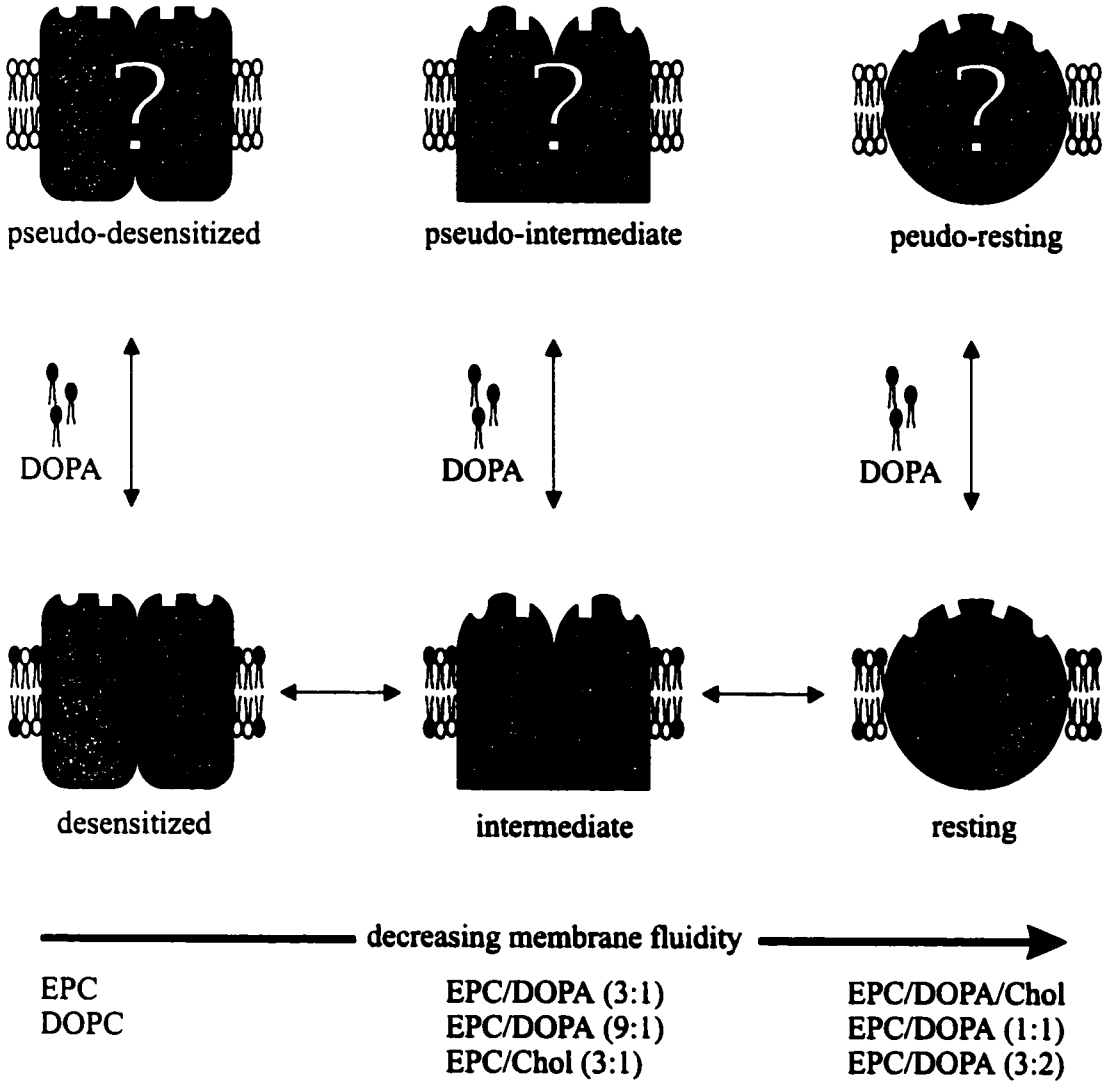
?
?
?
pseudo-desensitized
pseudo-intermediate
peudo-resting
DOPA
DOPA
DOPA
desensitized
intermediate
resting
decreasing membrane fluidity
EPC
DOPC
EPC/DOPA (3:1)
EPC/DOPA (9:1)
EPC/Chol (3:1)
EPC/DOPA/Chol
EPC/DOPA (1:1)
EPC/DOPA (3:2)

increasing levels of either DOPA or Chol, an increasing number of receptors regain the ability to undergo Carb-induced desensitization. The stabilization of the desensitized state in EPC, as suggested by the model, accounts for the observation that the nAChR is incapable of undergoing the Carb-induced conformational change. In addition, a shift in the resting-to-desensitized conformational equilibrium towards the resting state with increasing levels of either DOPA or Chol accounts for the increasing numbers of receptors that undergo Carb-induced desensitization. Note, however, that the data is also consistent with a locked resting conformation in EPC that is not responsive to Carb binding, as is suggested by Rankin *et al.* (167). The model does not favour the latter interpretation for two reasons.

First, the photoaffinity labeling pattern of the nAChR in EPC membranes by the conformationally sensitive probe [^{125}I]-TID is similar to that observed for the nAChR in both native and EPC/DOPA/Chol membranes after pre-exposure to Carb and thus receptor desensitization (143). These labeling experiments demonstrate that the nAChR in EPC alone is not locked in the resting state. Second, Rankin *et al.* (167) suggest that lipid composition has no effect on the conformational equilibrium of the nAChR. In the absence of a change in the relative populations of the nAChR found in either the resting or desensitized state, the nAChR can only be locked in the resting conformation in EPC if the activation energies between the resting and all other conformational states are so high that the kinetics of gating and desensitization become infinitely slow. In such a model, conformational transitions could occur on a biological time scale in the presence of Chol

and DOPA if each lipid lowers the activation energies between conformational states. A lowering of activation energies could arise from either the formation of specific physical interactions between each lipid and the nAChR, in a manner similar to that by which enzymes interact with substrates to lower activation energies and enhance reaction rates, or by a non-specific effect on some bulk property of the membrane. A mechanism involving the formation of specific interactions between either Chol or DOPA and the nAChR, however, is unlikely given the diverse structures of these two lipids as well as the generally 'loose' structural requirements of the nAChR for neutral and anionic lipids (see below). A change in some bulk property of the lipid membrane leading to lower activation energies is also unlikely since a gradual change in this bulk property with increasing levels of either DOPA or Chol would lead to a gradual change in activation energies and thus a gradual shift in the rates of transitions between the resting and other conformational states. The data presented by Rankin *et al.* (167), however, suggest that the *number* of nAChRs capable of undergoing Carb-induced conformational change, not the *rates* of the conformational changes themselves, are influenced by lipid composition. An effect of DOPA and Chol on the activation energies between the various conformational states of the nAChR, therefore, seems unlikely. Consequently, the nAChR cannot be locked in the resting state in EPC membranes. The most plausible interpretation of the data is thus in terms of a lipid-dependent modulation of the number of receptors present in the resting and desensitized states in the absence of bound agonist.

2) A second postulate of the model is that lipids influence the conformational equilibrium of the nAChR through a non-specific effect on some bulk property of the membrane. This postulate is based on several observations including those discussed in Chapter 3, where the addition of either Chol, DOPA, DOPS, or squalene to reconstituted EPC membranes was shown to influence the conformational equilibrium of the nAChR. Sunshine and McNamee (145) have also shown that mixtures of a variety of diverse neutral and anionic lipids are capable of substituting for DOPA and Chol in supporting a functional nAChR. In addition, Chol covalently-linked to a phospholipid in the bulk lipid is as effective as free Chol in stabilizing a conformationally-competent nAChR (172). While specific Chol binding sites on the nAChR are often invoked to explain the ability of Chol to enhance receptor activity, both the loose structural requirements of the nAChR for neutral and anionic lipids and the lack of experimentally documented Chol binding sites are suggestive of an indirect effect of lipids on bulk properties of the lipid membrane.

Consequently, as shown in Figure 4.6, the model proposes that both Chol and DOPA modulate the conformational equilibrium of the nAChR by influencing the bulk membrane fluidity. It is well documented that the presence of Chol in a membrane, including reconstituted membranes containing the nAChR, leads to an ordering of the fatty acyl chains and thus a decrease in fluidity (150, 173). In addition, it is possible that the very small head group of DOPA can lead to a lateral condensation of the lipid acyl chains and thus an increased ordering of the lipid bilayer (162, 174). In support of the

latter, it has been shown that increasing levels of DOPA in reconstituted EPC membranes leads to a decrease in the proportion of lipid ester carbonyls that are hydrogen bonded to water. This could represent a decreased penetration of water into the lipid head group region of the bilayer as a result of a lateral condensation of the phospholipids (171).

Although a role for membrane fluidity in modulating nAChR function has previously been suggested, molecular order parameters derived from fluorescent probe studies of the receptor in reconstituted membranes are not consistent with a correlation between bulk fluidity and function (145). However, a single order parameter describing the amplitudes of motion of a rigid fluorescent probe in a lipid bilayer may not be sufficient to accurately describe the complex motions and dynamics of the lipids themselves and thus the so-called membrane fluidity. It may be necessary to describe the rates and amplitudes for each type of lipid motion as well as other factors such as diffusion rates, lipid flip-flop times, etc. More comprehensive studies aimed at elucidating the role of membrane fluidity in modulating the conformational equilibria of the nAChR are, therefore, required.

3) A third postulate of the model is that the nAChR requires the specific presence of anionic lipids, in addition to the proper membrane fluidity noted above, in order to adopt a fully functional resting conformation. This postulate is based on the observation that Carb-difference spectra recorded from the nAChR in membranes containing high levels of DOPA are essentially equivalent to those recorded from the nAChR in functional EPC/DOPA/Chol and native membranes whereas Carb-difference spectra

recorded from the nAChR in EPC membranes with high levels of Chol are not. Specifically, Carb-difference spectra recorded from the nAChR in EPC/Chol (3:2) do not exhibit the same band intensity near 1740 and 1059 cm^{-1} that are observed in Carb-difference spectra recorded from the nAChR in either EPC/DOPA/Chol, EPC/DOPA (3:2), or EPC/DOPA (1:1) membranes. Although the significance of these subtle vibrational differences remains to be established, they could indicate that certain residues in the nAChR are not found in a fully functional resting conformation in the absence of anionic lipids. The preliminary evidence presented here suggests that subtle variations in the Carb-difference spectra recorded from the nAChR in EPC membranes either with or without DOPA may correlate with functional consequences for the nAChR. As a result, the resting and desensitized conformations of the nAChR stabilized in the absence of anionic lipids are tentatively referred to as pseudo-resting and pseudo-desensitized states, respectively (Figure 4.6)

The observed ability of EPC/DOPA membranes to support a functional nAChR is consistent with the work of McCarthy and Moore (143), who showed that the nAChR in EPC/DOPA (3:1) membranes is capable of undergoing agonist-induced conformational change. Although usually treated as non-functional, the nAChR in DOPC/DOPA (3:1) does exhibit a small cation flux in response to the binding of Carb (141, 145). In contrast to the data presented here, most recent studies have concluded that the nAChR has an absolute structural requirement for Chol. However, studies designed to test the functional state of the nAChR in the presence of anionic lipids have always assayed receptor

function in DOPC membranes with the anionic lipid of interest at a level of 25% or less of the total lipids. Carb-difference spectra suggest that only a small proportion of the nAChRs in EPC membranes containing 25% or less DOPA are stabilized in the functional resting state, consistent with the low cation flux observed in similar membranes. It may also be that the DOPC/DOPA mixtures used by others are slightly more fluid than the EPC/DOPA mixtures used here (DOPC has two unsaturated oleoyl chains whereas EPC has predominantly one), which may lead to a greater proportion of the nAChRs in the non-functional desensitized state. It is interesting to note that while the nAChR in DOPC/Chol mixtures does not flux cations, it does in neutral lipid-depleted asolectin supplemented with Chol (150). This latter study concluded that a component other than Chol is critical for the nAChR to adopt the functional resting state. Carb-difference spectra suggest that the high levels of Chol in both of these membranes may provide a proper fluidity and that the missing component in the DOPC/Chol mixtures may be an anionic lipid, such as DOPA. The specific mechanism by which anionic lipids alone influence nAChR conformation, however, remains to be established.

4) The final postulate of the model is that lipids influence the conformational equilibrium of the nAChR between more than a single resting (or pseudo-resting) and a single desensitized (or pseudo-desensitized) state. This postulate is based on the observation that Carb-difference spectra recorded from the nAChR in EPC/DOPA (3:1) and EPC/Chol (3:1) membranes exhibit a pattern of bands that is suggestive of the stabilization of the nAChR in a conformation that is a structural intermediate between the

resting and desensitized states. Specifically, the spectra recorded from the nAChR in both membranes exhibit intensities of the conformationally-sensitive vibrational bands near 1663 and 1059 cm^{-1} that are similar to those observed in Carb-difference spectra recorded from the nAChR in EPC membranes alone while the intensities near 1655 and 1547 cm^{-1} are closer to those found in Carb-difference spectra recorded from the nAChR in EPC/DOPA/Chol. At these low levels of either anionic or neutral lipids, some residues within the nAChR appear to adopt a desensitized-like conformation while others appear to adopt a resting-like conformation. Lipids may, therefore, influence the equilibrium between at least three different conformational states of the nAChR: resting, intermediate and desensitized (Figure 4.6).

The results of this study illustrate the potential complexity of the mechanisms by which lipids influence nAChR function. These complexities have been incorporated into the speculative model presented in Figure 4.6, which accounts for many observations in the literature regarding the effects of lipids on nAChR function. This model presents clear hypotheses that can be tested with definitive experiments. To fully understand the mechanisms of lipid-protein interactions at the nAChR, however, comprehensive studies of the effects of lipids on nAChR structure and function in conjunction with detailed characterizations of the physical properties of reconstituted nAChR membranes are required.

CONCLUSIONS

In this study, the nAChR was reconstituted into EPC membranes with increasing levels of either DOPA or Chol. Increasing levels of either lipid increasingly stabilize the nAChR in a conformation(s) that is/are capable of undergoing agonist-induced desensitization, although only DOPA stabilizes the receptor in what appears to be the fully functional resting state. The results have been interpreted in terms of a speculative model that describes the mechanisms by which lipids influence nAChR function. This model suggests that membrane fluidity or some other bulk property of the membrane modulates the conformational equilibrium of the nAChR between the resting and desensitized states. A membrane with a relatively low fluidity may be required to stabilize the nAChR in the functional resting conformation whereas a relatively fluid membrane may lead to the stabilization of the desensitized state. At least one conformational intermediate between the resting and desensitized states also likely exists. Finally, the model suggests that in addition to an indirect effect of lipids via the bulk fluidity, the nAChR requires anionic lipids, such as DOPA, to adopt a fully functional resting conformation. This specific requirement for anionic lipids could result from either the binding to a distinct site on the nAChR or a less specific effect of charge on nAChR conformation.

CHAPTER 5

STRUCTURAL CONSEQUENCES OF LOCAL ANESTHETIC BINDING TO THE NICOTINIC ACETYLCHOLINE RECEPTOR

INTRODUCTION

The molecular mechanisms of anesthetic action have been the subject of intensive investigations for over a century. While initial studies attempted to explain phenomenological aspects of anesthesia, such as the correlation between lipid solubility and anesthetic potency, recent work has focused on defining the interactions between anesthetics and specific integral membrane proteins involved in the generation and propagation of action potentials (175). The nAChR is a well characterized component of the postsynaptic membrane that has been used extensively as a model for probing the molecular details of both local and general anesthesia (69, 115, 176). In the absence of high resolution structural information, however, the precise mechanisms of anesthetic action at the nAChR remain unclear.

Within its native membrane, the nAChR exists within an equilibrium between at least two distinct conformations, a channel-competent resting and channel-inactive desensitized state, that can be distinguished pharmacologically by their relative affinities for agonists such as ACh and Carb. In the absence of agonist, this equilibrium heavily favours the low affinity resting state with only approximately 20% of the receptors adopting the high affinity desensitized state (178). Although the mechanism of general anesthetic action at the nAChR has yet to be fully elucidated, the current model of local anesthetic action suggests that they modulate receptor structure and function by binding to a distinct allosteric non-competitive blocker site located within the receptor's ion channel pore. For the most part, the binding of local anesthetic to this site both sterically

blocks the ability of the nAChR to conduct cations across the membrane and stabilizes the receptor in a high affinity ACh binding conformation that has been presumed to be analogous to the agonist-induced desensitized state (158, 177). Consequently, it has been proposed that such 'desensitizing' local anesthetics shift the conformational equilibrium of the nAChR towards a predominantly desensitized population of receptors (178). Other local anesthetics compete for binding to the same non-competitive blocker site but either have no effect on the affinity of the nAChR for agonist or stabilize a low affinity ACh binding conformation, the latter effect being presumably a consequence of a shift in the conformational equilibrium towards the resting state (178). Some local anesthetics also bind to the receptor's two neurotransmitter binding sites as well as to a large number of low affinity sites located at the protein-lipid interface, although the functional consequences of these interactions remain poorly understood (179).

The objective of this study was to exploit the structural sensitivity of FTIR difference spectroscopy to gain insight into the molecular details of local anesthetic action at the nAChR. The results suggest that in the absence of agonist and local anesthetic, the nAChR exists within an equilibrium between at least three distinct conformations: resting, desensitized and a novel intermediate state. At low concentrations of desensitizing local anesthetics, where binding occurs predominantly to the non-competitive blocker site, the conformational equilibrium of the nAChR is shifted towards the intermediate state. In contrast, low concentrations of the local anesthetic tetracaine, which stabilize the nAChR in a low affinity binding conformation, suggest a shift in the

conformational equilibrium towards the resting state. Regardless of the conformation stabilized by local anesthetic binding to the non-competitive blocker site, however, the additional binding of local anesthetic to the neurotransmitter binding sites stabilizes the nAChR in a conformation that is analogous to the agonist-induced desensitized state. The results also shed light on the nature of the physical interactions that occur between local anesthetics and individual neurotransmitter binding site residues.

EXPERIMENTAL PROCEDURES

NAChR Affinity Purification, Reconstitution and FTIR Difference Spectroscopy. For a detailed description, see Chapter 3, Experimental Procedures.

Local Anesthetic Solution Spectra. The absorbance spectra of dibucaine, prilocaine, lidocaine and tetracaine in Torpedo Ringer buffer (pH 7.0) were each recorded using the ATR technique. Each spectrum is an average of 250 scans acquired at a resolution of 2 cm^{-1}. The overlapping absorbance bands of the buffer were subtracted.

RESULTS

Carb-difference spectra recorded from the nAChR reconstituted into membranes composed of EPC/DOPA/Chol (3:1:1) exhibit a highly reproducible pattern of positive and negative bands that provides a spectral map of the structural changes that occur

within the receptor upon Carb binding and subsequent desensitization (Figure 5.1, scheme ii) (127-129). In particular, the difference bands represent vibrational changes associated with both the resting-to-desensitized conformational transition and the formation of physical interactions (i.e. hydrogen bonds, cation-π-electron interactions, etc...) between Carb and individual neurotransmitter binding site residues. Positive bands are also observed in the Carb-difference spectrum that reflect the vibrations of distinct functional groups within nAChR-bound Carb (denoted by a *c* in Figure 5.2, top trace).

The difference between infrared spectra recorded from the nAChR in the presence and absence of a local anesthetic should similarly exhibit spectral features that are indicative of local anesthetic-induced conformational change. In most cases, however, these features are masked by relatively large intensity variations that result from the local anesthetic partitioning into, and a resulting expansion of, the nAChR film on the surface of the germanium IRE (data not shown). An alternate approach for monitoring local anesthetic-induced conformational change is to record typical Carb-difference spectra while maintaining the nAChR in the continuous presence of a given concentration of local anesthetic (Figure 5.1, schemes iii and iv). Variations in the pattern of bands in Carb-difference spectra recorded under these conditions should reflect local anesthetic-induced variations in the structure of those residues that are involved in Carb binding and subsequent desensitization. As local anesthetics modulate the conformational equilibrium between the resting and desensitized states and, in turn, influence the affinity

Figure 5.1 Schematic diagram illustrating the conformational changes in the nAChR probed in this study using FTIR difference spectroscopy. In the absence of agonist, the nAChR exists within a conformational equilibrium between at least two distinct conformations: a low affinity channel-competent resting and a high affinity channel-inactive desensitized state (scheme i). A typical Carb-difference spectrum reveals those structural variations that exist between the resting and Carb-induced desensitized state (scheme ii). In contrast, Carb-difference spectra recorded from the nAChR while maintaining the receptor in contact with low concentrations of local anesthetic should reveal local anesthetic-induced variations in the structure of the nAChR that arise predominantly from the binding of the local anesthetic to the non-competitive blocker site. For most local anesthetics, binding to the non-competitive blocker site is thought to induce a shift in the conformational equilibrium of the nAChR towards the desensitized state (scheme iii). Some local anesthetics, however, are thought to instead shift the equilibrium towards the resting state (scheme iv). Maintaining the nAChR in contact with high concentrations of local anesthetic results in the additional binding of the local anesthetic to the neurotransmitter and/or low affinity sites located at the protein lipid interface. The structural and functional consequences of local anesthetic binding to these sites, however, have yet to be elucidated.

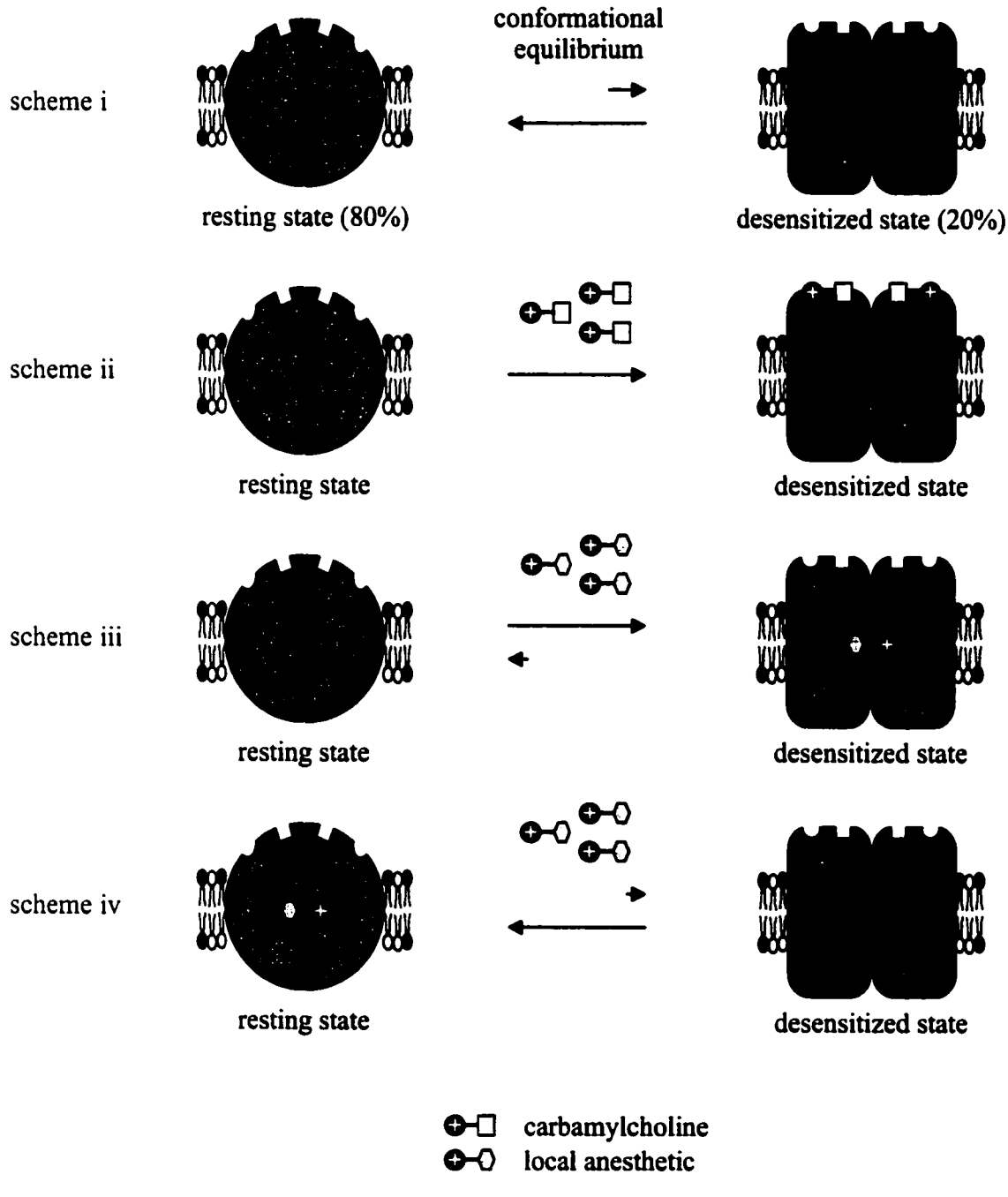
scheme i
conformational
equilibrium
resting state (80%)
desensitized state (20%)
scheme ii
resting state
desensitized state
scheme iii
resting state
desensitized state
scheme iv
resting state
desensitized state
carbamylcholine
local anesthetic

Figure 5.2 A comparison of Carb-difference spectra recorded from affinity purified nAChR reconstituted into membranes composed of EPC/DOPA/Chol (3:1:1), but while continuously maintaining the receptor in contact with increasing concentrations of the local anesthetic, dibucaine. The bottom trace is an absorbance spectrum recorded from a 50 mM aqueous solution of dibucaine (the overlapping absorbance bands of the buffer have been subtracted). The red dashed lines identify dibucaine-induced variations in the intensity of those five bands that are thought to reflect structural changes in the nAChR associated with the resting-to-desensitized conformational transition. The green dashed lines identify both a negative and positive vibrational band thought to reflect specific interactions between Carb and individual neurotransmitter binding site residues. The blue dashed lines identify band intensity variations due to the Carb-induced displacement of dibucaine from the nAChR. Positive bands reflecting the vibrations of nAChR-bound Carb are denoted by a *c* (top trace) (129).

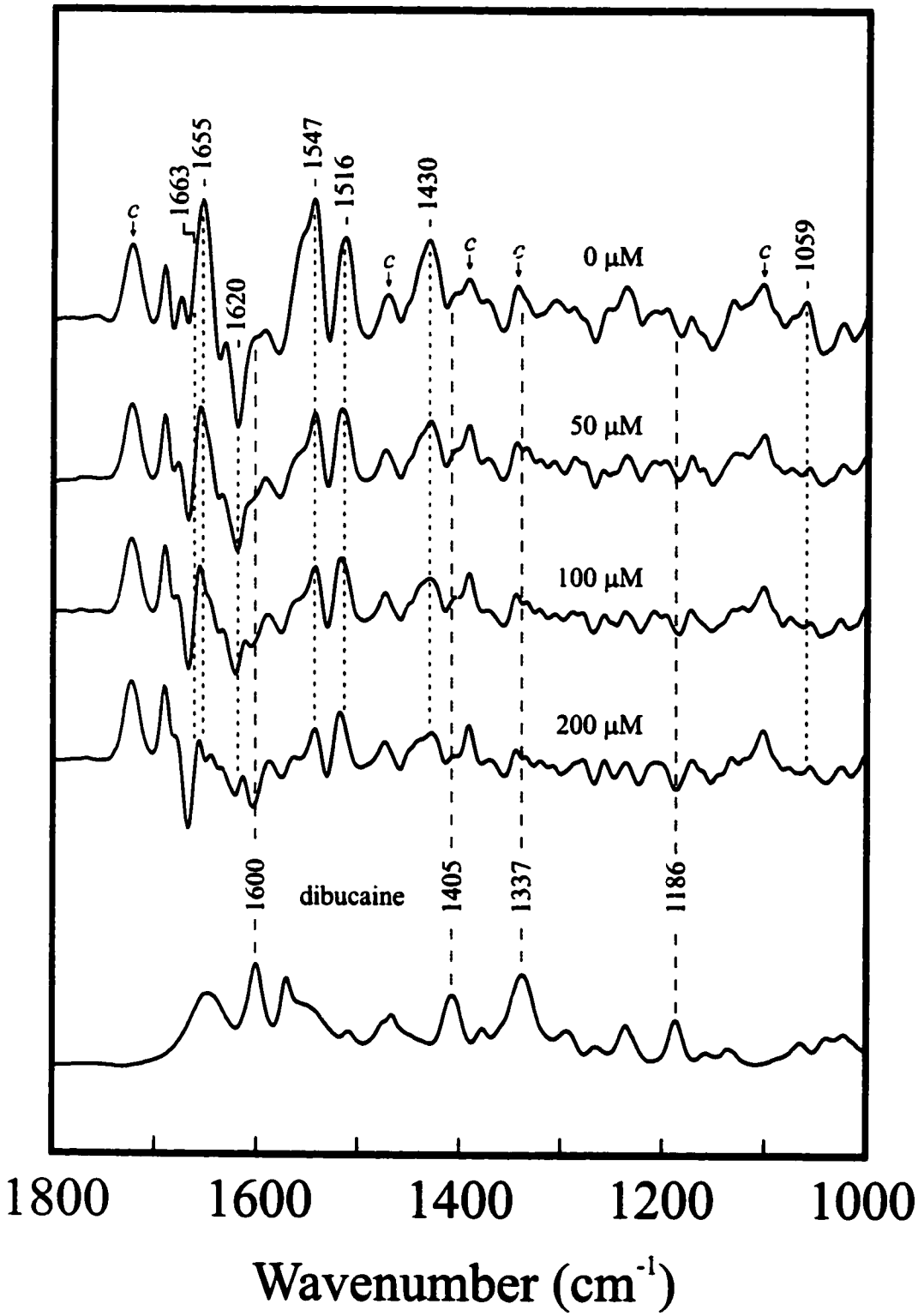
1663
1655
1547
1516
1430
1620
1059
0 μM
50 μM
100 μM
200 μM
1600
dibucaine
1405
1337
1186
1800
1600
1400
1200
1000
Wavenumber (cm-1)

of the nAChR for Carb, such spectral variations should provide insight into the structural basis of local anesthetic action at the nAChR.

Desensitizing Local Anesthetics. Carb-difference spectra recorded from the nAChR reconstituted into EPC/DOPA/Chol (3:1:1) membranes, but while continuously maintaining the receptor in contact with increasing concentrations of the desensitizing local anesthetics dibucaine, prilocaine, or lidocaine exhibit variations in the intensity of a number of positive and negative difference bands (Figures 5.2-5.4, red dashed lines). Significantly, these band intensity variations occur over a range of concentrations consistent with the known binding affinities of the local anesthetics for the non-competitive blocker and/or neurotransmitter binding sites suggesting that they reflect changes in nAChR structure that correlate with altered function (Table 5.1). The most notable variations include a marked decrease in the intensity of five positive bands centered near 1663, 1655, 1547, 1430 and 1059 cm^{-1}. The bands near 1663, 1655 and 1547 cm^{-1} occur in either the amide I (1600-1700 cm^{-1}) or amide II (1520-1580 cm^{-1}) region and thus likely reflect a change in the conformation of the nAChR's polypeptide backbone. The difference bands near 1430 and 1059 cm^{-1}, on the other hand, likely reflect a change in the structure and/or environment surrounding individual amino acid side chains. As all three local anesthetics stabilize a desensitized nAChR, they should eliminate bands in the Carb-difference spectrum that result from the resting-to-desensitized conformational transition itself. The loss of intensity at these five frequencies thus likely reflects the formation of a desensitized nAChR. This possibility is

Figure 5.3 A comparison of Carb-difference spectra recorded from affinity purified nAChR reconstituted into membranes composed of EPC/DOPA/Chol (3:1:1), but while continuously maintaining the receptor in contact with increasing concentrations of the local anesthetic, prilocaine. The bottom trace is an absorbance spectrum recorded from a 50 mM aqueous solution of prilocaine (the overlapping absorbance bands of the buffer have been subtracted). The red dashed lines identify prilocaine-induced variations in the intensity of those five bands that are thought to reflect structural changes in the nAChR associated with the resting-to-desensitized conformational transition. The green dashed lines identify both a negative and positive vibrational band thought to reflect specific interactions between Carb and individual neurotransmitter binding site residues. The blue dashed lines identify band intensity variations due to the Carb-induced displacement of prilocaine from the nAChR. These latter variations, however, are difficult to observe due to the extremely weak intrinsic absorbance intensity of prilocaine.

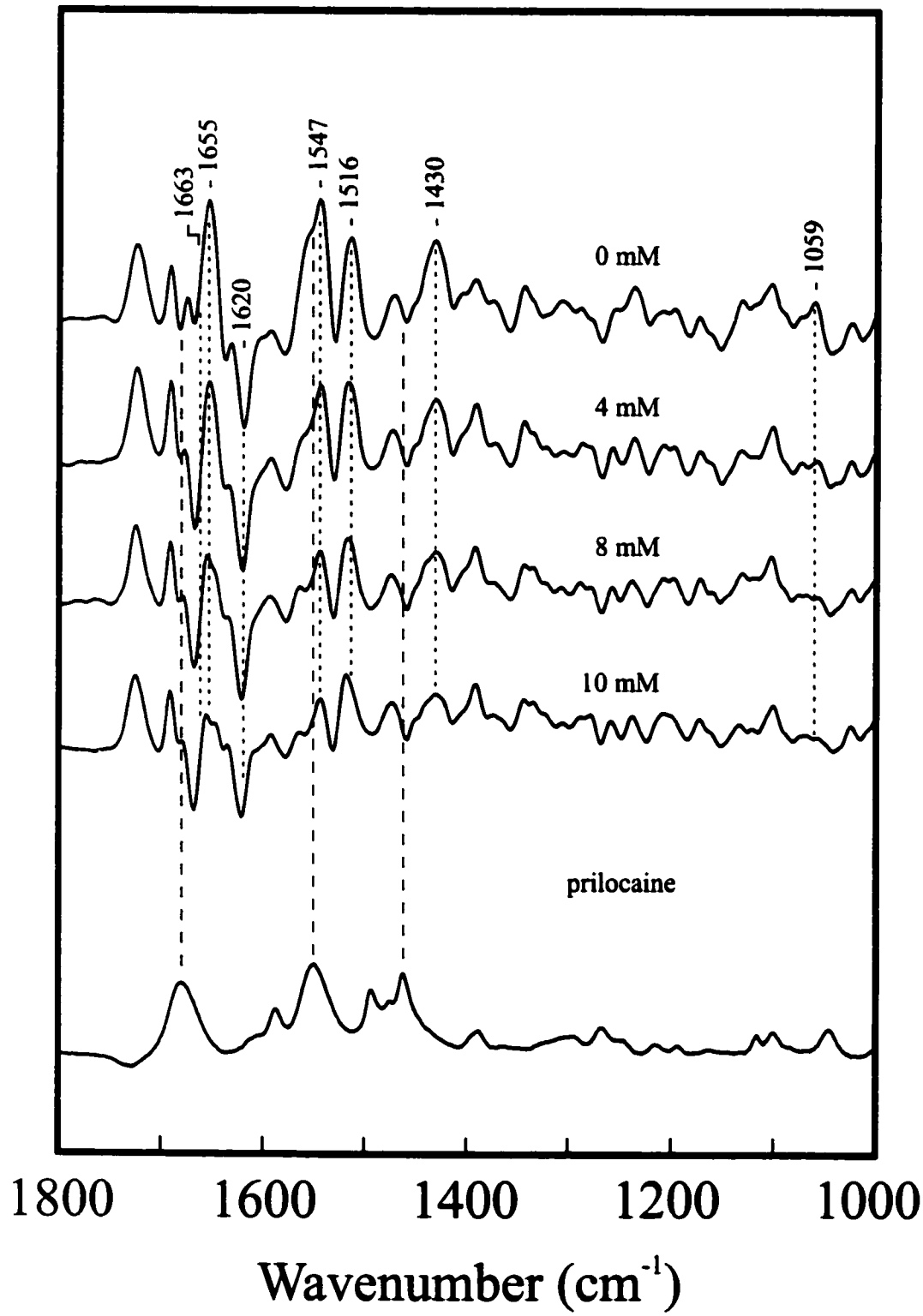
1663
1655
1620
1547
1516
1430
1059
0 mM
4 mM
8 mM
10 mM
prilocaine
1800
1600
1400
1200
1000
Wavenumber (cm-1)

Figure 5.4 A comparison of Carb-difference spectra recorded from affinity purified nAChR reconstituted into membranes composed of EPC/DOPA/Chol (3:1:1), but while continuously maintaining the receptor in contact with increasing concentrations of the local anesthetic, lidocaine. The bottom trace is an absorbance spectrum recorded from a 50 mM aqueous solution of lidocaine (the overlapping absorbance bands of the buffer have been subtracted). The red dashed lines identify lidocaine-induced variations in the intensity of those five bands that are thought to reflect structural changes in the nAChR associated with the resting-to-desensitized conformational transition. The green dashed lines identify both a negative and positive vibrational band thought to reflect specific interactions between Carb and individual neurotransmitter binding site residues. The blue dashed lines identify band intensity variations due to the Carb-induced displacement of lidocaine from the nAChR. These latter variations, however, are difficult to observe due to the extremely weak intrinsic absorbance intensity of lidocaine.

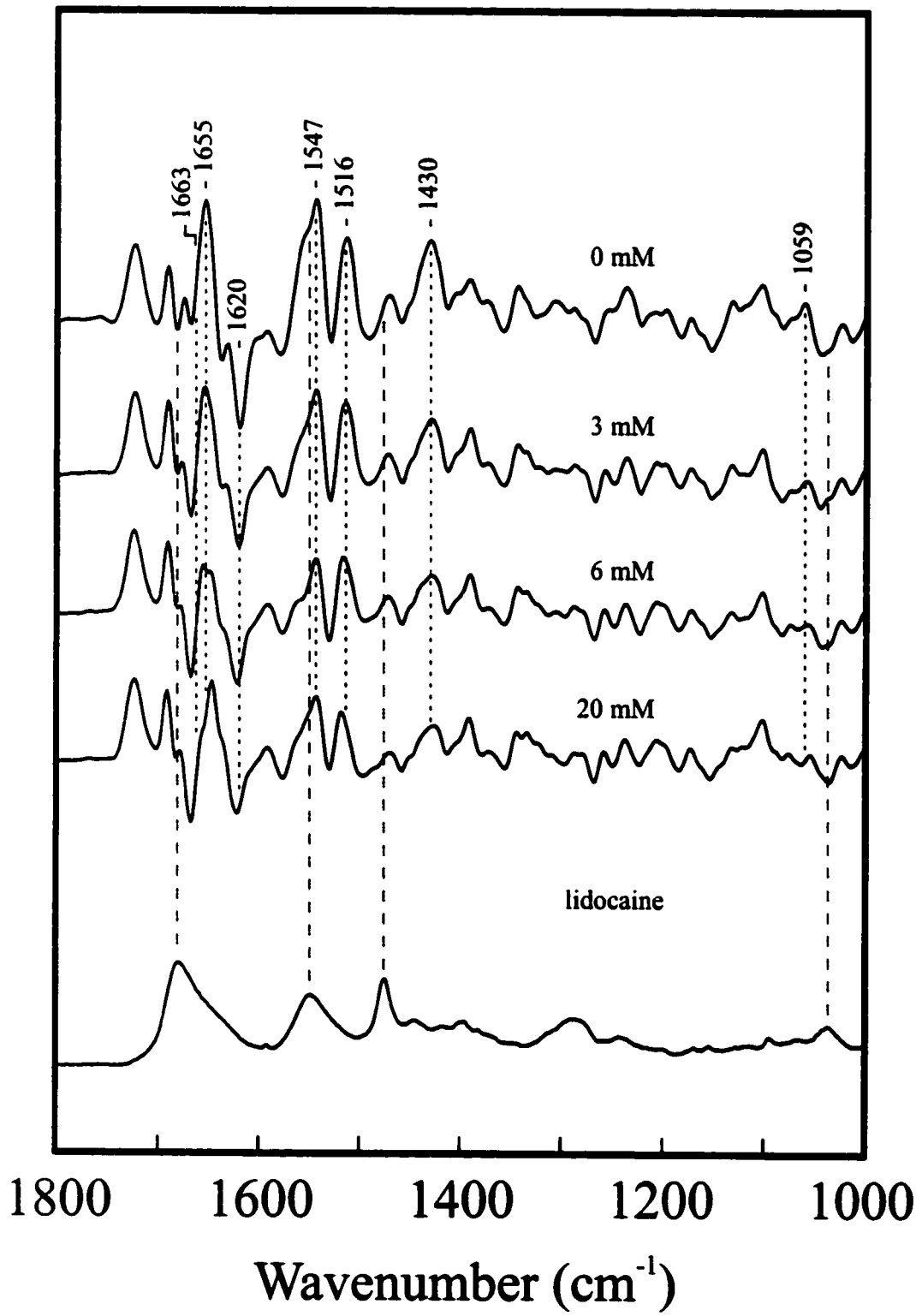
1663
1655
1620
1547
1516
1430
1059
0 mM
3 mM
6 mM
20 mM
lidocaine
1800
1600
1400
1200
1000
Wavenumber (cm-1)

Table 5.1 A comparison of both the binding affinities and conformational effects of the studied local anesthetics at the non-competitive blocker and neurotransmitter binding sites as determined by (**A**) various biochemical methods and (**B**) FTIR difference spectroscopy. [a]C_{50} represents the concentration of local anesthetic, in the absence of Carb, required to either reduce the specific binding of [^{3}H]perhydrohistrionicotoxin to the nAChR (dibucaine, lidocaine and tetracaine) (156) or the concentration required to cause half the maximal observed increase in the binding of a fluorescent ACh analogue to the neurotransmitter binding sites (prilocaine) (180). [b]Values presented in brackets represent the reported concentration of local anesthetic required to cause a maximal increase in fluorescent agonist binding to the neurotransmitter binding sites (180). [c]C_{50} represents the concentration of local anesthetic required to reduce the initial rate of [^{125}I]α-btx (dibucaine, lidocaine and tetracaine) or [^{3}H]α-toxin (prilocaine) by 50% (156, 181). [d]C_{max} represents the concentration of local anesthetic required to produce maximal changes in band intensity in the Carb-difference spectra. Values or conformational effects that have yet to be defined are identified by a question mark (?). D and R refer to the desensitized and resting states, respectively. The local anesthetics dibucaine, prilocaine and lidocaine are proposed to stabilize a novel intermediate (I) conformation upon binding to the non-competitive blocker site (see text).

A

Local Anesthetic	Non-Competitive Blocker Site		Neurotransmitter Binding Sites	
	C_{50} (μM)[a]	Effect	C_{50} (μM)[c]	Effect
dibucaine	80	D	56	?
lidocaine	2500 (2000)[b]	D	1100	?
prilocaine	3000 (4000)[b]	D	4500	?
tetracaine	1.5	R	800	?

B

Local Anesthetic	Non-Competitive Blocker Site		Neurotransmitter Binding Sites	
	C_{max} (μM)[d]	Effect	C_{max} (μM)[d]	Effect
dibucaine	?	I	200	D
lidocaine	3000	I	10000	D
prilocaine	4000	I	10000	D
tetracaine	10	R	1000	D

supported by the observation of similar band intensity changes in Carb-difference spectra recorded from the nAChR reconstituted into EPC membranes where the nAChR is incapable of undergoing agonist-induced conformational change and is thus presumed to be stabilized in the desensitized conformation (see Chapter 4, Figure 4.1) (155). In addition, the local anesthetic, tetracaine, which is thought to stabilize the nAChR in the resting state, leads to an increase as opposed to a decrease in intensity at each of these five frequencies (see below).

The loss in band intensity attributed to the formation of a desensitized nAChR occurs for all three local anesthetics concomitant with the appearance of negative bands at frequencies that correlate with the molecular vibrations of the local anesthetics themselves. These negative features are clearly detected near 1600, 1405, 1337 and 1186 cm^{-1} in the Carb-difference spectra recorded in the presence of dibucaine, but are only detected upon superimposition of the Carb-difference spectra recorded in the presence and absence of either prilocaine or lidocaine due to the extremely weak intrinsic absorbance intensity of the latter two local anesthetics (Figures 5.2-5.4, blue dashed lines). The appearance of negative local anesthetic bands indicates that the addition of Carb leads to the displacement of each local anesthetic from the nAChR membrane film. Carb does not bind to the ion channel pore at a concentration of 50 μM suggesting that the negative bands do not reflect the competitive displacement of local anesthetics from the non-competitive blocker site. The negative local anesthetic intensity cannot be due to a Carb-induced allosteric displacement of the local anesthetics from the non-competitive

blocker site since the reported affinities of all three local anesthetics are higher in the presence of Carb (156, 159). Control Carb-difference spectra recorded from α-btx treated nAChR membranes also indicate that the majority of the negative local anesthetic intensity is neither due to direct Carb/local anesthetic competition at a previously unidentified site distinct from the neurotransmitter and non-competitive blocker sites nor a non-specific Carb-induced displacement of the local anesthetics from the lipid bilayer (data not shown). The negative local anesthetic bands must, therefore, reflect the competitive displacement of the local anesthetics from the neurotransmitter binding sites upon the addition of Carb. This interpretation is consistent with the known binding of all three local anesthetics to the neurotransmitter binding sites over the studied ranges of local anesthetic concentration (Table 5.1).

The local anesthetics also have subtle effects on the intensity and possibly the frequency of Carb-difference bands that cannot be attributed to either the displacement of local anesthetics from the nAChR or an effect on the equilibrium between the resting and desensitized states. In particular, dibucaine leads to a marked reduction in the intensity of the negative and positive bands located near 1620 and 1516 cm^{-1}, respectively (Figure 5.2, green dashed lines). Lidocaine has a lesser effect on the intensity of both bands whereas prilocaine has no influence on the intensity near 1620 cm^{-1} but elicits a reduction in intensity of the band centered near 1516 cm^{-1} (Figures 5.3 and 5.4, green dashed lines). Note that neither the presence of tetracaine (see below) nor reconstitution of the nAChR

into EPC membranes, both of which influence the conformational status of the nAChR, have marked effects on the intensity of either band (155).

Vibrational bands within the Carb-difference spectrum that are not due to either the resting-to-desensitized conformational transition or the vibrations of nAChR-bound Carb must reflect the formation of physical interactions between Carb and individual neurotransmitter binding site residues. Although the band near 1620 cm^{-1} has yet to be assigned, the large downshift in the frequency of this band observed upon exposure of the nAChR to ^2H_2O suggests that it reflects a side chain vibration (166). The vibration near 1516 cm^{-1}, however, is highly characteristic of a ring stretching vibration of tyrosine and likely reflects an increase in vibrational intensity associated with the formation of cation-tyrosine interactions between Carb and the nAChR (see Discussion). The local anesthetic-induced decrease in intensity of the 1516 cm^{-1} difference band suggests that local anesthetics form similar cation-tyrosine interactions with the nAChR prior to the addition of Carb. In addition, the variable effects of the three local anesthetics on the intensity of these two bands could indicate subtle differences in the ability of the local anesthetics to mimic the binding of Carb to the neurotransmitter binding sites.

The concomitant appearance of spectral variations that are suggestive of the stabilization of a desensitized nAChR, the Carb-induced displacement of local anesthetics from the neurotransmitter binding sites, and the formation of Carb-like physical interactions between local anesthetics and neurotransmitter binding site residues implies that the main 'desensitizing' effect of each local anesthetic occurs as a consequence of

binding to the neurotransmitter binding sites. This interpretation contrasts the current model of local anesthetic action at the nAChR, which suggests that local anesthetics stabilize a desensitized receptor by binding to the non-competitive blocker site and questions whether the binding of local anesthetics to the non-competitive blocker site in fact modulates the conformational equilibrium of the nAChR. A close examination of the concentration dependencies of the spectral variations observed in the presence of prilocaine and lidocaine, however, reveals that there are structural changes that occur exclusively as a result of local anesthetic binding to the non-competitive blocker site.

Prilocaine and lidocaine at concentrations of 4 and 3 mM, respectively, elicit close to maximal changes in the intensity of the two conformationally-sensitive bands near 1663 and 1059 cm^{-1} whereas the bands near 1655 and 1430 cm^{-1} remain largely unaffected (the amide II band near 1547 cm^{-1} is structurally coupled to both amide I bands near 1663 and 1655 cm^{-1} and thus exhibits intermediate changes in intensity) (Figures 5.3 and 5.4, red dashed lines). These local anesthetic concentrations are essentially equivalent to those at which prilocaine and lidocaine bind to the non-competitive blocker site and lead to a maximal increase in the binding of a fluorescent ACh analogue to the neurotransmitter binding sites (180). While the overlapping affinities of prilocaine and lidocaine for the non-competitive blocker and neurotransmitter binding sites prevents an unequivocal interpretation of the data, it appears that the binding of local anesthetics to the non-competitive blocker site induces those residues that vibrate near 1663 and 1059 cm^{-1} to adopt a structure similar to that found in the desensitized state while those

residues that vibrate near 1655 and 1430 cm^{-1} retain a predominantly resting-like structure. Local anesthetic binding to the non-competitive blocker site, therefore, appears to stabilize the nAChR in a conformation that is a structural intermediate between the resting and desensitized states.

Tetracaine Binding to the Non-Competitive Blocker and Neurotransmitter Binding Sites. The structural consequences of local anesthetic binding exclusively to the non-competitive blocker and neurotransmitter binding sites were investigated further by recording Carb-difference spectra in the presence of increasing concentrations of the local anesthetic tetracaine. Tetracaine has more than a 100-fold stronger binding affinity for the non-competitive blocker versus the neurotransmitter binding sites. In addition, unlike dibucaine, prilocaine and lidocaine, the binding of tetracaine to the non-competitive blocker site stabilizes a low affinity ACh binding conformation and is thus presumed to shift the resting-to-desensitized equilibrium towards the resting state (recall that in the absence of agonist and local anesthetic, approximately 80% of the nAChR population adopts the resting state while the remaining 20% adopts the desensitized state) (178).

Carb-difference spectra recorded in the presence of up to 50 μM tetracaine, where binding is restricted to the non-competitive blocker site, exhibit variations in the intensity of the previously noted conformationally-sensitive bands centered near 1663, 1655, 1547, 1430 and 1059 cm^{-1}, although as expected, there is an increase as opposed to a decrease in the intensity of each band (Figure 5.5, red dashed lines). The reversed variations in the intensity of these five bands compared to those observed in the presence of desensitizing

Figure 5.5 A comparison of Carb-difference spectra recorded from affinity purified nAChR reconstituted into membranes composed of EPC/DOPA/Chol (3:1:1), but while continuously maintaining the receptor in contact with increasing concentrations of the local anesthetic, tetracaine. The bottom trace is an absorbance spectrum recorded from a 50 mM aqueous solution of tetracaine (the overlapping absorbance bands of the buffer have been subtracted). The red dashed lines identify tetracaine-induced variations in the intensity of those five bands that are thought to reflect structural changes in the nAChR associated with the resting-to-desensitized conformational transition. The green dashed lines identify both a negative and positive vibrational band thought to reflect specific interactions between Carb and individual neurotransmitter binding site residues. Note that at these tetracaine concentrations, there are no band intensity variations suggestive of the Carb-induced displacement of tetracaine from the nAChR (blue dashed lines).

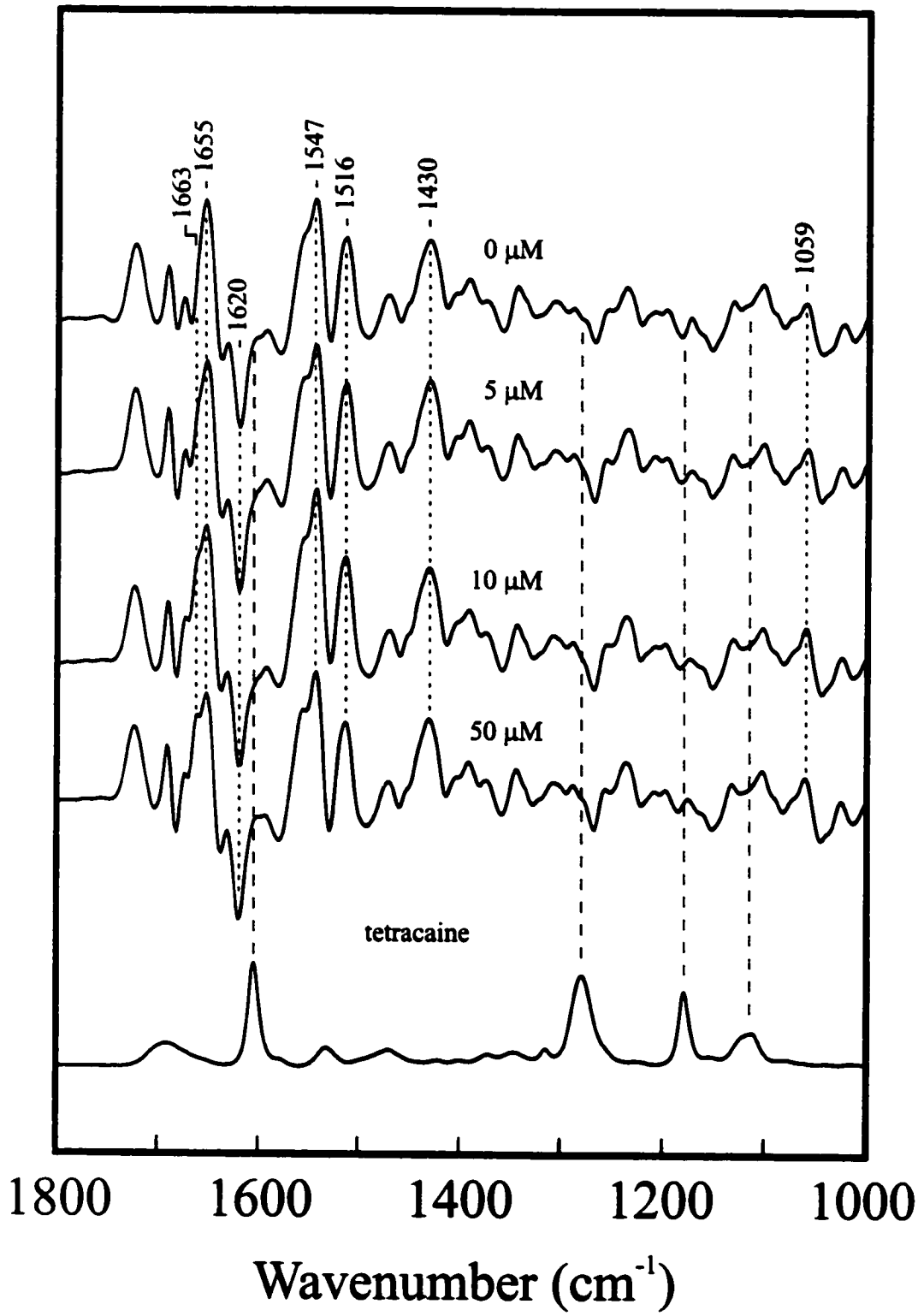
1663
1655
1620
1547
1516
1430
1059
0 μM
5 μM
10 μM
50 μM
tetracaine
1800
1600
1400
1200
1000
Wavenumber (cm-1)

local anesthetics is consistent with the stabilization of a low affinity resting as opposed to a high affinity desensitized state. However, it is significant to note that these concentrations of tetracaine lead to a relatively large increase in intensity near 1663 and 1059 cm^{-1} while the variations in intensity of the bands near 1655 and 1430 cm^{-1} are much less intense (Figures 5.5 and 5.6B). The tetracaine-induced spectral variations are essentially the reverse of those observed at concentrations of prilocaine and lidocaine where maximal structural effects are expected due to local anesthetic binding to the non-competitive blocker site. The binding of local anesthetics to the non-competitive blocker site thus appears to lead to changes in nAChR structure that are reflected predominantly through alterations in the intensity of the two Carb-difference bands near 1663 and 1059 cm^{-1}. Since previous studies have shown that local anesthetics allosterically influence ACh binding affinity by binding to the non-competitive blocker site, the structural changes in the nAChR reflected by these two bands may perform a substantial role in governing agonist affinity, even though they may not constitute the formation of a fully desensitized or resting state receptor (see Discussion). Note that at these low concentrations of tetracaine, there are no bands indicative of the Carb-induced displacement of tetracaine from the neurotransmitter binding sites and minimal, if any, effects on the difference bands near 1620 and 1516 cm^{-1} (Figure 5.5, blue and green dashed lines, respectively).

In contrast, higher concentrations of tetracaine that result in the additional binding to the neurotransmitter binding sites lead to a marked decrease in positive intensity near

Figure 5.6 A comparison of a Carb-difference spectrum recorded from the nAChR reconstituted into membranes composed of EPC/DOPA/Chol (3:1:1) [solid line in (A) and (B)] with those recorded under the same conditions, but while continuously maintaining the receptor in contact with **(A)** 4 mM (---) and 10 mM (– · –) prilocaine and **(B)** 10 μM (---) and 1 mM (– · –) tetracaine. A multiple point baseline correction was performed on all spectra in order to reduce small baseline fluctuations and thus allow for the spectra to be superimposed. Note that the baseline corrections do not affect the intensity or the frequencies of the individual bands (compare the spectra presented here with those presented in Figures 5.3, 5.5 and 5.7, which are not baseline corrected). The negative band near 1605 cm^{-1} in (B) reflects an increase in negative intensity due to the Carb-induced displacement of tetracaine from the neurotransmitter binding sites.

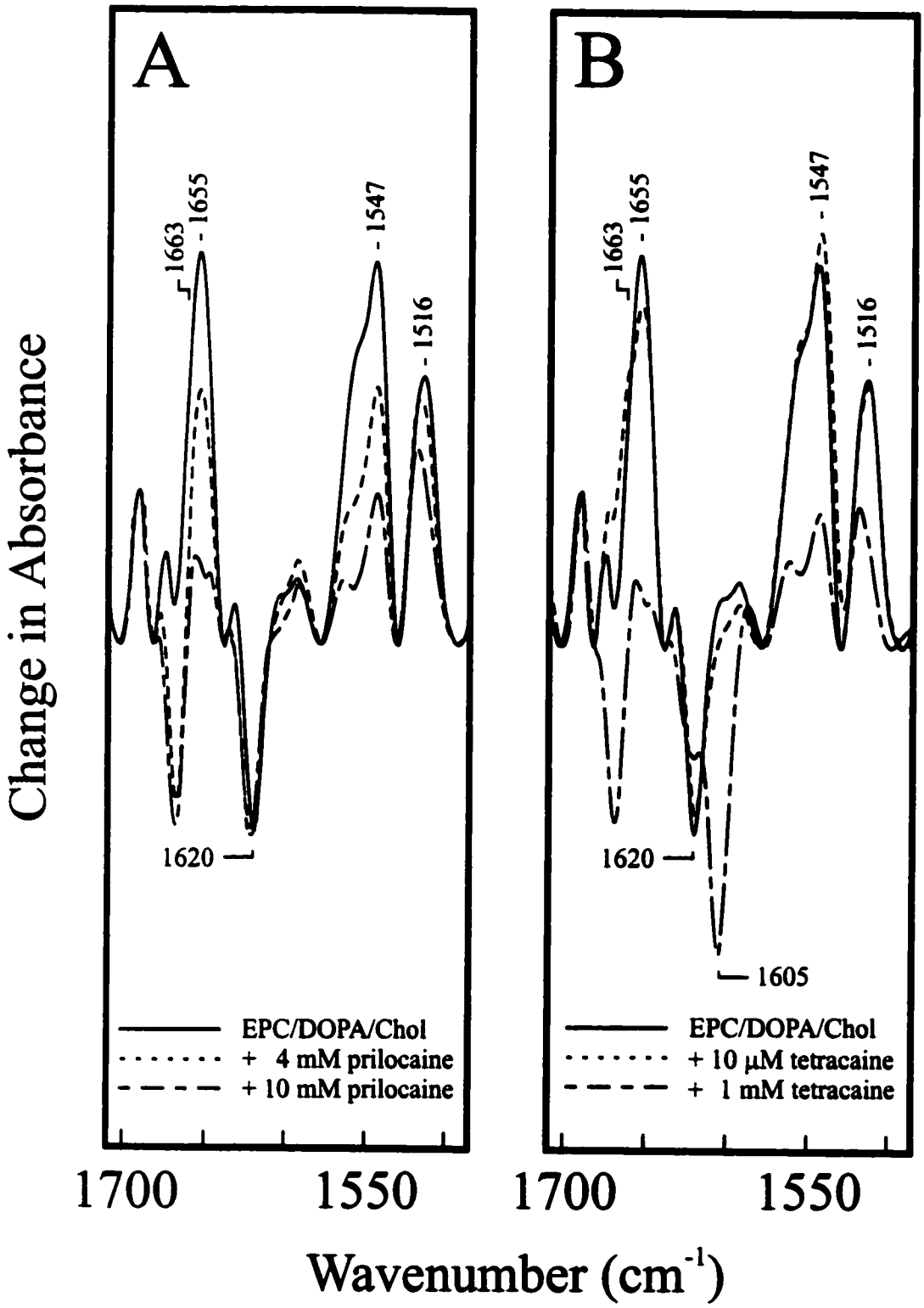
A
B
1663
1655
1547
1516
1620
1605
EPC/DOPA/Chol
+ 4 mM prilocaine
+ 10 mM prilocaine
+ 10 μM tetracaine
+ 1 mM tetracaine
Change in Absorbance
1700
1550
Wavenumber (cm-1)

1663, 1655, 1547, 1430 and 1059 cm^{-1} suggesting a shift back towards a desensitized nAChR (Figures 5.6B and 5.7, red dashed lines). This decrease in intensity of all five bands occurs with similar concentration dependencies suggesting that the structural effects result from tetracaine binding to a single class of sites. The spectra also exhibit negative bands indicative of the Carb-induced displacement of tetracaine from the neurotransmitter binding sites as well as a decrease in the intensity of the two noted bands near 1620 and 1516 cm^{-1} suggesting the formation of direct physical interactions between tetracaine and individual neurotransmitter binding site residues (Figure 5.7, green dashed lines). Together the data indicate that desensitization can occur exclusively as a result of local anesthetic binding to the neurotransmitter binding sites. This finding is consistent with and explains the previously reported increase in ACh binding affinity that is observed at tetracaine concentrations above those necessary to saturate the non-competitive blocker site (178). Note also that the conformational effects of tetracaine binding to the neurotransmitter binding sites overcome any changes in the conformational equilibrium of the nAChR that result from tetracaine binding to the non-competitive blocker site.

DISCUSSION

Previous studies have shown that the positive and negative bands that are observed in the Carb-difference spectrum reflect structural changes in the nAChR that

Figure 5.7 A comparison of Carb-difference spectra recorded from affinity purified nAChR reconstituted into membranes composed of EPC/DOPA/Chol (3:1:1), but while continuously maintaining the receptor in contact with increasing concentrations of the local anesthetic, tetracaine. The bottom trace is an absorbance spectrum recorded from a 50 mM aqueous solution of tetracaine (the overlapping absorbance bands of the buffer have been subtracted). The red dashed lines identify tetracaine-induced variations in the intensity of those five bands that are thought to reflect structural changes in the nAChR associated with the resting-to-desensitized conformational transition. The green dashed lines identify both a negative and positive vibrational band thought to reflect specific interactions between Carb and individual neurotransmitter binding site residues. The blue dashed lines identify band intensity variations due to the Carb-induced displacement of tetracaine from the nAChR.

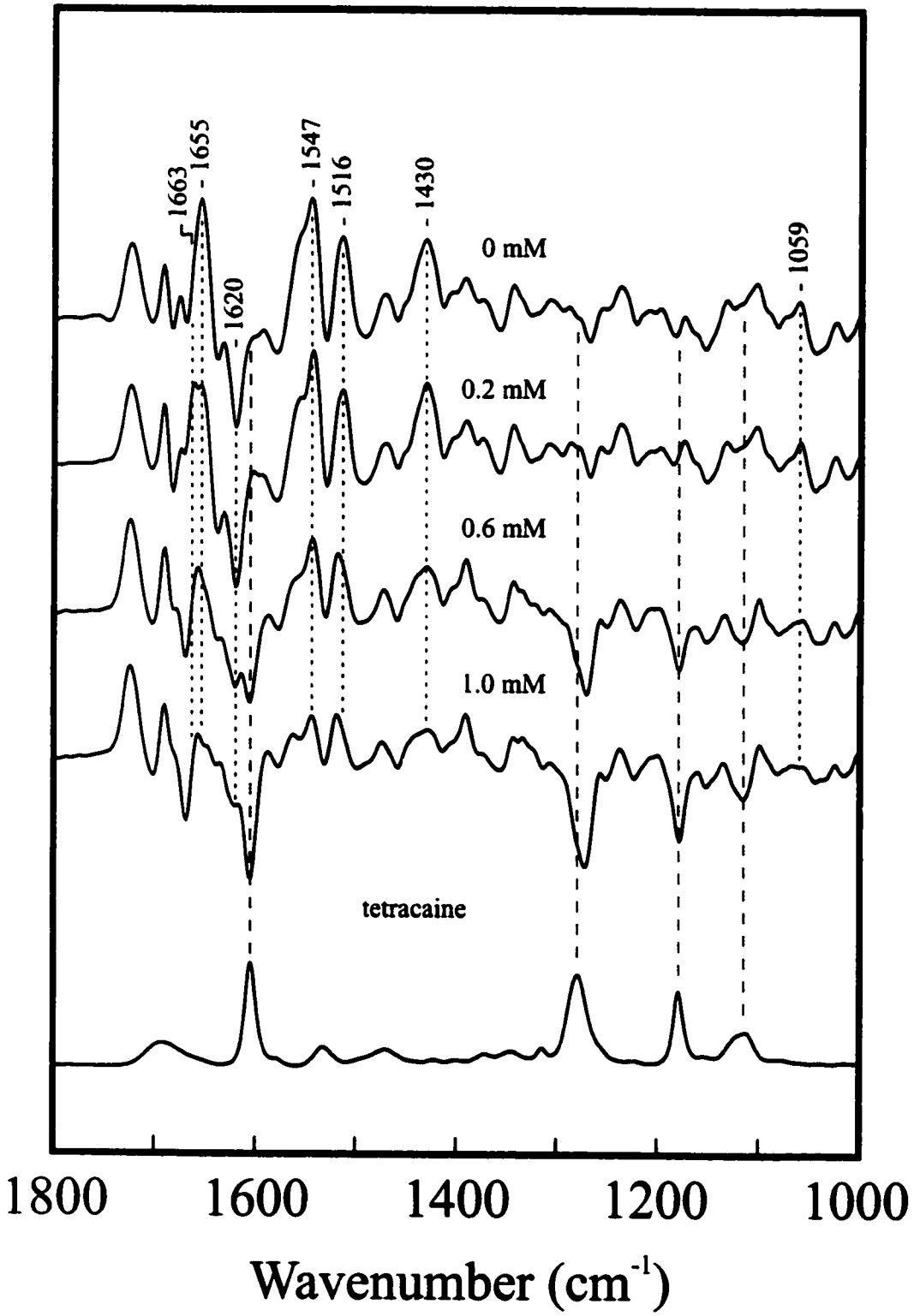
1663
1655
1620
1547
1516
1430
1059
0 mM
0.2 mM
0.6 mM
1.0 mM
tetracaine
1800
1600
1400
1200
1000
Wavenumber (cm-1)

occur specifically from the binding of Carb and subsequent receptor desensitization (127-129). Here it is shown that local anesthetics elicit variations in the intensity of these positive and negative Carb-difference bands at concentrations consistent with the known binding affinities of the local anesthetics for both the non-competitive blocker and/or neurotransmitter binding sites on the nAChR. The close correlation between the dose dependencies of the spectral variations and the reported pharmacological properties of the nAChR provides compelling evidence that the reported spectral variations reflect changes in receptor structure that are responsible for altered function.

The Carb-difference spectra show that dibucaine, prilocaine, lidocaine and tetracaine all bind to the neurotransmitter binding sites and that neurotransmitter site binding leads to a conformational change in the nAChR. This conformational change is characterized by a loss of intensity in the Carb-difference spectrum at five frequencies centered near 1663, 1655, 1547, 1430 and 1059 cm^{-1}. The similarity of the spectral variations elicited by each local anesthetic suggests that each stabilize a similar conformation of the nAChR by binding to the neurotransmitter binding sites. As the local anesthetic-induced conformational change results from a mimicking of Carb binding to these sites (see below), the loss of intensity at these five frequencies likely reflects the formation of a desensitized conformation equivalent to that stabilized by prolonged exposure to agonist. This interpretation is consistent with the observation of similar band intensity changes in Carb-difference spectra recorded from the nAChR reconstituted into

EPC membranes where the nAChR is incapable of undergoing agonist-induced desensitization and is thus assumed to be stabilized in the desensitized state (143, 155).

The Carb-difference spectra also show that local anesthetic binding to the non-competitive blocker site leads to conformational changes in the nAChR, but that these changes are characterized mainly by variations in band intensity near 1663 and 1059 cm^{-1}. Prilocaine and lidocaine both lead to a loss of intensity near 1663 and 1059 cm^{-1}. In contrast, tetracaine leads mainly to an increase in intensity of both bands. Significantly, the opposing structural effects of prilocaine/lidocaine and tetracaine are consistent with the opposing allosteric effects of these local anesthetics on ACh binding affinity at the neurotransmitter binding sites. The binding of either prilocaine or lidocaine to the non-competitive blocker site leads to an increase in binding affinity for ACh whereas the binding of tetracaine leads to a decrease (178, 180). The structural changes reflected by the vibrations near 1663 and 1059 cm^{-1} may, therefore, be largely responsible for variations in agonist affinity even though they do not represent the formation of either a fully desensitized or resting state receptor.

The data, therefore, suggest that a limited region of the polypeptide backbone, represented by the vibrational bands near 1663 and 1059 cm^{-1}, can independently interconvert between the resting and desensitized conformations. The binding of desensitizing local anesthetics to the non-competitive blocker site appears to cause this region or loop of the polypeptide backbone to shift from a resting to a desensitized-like conformation while the remainder of the nAChR retains a predominantly resting-like

conformation. In contrast, tetracaine binding to the non-competitive blocker site appears to shift the same region from a desensitized-like conformation to a resting conformation.

The results suggest a revised model of local anesthetic action at the nAChR (Figure 5.8). In this model, the nAChR, in the absence of agonist and local anesthetics, exists within a conformational equilibrium between not two, but at least three distinct conformations: resting, desensitized and a novel intermediate state. Within the intermediate state, the nAChR's ion channel is proposed to adopt a predominantly desensitized-like conformation while the neurotransmitter binding sites retain a predominantly resting-like conformation. There are, however, likely subtle changes in the neurotransmitter binding sites that provide the intermediate state with an affinity for agonist somewhere between that of both the resting and desensitized states. The binding of so-called 'desensitizing' local anesthetics, such as prilocaine and lidocaine to the non-competitive blocker site induces a shift in the nAChR's conformational equilibrium towards the intermediate state (characterized by a decrease in vibrational intensity in the Carb-difference spectrum near 1663 and 1059 cm^{-1}). In contrast, the local anesthetic tetracaine, which stabilizes a low affinity binding conformation, binds to the non-competitive blocker site and induces a shift in the conformational equilibrium towards the resting state (characterized by an increase in intensity in the Carb-difference spectrum near 1663 and 1059 cm^{-1}). In addition, the model proposes that regardless of the conformation stabilized by local anesthetic binding to the non-competitive blocker site, higher concentrations of local anesthetics, where the additional binding to the

Figure 5.8 A revised model of local anesthetic action at the nAChR. In the absence of agonist and local anesthetic, the nAChR exists within an equilibrium between not two, but at least three distinct conformations: resting, desensitized and a novel intermediate state (grey box). The channel-competent resting state is characterized by its low affinity for agonist while the channel-inactive desensitized state is characterized by its high affinity for agonist. In contrast, the intermediate state displays structural features in common with both the resting and desensitized states. In the intermediate state, the nAChR's ion channel is proposed to adopt a predominantly desensitized-like conformation while the neurotransmitter binding sites retain a predominantly resting-like conformation. There are, however, likely subtle changes in the neurotransmitter binding sites that provide the intermediate state with an affinity for agonist somewhere between that of both the resting and desensitized states. The results suggest that the binding of so-called 'desensitizing' local anesthetics, such as prilocaine and lidocaine, to the non-competitive blocker site, induces a shift in the nAChR's conformational equilibrium towards the intermediate state (bottom pathway). In contrast, some local anesthetics, such as tetracaine, bind to the non-competitive blocker site and induce a shift towards the resting state (top pathway). Regardless of the conformational state stabilized by local anesthetic binding to the non-competitive blocker site, however, the additional binding to the neurotransmitter binding sites results in the stabilization of the nAChR in a conformation that is analogous to the agonist-induced desensitized state.

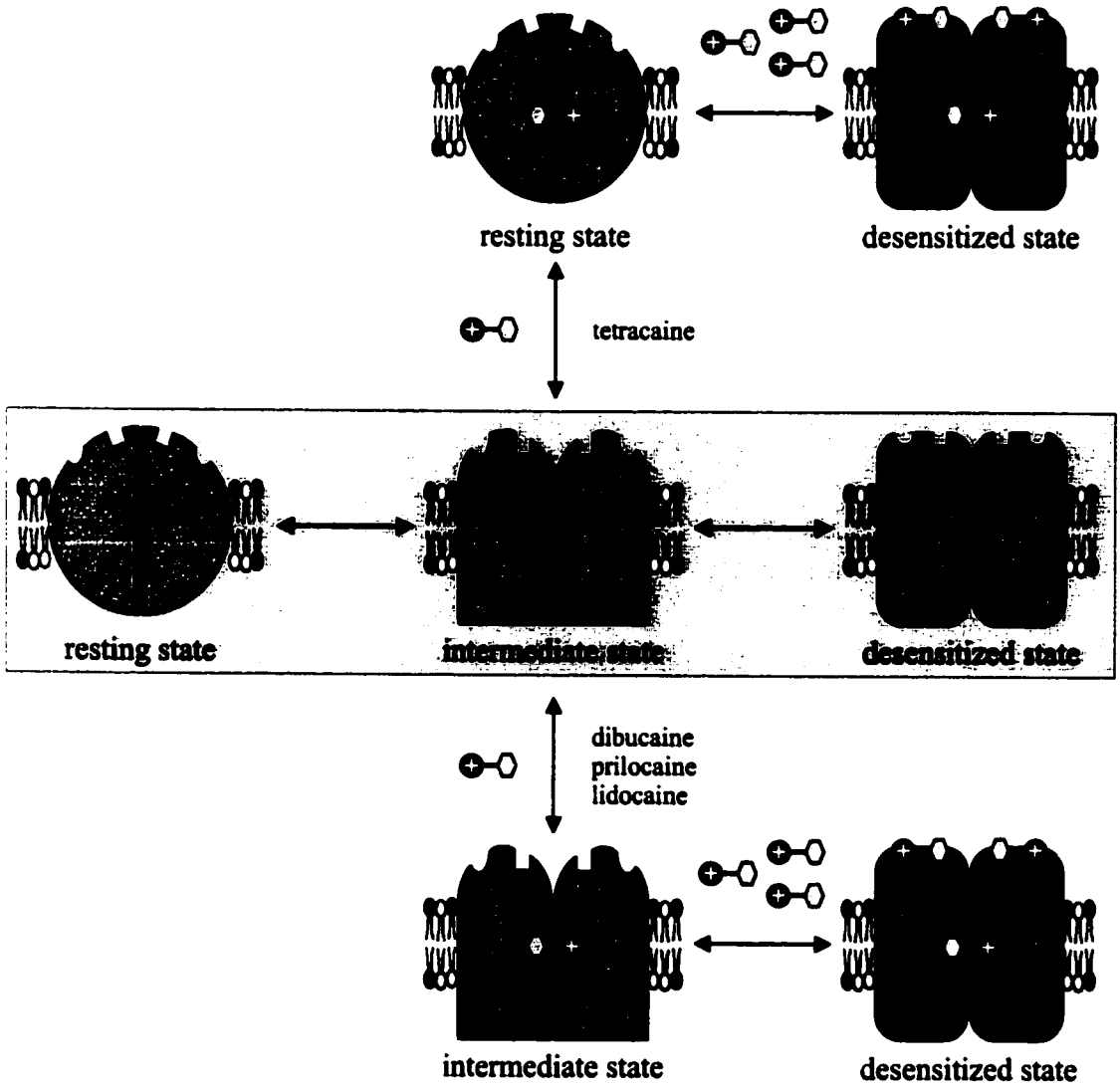
resting state
desensitized state
tetracaine
resting state
intermediate state
desensitized state
dibucaine
prilocaine
lidocaine
intermediate state
desensitized state
local anesthetic

neurotransmitter binding sites occurs, stabilizes the nAChR in a conformation that is analogous to the agonist-induced desensitized state.

Further studies with local anesthetics that bind exclusively to the non-competitive blocker site with high potency are clearly required to test the above model. Kinetic ACh binding studies are also necessary to relate any newly defined structural conformations to the various fast and slow desensitized states that have been identified previously (114, 158, 182-184). However, it is clear that the effects of local anesthetics on nAChR conformation are complex and result from binding to at least two distinct pharmacological sites, in agreement with the previous studies of Heidmann et al. (179). The conformation of the nAChR that is stabilized by a particular local anesthetic at a given concentration is dependent upon the relative affinities of the local anesthetic for the neurotransmitter and non-competitive blocker sites and either the complimentary or competing conformational effects that result from local anesthetic binding to each of these two sites. As an example, tetracaine stabilizes a desensitized conformation by binding to the neurotransmitter binding sites even though simultaneous binding to the non-competitive blocker site favours the formation of the resting state.

In addition to binding to both the non-competitive blocker and neurotransmitter binding sites, some local anesthetics, such as chlorpromazine and trimethisoquin, bind to saturable low affinity allosteric sites on the nAChR thought to be located near the lipid-protein interface (179). While such low affinity sites have yet to be demonstrated for dibucaine, lidocaine and prilocaine, these local anesthetics could bind to such low affinity

sites leading to some of the vibrational changes observed here in the Carb-difference spectra. However, despite large differences in the potencies of the three local anesthetics, there is a close correlation between the concentrations of the local anesthetics required to elicit the observed vibrational changes and the reported nAChR binding affinities (Table 5.1). This suggests that the observed structural changes result from local anesthetic interactions at the non-competitive blocker and neurotransmitter binding sites. Consistent with this interpretation, all the vibrational changes attributed to local anesthetic binding to the neurotransmitter binding sites occur concomitant with the appearance of spectral features indicative of Carb-induced displacement of the local anesthetics from the neurotransmitter binding sites. In addition, the vibrational changes attributed to a conformational change resulting from tetracaine binding to the non-competitive blocker site occur at micromolar concentrations that are well below those expected for binding to the low affinity nAChR sites. Consequently, although subtle structural effects of local anesthetic binding to low affinity sites are possible, the observed spectral changes likely arise as a result of local anesthetic binding to either the non-competitive blocker or neurotransmitter binding sites.

The local anesthetic-induced changes in the Carb difference spectra also provide insight into the nature of the physical interactions that occur between the local anesthetics and individual neurotransmitter binding site residues. The relatively high concentrations of dibucaine, prilocaine, lidocaine, and tetracaine that result in binding to the neurotransmitter sites lead to a reduction in the intensity of the two difference bands near

1620 and 1516 cm^{-1}. The vibration near 1516 cm^{-1} is highly characteristic of a tyrosine ring stretching vibration. Several tyrosine residues are found in the neurotransmitter binding sites and perform a critical role in agonist binding likely via the formation of cation-tyrosine-π-electron interactions (66, 71, 73, 75, 185). Carb-tyrosine interactions have also been shown to be critical for gating the nAChR ion channel. Difference spectra recorded in the absence of local anesthetics using the Carb analog, tetramethylammonium (Figure 5.9), exhibit a 1516 cm^{-1} band of comparable intensity to that observed in Carb-difference spectra indicating that the vibration is specific to interactions with the cationic ammonium group of Carb (data not shown). A substantial portion of the 1516 cm^{-1} difference band may, therefore, be due to an increase in tyrosine vibrational intensity that results from the formation of cation-π–electron interactions. The ability of some local anesthetics to substantially reduce the intensity of this vibration upon binding to the neurotransmitter binding site suggests that local anesthetics mimic the cation-tyrosine interactions that perform a key role in agonist action at the nAChR.

Compared to dibucaine and tetracaine, neither prilocaine nor lidocaine has as dramatic an effect on the intensity of the two vibrations near 1620 and 1516 cm^{-1}. The binding of both prilocaine and lidocaine to the neurotransmitter binding sites is much weaker than the binding of dibucaine and tetracaine (Table 5.1). In addition, prilocaine and lidocaine differ structurally from the other two local anesthetics in that they have only one instead of three atoms between the charged nitrogen and the carbonyl carbon (Figure 5.9). The reduced distance between the nitrogen and ester carbonyl could prevent binding

Figure 5.9 A comparison of the structures of the local anesthetics dibucaine, prilocaine, lidocaine and tetracaine with those of the agonists ACh, Carb and tetramethylammonium.

ACh

Carb

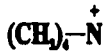

tetramethylammonium

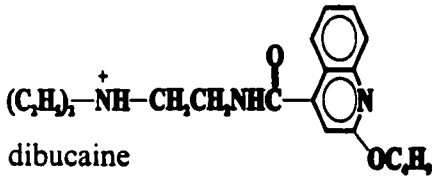

dibucaine

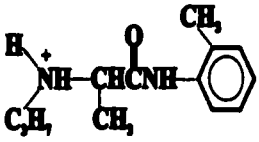

prilocaine

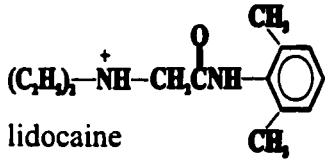

lidocaine

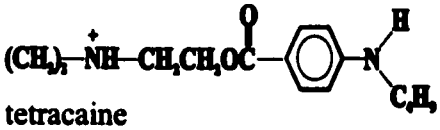

tetracaine

to the neurotransmitter binding sites in a manner that allows both prilocaine and lidocaine to interact simultaneously at both the cationic and esterophilic subsites (see Chapter 1, Figure 1.7) (187). Alternatively, the reduced number of carbon atoms could bring the bulky aromatic groups of the local anesthetics closer to the charged nitrogen and thus prevent tight binding of the local anesthetics to the cationic binding subsite. While more detailed studies are required in order to both assign the two vibrations to specific amino acids and to interpret the local anesthetic induced changes in intensity, the variable influence of the local anesthetics likely reflect subtle differences in the manner in which the local anesthetics bind to the neurotransmitter sites as a consequence of their slightly different chemical structures.

The binding of local anesthetics to the neurotransmitter binding sites and mimicry of agonist-induced desensitization is likely governed by the ammonium cation. All local anesthetics that have been studied here both possess a positively charged nitrogen moiety and appear to stabilize the same desensitized conformation of the nAChR by forming interactions between the charged nitrogen and neurotransmitter binding site tyrosine residues. In contrast, local anesthetic action at the non-competitive blocker site is likely governed by the hydrophobic substituents on the local anesthetics. ACh and Carb, which lack large hydrophobic substituents, bind to the non-competitive blocker site with extremely weak affinity while the interactions of neutral general anesthetics within the ion channel pore are governed by hydrophobicity (188). A greater structural diversity is also found in the hydrophobic substituents of the various local anesthetics than is found

with the charged nitrogen substituents. These structural differences may be responsible for the contrasting conformational effects of lidocaine/prilocaine and tetracaine at the non-competitive blocker site.

The ability to probe both the physical interactions that occur between local anesthetics and amino acid side chains and the conformational states of the nAChR using a structure based approach represents a step towards defining the molecular details of local anesthetic action at the nAChR. Further technical advancements should lead to kinetic infrared studies of ACh binding to the various conformational states and thus allow the conformations defined here to be correlated with those identified previously using ACh kinetic binding studies. The use of site-directed mutagenesis should also lead to the identification of both those regions of the nAChR that are involved in the specific conformational changes and the specific residues that are involved in direct physical interactions with the bound local anesthetics.

CONCLUSIONS

The primary goal of this study was to employ FTIR difference spectroscopy to probe the structural consequences of local anesthetic binding to the nAChR in the hope of gaining insight into the molecular details of local anesthetic action at the nAChR. The results reveal that the effects of local anesthetics on the conformation of the nAChR are complex and arise from local anesthetic binding to at least two distinct pharmacological

sites. The binding of local anesthetics to the neurotransmitter binding sites and mimicry of specific cation-tyrosine interactions stabilizes the nAChR in a conformation that is analogous to the agonist-induced desensitized state. In contrast, the binding of local anesthetics to the non-competitive blocker site appears to modulate the conformational equilibrium of the nAChR between the resting, desensitized and a novel intermediate state. The binding of so-called 'desensitizing' local anesthetics, such as prilocaine and lidocaine, to the non-competitive blocker site induces a shift in this equilibrium towards the intermediate state. The local anesthetic tetracaine, on the other hand, induces a shift in this equilibrium towards the resting state.

CHAPTER 6

A STRUCTURAL INTERMEDIATE BETWEEN THE RESTING AND DESENSITIZED STATES OF THE NICOTINIC ACETYLCHOLINE RECEPTOR

INTRODUCTION

The magnitude of the cation flux response elicited by ACh at the postsynaptic membrane is dependent upon a variety of factors. These factors include both the number of nAChRs present within the postsynaptic membrane and the proportion of these receptors that exist in active versus inactive conformations. As an example, within its native membrane, the nAChR from *Torpedo* exists within an equilibrium between at least two distinct conformations: a low affinity channel-competent resting state and a high affinity channel-inactive desensitized state (178). In the absence of ACh this equilibrium strongly favours the resting conformation with only approximately 20% of the receptors adopting the desensitized state (178). Prolonged exposure to ACh, however, induces a shift in this equilibrium towards the desensitized state thus diminishing the postsynaptic response. In addition, the equilibrium between the resting and desensitized states and/or the kinetics of the resting-to-desensitized conformational transition can be influenced by a variety of endogenous factors including receptor phosphorylation and membrane lipid composition.

The ability of the nAChR to conduct cations across the membrane can be modulated further by a class of structurally diverse compounds collectively referred to as non-competitive blockers. These non-competitive blockers, which include both general and local anesthetics, the hallucinogenic drug phencyclidine hydrochloride (PCP) and the frog toxin histrionicotoxin and its derivatives, sterically inhibit the cation flux capabilities of the nAChR by binding to a distinct non-competitive blocker site located within the

receptor's ion channel pore (158, 159, 180, 181, 183, 189, 190-193). The binding of non-competitive blockers to the ion channel pore also modulates the affinity of the nAChR for ACh. Both the local anesthetics dibucaine, prilocaine, lidocaine and proadifen and the hallucinogen, PCP increase the affinity of the nAChR for ACh and are thus thought to shift the conformational equilibrium of the receptor towards the desensitized state. Other local anesthetics, such as tetracaine and adiphenine, decrease the affinity of the nAChR for ACh and are thus thought to shift the conformational equilibrium towards the resting state (158, 177, 178).

Previously, the structural consequences of local anesthetic binding to the nAChR were investigated using FTIR difference spectroscopy (170). In agreement with the current model of non-competitive blocker action, Carb-difference spectra recorded from the nAChR while maintaining the receptor in continuous contact with a variety of local anesthetics suggest that local anesthetics stabilize a desensitized conformation. Contrary to this model, however, the FTIR data suggest that desensitization occurs not through interactions at the non-competitive blocker site, but solely as a result of local anesthetic binding to the neurotransmitter binding sites. The data also suggest that the binding of local anesthetics to the non-competitive blocker site stabilizes a novel intermediate conformation that exhibits structural features in common with both the resting and desensitized states. Unfortunately, the overlapping binding affinities of the studied local anesthetics for both the non-competitive blocker and neurotransmitter binding sites

prevented an unequivocal assessment of the structural changes elicited specifically upon local anesthetic binding to the non-competitive blocker site.

The possible existence of a stable structural intermediate between the resting and desensitized states has implications for understanding the mechanisms of agonist-induced nAChR conformational change. The existence of such an intermediate state in vivo could also play an important role in modulating the postsynaptic response to ACh. In this study, FTIR difference spectroscopy has been employed to directly monitor the structural changes that occur upon the binding of the local anesthetic, proadifen, and the hallucinogen, PCP, to the nAChR. Both proadifen and PCP have widely disparate affinities for both the non-competitive blocker and neurotransmitter binding sites and thus should allow those structural changes that occur as a consequence of binding to the non-competitive blocker site to be resolved with little interference from the structural changes that occur as a consequence of binding to the neurotransmitter binding sites. The results support the findings of the previous study and show conclusively that both local anesthetics and PCP bind to the non-competitive blocker site and stabilize the nAChR in a novel intermediate conformation that is distinct from both the resting and agonist-induced desensitized state.

EXPERIMENTAL PROCEDURES

Materials. PCP was generously provided as a gift from Health Canada.

NAChR Affinity Purification, Reconstitution and FTIR Difference Spectroscopy. For a detailed description, see Chapter 3, Experimental Procedures.

Hydrogen/Deuterium Exchange FTIR Difference Spectroscopy. Carb-difference spectra in ^2H_2O were recorded as described in Chapter 3, Experimental Procedures, with the following modifications. First, the affinity purified nAChR sample in ^1H_2O phosphate buffer (pH 8.0) was centrifuged and the supernatant removed with a glass pipette. The pellet was re-suspended in 1 ml of ^2H_2O phosphate buffer (pH 8.0), centrifuged and the supernatant again discarded. The pellet was then re-suspended in 1 ml of ^2H_2O phosphate buffer and left at 4 °C for three days to allow for complete $^1H/^2H$ exchange. Second, both the +Carb and –Carb flowing buffers were made using ^2H_2O. Finally, to reduce the amount of ^2H_2O required for the acquisition of the Carb-difference spectra, only one resting state spectra, rather than two, was recorded.

Proadifen and PCP Solution Spectra. An absorbance spectrum of proadifen in Torpedo Ringer buffer (pH 7.0) was recorded using the ATR technique. The spectrum is an average of 250 scans acquired at a resolution of 2 cm^{-1}. The overlapping absorbance bands of the buffer were subtracted. For PCP, 50 µl of a 50 mM PCP stock solution was spread on the surface of a germanium IRE and the bulk solvent evaporated using a gentle stream of N_2 gas. An absorbance spectrum of dry PCP was then recorded using the ATR technique. The spectrum is an average of 250 scans acquired at a resolution of 2 cm^{-1}.

RESULTS

Carb-difference spectra recorded from the nAChR reconstituted into membranes composed of EPC/DOPA/Chol (3:1:1) reveal a complicated pattern of positive and negative bands that reflect variations in the vibrations of those amino acid residues whose structures and/or surrounding environments differ between the resting and Carb-induced desensitized state (127-129). In particular, the Carb-difference spectrum exhibits bands that reflect 1) the vibrations of distinct functional groups within nAChR-bound Carb, 2) vibrational changes associated with the formation of direct physical interactions between Carb and individual neurotransmitter binding site residues and 3) vibrational changes associated with the resting-to-desensitized conformational transition. Comprehensive studies with local anesthetics and with the nAChR reconstituted into membranes of defined lipid composition indicate that those positive vibrational bands centered near 1663, 1655, 1547, 1430 and 1059 cm^{-1} reflect structural changes in the nAChR associated with the resting-to-desensitized conformational transition (155, 170, 194). Variations in the intensity of these five bands can thus serve as a marker of the ability of the nAChR to undergo the resting-to-desensitized conformational transition.

Proadifen-Induced Variations in NAChR Structure. Carb-difference spectra recorded from the nAChR while maintaining the receptor in continuous contact with the local anesthetic proadifen exhibit dose dependent band intensity variations that reflect the structural consequences of proadifen binding to the nAChR (Figures 6.1 and 6.2). Proadifen binds with a relatively high affinity to the ion channel pore (K_D = ~3 μM) and

Figure 6.1 A comparison of selected regions of Carb-difference spectra recorded from the nAChR while continuously maintaining the receptor in contact with low concentrations of the local anesthetic, proadifen. The bottom trace is an absorbance spectrum recorded from a 50 mM aqueous solution of proadifen (the overlapping absorbance bands of the buffer have been subtracted). At concentrations up to 50 μM proadifen, where binding occurs predominantly to the non-competitive blocker site, there is a substantial reduction in the intensity of two of the conformationally sensitive bands near 1663 and 1059 cm^{-1}. In contrast, the intensity of the vibrational bands near 1655 and 1430 cm^{-1} remain largely unaffected. The amide II band near 1547 cm^{-1} is structurally coupled to both amide I bands near 1663 and 1655 cm^{-1} and thus exhibits intermediate changes in intensity. Note that at 50 μM proadifen, negative bands are beginning to appear at frequencies that match those of the vibrations of proadifen itself (blue dashed lines). This suggests that proadifen is being competitively displaced from the neurotransmitter binding sites by Carb and that further band intensity variations observed at higher proadifen concentrations reflect additional structural changes in the nAChR that arise as a consequence of proadifen binding to the neurotransmitter binding sites.

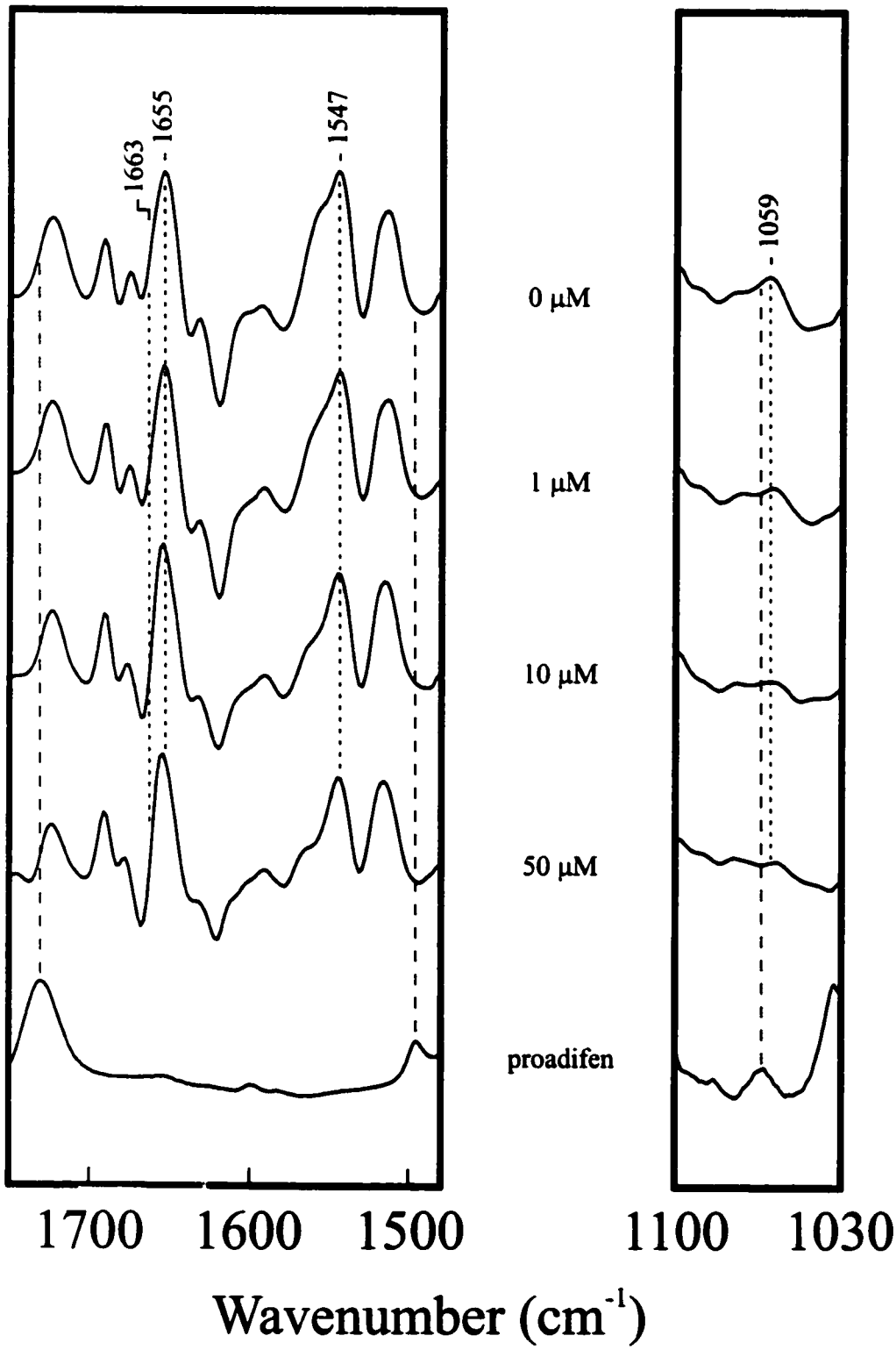
1663
1655
1547
1059
0 μM
1 μM
10 μM
50 μM
proadifen
1700
1600
1500
1100
1030
Wavenumber (cm-1)

Figure 6.2 A comparison of selected regions of Carb-difference spectra recorded from the nAChR while continuously maintaining the receptor in contact with high concentrations of the local anesthetic, proadifen. The bottom trace is an absorbance spectrum recorded from a 50 mM aqueous solution of proadifen (the overlapping absorbance bands of the buffer have been subtracted). High concentrations of proadifen, where the additional binding to the neurotransmitter binding sites occurs, results in no further band intensity variations near 1663 and 1059 cm^{-1}. There is, however, a dose dependent reduction in the intensity of the two conformationally sensitive bands near 1655 and 1430 cm^{-1}. Due to the presence of a large positive spectral distortion in the 1700-1500 cm^{-1} region, the decrease in intensity near 1655 cm^{-1} can be most easily visualized by comparing the intensity of this band relative to the inflection point centered near 1632 cm^{-1} (green dashed line). Note that the reduction in intensity near 1655 and 1430 cm^{-1} occurs concomitantly with an increase in negative intensity at frequencies that match the vibrational frequencies of proadifen itself (blue dashed lines). This suggests that proadifen is being competitively displaced from the neurotransmitter binding sites by Carb and provides further support that the additional structural changes in the nAChR reflected by the decrease in intensity near 1655 and 1430 cm^{-1} arise as a consequences of proadifen binding to the neurotransmitter binding sites.

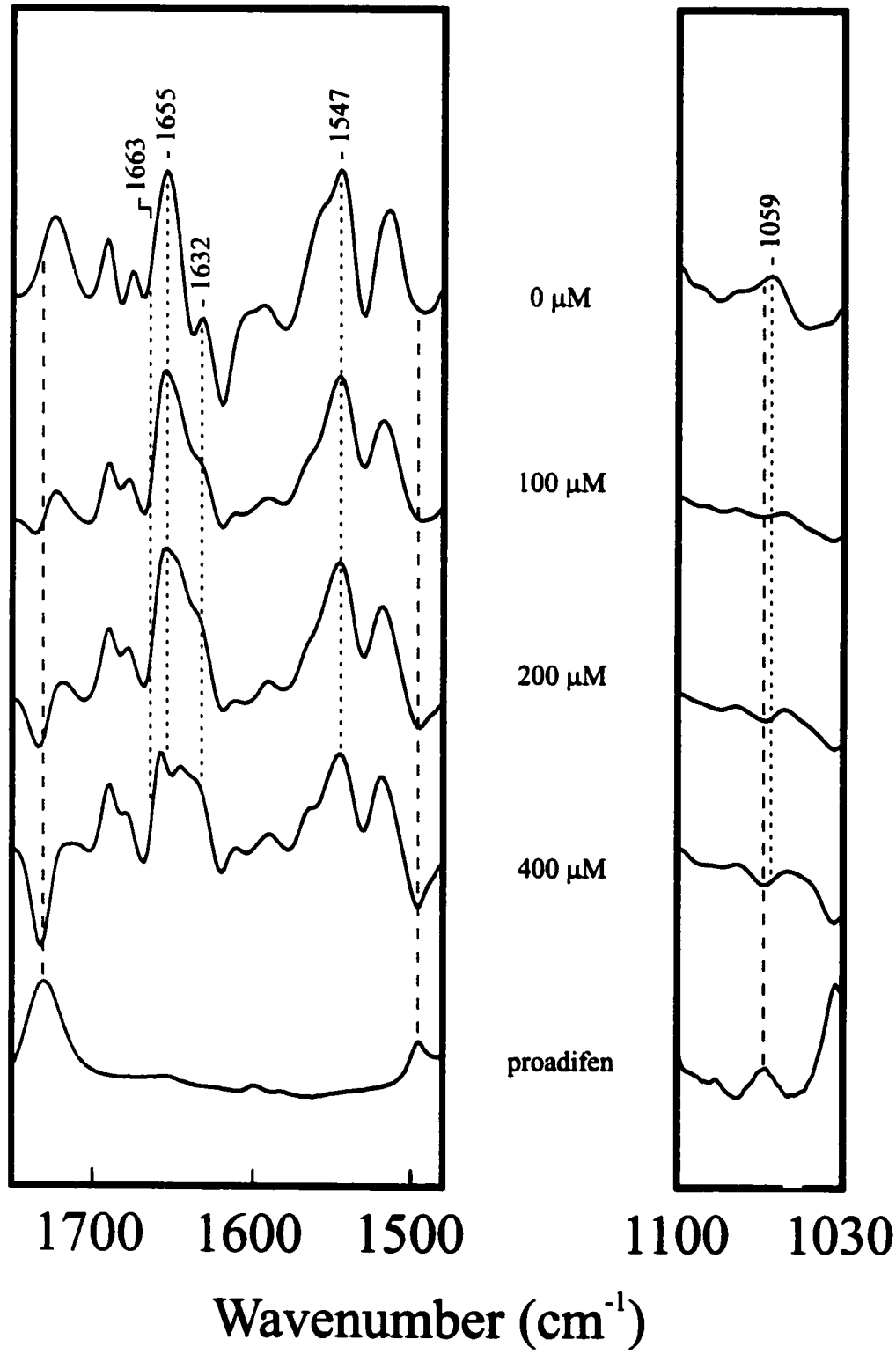
1663
1655
1632
1547
1059
0 μM
100 μM
200 μM
400 μM
proadifen
1700
1600
1500
1100
1030
Wavenumber (cm-1)

with a relatively low affinity to the neurotransmitter binding sites (K_D = ~400 μM) (156). Band intensity variations observed in Carb-difference spectra recorded at proadifen concentrations up to 50 μM thus reflect structural changes in the nAChR that result predominantly from proadifen binding to the non-competitive blocker site (Figure 6.1). Specifically, the Carb-difference spectra exhibit a marked reduction in the intensity of two of the five noted conformationally-sensitive bands near 1663 and 1059 cm^{-1} whereas the intensity of the vibrational bands centered near 1655 and 1430 cm^{-1} remain largely unaffected (the positive amide II band near 1547 cm^{-1} is structurally coupled to both amide I bands near 1663 and 1655 cm^{-1} and thus exhibits intermediate changes in intensity). The reduction in band intensity near 1663 and 1059 cm^{-1} is evident at 10 μM proadifen but becomes much more pronounced at 50 μM proadifen where the positive intensity at both frequencies is almost completely absent. These results suggest that the binding of proadifen to the non-competitive blocker site induces those residues that vibrate near 1663 and 1059 cm^{-1} to adopt a predominantly desensitized-like conformation prior to the addition of Carb, while those residues that vibrate near 1655 and 1430 cm^{-1} retain a predominantly resting-like conformation. In agreement with previous Carb-difference spectra recorded from the nAChR in the presence of low concentrations of the local anesthetics prilocaine and lidocaine, proadifen appears to bind to the non-competitive blocker site and stabilize the nAChR in a conformation that is a structural intermediate between the resting and desensitized states.

Carb-difference spectra recorded at higher concentrations of proadifen, where the additional binding to the neurotransmitter binding sites occurs, are presented in Figure 6.2. These spectra, however, are slightly distorted for two reasons. First, the partitioning of proadifen into the lipid bilayers causes the nAChR film on the germanium IRE to expand and contract, the result of which, is the appearance of a broad positive artifact in the 1500-1700 cm^{-1} region. Secondly, the Carb-difference spectra exhibit a number of large negative bands at frequencies that correlate with the molecular vibrations of proadifen itself (Figure 6.2, blue dashed lines). These negative bands occur over a range of concentrations consistent with the reported dissociation constant of proadifen for the neurotransmitter binding sites suggesting that they reflect the competitive displacement of proadifen from the neurotransmitter binding sites upon the addition of Carb.

Despite the noted spectral distortions, it is clear that the additional binding of proadifen to the neurotransmitter binding sites results in no further band intensity variations near 1663 and 1059 cm^{-1}. This suggests that the majority of those residues in the nAChR that give rise to the bands at these two frequencies are fully stabilized in a desensitized conformation solely upon proadifen binding to the non-competitive blocker site. In contrast, the binding of proadifen to the neurotransmitter binding sites results in a substantial loss in intensity near 1655 and 1430 cm^{-1}. For the band centered near 1655 cm^{-1}, this loss in intensity can be most easily visualized by comparing the intensity near 1655 cm^{-1} relative to that of the inflection point centered near 1632 cm^{-1} (compare the Carb-difference spectra recorded in the presence of 100 and 400 μM proadifen, which

both exhibit the spectral distortion) (Figure 6.2). The additional binding of proadifen to the neurotransmitter binding sites thus appears to induce those residues that vibrate near 1655 and 1430 cm^{-1} to adopt a desensitized conformation prior to the addition of Carb. In agreement with Carb-difference spectra recorded from the nAChR in the presence of high concentrations of the local anesthetics dibucaine, prilocaine, lidocaine and tetracaine, proadifen appears to stabilize the nAChR in a fully desensitized conformation only upon binding to the neurotransmitter binding sites (170).

PCP-Induced Variations in nAChR Structure. Additional evidence for the existence of a conformational intermediate between the resting and desensitized states of the nAChR was obtained from Carb-difference spectra recorded from the nAChR while continuously maintaining the receptor in contact with the hallucinogen, PCP (Figure 6.3). Like proadifen, PCP binds with a relatively high affinity to the non-competitive blocker site (K_D = ~5 μM), but with a low affinity to the neurotransmitter binding sites (K_D = ~250 μM) (179). At concentrations up to 100 μM PCP, where binding occurs predominantly to the non-competitive blocker site, the Carb-difference spectra exhibit similar, but less pronounced spectral variations to those observed in the presence of proadifen, including a dose-dependent decrease in intensity near 1663, 1547 and 1059 cm^{-1}. Furthermore, like proadifen, the binding of PCP to the non-competitive blocker site has little, if any, effect on the intensity of the Carb-difference bands centered near 1655 and 1430 cm^{-1}. Although PCP does not appear to be as efficient as proadifen in inducing those residues that vibrate near 1663 and 1059 cm^{-1} to adopt a desensitized-like

Figure 6.3 A comparison of selected regions of Carb-difference spectra recorded from the nAChR while continuously maintaining the receptor in contact with increasing concentrations of the hallucinogen, PCP. Low concentrations of PCP, where binding occurs predominantly to the non-competitive blocker site, results in a dose dependent decrease in the intensity of two of the conformationally sensitive bands near 1663 and 1059 cm^{-1}. In addition, the intensity of the bands near 1655 and 1430 cm^{-1} remain largely unaffected while the amide II band near 1547 cm^{-1} exhibits intermediate changes in intensity.

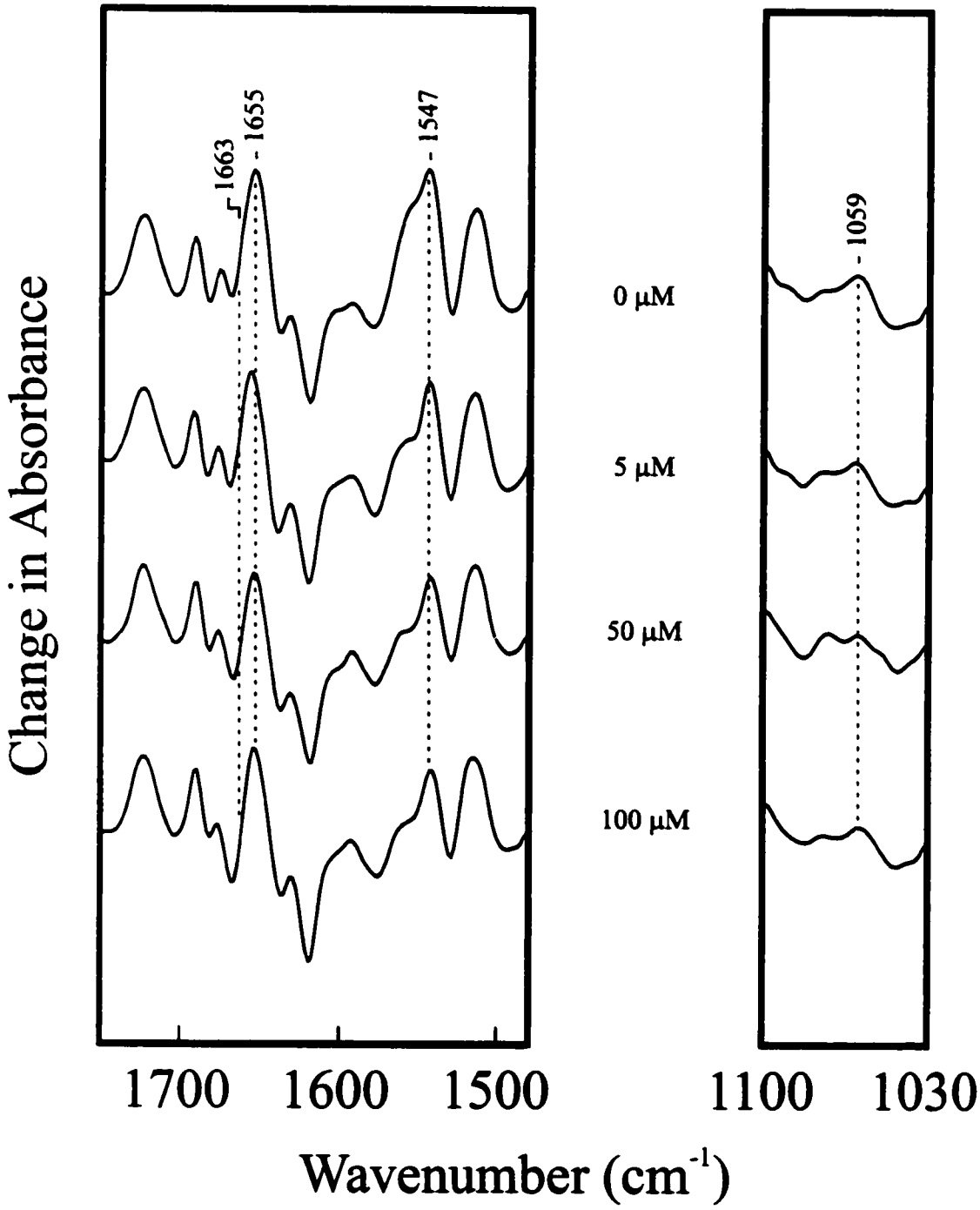
Change in Absorbance
1663
1655
1547
1059
0 μM
5 μM
50 μM
100 μM
1700
1600
1500
1100
1030
Wavenumber (cm-1)

conformation, it is evident that the binding of both PCP and proadifen to the non-competitive blocker site stabilizes the nAChR in an identical conformation that is distinct from both the resting and agonist-induced desensitized states.

Ideally, the structural consequences of both proadifen and PCP binding to the non-competitive blocker site should be investigated directly by acquiring the difference between spectra recorded from the nAChR in the presence and absence of either ligand. As mentioned above, however, like most local anesthetics, proadifen partitions into the lipid membrane causing the nAChR film on the surface of the germanium IRE to expand and contract. This results in a severely distorted spectrum that masks any vibrational bands reflecting either specific proadifen-nAChR interactions or the effects of these interactions on nAChR structure (data not shown). Fortunately, these spectral distortions are absent in spectra recorded in the presence and absence of PCP thus providing a clear window into the structural consequences of PCP binding to the non-competitive blocker site.

PCP-Difference Spectrum. The difference between spectra recorded from the nAChR in the presence and absence of 50 μM PCP, referred to as a PCP-difference spectrum, reveals a number of positive and negative vibrational bands (Figure 6.4). Since at 50 μM PCP binding occurs almost exclusively to the non-competitive blocker site, these positive and negative bands reflect variations in the vibrations of individual residues within the nAChR that arise specifically from the binding of PCP to the non-competitive blocker site. The assignment of the vibrational bands to PCP-induced changes in nAChR

Figure 6.4 A comparison of the band intensity variations observed in Carb-difference spectra recorded from the nAChR while continuously maintaining the receptor in contact with 50 μM PCP (second trace from the top) with those observed in the PCP-difference spectrum (second trace from the bottom). The top trace is a typical Carb difference spectrum while the bottom trace is the absorption spectrum of PCP itself. Significantly, the PCP-difference spectrum exhibits an essentially identical pattern of band intensity variations as that observed in Carb-difference spectra recorded in the presence of PCP except that there is an increase, as opposed to a decrease, in intensity near 1663, 1547 and 1059 cm^{-1}. The PCP-difference spectrum also exhibits no significant band intensity near 1655 cm^{-1}. In contrast, there is an increase in positive intensity near 1430 cm^{-1} that does not correlate with a similar decrease in intensity in Carb-difference spectra recorded in the presence of PCP. This positive intensity, however, likely reflects the vibrations of nAChR-bound PCP (blue dashed lines) rather than PCP-induced changes in nAChR structure.

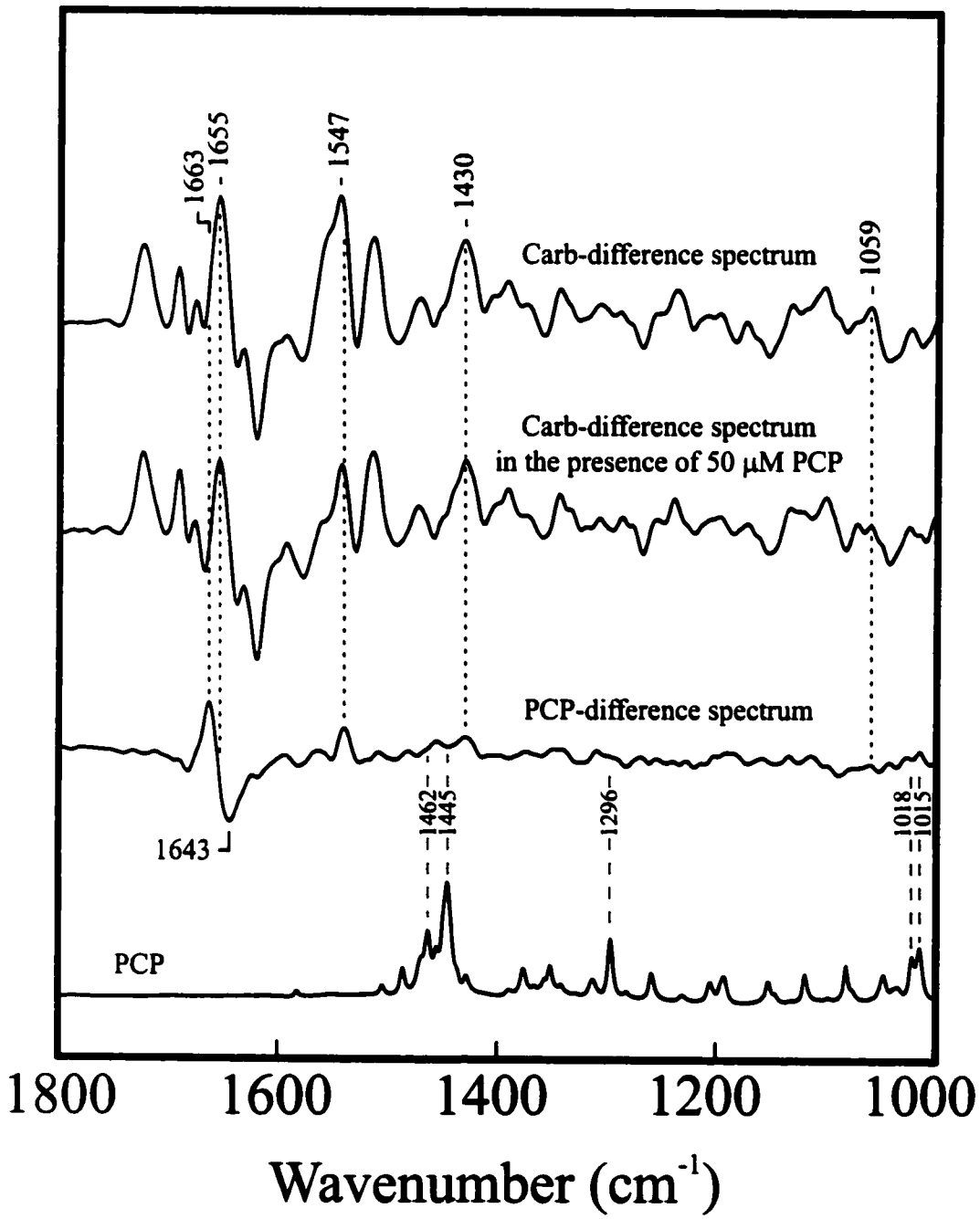
1663
1655
1547
1430
1059
Carb-difference spectrum
Carb-difference spectrum
in the presence of 50 μM PCP
PCP-difference spectrum
1643
1462
1445
1296
1018
1015
PCP
1800
1600
1400
1200
1000
Wavenumber (cm-1)

structure is supported further by the presence of a number of positive bands, including those near 1462, 1445, 1296, 1018 and 1015 cm^{-1}, whose frequencies match the vibrational frequencies of PCP itself suggesting that they reflect the vibrations of distinct functional groups within nAChR-bound PCP (Figure 6.4, blue dashed lines).

The most striking feature of the PCP-difference spectrum is that it exhibits an essentially identical pattern of band intensity variations as that observed in Carb-difference spectra recorded in the presence of low concentrations of either proadifen or PCP, except that as expected, there is an increase, as opposed to a decrease, in intensity near 1663, 1547 and 1059 cm^{-1}. The PCP-difference spectrum also does not exhibit any significant positive intensity near 1655 cm^{-1}, although there is an increase in intensity near 1430 cm^{-1} that does not correlate with a similar decrease in intensity at the same frequency in Carb-difference spectra recorded in the presence of PCP. This latter positive intensity, however, likely reflects the vibrations of nAChR-bound PCP rather than PCP-induced changes in nAChR structure. The PCP-difference spectrum thus clearly shows that the binding of PCP to the non-competitive blocker site stabilizes the nAChR in a novel intermediate conformation that is structurally distinct from both the resting and agonist-induced desensitized states.

In addition to the band intensity variations described above, the PCP-difference spectrum exhibits both a strong negative vibrational band near 1643 cm^{-1} and several smaller positive vibrational bands whose frequencies are distinct from those of nAChR-bound PCP. These bands reflect either additional structural variations between the

resting and intermediate state and/or direct interactions between PCP and individual residues within the non-competitive blocker site. Although further studies are required to assign these bands to the vibrations of specific amino acid residues, it is interesting to note that both the negative band near 1643 cm^{-1} and the positive band near 1663 cm^{-1} occur within the amide I (1600-1700 cm^{-1}) region of the infrared spectrum. Bands within this region are highly characteristic of vibrational changes associated with a change in the conformation of a protein's polypeptide backbone. It is likely then that the negative band near 1643 cm^{-1} reflects the vibrations of a region of the nAChR's polypeptide backbone as it is found in the resting conformation while the positive band near 1663 cm^{-1} reflects the vibrations of the same region as it is found in the intermediate state.

The nature of the PCP-induced conformational change reflected in the PCP-difference spectrum was also probed by recording PCP-difference spectra in ^2H_2O buffer after prior exposure of the nAChR to ^2H_2O for three days (Figure 6.5). Prolonged exposure of the nAChR to ^2H_2O induces those residues that are accessible to solvent to exchange their protons for the heavier deuterium thus leading to a downshift in the frequency of the residue's molecular vibration. A comparison of the PCP-difference spectrum recorded from the nAChR in ^1H_2O with that recorded from the nAChR in ^2H_2O reveals that the three relatively intense vibrational bands within the PCP difference spectrum, near 1663, 1643 and 1547 cm^{-1}, are unaffected by exposure of the nAChR to ^2H_2O. This indicates that the peptide carbonyl and N-H groups whose structure changes upon PCP binding to the non-competitive blocker site remain in the protiated form after

Figure 6.5 A comparison of a PCP-difference spectrum recorded from the nAChR in $^{1}H_2O$ with that recorded from the nAChR in $^{2}H_2O$ after prior exposure of the receptor to $^{2}H_2O$ for three days. Prolonged exposure of the nAChR to $^{2}H_2O$ does not induce a shift in the frequency of the vibrational bands centered near 1663, 1643 and 1547 cm^{-1} suggesting that these bands reflect the vibrations of residues within solvent inaccessible regions of the nAChR.

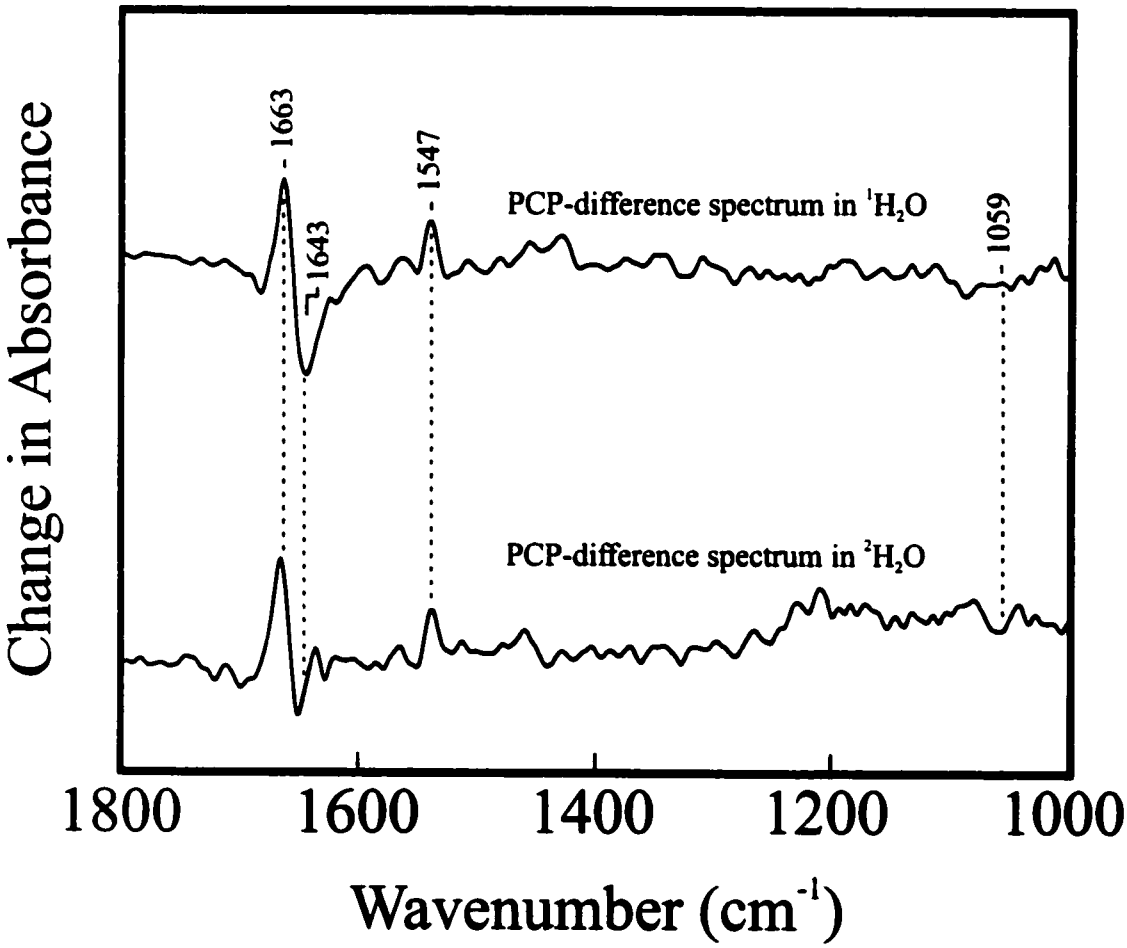
Change in Absorbance
1663
1643
1547
1059
PCP-difference spectrum in ^1H_2O
PCP-difference spectrum in ^2H_2O
1800
1600
1400
1200
1000
Wavenumber (cm^{-1})

three days of exposure of the nAChR to ^2H_2O and thus must be located in a solvent inaccessible region of the nAChR. This strongly suggests that the conformational change elicited by PCP binding to the non-competitive blocker site is restricted mainly to the transmembrane domain of the nAChR.

DISCUSSION

Control studies have previously shown that the positive and negative bands observed in Carb-difference spectra recorded from the nAChR reflect vibrational changes in the receptor that occur as a consequence of Carb binding and subsequent desensitization (127-129). Extensive studies have also identified five distinct positive bands within the Carb-difference spectrum, located near 1663, 1655, 1547, 1430, and 1059 cm^{-1}, that reflect the specific vibrational changes in the nAChR associated with the resting-to-desensitized conformational transition (155, 170, 194). These five bands can thus serve as markers of the ability of the nAChR to undergo Carb-induced conformational change. The presence of each in a Carb-difference spectrum indicates that the nAChR retains the ability to undergo the Carb-induced resting-to-desensitized conformational transition. Similarly, the absence of each indicates that the nAChR is incapable of undergoing Carb-induced conformational change. In the latter case, the nAChR can be either locked in a resting conformation that is unable to respond to the binding of Carb or stabilized in a desensitized conformation prior to the addition of Carb.

The results of this study clearly show that the binding of both the local anesthetic, proadifen, and the hallucinogen, PCP, stabilizes the nAChR in a conformation that is a structural intermediate between the resting and desensitized states. Carb-difference spectra recorded from the nAChR in the presence of concentrations of both proadifen and PCP consistent with their binding to the non-competitive blocker site exhibit a substantial loss of intensity near 1663 and 1059 cm^{-1} with no change in intensity near either 1655 or 1430 cm^{-1}. This pattern of band intensity variations indicates that those conformationally active residues of the nAChR that vibrate near 1663 and 1059 cm^{-1} are incapable of undergoing the resting-to-desensitized conformational transition upon the binding of Carb, whereas those residues that vibrate near 1655 and 1430 cm^{-1} retain the ability to undergo the Carb-induced conformational transition in the presence of either ligand. While the loss of positive intensity near 1663 and 1059 cm^{-1} could reflect the stabilization of either a locked resting or a desensitized conformation for the conformationally sensitive residues that vibrate at these frequencies, PCP-difference spectra, which detect the structural changes in the nAChR elicited directly by the binding of PCP, support the latter interpretation. The PCP-difference spectra show that PCP binding to the ion channel pore leads to a conformational change in those residues within the nAChR that vibrate near 1663 and 1059 cm^{-1}. It can thus be concluded that the binding of both PCP and proadifen to the non-competitive blocker site induces a conformational change in the nAChR and thus stabilizes a structural intermediate between the resting and desensitized states. Within this intermediate state, some residues within the nAChR retain a resting-

like conformation that is capable of responding to the binding of Carb while others adopt a desensitized-like conformation.

The nature of the conformational change induced in the nAChR by the binding of both proadifen and PCP to the non-competitive blocker site was also investigated by acquiring PCP-difference spectra in ^2H_2O buffer after prior exposure of the nAChR to ^2H_2O for three days. The results reveal that the majority of those residues that undergo a structural change upon either PCP or proadifen binding to the non-competitive blocker site are highly resistant to peptide $^1H/^2H$ exchange suggesting that they are located within solvent inaccessible regions of the nAChR. The majority of the structural changes elicited by PCP and/or proadifen binding to the non-competitive blocker site thus likely occur within the transmembrane domain of the nAChR.

The results of this study have two important implications. First, it is clear from the data presented here, and in a previous study investigating the structural effects of local anesthetic binding to the nAChR, that the mechanisms by which both local anesthetics and PCP modulate nAChR function is more complex than suggested by current models. Current models propose that both local anesthetics and PCP bind to the non-competitive blocker site sterically hindering cation flux and stabilizing the nAChR in a high affinity, presumably desensitized conformation (158, 177, 179). In contrast, the FTIR data show that nAChR desensitization occurs only upon local anesthetic binding to the neurotransmitter binding sites. In addition, the binding of both local anesthetics and PCP to the non-competitive blocker site leads to the formation of a conformational

intermediate between the resting and desensitized states. Local anesthetic binding to the ion channel pore does lead to a change in agonist binding affinity (158, 177, 179). While such changes in binding affinity are compatible with the FTIR data, it is clear that a change in binding affinity is not sufficient to define the conformational state of the nAChR.

Second, the FTIR data suggest that the conformational spectrum that can be sampled by the nAChR may be more complex than currently thought. It has generally been assumed that the nAChR can adopt a resting, open, or desensitized state depending upon the presence and concentration of agonist. A fast-desensitized state has also been detected (114, 184). The intermediate conformation detected in this study also appears to be stabilized under additional conditions. Carb-difference spectra recorded in the presence of prilocaine and lidocaine or upon reconstitution of the nAChR into EPC membranes containing low concentrations of either DOPA or Chol also suggest the formation of an intermediate conformation (170, 194). The intermediate conformation detected here is thus not unique to both PCP and proadifen but may be stabilized under a variety of physiological conditions. This intermediate conformation may form *in vivo* and may play an important role in enabling both endogenous and exogenous factors to modulate the postsynaptic response elicited by the nAChR in response to the binding of ACh. Further studies, however, are clearly required to define the biophysical properties of such an intermediate conformation in order to understand its function *in vivo*.

CONCLUSIONS

The objective of this study was to investigate the structural consequences of both proadifen and PCP binding to the nAChR. The results show conclusively that the binding of both proadifen and PCP to the non-competitive blocker site stabilizes the nAChR in a novel intermediate conformation that is structurally distinct from both the resting and desensitized states. Within this intermediate state, some residues within the nAChR retain a predominantly resting-like conformation while others adopt a predominantly desensitized-like conformation. A $^{1}H/^{2}H$ exchange study further reveals that the majority of those residues involved in the conformational transition from the resting to the intermediate state reside within solvent inaccessible regions of the nAChR, likely implicating a region within the receptor's transmembrane domain.

General Conclusions

The objective of the research presented in this thesis was to employ the novel technique of FTIR difference spectroscopy to investigate the structural consequences of both lipid and local anesthetic action at the nAChR. FTIR difference spectroscopy exists as one of the few techniques capable of abstracting detailed structural information from large integral membrane proteins, such as the nAChR, by providing insight into the molecular vibrations of individual amino acids, which are extremely sensitive to changes in molecular structure and local environment. Together, the results have been incorporated into two speculative models that describe the mechanisms by which both lipids and local anesthetics modulate the structure, and thus function, of the nAChR.

Lipid-Induced Modulations in the Conformational Equilibrium of the NAChR

Initial studies focussing on the specific functional requirement of the nAChR for both neutral and anionic lipids, such as Chol and DOPA, suggested that each lipid modulated the structure and function of the nAChR by binding to discrete sites on the nAChR with distinct effects on the receptor's gross secondary structure. As an example, it was proposed that the rigid sterol ring of Chol could intercalate into the grooves of α-helical segments, thus leading to the stabilization of transmembrane α-helices. Similarly, it was proposed that the negatively charged head group of DOPA could form electrostatic interactions with extramembranous regions of the nAChR, thus leading to the stabilization of β-sheet secondary structures. In addition, in the absence of both neutral and anionic lipids, the nAChR appeared to be stabilized in a channel-inactive conformation analogous to that of the agonist-induced desensitized state.

Carb-difference spectra recorded from the nAChR reconstituted into EPC membranes void of both neutral and anionic lipids do in fact suggest that the nAChR is stabilized in the desensitized state. The Carb-difference spectra also reveal, however, that rather than stabilizing distinct nAChR secondary structures, the predominant effect of both neutral and anionic lipids within a reconstituted membrane is to stabilize the nAChR in an equivalent resting conformation. In addition, the proportion of receptors adopting either the resting or desensitized state appears to be dependent upon the final lipid composition of the reconstituted membrane. Initially the results were interpreted to suggest that diverse lipid structures influence the conformational equilibrium of the nAChR between the resting and desensitized states through an indirect affect on some physical property of the lipid bilayer, possibly bulk fluidity. In other words, the presence of both neutral and anionic lipids within an EPC membrane could lead to a relatively ordered lipid membrane that may be required for maintaining the receptor in a predominantly resting conformation. Conversely, the absence of either or both lipids could lead to a more fluid membrane that may increasingly enhance the formation of the desensitized state.

Further studies focussing on the specific effects of increasing levels of either DOPA or Chol within an EPC membrane, however, show that the effects of lipids on nAChR function is more complex than the modulation of a simple two state equilibrium. Carb-difference spectra recorded from the nAChR in EPC membranes with relatively low levels of either DOPA or Chol exhibit a pattern of band intensity variations suggestive of the stabilization of a structural intermediate between the resting and desensitized states.

The Carb-difference spectra also suggest that the resting, intermediate and desensitized states adopted by the nAChR in the absence of the anionic lipid, DOPA, differ slightly in structure from the corresponding states stabilized in its presence.

Consequently, Figure 7.1 depicts a revised model of the effects of membrane lipid composition on the structure and function of the nAChR. In this model, the nAChR is proposed to exist, in the absence of agonist, within a conformational equilibrium between at least three distinct conformations: a low affinity channel-competent resting state, a high affinity channel-inactive desensitized state and a novel intermediate state. Within a relatively ordered membrane, such as that formed by native or EPC/DOPA/Chol membranes, the nAChR is stabilized predominantly in the resting state. An increase in membrane fluidity, such as that found with decreasing concentrations of either neutral and/or anionic lipids, leads initially to a shift in the conformational equilibrium of the nAChR towards the intermediate state, and then finally towards the desensitized state. In the absence of anionic lipids, however, the nAChR adopts a conformation similar to either the resting, intermediate or desensitized states, as dictated by the membrane fluidity, but one that has a subtle unidentified structural difference. These putative conformational states are tentatively described as pseudo-resting, pseudo-intermediate and pseudo-desensitized.

Figure 7.1 A revised model of the effects of membrane lipid composition on the structure and function of the nAChR (see text for details).

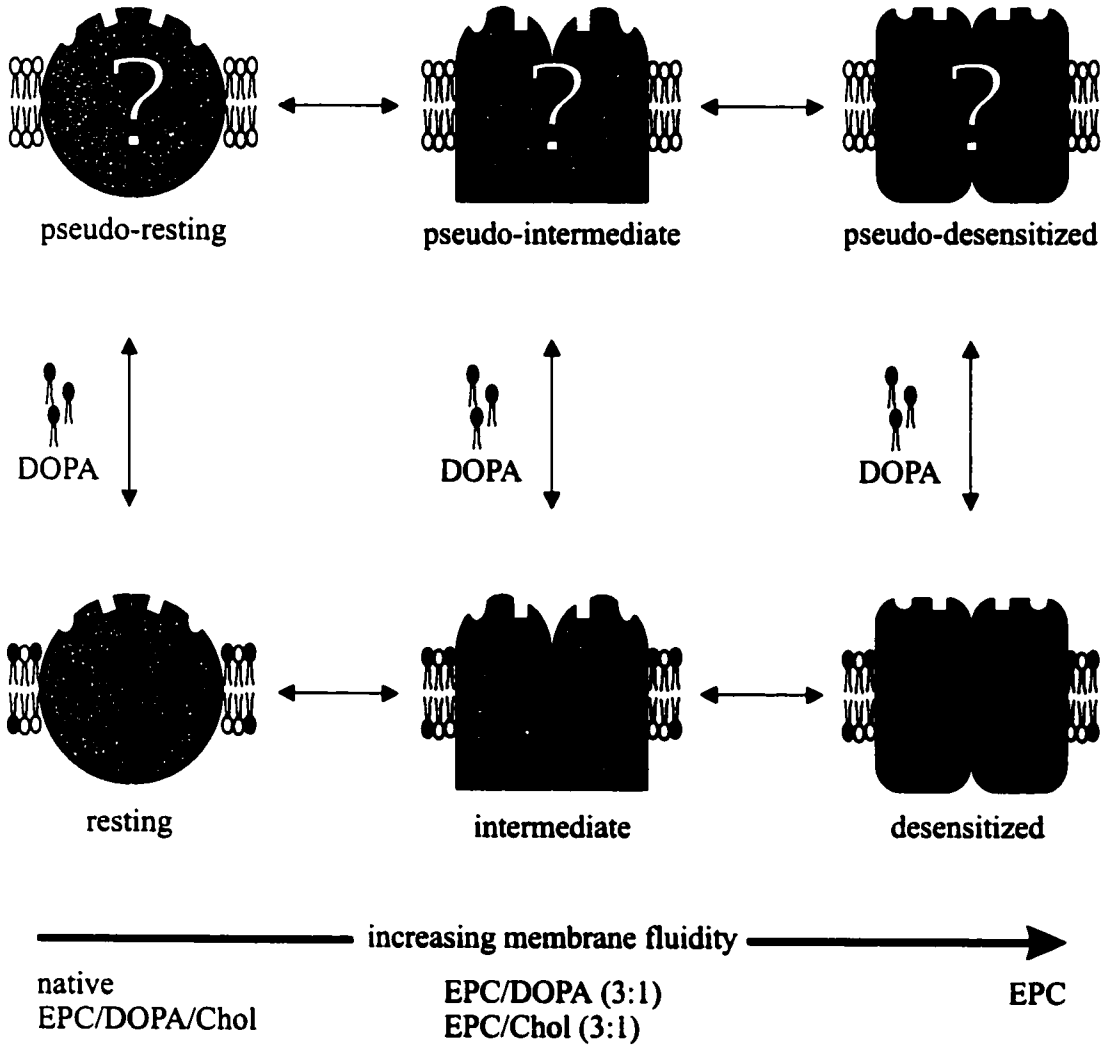
?
?
?
pseudo-resting
pseudo-intermediate
pseudo-desensitized
DOPA
DOPA
DOPA
resting
intermediate
desensitized
increasing membrane fluidity
native
EPC/DOPA/Chol
EPC/DOPA (3:1)
EPC/Chol (3:1)
EPC

Local Anesthetic-Induced Modulations in the Conformational Equilibrium of the NAChR

The ability of the nAChR to conduct cations across the postsynaptic membrane in response to the binding of ACh is also sensitive to the presence of both local anesthetics and the hallucinogen, PCP. Local anesthetics and PCP belong to a class of structurally diverse compounds that modulate nAChR activity by binding to a distinct non-competitive blocker site located within the receptor's ion channel pore. For most local anesthetics, as well as for PCP, binding to the non-competitive blocker site stabilizes the nAChR in a high-affinity ACh binding conformation that has been presumed to be analogous to the agonist-induced desensitized state. As a result, the current model of local anesthetic action at the nAChR proposes that these compounds bind to the non-competitive blocker site and induce a shift in the conformational equilibrium of the receptor towards the desensitized state. Similarly, some local anesthetics, such as tetracaine, bind to the non-competitive blocker site and stabilize the nAChR in a low affinity ACh binding conformation and are thus presumed to shift the conformational equilibrium of the receptor towards the resting state.

In agreement with the current model, Carb-difference spectra recorded in the presence of a variety of local anesthetics suggest that local anesthetics do in fact bind to the nAChR and stabilize the receptor in a desensitized conformation. Contrary to the model, however, the FTIR data reveal that nAChR desensitization occurs not through interactions at the non-competitive blocker site, but solely as a result of local anesthetic binding to the neurotransmitter binding sites. In fact, the main 'desensitizing' effect of

local anesthetics appears to occur as a result of their binding to the neurotransmitter binding sites and mimicking many of the same interactions as those formed between agonist and individual neurotransmitter binding site residues.

The Carb-difference spectra also reveal that both the local anesthetics prilocaine, lidocaine and proadifen and the hallucinogen, PCP, bind to the non-competitive blocker site and stabilize the nAChR in an intermediate conformation similar to that stabilized upon reconstitution of the nAChR into EPC membranes containing low concentrations of either Chol or DOPA. Based on both the pattern of vibrational changes induced in the nAChR upon transition from the resting to the intermediate state and the susceptibility of these changes to $^{1}H/^{2}H$ exchange, it is proposed that within the intermediate state, the nAChR's ion channel adopts a predominantly desensitized-like conformation while the neurotransmitter binding sites retain a predominantly resting-like conformation. There are however, likely subtle changes in the neurotransmitter binding sites that provide the intermediate state with an affinity for agonist somewhere between that of both the resting and desensitized states.

Consequently, Figure 7.2 depicts a revised model of the effects of local anesthetic binding on the structure and function of the nAChR. In this model, the nAChR is again proposed to exist, in the absence of agonist, within a conformational equilibrium between the resting, intermediate and desensitized state. At low concentrations of so-called 'desensitizing' local anesthetics, where binding occurs predominantly to the non-competitive blocker site, the conformational equilibrium of the nAChR is shifted towards the intermediate state. In contrast, the binding of the local anesthetic, tetracaine, to the

Figure 7.2 A revised model of the effects of local anesthetic binding on the structure and function of the nAChR (see text for details).

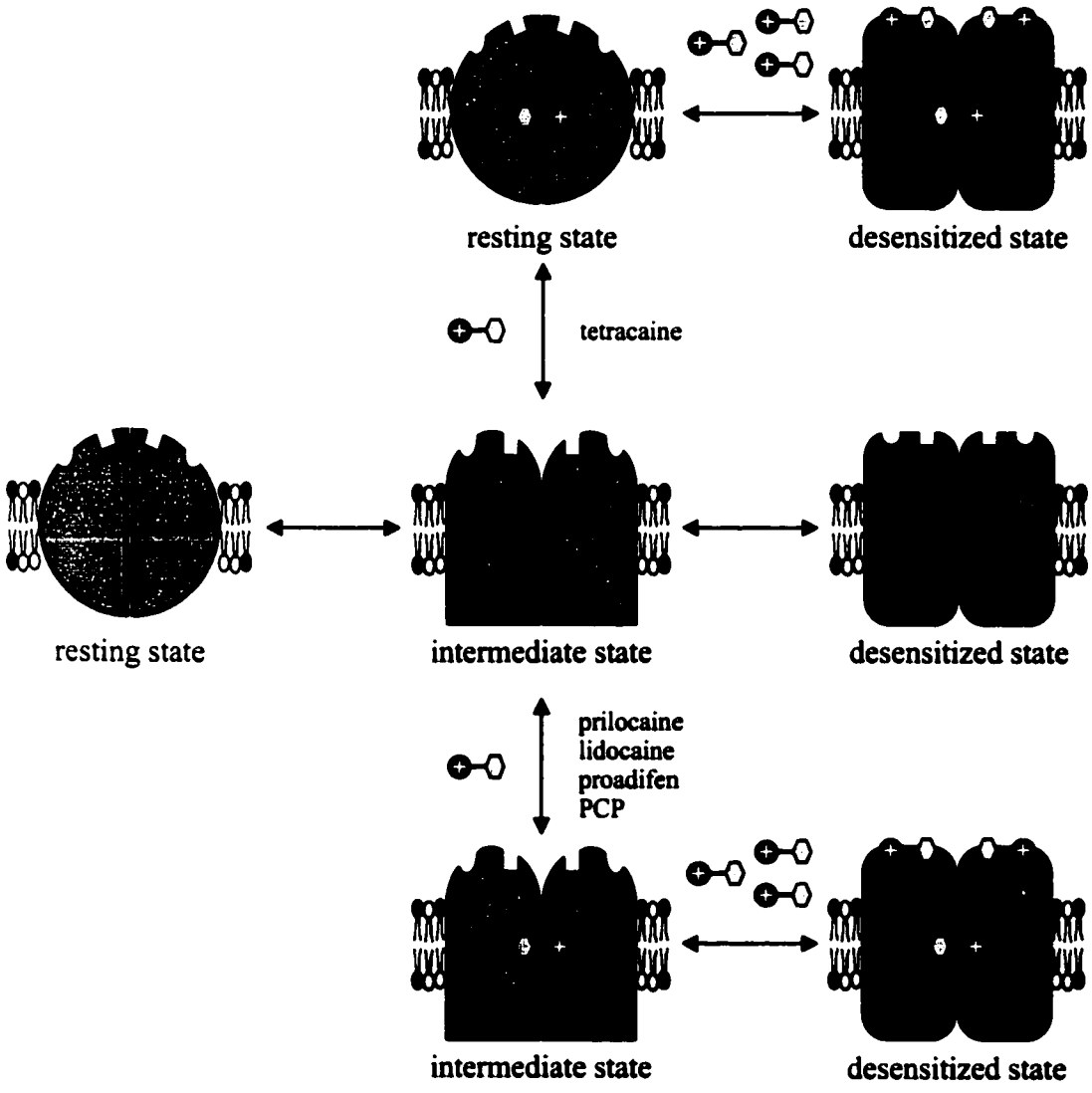
resting state
desensitized state
tetracaine
resting state
intermediate state
desensitized state
prilocaine
lidocaine
proadifen
PCP
intermediate state
desensitized state
local anesthetic

non-competitive blocker site induces a shift in the conformational equilibrium of the nAChR towards the resting state. Regardless of the conformation stabilized by local anesthetic binding to the non-competitive blocker site, however, the additional binding of local anesthetic to the neurotransmitter binding sites stabilizes the nAChR in a desensitized conformation analogous to that stabilized upon prolonged exposure to agonist.

Although further studies are required to fully elucidate the molecular details surrounding both lipid and local anesthetic action at the nAChR, the results of this research clearly show that the nAChR is capable of adopting a diversity of conformational states, each likely possessing its own unique functional characteristics (i.e. agonist affinity, channel gating and/or desensitization kinetics etc...). The ability of various endogenous and exogenous factors to influence the proportion of receptors adopting either conformation suggests that this conformational diversity may perform a central role in affording neurons the necessary flexibility to not only respond and adapt to changes in both their internal and external environment but to also perform such complex functions as thought, memory and learning.

REFERENCES

1. Kandel, E.R., Schwartz, J.H. and Jessell, T.M. (1995) In: Essentials of neural science and behaviour. Eds. Kandel, E.R., Schwartz, J.H. and Jessell, T.M., Appleton & Lange, Norwalk, Connecticut.

2. Schauf, C., Moffet, D. and Moffet, S. (1990) In: Human physiology: foundations and frontiers. Ed. Allen, D., Times Mirror/Mosby College Publishing, Toronto.

3. Aronstam, R.S. (1982) In: Progress in cholinergic biology: model cholinergic synapses. Eds. Hanin, I. and Goldberg, A.M., Raven Press, New York.

4. Lindstrom, J., Einarson, B. and Merlie, J. (1978) Immunization of rats with polypeptide chains from torpedo acetylcholine receptor causes an autoimmune response to receptors in rat muscle. Proc. Natl. Acad. Sci. U.S.A. 75, 769-773.

5. Conti-Tronconi, B.M., and Raftery, M.A. (1982) The nicotinic cholinergic receptor: correlation of muscle structure with functional properties. Annu. Rev. Biochem. 51, 491-530.

6. Changeux, J.-P. (1993) Chemical signaling in the brain. Scientific American 269, 58-62.

7. Unwin, N. (1993) The nicotinic acetylcholine receptor at 9 Å resolution. J. Mol. Biol. 229, 1101-1124.

8. Reynolds, J.A. and Karlin, A. (1978) Molecular weight in detergent solution of acetylcholine receptor from Torpedo californica. Biochemistry 17, 2035-2038.

9. Lindstrom, J., Walter, B. and Einarson, B. (1979) Immunochemical similarities between subunits of acetylcholine receptors from Torpedo, Electrophorus, and mammalian muscle. Biochemistry 18, 4470-4480.

10. Raftery, M.A., Hunkapiller, M.W., Strader, C.D. and Hood, L.E. (1980) Acetylcholine receptor: complex of homologous subunits. Science 208, 1454-1456.

11. Fairclough, R.H., Finer-Moore, J., Love, R.A., Kristofferson, D., Desmeules, P.J. and Stroud, R.M. (1983) Subunit organization and structure of an acetylcholine receptor. Cold Spring Harbor Symp. Quant. Biol. 48, 9-20.

12. Kistler, J., Stroud, R.M., Klymkowsky, M.W., Lalancette, R.A., and Fairclough, R.H. (1982) Structure and function of an acetylcholine receptor. Biophys. J. 37, 371-383.

13. Hamilton, S.L., Pratt, D.R. and Eaton, D.C. (1985) Arrangement of the subunits of the nicotinic acetylcholine receptor of Torpedo californica as determined by alpha-neurotoxin cross-linking. Biochemistry 24, 2210-2219.

14. Kubalek, E., Ralston, S., Lindstrom, J. and Unwin, N. (1987) Location of subunits within the acetylcholine receptor by electron image analysis of tubular crystals from *Torpedo marmorata*. J. Cell Biol. 105, 9-18.

15. Mishina, M., Toshiyuki, T., Imoto, K., Noda, M., Takahashi, T., Numa, S., Methfessel, C. and Sakmann, B. (1986) Molecular distinction between fetal and adult forms of muscle acetylcholine receptor. Nature 321, 406-411.

16. Gu, Y. and Hall, Z.W. (1988) Characterization of acetylcholine receptor subunits in developing and in denervated mammalian muscle. J. Biol. Chem. 263, 12878-12885.

17. Goldman, D. and Tanai, K. (1989) Coordinate regulation of RNAs encoding two isoforms of rat muscle nicotinic acetylcholine receptor β-subunit. Nucleic Acids Res. 25, 3049-3056.

18. Hartman, D.S. and Claudio, T. (1990) Coexpression of two distinct muscle acetylcholine receptor α subunits during development. Nature 343, 372-373.

19. Beeson, D., Morris, A., Vincent, A. and Newsom-Davis, J. (1990) The human muscle nicotinic acetylcholine receptor α subunit exists as two isoforms: a novel exon. EMBO J. 9, 2101-2106.

20. Boulter, J., Evans, K., Goldman, D., Martin, G., Treco, D., Heinemann, S. and Patrick, J. (1986) Isolation of a cDNA clone coding for possible neuronal nicotinic acetylcholine receptor α-subunit. Nature 319, 368-374.

21. Couturier, S., Bertrand, D., Matter, J.-M., Hernandez, M.-C., Bertrand, S., Millar, N., Valera, S., Barkas, T. and Ballivet, M. (1990) A neuronal nicotinic acetylcholine receptor subunit (α7) is developmentally regulated and forms a homooligomeric channel blocked by alpha-BTX. Neuron 5, 847-856.

22. Bertrand, D., Devillers-Thiery, A., Revah, F., Galzi, J.-L., Hussy, N., Mulle, C., Bertrand, S., Ballivet, M. and Changeux, J.-P. (1992) Unconventional pharmacology of a neuronal nicotinic acetylcholine receptor mutated in the channel domain. Proc. Natl. Acad. Sci. U.S.A. 89, 1261-1265.

23. Sawruck, E., Udri, C., Betz, H. and Schmitt, B. (1990) SBD, a novel structural subunit of the *Drosophila* nicotinic acetylcholine receptor, shares its genomic localization with two alpha-subunits. FEBS Lett. 273, 177-181.

24. Sawruck, E., Scloss, P., Betz, H. and Schmitt, B. (1990) Heterogeneity of *Drosophila* nicotinic acetylcholine receptors: SAD, a novel developmentally regulated alpha-subunit. EMBO J. 9, 2671-2677.

25. Marshall, J., Buckingham, S.D., Shingai, R., Lunt, G.G., Goosey, M.W., Darlison, M.G., Sattelle, D.B. and Barnard, E.A. (1990) Sequence and functional expression of a single alpha subunit of an insect nicotinic acetylcholine receptor. EMBO J. 9, 4391-4398.

26. Sumikawa, K., Houghton, M., Smith, J.C., Richards, B.M. and Barnard, E.A. (1982) The molecular cloning and characterization of cDNA coding for the α subunit of the acetylcholine receptor. Nucleic Acids Res. 10, 5809-5822.

27. Noda, M., Takahashi, H., Tanabe, T., Toyosato, M., Furutani, Y., Hirose, T., Asai, M., Inayama, S., Miyata, T. and Numa, S. (1982) Primary structure of α-subunit precursor of *Torpedo californica* acetylcholine receptor deduced from cDNA sequence. Nature 299, 793-797.

28. Devillers-Thiery, A., Giraudat, J., Bentaboulet, M. and Changeux, J.-P. (1983) Complete mRNA coding sequence of the acetylcholine binding α-subunit of *Torpedo marmorata* acetylcholine receptor: a model for the transmembrane organization of the polypeptide chain. Proc. Natl. Acad. Sci. U.S.A. 80, 2067-2071.

29. Noda, M., Takahashi, H., Tanabe, T., Toyosato, M., Kikykotani, S., Hirose, T., Asai, M., Takashima, H., Inayama, S., Miyata, T. and Numa, S. (1983) Primary structures of β-and δ-subunit precursor of *Torpedo californica* acetylcholine receptor deduced from cDNA sequence. Nature 301, 251-255.

30. Claudio, T., Ballivet, M., Patrick, J. and Heinemann, S. (1983) Nucleotide and deduced amino acid sequences of *Torpedo californica* acetylcholine receptor γ subunit. Proc. Natl. Acad. Sci. U.S.A. 80, 1111-1115.

31. Noda, M., Takahashi, H., Tanabe, T., Toyosato, M., Kikykotani, S., Furutani, Y., Hirose, T., Takashima, H., Inayama, S., Miyata, T. and Numa, S. (1983) Structural homology of *Torpedo californica* acetylcholine receptor subunits. Nature 302, 528-532.

32. Anderson, D.J., Walter, P. and Blobel, G. (1982) Signal recognition protein is required for the integration of acetylcholine receptor δ subunit, a transmembrane glycoprotein, into the endoplasmic reticulum. J. Cell Biol. 93, 501-506.

33. Nomoto, H., Takahashi, N., Nagaki, Y., Endo, S., Arata, Y. and Hayashi, K. (1986) Carbohydrate structures of acetylcholine receptors from *Torpedo californica* and distribution of oligosaccharides among the subunits. Eur. J. Biochem. 157, 133-242.

34. Poulter, L., Earnest, J.P., Stroud, R.M. and Burlingame, A. (1989) Structure, oligosaccharide structures, and posttranslationally modified sites of the nicotinic acetylcholine receptor. Proc. Natl. Acad. Sci. U.S.A. 86, 6645-6649.

35. Ross, M.J., Klymkowsky, M.W., Agard, D.A. and Stroud, R.M. (1977) Structural studies of a membrane-bound acetylcholine receptor from Torpedo californica. J. Mol. Biol. 116, 635-659.

36. Stroud, R.M. and Agard, D.A. (1979) Structure determination of asymmetric membrane profiles using an iterative Fourier method. Biophys. J. 25, 495-512.

37. Baenziger, J.E. and Méthot, N. (1995) Fourier transform infrared and hydrogen/deuterium exchange reveal an exchange-resistant core of α-helical peptide hydrogens in the nicotinic acetylcholine receptor. J. Biol. Chem. 270, 29129-29137.

38. Corbin, J., Méthot, N., Wang, H.H., Baenziger, J.E. and Blanton, M.P. (1998) Secondary structure analysis of individual transmembrane segments of the nicotinic acetylcholine receptor by circular dichroism and Fourier transform infrared spectroscopy. J. Biol. Chem. 273, 771-777.

39. Méthot, N. and Baenziger, J.E. (1998) Secondary structure of the exchange resistant core from the nicotinic acetylcholine receptor revealed by Fourier transform infrared spectroscopy. Biochemistry 37, 14815-14822.

40. Giraudat, J., Dennis, M., Heidmann, T., Haumont, P.-Y., Lederer, F. and Changeux, J.-P. (1987) Structure of the high-affinity binding site for noncompetitive blockers of the acetylcholine receptor: [^{3}H]chlorpromazine labels homologous residues in the β and δ chains. Biochemistry 26, 2410-2418.

41. Charnet, P., Labarca, C., Leonard, R.J., Vogelaar, N.J., Czyzyk, L., Gouin, A., Davidson, N. and Lester, H.A. (1990) An open-channel blocker interacts with adjacent turns of α-helices in the nicotinic acetylcholine receptor. Neuron 4, 87-95.

42. Blanton, M.P. and Cohen, J.B. (1992) Mapping the lipid-exposed regions in the *Torpedo californica* nicotinic acetylcholine receptor. Biochemistry 31, 3738-3750.

43. Villarroel, A. and Sakmann, B. (1992) Threonine in the selectivity filter of the acetylcholine receptor channel. Biophys. J. 62, 196-205.

44. Akabas, M.H., Kaufmann, C., Archdeacon, P. and Karlin, A. (1994) Identification of acetylcholine receptor channel-lining residues in the entire M2 segment of the α subunit. Neuron 13, 919-927.

45. Blanton, M.P. and Cohen, J.B. (1994) Identifying the lipid-protein interface of the *Torpedo* nicotinic acetylcholine receptor: secondary structure implications. Biochemistry 33, 2859-2872.

46. Ratnam, M., Sargent, P.B., Sarin, V., Fox, J.L., Nguyen, D.L. Rivier, J., Criado, M. and Lindstrom, J.M. (1986) Location of antigenic determinants on primary sequences of subunits of nicotinic acetylcholine receptors by peptide mapping. Biochemistry 25, 2621-2632.

47. Ratnam, M., Manohar, Le Nguyen, D., Rivier, J., Sargent, P.B. and Lindstrom, J. (1986) Transmembrane topography of nicotinic acetylcholine receptor: immunochemical tests contradict theoretical predictions based on hydrophobicity profiles. Biochemistry 25, 2633-2643.

48. Kordossi, A.A. and Tzartos, S.J. (1987) Conformation of cytoplasmic segments of acetylcholine receptor α- and β-subunits probed by monoclonal antibodies: sensitivity of the antibody competition approach. EMBO J. 6, 1605-1610.

49. LaRochelle, W.J., Wray, B.E., Sealock, R. and Froehner, S.C. (1985) Immunochemical demonstration that amino acids 360-377 of the acetylcholine receptor gamma-subunit are cytoplasmic. J. Cell Biol. 100, 684-691.

50. Lei, S.J., Raftery, M.A. and Conti-Tronconi, B.M. (1993) Monoclonal antibodies against synthetic sequences of the nicotinic receptor cross-react fully with the native receptor, and reveal the transmembrane disposition of the epitopes. Biochemistry 32, 91-100.

51. Huganir, R.L. (1987) Regulation of the nicotinic acetylcholine receptor by protein phosphorylation. J. Recept. Res. 7, 241-256.

52. Haggerty, J.G. and Froehner, S.C. (1981) Restoration of the ^{125}I-α-bungarotoxin binding activity to the α subunit of *Torpedo* acetylcholine receptor isolated by gel electrophoresis in sodium dodecyl sulfate. J. Biol. Chem. 256, 8294-8297.

53. Tzartos, S.J. and Changeux, J.-P. (1983) High affinity binding of alpha-bungarotoxin to the purified alpha-subunit and to its 27000-dalton proteolytic peptide from *Torpedo marmorata* acetylcholine receptor. EMBO J. 2, 381-387.

54. Gershoni, J.M., Hawrot, E. and Lentz, T.L. (1983) Binding of α-bungarotoxin to isolated α subunit of the acetylcholine receptor of *Torpedo californica*: quantitative analysis with protein blots. Proc. Natl. Acad. Sci. U.S.A. 80, 4973-4977.

55. Reiter, M.J., Cowburn, D.A., Prives, J.M. and Karlin, A. (1972) Affinity labelling of the acetylcholine receptor in the electroplax: electrophoretic separation in sodium dodecyl sulphate. Proc. Natl. Acad. Sci. U.S.A. 69, 1168-1172.

56. Karlin, A. and Cowburn, D.A. (1973) The affinity labelling of partially purified acetylcholine receptor from electric tissue of *Electrophorus*. Proc. Natl. Acad. Sci. U.S.A. 70, 3636-3640.

57. Weiland, G., Frisman, D. and Taylor, P. (1979) Affinity labelling of the subunits of the membrane associated cholinergic receptor. Mol. Pharmacol. 15, 213-226.

58. Langenbuch-Cachat, J., Bon, C., Goeldner, M., Hirth, C. and Changeux, J.-P. (1988) Photoaffinity labelling by aryldiazonium derivatives of *Torpedo marmorata* acetylcholine receptor. Biochemistry 27, 2337-2345.

59. Valenzuela, C.F., Weigh, P., Yguerabide, J. and Johnson, D.A. (1994) Transverse distance between the membrane and the agonist binding sites on the *Torpedo* acetylcholine receptor: A fluorescence study. Biophys. J. 66, 674-682.

60. Unwin, N. (1996) Acetylcholine receptor imaged in the open state. Nature 373, 37-43.

61. Miyazawa, A., Fujiyoshi, Y., Stowell, M. and Unwin, N. (1999) Nicotinic acetylcholine receptor at 4.6 Å resolution: transverse tunnels in the channel wall. J. Mol. Biol. 288, 765-786.

62. Kao, P.N., Dwork, A.J., Kaldany, R.-R.J., Silver, M.L., Wideman, J., Stein, S. and Karlin, A. (1984) Identification of the α subunit half-cystine specifically labeled by an affinity reagent for the acetylcholine receptor binding site. J. Biol. Chem. 259, 11662-11665.

63. Kao, P.N. and Karlin, A. (1986) Acetylcholine receptor binding site contains a disulfide crosslink between adjacent half-cystinyl residues. J. Biol. Chem. 261, 8085-8088.

64. Abramson, S.N., Li, Y., Culver, P. and Taylor, P. (1989) An analog of lophotoxin reacts covalently with Tyr190 in the α-subunit of the nicotinic acetylcholine receptor. J. Biol. Chem. 264, 12666-12672.

65. Galzi, J.-L., Revah, F., Black, D., Goeldner, M., Hirth, C. and Changeux, J.-P. (1990) Identification of a novel amino acid α-tyrosine 93 within the cholinergic ligands-binding sites of the acetylcholine receptor by photoaffinity labeling. Additional evidence for a three-loop model of the cholinergic ligands-binding sites. J. Biol. Chem. 265, 10430-10437.

66. Cohen, J.B., Sharp, S.D. and Liu, W.S. (1991) Structure of the agonist-binding site of the nicotinic acetylcholine receptor. [^{3}H]acetylcholine mustard identifies residues in the cation-binding sites. J. Biol. Chem. 266, 23354-23364.

67. Middleton, R.E. and Cohen, J.B. (1991) Mapping of the acetylcholine binding site of the nicotinic acetylcholine receptor: [^{3}H]nicotine as an agonist photoaffinity label. Biochemistry 30, 6987-6997.

68. Boulter, J., O'Shea-Greenfield, A., Duvoisin, R.M., Conolly, J.G., Wada, E., Jensen, A., Gardner, P.D., Ballivet, M., Deneris, E.S., McKinnon, D., Heinemann, S. and Patrick, J. (1990) α3, α5, and β4: three members of the rat neuronal nicotinic acetylcholine receptor-related gene family form a gene cluster. J. Biol. Chem. 265, 4472-4482.

69. Galzi, J.-L., Revah, F., Bessis, A. and Changeux, J.-P. (1991) Functional architecture of the nicotinic acetylcholine receptor: From electric organ to brain. A. Rev. Pharmac. Toxic. 31, 37-72.

70. Galzi, J.L., Revah, F., Bouet, F., Ménez, A., Goeldner, M., Hirth, C. and Changeux, J.-P. (1991) Allosteric transitions of the acetylcholine receptor probed at the amino acid level with a photolabile cholinergic ligand. Proc. Natl. Acad. Sci. USA 88, 5051-5055.

71. Tomaselli, G.F., McLaughlin, J.T., Jurman, M., Hawrot, E. and Yellen, G. (1991) Mutations affecting agonist sensitivity of the nicotinic acetylcholine receptor. Biophys. J. 60, 721-727.

72. O'Leary, M.E. and White, M.M. (1992) Mutational analysis of ligand-induced activation of the *Torpedo* acetylcholine receptor. J. Biol. Chem. 267, 8360-8365.

73. Sine, S.M., Quiram, P., Papanikolaou, F., Kreienkamp, H.J. and Taylor, P. (1994) Conserved tyrosines in the alpha-subunit of the nicotinic acetylcholine receptor stabilize quaternary ammonium groups of agonists and curariform antagonists. J. Biol. Chem. 269, 8808-8816.

74. Corringer, P.J., Galzi, J.L., Eisele, J.L., Bertrand, S., Changeux, J.-P. and Bertrand, D. (1995) Identification of a new component of the agonist site of the nicotinic α7 homooligomeric receptor. J. Biol. Chem. 270, 11749-11752.

75. Dougherty, D.A. and Stauffer, D.A. (1990) Acetylcholine binding by a synthetic receptor: implications for biological recognition. Science 250, 1558-1560.

76. Sussman, J.L., Harel, M., Frolow, F., Oefner, C., Goldman, A., Toker, L. and Silman, I. (1991) Atomic structure of acetylcholinesterase from *Torpedo californica*: a prototypic acetylcholine-binding protein. Science 253, 872-879.

77. Satow, Y., Cohen, G.H., Padlan, E.A. and Davies, D.R. (1986) Phosphocholine binding immunoglobulin Fab McPC603. An X-ray diffraction study at 2.7 Å. J. Mol. Biol. 190, 593-604.

78. Glockshuber, R., Stadlmuller, J. and Pluckthun, A. (1991) Mapping and modification of an antibody hapten binding site: a site directed mutagenesis study of McPC603. Biochemistry 30, 3049-3054.

79. Neubig, R.R. and Cohen, J.B. (1979) Equilibrium binding of [^{3}H]tubocurarine and [^{3}H]acetylcholine by *Torpedo* postsynaptic membranes: stoichiometry and ligand interactions. Biochemistry 18, 5464-5475.

80. Neubig, R.R. and Cohen, J.B. (1980) Permeability control by cholinergic receptors in *Torpedo* postsynaptic membranes: agonist dose response relations measured at second and millisecond times. Biochemistry 19, 2770-2779.

81. Pedersen, S.E. and Cohen, J.B. (1990) *d*-tubocurarine binding sites are located at α-γ and α-δ subunit interfaces of the nicotinic acetylcholine receptor. Proc. Natl. Acad. Sci. U.S.A. 87, 2785-2789.

82. Damle, V.N. and Karlin, A. (1978) Affinity labeling of one of two α-neurotoxin binding sites in acetylcholine receptor from *Torpedo californica*. Biochemistry 17, 2039-2045.

83. Deleglane, A.M. and McNamee, M.G. (1980) Independent activation of the acetylcholine receptor from *Torpedo californica* at two sites. Biochemistry 19, 890-895.

84. Ratnam, M., Gullick, W., Spiess, J., Wan, K., Criado, M. and Lindstrom, J. (1986c) Structural heterogeneity of the alpha-subunits of the nicotinic acetylcholine receptor in relation to agonist affinity and antagonist binding. Biochemistry 25, 4268-4275.

85. Kurosaki, T., Fukuda, K., Konno, T., Mori, Y., Tanaka, K., Mishina, M. and Numa, S. (1987) Functional properties of nicotinic acetylcholine receptor subunits expressed in various combinations. FEBS Lett. 214, 253-258.

86. Czajkowski, C. and Karlin, A. (1991) Agonist binding site of *Torpedo* electric tissue nicotinic acetylcholine receptor. A negatively charged region of the δ subunit within 0.9 nm of the α subunit binding site disulfide. J. Biol. Chem. 266, 22603-22612.

87. Czajkowski, C. and Karlin, A. (1995) Structure of the nicotinic acetylcholine-binding site: identification of acidic residues in the δ subunit within 0.9 nm of the α subunit binding site disulfide. J. Biol. Chem. 270, 3160-3164.

88. Dowding, A.J. and Hall, Z.W. (1987) Monoclonal antibodies specific for each of the two toxin-binding sites of *Torpedo* acetylcholine receptor. Biochemistry 26, 6372-6381.

89. Sine, S.M. (1993) Molecular dissection of subunit interfaces in the acetylcholine receptor: identification of residues that determine curare selectivity. Proc. Natl. Acad. Sci. U.S.A. 90, 9436-9440.

90. Hann, R.M., Pagan, O.R. and Eterovic, V.A. (1994) The α-conotoxins GI and MI distinguish between the nicotinic acetylcholine agonist sites while SI does not. Biochemistry 33, 14058-14063.

91. Hucho, F. (1986) The nicotinic acetylcholine receptor and its ion channel. Eur. J. Biochem. 158, 211-226.

92. Hucho, F.L., Oberthür, W. and Lottspeich, F. (1986) The ion channel of the nicotinic acetylcholine receptor is formed by the homologous helices MII of the receptor subunits. FEBS Lett. 205, 137-142.

93. Giraudat, J., Dennis, M., Heidmann, T., Chang, J,Y., and Changeux, J.-P. (1986) Structure of the high-affinity binding site for noncompetitive blockers of the acetylcholine receptor: serine-262 of the delta subunit is labelled by [^{3}H]chlorpromazine. Proc. Natl. Acad. Sci. U.S.A. 83, 2719-2723.

94. Giraudat, J., Galzi, J.-L., Revah, F., Changeux, J.-P., Haumont, P.-V. and Lederer, F. (1989) The noncompetitive blocker [^{3}H]chlorpromazine labels segment M2 but not segment M1 of the nicotinic acetylcholine receptor α-subunit. FEBS Lett. 253, 190-198.

95. Imoto, K., Busch, C., Sakmann, B., Mishina, M., Konno, T., Nakai, J., Bujo, H., Mori, Y., Fukuda, K. and Numa, S. (1988) Rings of negatively charged amino acids determine the acetylcholine receptor channel conductance. Nature 335, 645-648.

96. Leonard, R.J., Labarca, C.G., Charnet, P., Davidson, N. and Lester, H.A. (1988) Evidence that the M2 membrane-spanning region lines the ion channel pore of the nicotinic receptor. Science 242, 1578-1581.

97. Oiki, S., Danho, W., Madison, V. and Montal, M. (1988) M2 δ, a candidate for the structure lining the ionic channel of the nicotinic cholinergic receptor. Proc. Natl. Acad. Sci. U.S.A. 85, 8703-8707.

98. Xu, M. and Akabas, M.H. (1993) Amino acids lining the channel of the gamma-aminobutyric acid type A receptor identified by cysteine substitution. J. Biol. Chem. 268, 21505-21508.

99. Xu, M., Covey, D.F. and Akabas, M.H. (1995) Interaction of picrotoxin with GABAA receptor channel-lining residues probed in cysteine mutants. Biophys. J. 69, 1858-1867.

100. Galzi, J.-L., Devillers-Thiery, A., Hussy, N., Bertrand, S., Changeux, J.-P. and Bertrand, D. (1992) Mutations in the ion channel domain of a neuronal nicotinic receptor convert ion selectivity from cationic to anionic. Nature 359, 500-505.

101. Bertrand, D., Galzi, J.-L., Devillers-Thiery, A., Bertrand, S. and Changeux, J.-P. (1993) Stratification of the channel domain in neurotransmitter receptors. Curr. Opin. Cell Biol. 5, 688-693.

102. Unwin, N. (1995) Acetylcholine receptor channel imaged in the open state. Nature 373, 37-43.

103. Revah, F., Galzi, J.L., Giraudat, J., Haumont, P.Y., Lederer, F. and Changeux, J. P. (1990) The noncompetitive blocker [^{3}H]chlorpromazine labels three amino acids of the acetylcholine receptor γ subunit: implications for the α-helical organization of the MII segments and the structure of the ion channel. Proc. Natl. Acad. Sci. U.S.A. 87, 4675-4679.

104. DiPaola, M., Czajkowski, C. and Karlin, A. (1990) The sidedness of the COOH terminus of the acetylcholine receptor δ-subunit. J. Biol. Chem. 264, 15457-15463.

105. Akabas, M.H. and Karlin, A. (1995) Identification of acetylcholine receptor channel-lining residues in the M1 segment of the α-subunit. Biochemistry 34, 12496-12500.

106. Brandl, C.J. and Deber, C.M. (1986) Hypothesis about the function of membrane-buried proline residues in transport proteins. Proc. Natl. Acad. Sci. U.S.A. 83, 917-921.

107. Katz, B. and Thesleff, S. (1957) A study of the desensitization produced by acetylcholine at the motor end-plate. J. Physiol. 138, 63-80.

108. Sakmann, B., Patlack, J. and Neher, E. (1980) Single acetylcholine activated channels show burst-kinetics in presence of desensitizing concentrations of agonist. Nature 286, 71-73.

109. Neubig, R.R., Boyd, N.D. and Cohen, J.B. (1982) Conformations of *Torpedo* acetylcholine receptor associated with ion transport and desensitization. Biochemistry 21, 3460-3467.

110. Heidmann, T., Bernhardt, J., Neumann, E. and Changeux, J.-P. (1983) Rapid kinetics of agonist-binding and permeability response analyzed in parallel on acetylcholine receptor rich membranes from *Torpedo marmorata*. Biochemistry 22, 5452-5459.

111. Jackson, M.B. (1989) Perfection of a synaptic receptor: kinetics and energetics of the acetylcholine receptor. Proc. Natl. Acad. Sci. U.S.A. 86, 2199-2203.

112. Auerbach, A. (1993) A statistical analysis of acetylcholine receptor activation in *Xenopus* myocytes: stepwise versus concerted models of gating. J. Physiol. 461, 339-378.

113. Hess, G.P. (1993) Determination of the chemical mechanism of neurotransmitter receptor-mediated reactions by rapid chemical kinetic techniques. Biochemistry 32, 989-1000.

114. Boyd, N.D. and Cohen, J.B. (1980) Kinetics of binding of [^{3}H]acetylcholine and [^{3}H]carbamoylcholine to Torpedo postsynaptic membranes: slow conformational transitions of the cholinergic receptor. Biochemistry 19, 5344-5353.

115. Stroud, R.M., McCarthy, M.P. and Shuster, M. (1990) Nicotinic acetylcholine receptor superfamily of ligand-gated ion channels. Biochemistry 29, 11009-11023.

116. Weber, M., David-Pfeuty, M.T. and Changeux, J.-P. (1975) Regulation of binding properties of the nicotinic receptor protein by cholinergic ligands in membrane fragments from *Torpedo marmorata*. Proc. Natl. Acad. Sci. U.S.A. 72, 3443-3447.

117. Unwin, N. (1996) Projection structure of the nicotinic acetylcholine receptor: distinct conformations of the α subunits. J. Mol. Biol. 257, 586-596.

118. Unwin, N., Toyoshima, C. and Kubalek, E. (1988) Arrangement of the acetylcholine receptor subunits in the resting and desensitized states, determined by cryoelectron microscopy of crystallized *Torpedo* postsynaptic membranes. J. Cell Biol. 107, 1123-1138.

119. Huganir, R.L., Delcour, A.H., Greengard, P. and Hess, P. (1986) Phosphorylation of the nicotinic acetylcholine receptor regulates its rate of desensitization. Nature 321, 774-776.

120. Miles, K., Anthony, D.T., Rubin, L.L., Greengard, P. and Huganir, R.L. (1987) Regulation of nicotinic acetylcholine receptor phosphorylation in rat myotubes by forskolin and cAMP. Proc. Acad. Sci. USA 84, 6591-6596.

121. Elliot and Ambrose (1950).

122. Ludlam, C.F.C., Sonar, S., Lee, C.-P., Coleman, M., Herzfeld, J., RajBhandary, U.L. and Rothschild, K.J. (1995) Site-directed isotope labeling and ATR-FTIR difference spectroscopy of bacteriorhodopsin: the peptide carbonyl group of Tyr 185 is structurally active during the bR-->N transition. Biochemistry 34, 2-6.

123. Rothschild, K.J. (1992) FTIR difference spectroscopy of bacteriorhodopsin: toward a molecular model. J. Bioenerg. Biomembr. 24, 147-167.

124. Hienerwadel, R., Grzybek, S., Fogel, C., Kreytz, W., Okamura, M.Y., Paddock, M.L., Breton, J., Nabedryk, E. and Mantele, W. (1995) Protonation of Glu L212 following QB- formation in the photosynthetic reaction center of Rhodobacter sphaeroides: evidence from time-resolved infrared spectroscopy. Biochemistry 34, 2832-2843.

125. Gregoriou, V. G., Jayaraman, V., Hu., X. and Spiro, T.G. (1995) FT-IR difference spectroscopy of hemoglobins A and Kempsey: evidence that a key quaternary interaction induces protonation of Asp beta 99. Biochemistry 34, 6876-6882.

126. Braiman, M.S., Walter, T.J. and Briercheck, D.M. (1994) Infrared spectroscopic detection of light-induced change in chloride-arginine interaction in halorhodopsin. Biochemistry 33, 1629-1635.

127. Baenziger, J.E., Miller, K.W. and Rothschild, K.J. (1992) Incorporation of the nicotinic acetylcholine receptor into planar multilamellar films: characterization by fluorescence and Fourier transform infrared difference spectroscopy. Biophys. J. 61, 983-992.

128. Baenziger, J.E., Miller, K.W., McCarthy, M.P. and Rothschild, K.J. (1992) Probing conformational changes in the nicotinic acetylcholine receptor by Fourier transform infrared difference spectroscopy. Biophys. J. 62, 64-66.

129. Baenziger, J.E., Miller, K.W. and Rothschild, K.J. (1993) Fourier transform infrared difference spectroscopy of the nicotinic acetylcholine receptor: evidence for specific protein structural changes upon desensitization. Biochemistry 32, 5448-5454.

130. Michelson, A.A. (1891) Philos. Mag. 31, 256.

131. Michelson, A.A. (1892) Philos. Mag. 34, 28.

132. Cooley, J.W. and Tukey, J.W. (1965) Math. Comput. 19, 297.

133. Fahrenfort, J. (1961) Spectrochim. Acta 17, 698.

134. Harrick, N.J. (1963) N.Y. Acad. Sci. 101, 928.

135. Harrick, N.J. (1965) J. Opt. Soc. Amer. 55, 851.

136. Harrick, N.J. (1967) In: Internal reflection spectroscopy. Ed. Harrick, N.J., Wiley Interscience, New York.

137. Braiman, M. and Rothschild, K.J. (1988) Fourier transform infrared techniques for probing membrane protein structure. Annu. Rev. Biophys. Biophys. Chem. 17, 541-570.

138. Pimentel, G.C. and Sederholm, C.H. (1956) J. Chem. Phys. 24, 639-641.

139. Parker, F.S. (1983) In: Applications of infrared, raman and resonance raman spectroscopy in biochemistry. Ed. Parker, F.S., Plenum Press, New York.

140. Venyaminov, S.Y. and Kalnin, N.N. (1990) Quantitative IR spectrophotometry of peptide compounds in water (H2O) solutions. I. Spectral parameters of amino acid residue absorption bands. Bipolymers 30, 1243-1257.

141. Ochoa, E.L.M., Dalziel, A.W. and McNamee, M.G. (1983) Reconstitution of acetylcholine receptor function in lipid vesicles of defined composition. Biochim. Biophys. Acta. 727, 151-162.

142. Fong, T.M. and McNamee, M.G. (1986) Correlation between acetylcholine receptor function and structural properties of membranes. Biochemistry 25, 830-40.

143. McCarthy, M.P. and Moore, M.A. (1992) Effects of lipids and detergents on the conformation of the nicotinic acetylcholine receptor from Torpedo californica. J. Biol. Chem. 267, 7655-7663.

144. Sunshine, C. and McNamee, M.G. (1992) Lipid modulation of nicotinic acetylcholine receptor function: the role of neutral and negatively charged lipids. Biochim. Biophys. Acta. 1108, 240-246.

145. Sunshine, C. and McNamee, M.G. (1994) Lipid modulation of nicotinic acetylcholine receptor function: the role of membrane lipid composition and fluidity. Biochim. Biophys. Acta. 1191, 59-64.

146. Jones, O.T. and McNamee, M.G. (1988) Annular and nonannular binding sites for cholesterol associated with the nicotinic acetylcholine receptor. Biochemistry 27, 2364-2374.

147. Bhushan, A. and McNamee, M.G. (1993) Correlation of phospholipid structure with functional effects on the nicotinic acetylcholine receptor. A modulatory role for phosphatidic acid Biophys. J. 64, 716-723.

148. Fong, T.M. and McNamee, M.G. (1987) Stabilization of acetylcholine receptor secondary structure by cholesterol and negatively charged phospholipids in membranes. Biochemistry. 26, 3871-3880.

149. Butler, D.H. and McNamee, M.G. (1993) FTIR analysis of nicotinic acetylcholine receptor secondary structure in reconstituted membranes. Biochim. Biophys. Acta. 1150, 17-24.

150. Fernandez-Ballester, G., Castresana, J., Fernandez, A.M., Arrondo, J.-L.R., Ferragut, J.A. and Gonzalez-Ros, J.M. (1994) A role for cholesterol as a structural effector of the nicotinic acetylcholine receptor. Biochemistry 33, 4065-4071.

151. Méthot, N., McCarthy, M.P. and Baenziger, J.E. (1994) Secondary structure of the nicotinic acetylcholine receptor: implications for structural models of a ligand-gated ion channel. Biochemistry 33, 7709-7717.

152. Ellena, J.F., Blazing, M.A. and McNamee, M.G. (1983) Lipid-protein interactions in reconstituted membranes containing acetylcholine receptor. Biochemistry 22, 5523-5535.

153. Lowry, O.H., Rosebrough, N.J., Farr, A.L. and Randall, R.J. (1951) J. Biol. Chem. 193, 265-275.

154. Hartree, E.F. (1972) Determination of protein: a modification of the Lowry method that gives a linear photometric response. Anal. Biochem. 48, 422-427.

155. Ryan, S.E., Demers, C.N., Chew, J.P. and Baenziger, J.E. (1996) Structural effects of neutral and anionic lipids on the nicotinic acetylcholine receptor. J. Biol. Chem. 271, 24590-24597.

156. Blanchard, S.G., Elliot, J. and Raftery, M.A. (1979) Interaction of local anesthetics with Torpedo californica membrane-bound acetylcholine receptor. Biochemistry 18, 5880-5885.

157. Moore, M.A. and McCarthy, M.P. (1994) The effects of drugs on the incorporation of a conformationally-sensitive, hydrophobic probe into the ion channel of the nicotinic acetylcholine receptor. Biochim. Biophys. Acta. 1190, 457-464.

158. Weiland, G., Georgia, B., Lappi, S., Chignell, C.F. and Taylor, P. (1977) Kinetics of agonist-mediated transitions in state of the cholinergic receptor. J. Biol. Chem. 252, 7648-7656.

159. Krodel, E.K., Beckman, R.A. and Cohen, J.B. (1979) Identification of a local anesthetic binding site in nicotinic post-synaptic membranes isolated from Torpedo marmorata electric tissue. Mol. Pharmacol. 15, 294-312.

160. Méthot, N., Demers, C.N. and Baenziger, J.E. (1995) Structure of both the ligand- and lipid-dependent channel-inactive states of the nicotinic acetylcholine receptor probed by FTIR spectroscopy and hydrogen exchange. Biochemistry 34, 15142-15149.

161. Reid, S.E., Moffat, D.J. and Baenziger, J.E. (1996) The selective enhancement and subsequent subtraction of atmospheric water vapour contributions from Fourier transform infrared spectra of proteins. Spectrochim. Acta 52, 1347-1356.

162. Salmon, A., Dodd, S.W., Williams, G.D., Beach, J.M. and Brown, M.F. (1987) J. Am. Chem. Soc. 109, 2600-2609.

163. Raines, D.E. and Miller, K.W. (1993) The role of charge in lipid selectivity for the nicotinic acetylcholine receptor. Biophys. J. 64, 632-641.

164. Marsh, D. and Watts, A. (1982) In: Lipid protein interactions, Vol. 2. Eds. Jost, J.C. and Griffith, O.H., Wiley, New York, pp. 53-126.

165. Auger, M., Carrier, D., Smith, I.C.P. and Jarrell, H.J. (1987) J. Amer. Chem. Soc. 112, 1373-1381.

166. Baenziger, J.E. and Chew, J.P. (1997) Desensitization of the nicotinic acetylcholine receptor mainly involves a structural change in solvent-accessible regions of the polypeptide backbone. Biochemistry 36, 3617-3624.

167. Rankin, S.E., Addona, G.H., Kloczewiak, M.A., Bugge, B. and Miller, K.W. (1997) The cholesterol dependence of activation and fast desensitization of the nicotinic acetylcholine receptor. Biophys. J. 73, 2446-2455.

168. Baenziger, J. E., Miller, K. W., and Rothschild, K. J., unpublished observations

169. Williamson, P.T., Grobner, G., Spooner, P.J., Miller, K.W. and Watts, A. (1998) Probing the agonist binding pocket in the nicotinic acetylcholine receptor: a high-resolution solid-state NMR approach. Biochemistry 37, 10854-10859.

170. Ryan, S.E and Baenziger, J.E. (1999) A structure-based approach to nicotinic receptor pharmacology. Mol. Pharm. 55, 348-355.

171. Baenziger, J.E., Darsaut, T.E. and Morris, M.-L. (1999) Title Biochemistry 38, 4905-4911.

172. Addona, G.H., Sandermann, H. Jr., Kloczewiak, M.A., Husain, S.S. and Miller, K.W. (1998) Where does cholesterol act during activation of the nicotinic acetylcholine receptor? Biochim. Biophys. Acta 1370, 299-309.

173. Yeagle, P.L. (1998) In: Biology of Cholesterol. Ed. Yeagle, P.L., CRC Press Inc., Boca Raton, pp. 121-146.

174. Marcelja, S. (1974) Chain ordering in liquid crystals. II. Structure of bilayer membranes. Biochim. Biophys. Acta 367, 165-176.

175. Meyer, 1899.

176. Forman, S.A, and Miller, K.W. (1989) Molecular sites of anesthetic action in postsynaptic nicotinic membranes. Trends Pharmacol. Sci. 10, 447-452.

177. Cohen, J.B., Correll, L.A., Dreyer, E.B., Kuisk I.R., Medynski, D.C. and Strand N.P. (1986) Interactions of local anesthetics with *Torpedo* nicotinic acetylcholine receptors. In: Molecular and cellular mechanisms of anesthetics. Eds. Roth, S.H. and Miller, K.W., Plenum, New York, pp. 111-124.

178. Boyd, N.D. and Cohen, J.B. (1984) Desensitization of membrane-bound *Torpedo* acetylcholine receptor by amine noncompetitive antagonists and aliphatic alcohols: studies of [^{3}H]acetylcholine binding and $^{22}Na^+$ ion fluxes. Biochemistry 23, 4023-4033.

179. Heidmann, T., Oswald, R.E. and Changeux, J.-P. (1983) Multiple sites of action for non-competitive blockers on acetylcholine receptor rich membranes from *Torpedo marmorata*. Biochemistry 22, 3112-3127.

180. Cohen, J.B., Weber, M. and Changeux, J.-P. (1974) Effects of local anesthetics and calcium on the interaction of cholinergic ligands with the nicotinic acetylcholine receptor protein from *Torpedo marmorata*. Mol. Pharmacol. 10, 904-932.

181. Weber, M. and Changeux, J.-P. (1974) Binding of *Naja nigricollis* [^{3}H]α-toxin to membrane fragments from *Electrophorus* and *Torpedo* electric organs. Mol. Pharmacol. 10, 35-40.

182. Heidmann, T. and Changeux, J.-P. (1979) Fast kinetic studies on the interaction of a fluorescent agonist with the membrane-bound acetylcholine receptor from *Torpedo marmorata*. Eur. J. Biochem. 94, 255-279.

183. Heidmann, T. and Changeux, J.-P. (1979) Fast kinetic studies on the allosteric interactions between acetylcholine receptor and local anesthetic binding sites. Eur. J. Biochem. 94, 281-296.

184. Boyd, N.D. and Cohen, J.B. (1980) Kinetics of binding of [^{3}H]acetylcholine to *Torpedo* postsynaptic membranes: association and dissociation rate constants by rapid mixing and ultrafiltration. Biochemistry 19, 5353-5358.

185. Dennis, M., Giraudat, J., Kotzyba-Hibert, F., Goeldner, M., Hirth, C., Chang, J.-Y., Lazure, C., Chretien, M. and Changeux, J.-P. (1988) Amino acids of the *Torpedo marmorata* acetylcholine receptor α-subunit labeled by a photoaffinity ligand for the acetylcholine binding site. Biochemistry 27, 2346-2357.

186. Aylwin, M.L. and White, M.M. (1994) Ligand-receptor interactions in the nicotinic acetylcholine receptor probed using multiple substitutions at conserved tyrosines on the alpha subunit. FEBS Lett. 349, 99-103.

187. Michelson, M.J. and Zeimal, E.V. (1973) In: Acetylcholine: an approach to the molecular mechanism of action. Pergamon press, New York.

188. Forman, S.A., Miller, K.W. and Yellen, G. (1995) A discrete site for general anesthetics on a postsynaptic receptor. Mol. Pharmacol. 48, 574-581.

189. Arias, H.R. (1996) Luminal and non-luminal non-competitive inhibitor binding sites on the nicotinic acetylcholine receptor. Mol. Membr. Biol. 13, 1-17.

190. Kloog, Y., Kalir, A., Buchman, O. and Sokolovsky, M. (1980) Specific binding of [^{3}H]phencyclidine to membrane preparation. Possible interaction with the cholinergic ionophore. FEBS Lett. 109, 125-128.

191. Albuquerque, E.X., Tsai, M.-C., Aronstam, R., Witkop, B., Eldefrawi, A.T., and Eldefrawi, M.E. (1980) Sites of action of phencyclidine. II. Interaction with the ionic channel of the nicotinic receptor. Mol. Pharmacol. 18, 159-178.

192. Oswald, R.E. and Changeux, J.-P. (1981) Proc. Natl. Acad. Sci. U.S.A. 78, 3925-3929.

193. Oswald, R.E. and Changeux, J.-P. (1981) Selective labeling of the delta subunit of the acetylcholine receptor by a covalent local anesthetic. Biochemistry 20, 7166-7174.

194. Baenziger, J.E., Morris, M.-L., Darsaut, T.E. and Ryan, S.E. (2000) Effect of membrane lipid composition on the conformational equilibria of the nicotinic acetylcholine receptor. J. Biol. Chem. 275, 777-784.

CURRICULUM VITAE

Name: **RYAN, Stephen Edward**

Degrees Obtained:

Ph. D. Biochemistry, University of Ottawa, 2000

B. Sc. (Honours), Biochemistry, University of Ottawa, 1994

Research Experience:

1994 - 2000	Doctoral thesis entitled: "Conformational Effects of Lipids and Local Anesthetics on the Nicotinic Acetylcholine Receptor". Carried out under the supervision of Dr. John Baenziger, University of Ottawa.
1994	Summer research student – Continuation of undergraduate honours project.
1993 - 1994	Undergraduate honours project: Identification and characterization of the factor IXa and factor X binding domains of factor VIII. Carried out under the supervision of Dr. Peter Ganz, The Canadian Red Cross Society.

Scholarships:

1998 - 2000	Ontario Graduate Scholarship
1996 - 2000	University of Ottawa Excellence Scholarship
1996 - 1998	NSERC Post-Graduate Scholarship
1996	University of Ottawa Entrance Scholarship

Research Achievements and Awards:

1999	American Biophysical Society Student Travel Award
1998	Biophysical Society of Canada Student Poster Award (first place).
1996 - 1998	Graduate Student Travel Awards, Department of Biochemistry, University of Ottawa.

1997	School of Graduate Studies and Research Travel Award, University of Ottawa.
1996	Graduate Student's Association of the University of Ottawa Travel Award.
1996	Biophysical Society of Canada Student Poster Award (first place).

Papers Published in Refereed Journals:

5. Baenziger, J.E., Morris, M.L., Darsaut, T.E. and **Ryan, S.E.**
"Effect of Membrane Lipid Composition on the Conformational Equilibria of the Nicotinic Acetylcholine Receptor."
Journal of Biological Chemistry (2000) **275**, 777-784.

4. **Ryan, S.E.** and Baenziger, J.E.
"A Structure Based Approach to Nicotinic Receptor Pharmacology."
Molecular Pharmacology (1999) **55**, 348-355.

3. **Ryan, S.E.**, Nguyen, H.P. and Baenziger, J.E.
"Anaesthetic Induced Structural Changes in the Nicotinic Acetylcholine Receptor."
Toxicology Letters (1998) **100**, 179-183.

2. Patenaude, S.I., MacKenzie, C.R., Bilous, D., To, R.J., **Ryan, S.E.**, Young, N.M. and Evans, S.V. "Production, Crystallization and Diffraction of an Antibody Fv Specific for the Blood Group A Oligosaccharide Antigen."
Acta Crystallographica (1998) **D54**, 1456-1459.

1. **Ryan, S.E.**, Demers, C.N., Chew, J.P. and Baenziger, J.E.
"Structural Effects of Neutral and Anionic Lipids on the Nicotinic Acetylcholine Receptor: An Infrared Difference Spectroscopy Study."
Journal of Biological Chemistry (1996) **271**, 24590-24597.

Papers in Preparation:

2. **Ryan, S.E.**, Blanton, M.P. and Baenziger, J.E.
"The Stabilization of a Structural Intermediate Between the Resting and Desensitized States of the Nicotinic Acetylcholine Receptor. "
To be submitted to *Journal of Biological Chemistry* June (2000).

1. **Ryan, S.E.** and Baenziger, J.E.
"Multiple Conformational Effects of Local Anaesthetics at the Nicotinic Acetylcholine Receptor."
To be submitted to *Biochemistry* July (2000).

Non-Refereed Publications:

1. **S.E. Ryan**
"The Mechanism of Drug Action at an Integral Membrane Receptor Probed by FTIR Difference Spectroscopy."
Biophysical Society of Canada Newsletter (1998) 10-14.

Conference Presentations:

14. **Ryan, S.E.** and Baenziger, J.E.
"Stabilization of an Intermediate State of the Nicotinic Acetylcholine Receptor."
Proceedings of the Canadian Federation of Biological Sciences, Ottawa, ON (2000) 117.

13. **Ryan, S.E.** and Baenziger, J.E.
"The Interaction of Phencyclidine with the Non-Competitive Blocker Site of the Nicotinic Acetylcholine Receptor Stabilizes a Unique Conformation that is a Structural Intermediate Between the Resting and Agonist-Induced Desensitized State."
44th Annual Meeting of the Biophysical Society, New Orleans, LA, *Biophysical Journal* (2000) **78** 360A.

12. **Ryan, S.E.** and Baenziger, J.E.
"Conformational Diversity Within the Nicotinic Acetylcholine Receptor."
43rd Annual Meeting of the Biophysical Society, Baltimore, MD, *Biophysical Journal* (1999) **76** A373.

11. Baenziger, J.E. and **Ryan, S.E.**
"Multiple Conformational Effects of Local Anesthetics at the Nicotinic Acetylcholine Receptor."
43rd Annual Meeting of the Biophysical Society, Baltimore, MD, *Biophysical Journal* (1999) **72** A22.

10. Baenziger, J.E. and **Ryan, S.E.**
"Attenuated Total Reflectance Infrared Spectroscopy: A Novel Method For Probing Membrane Protein Conformational Change."
44th International Conference on Analytical Sciences and Spectroscopy, Kingston, ON (1998) SP-24.

9. **Ryan, S.E.** and Baenziger, J.E.
"A Structure Based Approach to Nicotinic Receptor Pharmacology."
Proceedings of the Canadian Federation of Biological Sciences, Edmonton, AB (1998) 217.

8. Baenziger, J.E., Darsaut, T.E., Morris, M.L. and **Ryan, S.E.**
"Lipid Dependent Modulation of the Conformational State of the Nicotinic Acetylcholine Receptor."
Proceedings of the Canadian Federation of Biological Sciences Edmonton, AB (1998) 216.

7. **Ryan, S.E.** and Baenziger, J.E.
"A Structure Based Approach to Nicotinic Receptor Pharmacology."
IBC International Conference on Nicotinic Acetylcholine Receptors as Pharmaceutical Targets, Washington, DC (1997).

6. **Ryan, S.E.** and Baenziger, J.E.
"The Molecular Details of Anaesthetic-Nicotinic Receptor Interactions Probed Using FTIR Difference Spectroscopy."
5th International Meeting on the Cellular and Molecular Mechanisms of Anaesthesia, Calgary, AB (1997).

5. **Ryan, S.E.** and Baenziger, J.E.
"Anaesthetic Induced Conformational Changes in the Nicotinic Acetylcholine Receptor Probed by Fourier Transform Infrared Difference Spectroscopy."
41st Annual Meeting of the Biophysical Society, New Orleans, LA, *Biophysical Journal* (1997) **72**, A81.

4. Baenziger, J.E., **Ryan, S.E.**, Méthot, N. and Demers, C.N.
"Les Interactions Protéine-Lipide du Récepteur Nicotinique d'Acétylcholine."
64e Congrès de l'Association Canadienne-Française pour l'Avancement des Sciences, Quebec City, QC (1996) 57.

3. **Ryan, S.E.** and Baenziger, J.E.
"Anaesthetic Induced Conformational Changes in the Nicotinic Acetylcholine Receptor Probed by Fourier Transform Infrared Difference Spectroscopy."
Proceedings of the Canadian Federation of Biological Sciences, London, ON (1996) 101.

2. **Ryan, S.E.**, Demers, C.N. and Baenziger, J.E.
"Lipid-Protein Interactions in the Nicotinic Acetylcholine Receptor Probed by Fourier Transform Infrared (FTIR) Difference Spectroscopy."
Proceedings of the Canadian Federation of Biological Sciences, London, ON (1996) 100.

1. **Ryan, S.E.**, Demers, C.N. and Baenziger, J.E.
"Lipid- and Anaesthetic-Protein Interactions in the Nicotinic Acetylcholine Receptor Probed by FTIR Difference Spectroscopy."
40th Annual Meeting of the Biophysical Society, Baltimore, MD *Biophysical Journal* (1996) **70**, A197.

Societies:

1996 - present	Member of the Canadian Biophysical Society.
1995 - present	Member of the American Biophysical Society.